

**ENGINEERING RESEARCH UNIT
UNIVERSITY OF MORATUWA
SRI LANKA**

RESEARCH FOR INDUSTRY

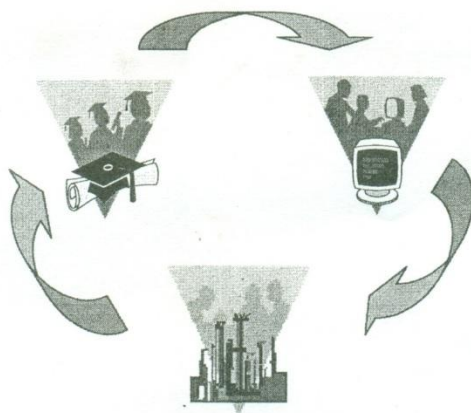
Proceedings of the 6th Annual Symposium 2000

December 2000

ISSN 1391-3999



**ENGINEERING RESEARCH UNIT
UNIVERSITY OF MORATUWA
SRI LANKA**



RESEARCH FOR INDUSTRY

Proceedings of the 6th Annual Symposium 2000

December 2000

DESIGN & CONSTRUCTION OF AN ENERGY-EFFICIENT FURNACE FOR MELTING NON-FERROUS ALLOYS IN THE LOCAL FOUNDRY INDUSTRY

S.R. Tittagala and N.P.N.M. Navarathna
Department of Mechanical Engineering, University of Moratuwa.

DESIGN & CONSTRUCTION OF AN ENERGY-EFFICIENT FURNACE FOR MELTING NON-FERROUS ALLOYS IN THE LOCAL FOUNDRY INDUSTRY

S.R. Tittagala and N.P.N.M. Navarathna
Department of Mechanical Engineering, University of Moratuwa.

ABSTRACT

A study has been carried out on the types of construction and factors affecting efficiency of metal melting furnaces currently used in the non-ferrous foundry sector with the objective of developing an oil-fired furnace with improved efficiency and reduced constructional and operating costs.

The project was initiated by the FDSI (Foundry Development and Services Institute) to meet a requirement of the small and medium-scale foundry industry. For example, there are many manufacturers of ornamental castings of Brass and Aluminum in the country, but they face the problem of the absence of a suitable furnace which could operate easily, efficiently and economically.

Following a preliminary survey and assessment of technical data, the main factors which affect performance were identified. Based on this a new design was evolved, the main features of which are that the charge is pre-heated, the flame retained in the furnace for longer duration and the fuel pre-heated and subjected to better atomised spray. The furnace, commissioned at a local foundry, demonstrated a significant improvement in performance over conventional types and acceptance by industry. A key feature was the improvement in overall working conditions and working environment. Based on this experience, a further improved version has been constructed and installed at the Mechanical Engineering Department – University of Moratuwa as a demonstration model for industry.

INTRODUCTION

History of Foundry Industry in Sri Lanka

In Sri Lanka during early colonial times, more affluent sectors of the population were involved with foundry industry for ornamental casting. Thus it is clear that the foundry industry has a long tradition in Sri Lanka. However, it has remained more a tradition or a custom with very little technological development over the years. As an example, Pilimathalawa in the Central Province is popular for ornamental castings but the profession is still practised using traditional methods. Elsewhere in the country, small-scale foundries are drying up as it is no longer an attractive or viable profession. Some foundrymen could not give up their traditional methods because of inadequate resources as well as lack of technological knowledge. Most of the people in this trade have limited resources to purchase new tools and equipment and to employ experienced and knowledgeable work force. Even though some may like to upgrade their industry with modern equipment, the prices of equipment such as furnaces are prohibitive. Also the sources of information and avenues available to improve the knowledge on foundry industry and to educate the work force is limited. On the other hand, the average foundryman does not trust modern technology and therefore hesitant to apply it. As a result, the quality of products is poor, production quantity is low and the cost of production is high.

State of Technology in Small-Scale Enterprises

Pattern making methods and moulding techniques have not changed much over the years. Due to the absence of efficient and low-cost furnaces, most persons practising the craft are not able to melt the metal properly. Also there is no temperature control and pouring methods are obsolete. As a result, solidification problems often arise. Gas contamination and porosity, and lack of metallurgical control of the product are common problems. The latter, however, is not given much consideration as the castings are used mostly for non-engineering purposes where the structure and mechanical properties are of not much significance. Due to these reasons, small-scale foundry industries are not in a position to sub-contract work from large industries. The quantity of production being insufficient and the quality being not acceptable, the small-scale industries have to survive on their own.

The Foundry Development and Services Institute (FDSI) has already identified the problems faced by the small-scale enterprises and is taking meaningful steps to uplift these industries. The main thrust at the present moment is to introduce an efficient furnace at a justifiable cost.

Information Survey

Important information was gathered by visiting small and medium sector local foundry industries involved with non-ferrous melting. These visits enabled the researchers to gain first hand experience about the nature and level of technology practised by these industries and also identify the problems faced by the small scale foundries. Construction and operation details of the different types of furnaces and the underlying principles of design were studied through discussions with industry personnel and survey of available literature. The knowledge thus gained formed the basis for the design and development procedure adopted.

TECHNOLOGY OF NON-FERROUS MELTING

The non-ferrous metal casting in Sri Lanka can be divided into two groups.

- (a) Heavy metal castings - for example Copper-alloy castings (Brasses and Bronzes).
- (b) Light metal castings - for example Aluminium-alloy castings.

It is essential that correct metallurgical practices are followed for each group as the quality of castings is greatly influenced by melting and pouring operations. These must be given due consideration at the furnace design stage.

Copper-Alloy Casting

In the sand casting method, the quality of the cast product is low if correct metallurgical practices are not followed. The quality of copper-base alloy castings is greatly dependent on melting and pouring operations. Copper-base alloys have high melting points of about 1000°C and more than 60% of heat is required to melt a unit weight of copper. This is due to greater heat capacity and latent heat of fusion. Copper-alloy sand casting is widely practised in cottage industries around Pilimathalawa area in Kandy.

Die-casting methods contribute to a large proportion of the total output of copper-alloy castings. However, die-casting of copper-alloys find very limited application in Sri Lanka. One example is water fittings being made by gravity die-casting.

Aluminium-Alloy Casting

Aluminium castings are one of the most widely used sectors of non-ferrous casting. Since most casting problems are directly related to incorrect procedures, adequate control has to be applied during the melting process. For die-casting, secondary aluminium is often used and it is approximately 15% cheaper than primary aluminium. Secondary aluminium means aluminium which is alloyed with Silicon.

Melting of Copper Alloys

In the case of melting of metals two main types of metallurgical problems arise. One is oxidation and the other is porosity. Oxidation produces metal oxide layers which may be entrapped and reduce strength of product. Porosity, whether at macro or micro level, affects casting quality. (Ref. 1)

Melting Procedure

The metal charge may consist of foundry scrap, ingots of desired composition and even good quality swarf. The metal is generally melted down under slightly oxidizing atmosphere if a fuel-fired furnace is used. This means about 0.5% free oxygen in the product of combustion. After melt down, additions of necessary alloying elements such as zinc, tin, lead can be made in order to get a specific composition. The melt is then heated to correct pouring temperature quickly to minimise gas absorption and compositional changes and then poured.

Dross Formation

Most copper alloys contain readily oxidizable elements such as zinc, tin, aluminium, manganese, and magnesium. The oxides separate completely or partially from the melt and form a "dross". Generally, oxide has low specific gravity and would be expected to float out of the melt. However, surface tension and other effects make separation difficult in some alloys such as high-zinc brasses and aluminium-bronzes. The dross may then entrap considerable metal and cause high melting loss. Sometimes charcoal covers or fluxes are employed to minimise dross formation. A cover of bottle glass thinned with borax is used as a covering flux and helps keep the metal surface clean. Charcoal as a protective cover is often used to minimise oxidation. Proprietary fluxes may be purchased which are claimed to cleanse the metal of oxides and prepare it for pouring. Minimum turbulence and melting under favourable combustion conditions will further reduce dross formation.

Oxygen in Copper Melting

Copper oxidises readily in molten condition and the solubility of oxygen in copper increases rapidly above its melting point. In solid state, copper dissolves oxygen only up to 0.0035% and the excess occurs as Cu_2O . Melting copper in an oxidising atmosphere favours oxidation of copper or an increased percentage of dissolved oxygen.

Another method of raising oxygen content of copper melt is to cover the melt with an oxidising flux, for example a mixture of 20 parts cupric oxide, 30 parts borax and 50 parts sand. Copper alloys contain substantially less oxygen under the same melting conditions than pure copper because the presence of more oxidisable elements prevent the maximum dissolved oxygen content from being reached (0.04 to 0.05% by wt. in pure copper.)

Hydrogen in Copper Melting

Solubility of hydrogen in copper alloys increase sharply with temperature particularly above their melting points. Solubility of hydrogen is lower in copper-tin bronzes than in pure copper. Hydrogen pickup comes from the furnace atmosphere, moulds and cores, dirty charge, moist ladles and melting accessories, moist melt additions etc. Dissolved hydrogen adds to the problem of dispersed shrinkage as it readily diffuses to shrinkage cavities and forms molecular hydrogen gas bubbles. This prevents the shrinkage cavities from being fed from the riser. In place of a pipe the riser top may swell. The risers may show exudations because of entrapment of gases (molecular hydrogen)

Oxygen-Hydrogen Interaction

Due to interaction, oxygen and hydrogen may form steam which can be entrapped in the solidifying casting giving defects. The two gases have a regulatory effect on each other. If high oxygen content is produced by melting under an oxidizing atmosphere, the hydrogen content of the melt can be held low by water vapour reaction. This is why most foundrymen prefer to melt copper alloys under oxidising condition; the hydrogen contamination is minimised. Reducing conditions will give the opposite result. Another method of reducing hydrogen is to flush it out with nitrogen, but this is not very common for various reasons like temperature loss, contamination through nozzle etc.

Zinc flare is another method to reduce the hydrogen in zinc containing copper alloys like brasses. The flare is due to high vapour pressure of zinc. The zinc vapour on reaction with oxygen forms brilliant white flame or flare. This occurs on raising the temperature above melting point. Flaring reduces hydrogen pickup but may cause zinc loss of 1% to 1.5%. If this practice is followed, additional zinc may be added before pouring to make up for the flare loss. If the charge is very dirty, then even high zinc brasses can have hydrogen porosity.

De-oxidation

Generally metals which oxidise more effectively (preferentially) than Copper is used as de-oxidants. When melting Copper-base alloys Phosphorous, Lithium, Boron, Calcium, Magnesium, Aluminium, Silicon and Beryllium are such de-oxidant elements. The most commonly used deoxidiser is low melting point phosphorus-copper alloy (15%P with 85% Cu). Equivalent of about 0.02% P is added to the melt for de-oxidation purposes. After addition is made, pouring should proceed at once. If a phosphorus residue takes place, the metal is no longer in an oxidised condition and it will pick up hydrogen again.

METAL MELTING FURNACES

There are several types of melting furnaces. Their economical and efficient performance depends upon :

1. The design of the melting chamber; shape and dimensions of the melting chamber and rate of heat input.
2. Control of process parameters.
3. Relatively small temperature gradient between flame and fuel, for effective combustion (for fuel-fired types). By supplying preheated air/fuel, combustion becomes more efficient.

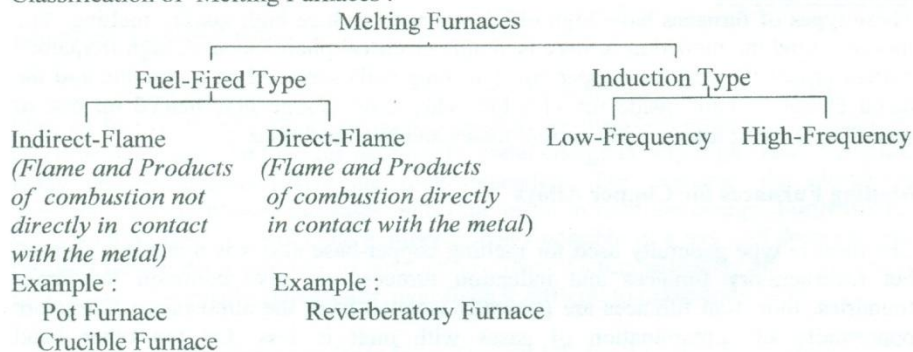
Process parameters can be monitored and controlled by using special instruments and thereby furnaces can be operated under optimum conditions. Some instruments used in conjunction with melting furnaces are,

1. Thermocouples, Radiation and Optical pyrometers for measuring temperature.
2. Fuel measuring appliances to monitor fuel consumption.
3. Pressure and Draught gauges.

Major types of metal melting furnaces are, Open-Hearth furnaces, Electric-Arc furnaces, Shaft type furnaces, Crucible furnaces, and Electric Induction furnaces.

Melting Furnaces Used in Non-Ferrous Foundry Industry

Classification of Melting Furnaces :



Pot Furnaces

Pot furnaces are of two types, Stationary pot furnaces and Tilting pot furnaces. Stationary furnace is used when the melting capacity is low. When the melting capacity is high, tilting furnace is normally used. In both cases molten metal is taken to ladles for distribution to the moulds.

Crucible Furnaces

Coke, gas or oil fired crucible furnaces are capable of giving high intensity of combustion with high temperature. In the case of coke-fired furnaces, the size and

quality of the coke is very important. The manner of combustion of coke is related to its physical properties. Harder cokes which have a higher ratio of carbon dioxide to carbon monoxide in the products of combustion, give higher intensity, and are more suitable for use in high temperature melting operations.

Capacity of the crucible furnace depends on the crucible size. Normally crucibles are made of a clay-graphite mixture or Silicon Carbide. Lift-out crucibles and crucibles with pouring spout are the most advantageous crucible furnaces. Lift-out crucibles are especially useful to obtain flexibility in small operations and when different types of alloys are to be melted. After the metal is melted, the crucible is lifted out of the furnace with tongs and placed in a ring shank ladle. Then it is poured directly from the ladle to moulds, after reaching the required temperature.

In oil-fired crucible furnaces the rate of fuel consumption should be controlled correctly. Fuel is wasted if too much or too little fuel or air is used. The optimum conditions are indicated from the shape and colour of the flame.

Reverberatory Furnaces

These furnaces are used mainly for large-scale production i.e. up to about 50,000 kg. of charge. Reverberatory furnace is a direct-flame furnace where the flame and combustion products are in contact with the metal being melted. These furnaces are mainly applied for bulk melting of ingots and scrap. After melting or holding, molten metal is then transferred to smaller furnaces, for example at a die-casting machine. The furnaces themselves are simply steel shelled and lined with refractory brick or having a monolithic lining. A burner is fixed to one end wall and the exhaust stack is at the other. Charging is carried out by either a separate door or through the exhaust stack. Metal is usually removed by either tilting the furnace or through a tap hole.

Induction Furnaces

These types of furnaces have high efficiency and produce high quality melting. The theory behind the induction furnace is simple electrical phenomena. A high frequency current passes through the copper coil (working coil) surrounding a crucible and the metal charge is kept inside the crucible. The metal charge gets heated up due to secondary current losses, eddy current losses and hysteresis losses.

Melting Furnaces for Copper Alloys

The furnace type generally used for melting copper-base alloys is a crucible furnace but reverberatory furnaces and induction furnaces are also common for larger foundries. Induction furnaces are generally isolated from the atmosphere. Therefore opportunity of contamination of gases with melt is less. On the other hand reverberatories and crucible furnaces have varying degrees of direct contact with furnace combustion gases and this affects metal quality.

Oil-fired crucible furnace is the furnace type widely used in local small-scale non-ferrous foundries. One of the most important components of such furnaces is the burner. The function of the burner unit is to atomise the fuel and allow complete combustion. The flame is directed to the crucible. Performance of an oil-fired crucible furnace depends on three major factors:

- (a) A suitable burner
- (b) A combustion chamber of right shape and size
- (c) Correct overall design

FURNACE USAGE: CURRENT SITUATION IN THE FOUNDRY INDUSTRY

In small-scale industry the furnaces used for melting non-ferrous metals such as brasses, bronzes, and aluminium alloys are mostly oil-fired pit furnaces. These are often not properly designed and constructed and also the maintenance is poor. Their poor performance is obvious even at first sight. There are many design defects which results in heavy heat losses, energy wastage etc. These also lead to uncomfortable working environment. Moreover, there is a very little control over the molten metal metallurgy and primitive technology is practised to obtain the possible best quality. (See Appendix – 1)

Identified Design and Operational Problems

- High fuel consumption.
- Flame is not properly controlled for heating.
- Very high time period for melting (for example about 3 hrs for 65kg of brass.)
- No proper temperature measuring method.
- Frequent crucible damage.
- Moisture contamination of the furnace.
- Long time taken for fuel line and air supply system repairs.
- Poor insulation.
- Uncomfortable working environment.
- Smoke spread all over the foundry.
- Furnace cannot be moved.

Economic Considerations

As stated above, fuel consumption is very high. For example to melt 1kg of Brass, 0.5 litres of fuel (burnt oil) has to be used. Therefore the fuel cost alone is very high. In this type of furnace the time for melting the metal charge is very high. Thus, there are many indirect expenses that are time dependent. For example, the electricity consumed for the blower increases with time taken to melt the charge. Furthermore, when melting time increases the number of heats possible in a day will decrease and this will lead to decreased rate of production. These factors adversely affect the profit margins and the small-scale foundryman finds it difficult to make ends meet.

Table 1: Performance Data for a Typical Oil-fired Crucible Furnace
(Metal Charge : Brass , Fuel : Diesel)

Weight of Charge (kg)	Volume of Fuel (Litres)	Furnace started at...	Furnace stopped at...
380	90	10.00 am	12.50 pm
416	92	10.00 am	01.00 pm
265	80	10.00 am	12.45 pm
306	85	10.00 am	01.00 pm
299	80	10.00 am	12.55 pm

By analysing the given set of observations :

(a) Efficiency

Weight of brass	= 380 kg	
Heat required to raise the temperature to 1100°C	= $(380 \times 0.385 \times 1070 + 380 \times 17) \text{ kJ}$	
	= $224.56 \times 10^3 \text{ kJ}$	
Calorific value of diesel	= 44,000 kJ/kg	
Required weight of diesel	= $\frac{224.56 \times 10^3}{44,000} \text{ kg}$	= 5.1 kg
Density of diesel	= 880 kg/m ³	
Required volume of diesel	= $(5.1/880) \times 10^3 \text{ l}$	= 5.8 l
Actual volume of diesel consumed	= 90 l	
Efficiency of the furnace	= $(5.8/90) \times 100\%$	= <u>6.45%</u>

(b) Operating Cost (Fuel cost only)

Price of diesel oil	= Rs. 13 per litre (say)
Diesel cost for a charge	= Rs. 13 x 90 = Rs. 1170
Diesel cost for melting 1 kg of brass	= Rs. 1170 / 380
	= <u>Rs. 3.00 (approx.)</u>

DESIGN & CONSTRUCTION CONSIDERATIONS

To overcome the shortcomings already identified, several improved design features were considered.

Increasing Heating Efficiency

- Covering the top of the furnace with a lid and introducing an exhaust pipe.
By covering top of the furnace, it is possible to use the flame more efficiently to heat the crucible and the furnace. At the same time the heat loss from the metal charge will be minimised.
The exhaust pipe helps to direct smoke (exhaust gases) and this in turn can be used to heat the fuel.
- Creating a spiral path to guide the flame which will help retain the flame for a longer duration inside the furnace and also ensure an increased flame contact area. The time required for the furnace to heat up can thus be considerably reduced.
- Using refractories having high insulating property and an outer steel cover to reduce moisture contamination.
- Using an additional flame initially at top of the furnace to pre-heat the metal charge by direct heating till the melting starts. This will help to reduce the time of heat up and heat losses.

Strategies to Recover Heat

To recover the useful heat in the exhaust gases and improve thermal efficiency, regenerative recuperation heating principles were considered.

- Pre-heat intake air using exhaust gas

- Pre-heat fuel oil using exhaust gas
This will also help to decrease viscosity of fuel, thereby enabling better atomisation and improved combustion efficiency.
- A “double atomising” nozzle to be used for better atomising. This would help better atomisation even with low blower pressures and gravity feed of fuel.
- A fuel cut-off system to be used to maintain the required temperature at constant level with saving of fuel. Also install a non-return valve in fuel feed line to eliminate the danger of backfire.
- To monitor the temperature of the melt using a Colour Chart.

Difficulties Encountered at the Design Stage

- Lack of information on available materials such as heat conductivity of firebricks, airflow rate of blower.
- Unaccountable heat losses.
When analyzing currently used furnaces or the new design, this is a major problem which affects the calculations, since it cannot be accurately quantified.
- Difficulty of taking measurements due to unavailability of equipment such as high temperature measuring equipment.

Difficulties Encountered in respect of Manufacture

- The strategy of pre-heating intake air using exhaust gas had to be abandoned.
The available burner supplied by the FDSI is of compact design with motor – blower – nozzle together on a single unit. Thus, if intake air is heated it would affect the motor windings.
(However this burner unit is of an improved design with a rotating nozzle which itself provides better atomization and therefore, efficient burning.)
- An additional flame to pre-heat the metal charge was not available.
(Such a pre-heating arrangement could be incorporated without any manufacturing modification, once such a unit is available)

Special Design Features

The special features which were to be finally incorporated in the new design to counter the identified shortcomings and improve efficiency can be summarised as follows:

- Spiral path on refractory brick lining
- Exhaust pipe with a heat exchanger
- Fuel cut-off system
- Lid lifting mechanism
- Steel outer casing
- Temperature estimation system

CONSTRUCTED FURNACE

The constructed furnace incorporates all the special design features summarised in the preceding Section. It is fitted with a special burner unit which is currently being introduced to the local foundry industry by the FDSI due to its efficient performance.

Main Parts and Functions

(See Appendix – 2)

Furnace Shell (Casing)

The furnace shell is a steel casing fabricated by welding. Steel plate bent to cylindrical shape is welded along the seam. Openings are provided for burner flame entry and exhaust. Features such as top and bottom flanges, exhaust fume box and brackets for lid lifting mechanism are all provided.

Combustion Chamber

The specially constructed combustion chamber provides for tangential entry of flame and guiding it around the crucible, thereby facilitating increased flame contact area. Fire bricks are suitably arranged around the steel casing and the gaps are filled with a mixture of fire clay and fine fire brick particles. To avoid thermal cracks in operation, care is exercised to provide even gaps between fire bricks and uniform bonding with clay.

Lift-off Lid

The furnace lid which has a center hole is made of refractory bricks clamped together by two semi-circular steel clamping rings. It is fitted with a swivel mechanism which enables the heavy lid to be easily moved to a side after lifting slightly.

Fuel Tank / Fuel Supply System

An oil barrel is used as the fuel tank with a gravity feed system. The function of the fuel tank is not only storing the fuel for combustion but maintaining the required fuel pressure. Thus it is kept at the required elevation:

An indicator on the fuel tank shows whether the fuel level is in the required range. A fuel shut-off valve controls the fuel supply as necessary.

Counter-flow Heat Exchanger

This is made of thin copper tube wound around the exhaust pipe to facilitate proper heat conduction and insulated with asbestos wool. The fuel oil circulation is carried out by the copper tube maintaining required oil flow and pressure.

Burner Unit

Burner is equipped with a motor, blower fan and a rotating nozzle. The motor driven fan supplies the combustion air and the rotating nozzle provides the atomized fuel.

Specifications of the blower motor are: ¼ HP, 3000 rev/min (Single phase - 220V)
Diesel or Kerosene can be used as the fuel oil. The burner needs no external pump to supply the fuel, since a gravity feed system is used.

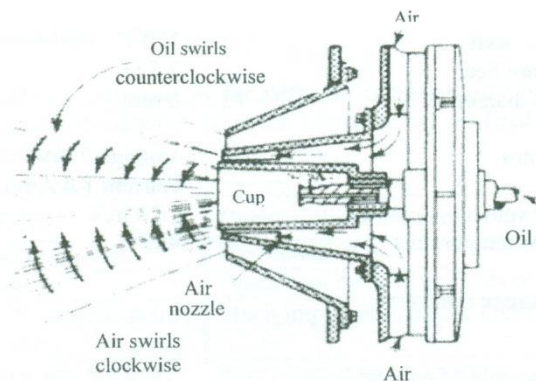


Figure 1: Components & Principle of Operation of the Burner Unit

Material & Construction Cost

	<u>Rs.</u>
Burner Unit	15,000
Crucible (50 kg)	8,000
Shell (steel casing)	6,000
Combustion Chamber (fire bricks, clay)	2,500
Other Components / Construction	3,500
Total	Rs. 35,000

COMMISSIONING OF FURNACE

The construction of the furnace was undertaken at Rohan Metal Industries Foundry at Dalugama under the supervision of the Foundry Development & Services Institute. The management and foundry staff extended their fullest co-operation at all stages. After trial firings some corrections were carried out to improve upon flame entry angle etc., following which the furnace was successfully commissioned.

Several trial melts were carried out to evaluate furnace performance. During these trials all important parameters were measured using equipment such as an anemometer, optical pyrometer and thermocouples.

Trial Data

A typical set of data obtained during commissioning trials is as follows :

Weight of charge (brass)	:	50 kg
Melting time – (Initial melt)	:	105 min.
- (Subsequent melts)	:	45 min. (average)
Melt temperature	:	1110°C
Ambient temperature	:	30°C
Diesel fuel consumption	:	7 l/h (average)
Fuel temp. – inlet	:	27°C

Fuel temp. – exit	:	120 ⁰ C
Fuel pressure head	:	2.5 m
Fuel outlet diameter	:	6 mm
Blower motor	:	Voltage 220V Current 1.8 Amp.
Blower air velocity	:	18.5 m/s
Exhaust gas temperature	:	485 ⁰ C

Furnace Performance Analysis

Symbols :

m	-	weight of charge
s	-	specific heat capacity of metal
L	-	Latent heat of metal
θ	-	Temperature difference
l	-	volume of fuel
ρ	-	density of fuel
C	-	calorific value of fuel
V	-	Blower motor voltage
A	-	Blower motor current
t	-	Time taken to melt the charge

Efficiency (η) :

Energy required to melt the charge	$= ms\theta + mL$
Energy supplied by the fuel	$= C(\rho l)$
Electrical energy absorbed by blower motor	$= VA (\cos \phi) t$
(For unity power factor)	$= VA t$

Total energy supplied = Energy supplied by the fuel
+ Electrical energy absorbed by the blower motor

$$\text{Furnace efficiency} = \frac{\text{Energy required to melt the charge}}{\text{Total energy supplied}}$$

$$= \frac{ms\theta + mL}{C\rho l + VA t}$$

For a specific trial :

Weight of charge (Brass)	=	50 kg
Volume of diesel	=	8 l
Time taken to melt the charge	=	105 min.
Thus Furnace Efficiency (η)	=	9.52%

Operating cost (Fuel cost only) :

Price of Diesel	=	Rs. 13 per litre (say)
Total cost of Diesel	=	Rs. 104
Diesel cost for melting 1 kg of Brass	=	Rs. 2.00 (approx.)

Performance Evaluation

Based on the limited experience so far with the industrial use of the constructed furnace, a comparative evaluation with the conventional oil-fired furnaces can be summarised as follows :

Conventional Type	Constructed Furnace
Very high fuel consumption.	Fuel economy.
High melting time.	Quick heat up & more heats per day.
Uncomfortable & unsatisfactory foundry environment.	Much improved working conditions.
No waste heat recovery methods.	Regenerative recuperation.
Melt contamination by flue gases.	Better metallurgical and defect control.
Start-up problems.	Can be fired easily.
Down-time due to frequent repair.	Durable and suitable for continuous operation.
Low initial cost.	Higher capital cost but, short-term cost recovery.

Not only improved design, but also controlled operation is critical for achieving maximum efficiency from a furnace. The crucial factors which affect the operation of oil-fired furnaces are discussed and the extent to which the designed furnace meets these requirements is analysed below.

Furnace Atmosphere Control

With few exceptions a slightly oxidizing flame should normally be used. For copper-base alloys, the flame will be tinged with green (due to pre-oxidation of the copper). A traditional test for the correct furnace atmosphere is to place a cold piece of zinc in the flame. A yellowish colour indicates an oxidizing flame, and a black colour indicates a reducing flame. The objective is to obtain a flame having a tinge of yellow, which indicates the presence of the desirable slightly oxidising atmosphere.

In the present design, the furnace lid effectively seals off the annular area between crucible and furnace brick lining, thereby preventing exhaust fumes contaminating the furnace atmosphere and melt. Therefore open-flame conditions in normal crucible melting are avoided. This minimises hydrogen contamination itself from the furnace atmosphere. However, if hydrogen pick-up is likely due to other adverse conditions, the desirable slightly oxidising atmosphere (in copper alloy melting) could still be provided by other means such as using an oxidising flux. Thus better metallurgical control over the cast product can be expected.

Burner Control

For efficient melting and optimum crucible life, it is necessary to have even heating of the crucible and to avoid hot and cold areas around the sides of the crucible bowl. Some furnace designers use two or four burners to minimise this problem. This will contribute to longer crucible life, better fuel economy, faster melting and lower noise levels. Precise periodic adjustment of the burner(s) is essential to efficient crucible furnace operation.

Special care is required to avoid over heating of bath. Normally 80% to 95% of the heat energy required to prepare a heat for the foundry is used to heat the charge to the

melting temperature. The melt is then quickly heated to correct pouring temperature and this is often the most critical step.

In the manufactured furnace, the special design of the combustion chamber provides for tangential flame entry and travel round the crucible thereby facilitating uniform crucible heating. Thus better melt-temperature control, particularly during the crucial period of quick heat up to pouring temperature after melting, is possible.

Oil Atomizing Burners :

Oil does not burn as a liquid; it is oil vapour that is burned. Quick combustion requires (among other factors) quick evaporation, which is attained by producing a very large surface area for a given quantity of oil. Since sub-divided oil (unless in contact with solids) assumes the shape of spheres, maximum surface area is obtained by extremely small droplets.

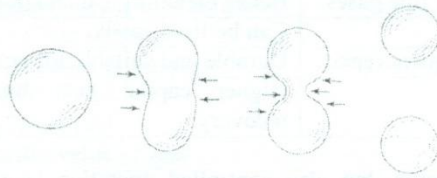


Figure 2: Subdivision of Liquid Droplets in Atomisation (Ref. 2)

Another important factor in vaporisation of oil is temperature of the surface of droplets because temperature increases vapour pressure. Temperature of the surface of a droplet is controlled by temperature of the oil itself and the temperature of surrounding gases (air plus products of combustion). Thus, either or both is beneficial. A third factor in quick combustion is thorough mixing of oil droplets with air.

The burner unit with rotary nozzle, currently promoted by FDSI and used in this instance, is capable of providing effective atomization and mixing, while fuel pre-heating is achieved in the 'heat exchanger'.

Even if all factors that favour rapid combustion are provided, combustion is not 'instantaneous' because of the size of the molecules. The effective time within which oil burns varies with size and design of furnace, with the demanded completeness of the combustion, and finally, with the fuel to air ratio. In the early stages of the combustion of an oil molecule, smaller molecules rich in carbon and also free carbon atoms are formed. If these particles, floating in a stream (the centre of which usually has a deficiency of air) squarely strike a wall, they adhere and form petroleum coke deposit which becomes progressively greater. If such a design is insisted on, more rapid combustion is the remedy.

The manufactured furnace avoids such an occurrence as the flame enters tangentially.

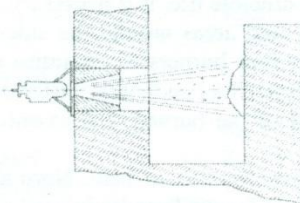


Figure 3: Formation of Carbon Deposit on Baffle in front of Oil Burner (Ref. 2)

FURTHER REFINEMENTS

The furnace installed at the laboratories of the Department of Mechanical Engineering is a further improved version of the furnace described in the preceding sections. Several refinements in construction have been carried out, particularly in the construction of the combustion chamber. A key additional feature is an attempt to reduce the time of heat up by directing exhaust gases on to the charge until melting starts. This is in lieu of the earlier strategy of pre-heating the charge using an extra gas flame at additional cost. A Silicon Carbide crucible is used in this furnace. Further possible improvements are the use of longer lasting refractory magnesite bricks instead of refractory alumina, backed by a layer of insulating type bricks in contact with the steel casing. The material and construction cost can be brought down to reasonable levels if there is a demand for a medium batch production.

At the time of writing this paper, the construction of the improved furnace has been completed and the furnace is about to be commissioned.

CONCLUSION

Industry trials indicate that the primary objectives of the study have been accomplished. These can be summarized as a marked improvement in working conditions together with a significant improvement in heating efficiency. Thus an overall gain in productivity and enhancement of quality through better metallurgical control can be envisaged. Further improvements to the furnace are possible but at an increased cost. The crucial decision the small-scale foundries will have to make sooner or later is whether to continue with current practices or to invest on improved equipment, with a short-term capital cost recovery strategy, for the sake of far reaching benefits for self and the foundry industry as a whole.

ACKNOWLEDGEMENT

The authors gratefully acknowledge the support extended towards this research by the Council of Management of the Foundry Development & Services Institute (FDSI) under the Chairmanship of Mr. Nihal Jinasena, and in particular, the valuable technical assistance and guidance received from Mr. Melvin Samarasinghe, Secretary – FDSI.

REFERENCES

1. **Richard W Heine, Carl R Loper and Philip C Rosenthal**, "Principles of Metal Casting", Second Edition, 1995, Tata McGraw-Hill
2. **G.S. Trinks and M.H. Mawhinney**, "Industrial Furnaces", Fifth Edition, 1961-1967, Newyork: Wiley

Appendix 1

Current Situation in small-scale Local Foundry Industry

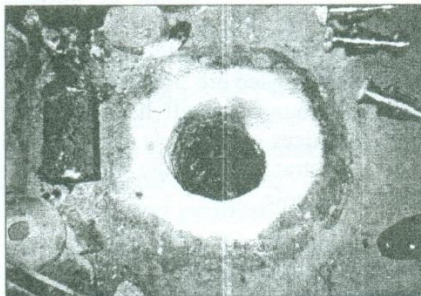


(a)



(b)

Pit Furnace for Aluminum melting



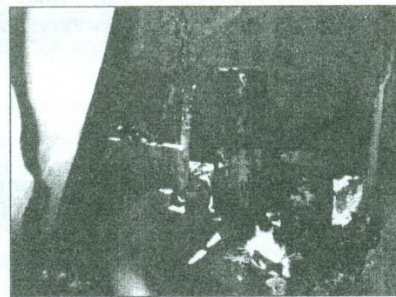
Pit furnace for Brass Melting



Pouring



(a)



(b)

Uncomfortable Working Environment

Appendix 2

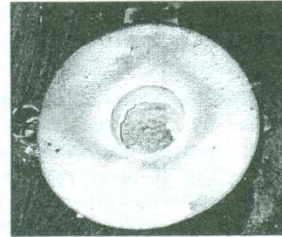
Constructed Furnace



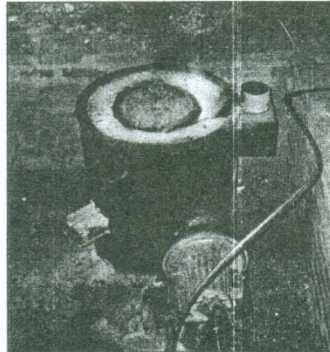
Oil Tank



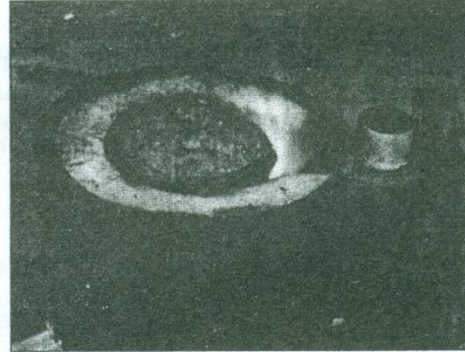
Steel Casing



Lid



(a)



(b)

Firing in Progress

CHEMICAL TREATMENT OF TIMBER, A NOVEL METHOD

Eng. (Dr) M.A.R.V.Fernando, B.Sc.(Eng), Ph.D., C.Eng., F.I.E.(SL),
Department of Mechanical Engineering, University of Moratuwa

CHEMICAL TREATMENT OF TIMBER, A NOVEL METHOD

Eng. (Dr) M.A.R.V.Fernando, B.Sc.(Eng), Ph.D., C.Eng., F.I.E.(SL),
Department of Mechanical Engineering, University of Moratuwa

ABSTRACT:

Dwindling resources of quality timber made manufacturers to look for alternatives. Species such as Rubber - "Hevea brasiliensis" were found to be good alternatives once treated against "Borer" attack. While expensive "Vacuum-Pressure Impregnation" provides total impregnation, cheaper methods such as "Dip" or "Spray" provides only a superficial treatment which may be removed during steps involved in furniture manufacture and similar processes. Analysis of "Mechanism of Impregnation in Vacuum-Pressure Process" indicate several short comings in the common explanation available. A new hypothesis suggested was verified with experimentation. Based on this explanation a "Novel Method", which uses simple equipment, yet ensuring total and perfect impregnation, though at a slightly lower rate, was developed. In this process the timber, immediately after sawing, is stacked in a tank (or a pit) to which the chemical solution pumped to completely submerge the timber. After the lapse of a specified period of time solution is pumped to a similar tank located adjoining (or close by) which too has a similar load of timber. While one tank is filled with chemical solution air is blown through the timber stacks of the dry tank. A spray of steam, if available, will be advantageous. While laboratory tests have proved the efficiency of the process field tests have proved the consistency of the process and durability of treated items. Cost analysis shows that the novel process is a very economical alternative, particularly attractive to Medium and Small Scale Industries.

INTRODUCTION:

With dwindling resources of quality timber the furniture and similar manufacturing industries, were forced to look for alternatives. Certain cheaper and abundant varieties while having most of the requirements such as strength, appearance, workability etc., were not durable due mainly to susceptibility to insect and fungal attacks. These then could be treated against such attacks and used as attractive alternatives to traditional high quality varieties.

Hevea basiliensis, commonly known as "Rubber Timber" is one such variety [1]. It's strength, nail holding and other physical properties are comparable with many quality varieties [2] such as Teak (*Tectona randis*), Beech (*Fagus sylvatia*), Light and Red Meranti (*Shorea leprosula* and *Shorea hemsleyane*) etc., [3],[4], but attracts borers very quickly. This is a common problem with many species where sapwood and heartwood cannot be easily separated or distinguished, as the insects are attracted to the "food" available in the sap [5]. Heartwood which actually consists of dead cells has no attraction for insects. Boron Treatment, which is basically impregnation of timber with Boron in the form of a mixture of Boric acid and Borax [6] to form a neutral solution, is particularly effective against borer attack [7]. This combined with a suitable fungicide makes such timbers very attractive alternatives to traditional "quality" timber in the furniture and related industries [8].

Surface treatment may be sufficient for certain applications such as handicrafts which are painted or protected by other means almost immediately after working [8]. However, steps such as band sawing, turning, or heavy planing involved in furniture manufacture may remove the surface layer and / or cut across the cross-section. Therefore, total impregnation is important to ensure durability of furniture [9]. While total impregnation could be achieved with "Vacuum-Pressure treatment", processes such as "Dip" or "Spray" treatment [10] often carried out with "Rubber" timber provides only a superficial protection [7]. Further while Vacuum-pressure impregnation can be carried out within a few hours [8][11], Dip and Spray treatments take several weeks.

However, Vacuum-Pressure impregnation plants are very expensive needing equipment including Pressure Chambers, Vacuum and Transfer Pumps, Valves, Solenoids and Controls etc. Further, it was observed that hardly any industry which has this facility is using it on a 24 hour basis. Operation of the plant around 4 to 6 hours a day is usually sufficient to treat the total needs of most of these industries. Thus a cheaper method, yet providing total impregnation, though perhaps at a little slower rate than Vacuum-pressure impregnation would be very attractive for furniture manufacturing and similar industries, particularly those of medium and small scale.

MECHANISM OF IMPREGNATION

All the analysis and experimentation described below were carried out with Rubber timber and Boron treatment. Same results may be applicable to other chemicals and species as well. However, they were not yet experimentally verified.

In both Dip and Spray treatments Boron ions are "**diffused**" into the cells of the "**wet**" timber. This is a very slow process [2]. The exact "Mechanism of Impregnation" during Vacuum-pressure treatment is also not fully established. It is presumed that during the vacuum cycle a part of the liquid (juices) in the cells (and lignin) is sucked out which then gets partly filled with chemical (boron) mixture during the pressure cycle. Next vacuum cycle removes a part of the chemicals and juice mixture from the cells replacing them with more chemicals during the next pressure cycle. This leads to increase of concentration, and thus the depth of penetration, of boron in to the cells during each cycle leading to substantial depth of penetration on repeating the process for a number of cycles. However, this mechanism is not fully established (to the best knowledge of author) theoretically or practically [7],[8] [and personal discussions with author of reference 7].

[Certain literature says that for vacuum-pressure impregnation to be effective the moisture content of the starting material should be less than 20% to 25 % [7]. However in practice in treatment of Rubber timber with Boron, unlike other species with other chemicals, sawn timber is put in to the impregnation plant as soon as possible [8] with the only delay perhaps being collecting sufficient quantity to fill the plant. Timber is not stacked for air drying as it may then be attacked by borer, and

are usually not pre dried in kilns or by other means as they substantially add to the cost of treatment].

Is this the correct explanation of the process ? Can the same result(s) be achieved by some other method(s)? The question whether the application of a hydrostatic pressure be able to compress a practically incompressible fluid (juices in cells) sufficiently to enable pumping in of some more liquid (boron mixture), will then arise. Can these fluids be sucked out by a vacuum? Both these questions are not properly answered in the existing literature (to the best knowledge of the author). Then **what are the other possible explanations?**

Evaporation of liquid on the surface of timber due to low partial pressure created during vacuum cycle may dry the surface of the timber to a certain degree. This causes some of the liquid (juices) inside the cells to be sucked out to the surface due to capillary action and surface tension as happens during kilning. As the chemical mixture is pumped back and the timber gets totally immersed in chemical solution the fluid depleted cells and porous matrix sucks back some chemical to replenish what was sucked out during vacuum period. As the cells are still interconnected in sapwood (and in rubber), as was needed for conveying food, chemicals so sucked in can mix well with the juices in the cells. Part of this mixture, of cell juices and chemicals, is then sucked out during the next vacuum cycle and penetrated during soaking. Thus a repetition of this process will gradually increase the concentration and thus the depth of penetration of chemicals.

This hypothesis could well be one possible explanation. If it is so even if a vacuum is not created, partial sucking out of the juices may be accomplished by drying the surface by any other means. If the surface is now fully soaked, or totally surrounded, with chemical solution suction of the chemical in to the liquid depleted cells should occur. This hypothesis could well be experimentally verified. Accordingly a set of experiments were designed and carried out.

EXPERIMENTATION:

Experiment 1.

Four pieces of 1" thick, 6" wide and 4' long planks of Rubber timber were prepared from timber sawn a day before. Out of these one piece was put into a vacuum-pressure impregnation plant while the other three pieces were treated as below.

a) Pieces were first exposed to a hot air draft around 50 °C in a drying kiln, for a sufficient time so that the surface felt dry to hand.

b) All the planks were then immersed in a bath of chemical (Boron mixture) that was being used for impregnation in the Vacuum-pressure chamber use with sample 1. Left for about 20 minutes.

c) A 6" long piece was cut from one plank for testing and the balance were again dried, and immersed in chemicals.

d) Cut piece was tested for depth of penetration with the standard Turmeric test. Measurement was carried out with instruments marked to 1/16" accuracy, and the variation over the cross section averaged to 1/32".

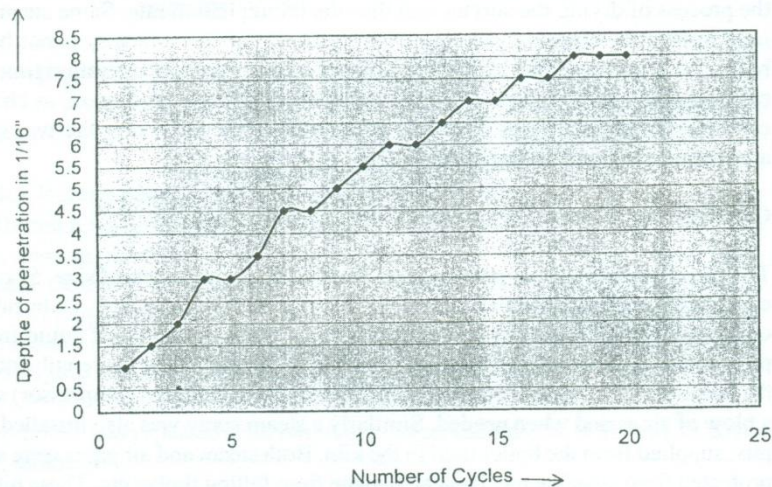
e) This process was repeated for 24 cycles.

This was compared with the sample, which was put into the vacuum-pressure impregnation plant and treated for approximately 4 hr and 30 minutes with alternate 15 minutes each vacuum and pressure cycles.

Results:

a). Vacuum-pressure impregnated plank had total penetration

b). The graph shows the depth of penetration of the test samples. It was observed that total penetration was achieved in about 18 to 20 cycles.



Discussion and Inferences:

The proposed hypothesis is valid, proved by the total penetration achieved.

Porosity of timber means presence of pores. These pores may be holding a small percentage of air or gasses. Application of pressure may compress these gasses, while the vacuum will expand them, thus accelerating the penetration process. This may

explain the shorter time of impregnation observed with vacuum-pressure process.

Pre-drying may increase the amount of gasses in pores and thus the rate of impregnation. This may explain the faster rate of impregnation with pre-dried timber as given in certain literature [7],[8].

INDUSTRIAL UNIT WITH THE NOVEL PROCESS:

Encouraged by above results a low cost industrial process was developed with a plant constructed at the factory of a leading furniture manufacturer. Obtaining a hot air blast needs heat exchangers which in turn escalate the cost of the plant. Considering financial constraints it was decided, therefore, to use an air blast for surface drying, with intermittent steam blast to raise the temperature of the surface of the timber thereby assisting the drying process. As this factory already has a waste wood fired boiler used with the seasoning plant (kiln), like in most of the medium scale wood working factories, and as the quantity of steam generated can be easily increased merely by increasing the fire (waste) wood fed to the boiler, steam in this instance is virtually free. Hardly any oil fired boilers are used in timber industry and therefore the cost of steam is minimal in most of the cases. Evaporation of fluids may cool the surface of timber due to latent heat and therefore heating the surface would accelerate the process of drying the surface and thus the impregnation rate. Same steam line is used to heat the chemical solution when needed. (In case a factory is not having a boiler the process may be carried out without steam. The total operation time in that case may have to be increased). Two pits (tanks) were decided upon, as chemicals can then be pumped from one tank to the other thus subjecting the two tanks to alternating cycles of drying and soaking.

CONSTRUCTION OF PLANT

The plant consists of two parallel steel lined concrete pits each of size 5' x 6' x 22' constructed 6 ft apart with a centre pit to accommodate a pump. Both pits were connected with 4" diameter pipes and valves to enable pumping of liquid from one pit (chamber) to the other. Pipes with small holes drilled along the length and laid at the bottom of the pits, and connected to an air blower fan (not a compressor) supplies a blow of air as and when needed. Similarly a steam spray was also installed at both pits, supplied from the boiler used in the kiln. Both steam and air pipes were suitably protected from possible mechanical damage from falling timber etc. These pits could take about 250 to 300 cu ft of timber each. (fig 1)

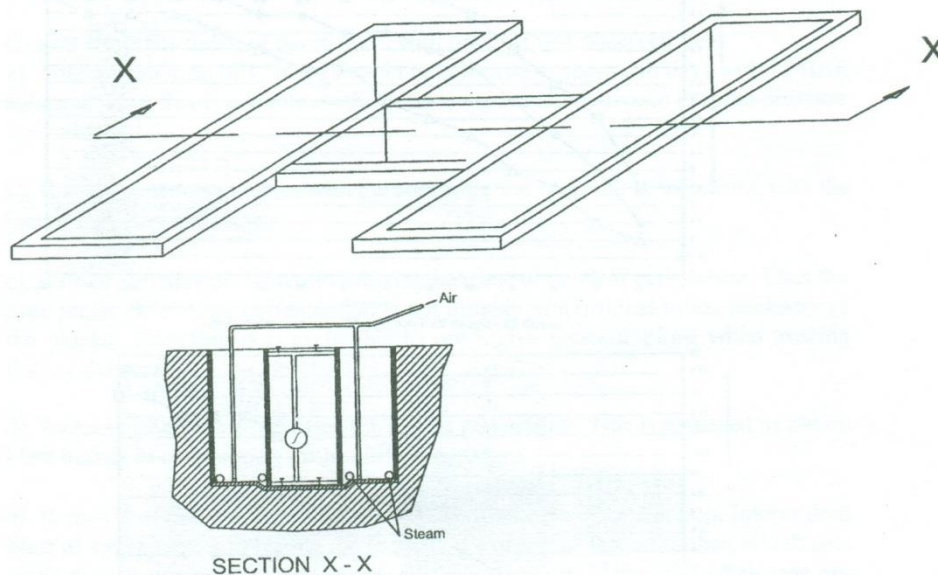


Fig. 1 - SKETCH OF TREATMENT PLANT

EXPERIMENT 2:

i). 1" thick Rubber planks were stacked with stickers as usual on both pits. An air blast with steam was sent to one of the pits for some time. Then it was filled up with 28 BAE neutral solution of Boric acid and Borax, while the air blasts with intermittent steaming was directed to the other pit. After about 2 hours chemical solution was pumped from first pit to the second pit and air blast re-directed to the first. This process was repeated. Samples were taken out after each cycle, ie; every 4 hrs (2 hrs drying and 2 hrs soaking), and tested for depth of penetration.

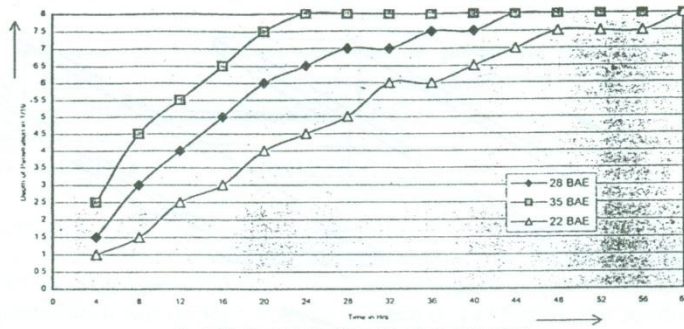
ii). Experiment was repeated with two more concentrations, 22 BAE and 35 BAE, with 1" planks.

iii). Experiment was repeated with 3/4" and 1 1/2" thick planks using 28 BAE solution.

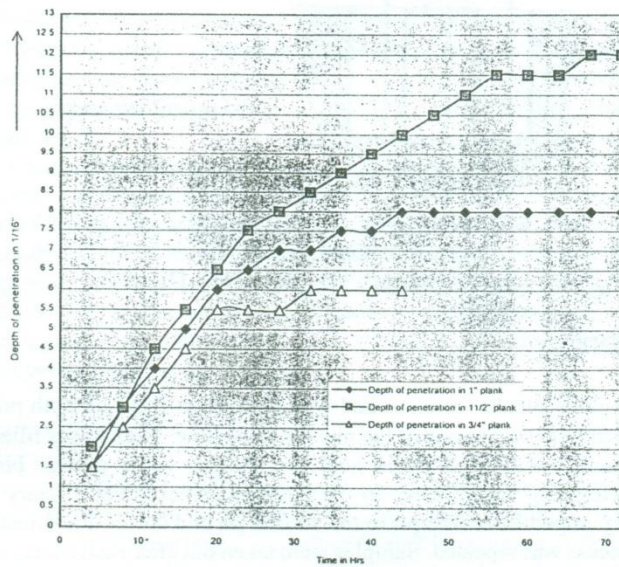
iv). Experiment was repeated with 28 BAE solution and 1" planks with increased air blast with intermittent steam, b) with air only (no steaming),

v). Experiment was repeated with 1" plank and 28 BAE solution with the temperature of the solution raised to about 45 °C

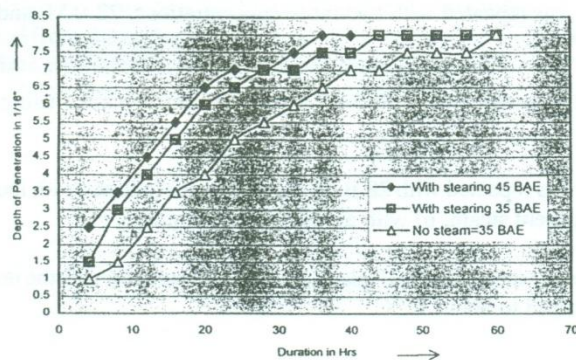
Accuracy of measurements approximately 1/16", variations averaged to 1/32"



Graph 02 - Depth Vs Time (for different concentration)



Graph 03 - Depth Vs Time (for different thickness)



Graph 04 - Depth Vs Time (with & without steam)

Observations and Discussion:

Graphs show the depth of penetration with time. It was observed that;

a). Total penetration of 1" planks could be achieved in about two days with 28 BAE solution. Thus this is a viable method and is a good alternative to vacuum-pressure treatment.

b). Rate of penetration varies with the concentration of solution, increasing with the increase of concentration.

c). Rate of penetration decreases with the increase of depth of penetration. Thus the time required for total impregnation is not directly proportional to the thickness of the planks. Therefore it is preferable to use higher concentrations when treating thicker planks.

d). Increase of air blast increases the rate of penetration. This is expected as the air blast assists in evaporation of the surface moisture.

e). Removal of intermittent steam blast reduces the rate of penetration. Intermittent blast of steam assists in raising the temperature of the surface of timber, which gets cools during evaporation of moisture due to latent heat. If the blast of air was dry (low R H) better results could have been expected. Thus, laying of an additional steam line to heat the blast of air, by blowing through it as in a kiln or any other suitable process, can be recommended when the additional expense can be afforded.

f). Increasing the temperature of the chemical solution increases the rate of penetration. However, use of steam blast to heat the bath dilutes the solution. An additional heat transfer arrangement as in "e", if available could be used for heating the bath as well.

COMMENTS:

This unit is in operation now for several years with very good results. The plant was continued to be supplied with steam as it can thus raise the temperature of the chemical solution, which was observed to have two additional advantages, viz; i). Chemical bath at a higher temperature accelerates the penetration, and ii). It prevents formation of fungus and bacteria in the bath thus preventing the severe pungent smell often observed with boron baths in vacuum-pressure plants. Need for frequent complete removal of liquor, which still contains a reasonable concentration of chemicals, from the bath replacing it with new chemicals, usually necessitated by this fungal formation in vacuum-pressure plants, thus is eliminated by the heating of the chemical bath with steam. It was found that replenishing the strength of the chemical, without disposing of the liquor, is sufficient and the same bath could be used for years.

As most of the medium scale timber working industries are having their own steam facility, cost of steam supply to the plant usually is only marginal. However, the process can be used even without steam where such facility is not available.

ECONOMICS OF PROCESS

The total construction cost of this plant was less than Rs 200,000/=. About 500 to 600 cuft of planks could be treated with these two baths alone in approximately two days. Capacity can easily be increased, if needed, simply by adding an additional pit. The cheapest Vacuum-Pressure impregnation plant available for the capacity requirements of this manufacturer was around Rs 7.5 million.

Operational costs of this plant are; a). Electricity for blower, b) cost of steam. At this unit, and at most of the medium industries, this is virtually nil as the only additional requirement is fire wood which is a waste from the saw mill. Hardly or no maintenance cost and need no skilled operators. Vacuum-pressure impregnation plants on the other hand consumes a considerable amount of electricity and needs skilled personnel for operation. Maintenance cost of valves, solenoids and controls involved too are considerable.

This amply demonstrate the economics of this process.

CONCLUSION:

1. In vacuum-pressure impregnation process, the suction of liquids from cells (and pores) may be due to capillary action (and surface tension) caused by the drying of the surface resulted by the evaporation of surface moisture due to reduced partial pressure.
2. Partial sucking in of chemicals to the cells is mainly due to replenishing of the fluid depleted cells when the surface is again soaked with chemicals. Application of pressure may be aiding this process.
3. The novel timber treatment plant and the Process described above ensures "total" and "complete" impregnation, though at a lower rate than with vacuum pressure plant.
4. The Plant is very simple and much cheaper, and therefore the process is much more economical, than using a Vacuum-Pressure impregnation plant of similar capacity. This process, therefore, would be particularly attractive to medium and small scale industries
5. Formation of bacteria which causes severe pungent smell, as often observed in vacuum-pressure impregnation plants, is eliminated with the heating of chemical bath with steam where available. Thus this saves chemicals by eliminating the need for frequent emptying of chemical baths.

6. Long term effectiveness of the process and the durability of the so treated products have already been proved in actual use.

REFERENCES:

- [1]. "Towards a wider use of Rubber wood", Planter's Bulletin 135, 1974, (pgs 181-194)
- [2]. TAN .A.G., MOHD ALI BIN SUJAN, "Rubber Wood for Furniture Manufacture", The Planter -Vol 57, No 668
- [3]. Hand Book of Hardwoods, Forestry Product Research Division Royal Forest Department, Bangkok.
- [4]. TISSEVERASINGHE. A.E.K., "A Manual of Timber Utilization for Ceylon", The Ceylon Forest Department, Colombo, 1970
- [5]. PIERIS. O.S., "Rubber Timber— a by-product of Natural Rubber Industry", Rubber News, 1982/2, RRI, Sri Lanka
- [6]. "Boron Diffusion Treatment for Timber", Internal report from CISIR
- [7]. TISSAVERASINGHE. A.E.K., "Preservative Treatment of Rubber (Hevea Brasiliensis) Wood by the Boron Diffusion Process., R.R.I.C Bulletin
- [8]. SONTI. V.R., CHATTERJEE. B., ASHROFF. M.S., "Utilization of Preserved Rubber woods -Preservatives and Methods of Treatment", 13 th Annual Meeting, 1982, International Research Group on Wood Preservation.
- [9]. WEERARATHNA. W.G.,- Consultant-, Forestry & Wood Industry, UNDP & ADB, Internal Report
- [10]. TISSAVERASINGHE A.E.K., "The Utilization of Rubber Wood", R.R.I.C Bulletin, Vol 5 – Nos 3 & 4,
- [11]. GRIFFIN. M.J., HEINBURGER. P., "Practical Extraction of Rubber Wood", Seminar on Rubber wood, 1982

APPLICATION OF MEBRANE SEPARATION PROCESSES TO THE SRI LANKAN INDUSTRY

B.M.W.P.K. Amarasinghe and I. M.B.M. De Silva
Dept. of Chemical Engineering, University of Moratuwa

APPLICATION OF MEBRANE SEPARATION PROCESSES TO THE SRI LANKAN INDUSTRY

B.M.W.P.K. Amarasinghe and I. M.B.M. De Silva
Dept. of Chemical Engineering, University of Moratuwa

ABSTRACT

Membranes and membrane based separation techniques have developed rapidly over the last two decades with a considerable technical and commercial impact. The technology is now widely used for a range of applications including water treatment, wastewater treatment, separations in the Chemical and Process industries, food and biotechnological industries and in the medical field. Micro Filtration, Ultra Filtration, Reverse Osmosis, Electro Dialysis and Dialysis are the commonly used processes. Nano Filtration, Pervaporation, Osmotic Distillation and Membrane Distillation are now becoming popular with the development of novel membranes, which withstand a wide range of operating conditions. The Membrane Separation technique is attractive due to many reasons, such as suitability of the processes for heat sensitive materials, high product quality and possibilities of recovery and recycle of valuable materials.

The survey shows very few applications of Membrane Processes in Sri Lankan industries. Normal Filtration and Ion Exchange are the widely used methods for water treatment. However, the application of a technique such as Reverse Osmosis or Ultra Filtration for water treatment in medical and pharmaceutical field, in drinking water production from high salinity level water and in food and beverage industries may largely help in improving the product quality. Wastewater is commonly treated using biological treatment and chemical treatment in combination with sedimentation. Approximately, 51% of the industries have the possibility of using Membrane Separation techniques not only to treat wastewater, but also to recover or recycle valuable materials, energy and water. Pulp and paper, Textile and Dairy industries are the major uses of Membrane technology for wastewater treatment. Further, the novel separation techniques such as Pervaporation and Osmotic distillation can be experimented for the manufacture of range of new products.

Application of Membrane Separation processes in Sri Lankan industry will be important in anticipation of future demands for high standards and minimal environmental impact.

INTRODUCTION

Membrane separation is a relatively new technology suitable for numerous processes. Membrane technologies have been widely applied to a range of conventionally difficult separations. For example conventional filtration cannot be applied for efficient processing of fine particles and colloids. Further the thermal processes such as distillation and evaporation are not suitable for heat sensitive food stuffs, pharmaceuticals and biological materials. The heat consumption is also very high for such thermal separations. Therefore, with the growth of new industries and the new concept of waste minimisation and cleaner technology necessity of advanced separation techniques arose and, membrane technology developed dramatically in the 1980's. The process is now used in the fields of water treatment, wastewater treatment, food and pharmaceutical industries and biotechnological and medical fields, either to improve established processes by improving product quality, minimising waste, treating waste or to process new materials.

This paper critically reviews membrane separation processes used for liquid systems and identifies the possibilities of applying the technique to the Sri Lankan Industry.

MEMBRANE TECHNOLOGY AND SEPARATION PROCESSES

A membrane is a permeable or semi-permeable phase, which restricts the motion of certain species in a mixture. The membrane introduces an interface between two bulk phases (liquid or gas) involved in the separation. Transport of selected species through the membrane is achieved by applying a driving force across the membrane. The driving force may be the pressure gradient, concentration gradient, temperature gradient, electrical potential gradient or combinations of above.

The schematic diagram of membrane separation is shown in Fig.1. The fraction which passes through the membrane is called the 'permeate' and its flow rate per unit area is the 'flux'. The 'concentrate' is rich in all components, which cannot pass through the membrane. The ratio between the flux and the feed is the 'recovery'. The separation factor between the concentrate and the permeate of one species is called the 'rejection'.

The heart of any membrane process is the membrane. The membranes can be polymeric, ceramic, metallic or modified natural products. Liquid membranes are also used. The membranes are manufactured by various chemical and heat treatment processes. The membrane may be symmetric or asymmetric. Figs 2a and 2b show electron micrographs of two membranes used in practice. The function of the membrane will depend on its structure as this essentially determines the mechanism of separation and thus the application. Therefore, careful selection of the membrane is extremely important and membranes and selection are described in detail by Scott[1,2] and Williams [3]. However that is beyond the scope of this paper.

Membranes need to be incorporated into modules or permeators. The module must support the membrane under high differential pressure, separate the feed side and the permeate side allowing permeate to pass through the membrane. Four main types of membrane modules are Tubular, Flat sheet, Spiral wound and Hollow fibre and are shown in Fig.3.

Membrane separations are used for various processes such as separation of solids from liquids, liquids from liquids, separation of miscible liquids, separation of dissolved solids and solutes from liquids and separation of mixtures of gases and vapours. Industrial membrane separation processes for liquid systems are classified in Table 1. However, the processes for the separation of gases are not discussed here. Micro Filtration (MF), Ultra Filtration (UF), Nano Filtration (NF) and Reverse Osmosis (RO) are the pressure driven processes used for the separation of fine particles, colloids, macromolecules and dissolved salts from liquids systems. The four processes are compared in Fig.4.

Table 1. Classification of Membrane separation processes used for liquid systems

MS processes	Driving Force and the Mechanism of separation	Separation achieved/ comments	Membrane types widely used
Micro Filtration	Pressure Sieving	Separates fine suspended solids and colloids. Operating modes: dead end mode and cross flow mode.	PTFE, Ceramic, Metallic
Ultra Filtration	Pressure Sieving (But particle surface charge and shape may play a role)	Separates dissolved molecules and fine particles.	CA, PA, PS, PAN
Nano Filtration	Pressure Sieving & Charge effects, Donnan exclusion	Separation of divalent ions but not monovalent ions.	PA
Reverse Osmosis (Hyper Filtration)	Pressure Size, shape, ionic charge interactions with the membrane	Separates Ionic solutes and macromolecules.	CA, PS, PA, PAN, PI
Dialysis	Concentration gradient Diffusion	Large molecules are separated from small molecules. A slow process.	CA
Electro Dialysis	Electrical potential Ionic charge	Ion free liquid can be obtained.	DVB, PTFE
Pervaporation	Partial pressure difference achieved using a vacuum Selective diffusion of one component with respect to others via the selected membrane	Separation of miscible liquids. Specially when conventional thermal processes are not applicable.	CA, PA, PS, PAN, PI
Osmotic Distillation	Partial pressure gradient achieved by differences in component activity in the mixture. Diffusion due to partial pressure gradient	Separates volatile components from a solution and concentrated solutions can be obtained.	PTFE, PVDF
Membrane Distillation	Partial pressure gradient achieved by the temperature gradient. Diffusion due to partial pressure gradient	Separates volatile components from a liquid and high purity distillate can be obtained	PTFE, PVDF, PP

PTFE - Polytetrafluoroethylene, CA - Cellulose esters, PA - Polyamide, PS - Polysulphone, PAN - Polyacrylonitrile, PI - Polyimide, DVB - Divinylbenzene, PVDF - Polyvinylidene fluoride, PP - Polypropylene

APPLICATIONS AND LIMITATIONS

Applications of membrane based separations of liquid streams can be broadly classified into three groups namely Water treatment, Wastewater treatment and Separations in the manufacturing processes. In a particular application permeate, concentrate or both streams may be important. Usually MS processes are used as a hybrid process in combination with other conventional processes, to reduce cost of operation and fouling problems.

Water Treatment

Water used for domestic purposes, medical and biotechnological applications and industries are obtained from various resources such as wells, rivers and lakes. Raw water contains ions, solutes, colloids and suspended solids etc. and should be treated before use. The required treatment largely depends on the necessary application and also on the raw water resource. For some applications, common water treatment methods such as coagulation/flocculation, sedimentation, filtration (F) and ion exchange (IX) can be used. However, appropriate membrane separation techniques, sometimes in combination with common separation methods should be used when high quality water is needed. Further application of membrane separation processes for water treatment avoids addition of chemicals such as coagulants and flocculants.

Some common applications of membrane separation techniques for purification of water are desalination of brackish water or sea water, production of electronic grade water, boiler feed water, pyrogen free water for medical and pharmaceutical industry, water for food and beverage and ultra pure water for biotechnological applications [1,15]. Fig.5 shows production of potable water using RO.

Waste Water Treatment

Membrane separation processes are widely used for wastewater (ww) treatment either to alleviate pollution problems or to recover valuables from waste streams. The type of pollutants in the wastewater has a major bearing on the selection of treatment technologies. Pollutants present in wastewater are particulates, suspended solids and micro-organisms, dissolved inorganics, volatile organics and non-volatile organics. Despite the fact that number of techniques such as biological treatments, chemical processes, physical processes are available for the removal of above contaminants from waste streams each method has its own disadvantages and limitations. Therefore, advanced membrane separation processes have come to play an increasingly important role in industrial wastewater treatment. Major applications of MS techniques for ww treatment includes pulp and paper [17,20,23,4,8,14,16], textile [9,11,13], electroplating, power station, dairy [10,21,22], latex, laundry, low grade radioactive plant, computer related industry [7] and oily waste water [19]. Figs 6 and 7 show MS applications in cheese whey production and paper

manufacturing process respectively. Comparison of conventional wastewater treatment techniques and with Membrane separations is shown in Table 2. Relative advantages and disadvantages of the techniques are described in detail by Scott [1] and Zinkus [18]. Table 2 shows that membrane separations and distillation are the only techniques suitable for all types of contaminants. The cost values in the table include installed capital costs, maintenance costs, chemical and power costs. Cost of some membrane techniques may be high compared to some of the conventional treatment methods. However, when compared with the advantages such as recovery of valuables and wide range of applications possible with Membrane Separations, the technique can be recommended for many applications.

Table 2: Applicability of wastewater treatment technologies

Treatment Process \ Type of pollutant	Suspended solids	Dissolved Organics	Dissolved Inorganics	Micro-organisms	Cost per million gallons treated *
Biological treatment	✓	✓	-	✓	40-1000
Chemical oxidation	-	✓	-	✓	200-10000
Chemical precipitation	-	-	✓	-	50-200
Adsorption	-	✓	-	-	70-1000
Filtration	✓	-	-	✓	20-100
Flotation	✓	-	-	-	20-100
Stripping	-	✓	-	-	40-250
Distillation	✓	✓	✓	✓	20-10000
Sedimentation (coagu/floccu)	✓	✓	-	✓	50-500
Ion exchange	-	-	✓	-	250-1000
Membrane separation	✓	✓	✓	✓	30-200

*- extracted from Zinkus [18]

Separations in the Manufacturing Processes

Membrane technology is now used in the manufacturing processes of many industries with the development of new types of membranes from a variety of materials. The ability of new membranes to tolerate all types of chemicals, extreme pH values and high temperature opens possibility of using membranes where conventional separation processes are inapplicable. Main applications of membrane separation processes lies on separations in food, biotechnological and pharmaceutical industries. MS processes are used for concentration of fruit juice and vegetable juice, milk, separation of enzymes, insulin, proteins, antibiotics etc., for hemodialysis, beverage industry, for purification of essential oils and production of anhydrous ethanol. Osmotic Distillation (OD) and Pervaporation (PV) are novel techniques and becoming popular in many industries. Mechanism of OD and use of OD for fruit juice concentration is shown in Fig.8.

Limitations

Membrane fouling and concentration polarisation are the two main phenomena which reduce the performance of the membranes. Fouling is the deposition of retained particles onto the membrane surface or in the pores. The build up of this deposit causes a continuous decline in flux with time. Concentration polarisation is the formation of a concentration gradient of solutes established at the membrane surface due to the preferential transport of solvent through the membrane. The higher solute concentration at the surface results in a higher osmotic pressure thereby reducing effective driving force. However, the above effects can be controlled by methods such as feed pre-treatment, adjustment of membrane properties, membrane cleaning and modification of operating conditions [1].

SRI LANKAN INDUSTRY

The main objective of this work was to gather information on current MS applications in Sri Lanka and find possibilities of future developments. A questionnaire was sent to approximately 45 Sri Lankan Chemical and Process industries, Textile industries, hospitals and hotels. The summarised format of the questionnaire is shown in the appendix. Data obtained were analysed considering source of feed, contaminants or components to be removed, capacity, necessity and possibility of recovering and recycling valuables, energy or water (for wastewater treatment) and final use of the product. The data was carefully compared with the literature on MS applications in developed countries and applicability to the Sri Lankan industry was decided. The survey shows that only 5% of the industries considered for the survey use MS technique in the process. However, 51% have the possibility of using MS techniques to improve product quality or to recover and recycle valuable materials and water and thereby increase profits. The results are summarised in Fig.9.

Fig.10 shows data collected on technologies used for water treatment. Municipal water supply, well water, deep well water and river water are the major sources of water used in Sri Lanka. The water is treated for drinking purposes, for the manufacturing processes, for boiler feed and for medical and surgical purposes. Normal Filtration and IX are the commonly used techniques for water treatment. Few applications of MS processes for water treatment in Sri Lanka includes use of RO and UF in hospitals and in the hotel sector.

Wastewater is hardly treated using MS in Sri Lanka. Biological treatment and Chemical treatment are the widely used separation techniques. However, only very few industries use wastewater treatment plants with recovery or recycle. But, if correctly used 56% of the industries have the possibility of using MS to treat wastewater, out of which 50% have the possibility of recovering valuable materials or energy or both (Fig.11).

Despite the wide range of applications of MS in food, biotechnological and medical fields, hemodialysis, which is dialysis of the blood against a physiological saline solution using UF membranes, is the only current usage of membrane technology for separations in Sri Lanka.

DISCUSSION

Electro Dialysis (ED) and RO are well-established techniques for desalination of seawater and brackish water. Distillation/Evaporation, Crystallisation, Ion exchange are the other processes used for desalination. Evaporation/Distillation and Crystallisation provide good quality water but the energy consumption is very high for these processes. IX is very popular in industries since the process produces good quality water. However if the dissolved solids concentration in water is high IX beds should be regenerated very often and may not be economical. Therefore IX is not normally used for water containing more than 1000 ppm of dissolved solids. RO is economically attractive for water containing high dissolved solids. In ED, transport of ions consumes electrical energy and therefore the higher the ion concentration the higher the energy consumption. Energy consumption for ED is less than that for RO at low dissolved solids concentrations. But for high dissolved ion concentrations energy consumption for ED is higher than that for RO. NF is now becoming popular with the development of novel membranes. NF can be used for water purification if the permeate can contain monovalent salts such as Na. This is advantageous since NF can be used at low pressures such as 6-15 bar compared with 30 bar for RO. Membrane Distillation (MD) can also be used for water purification, this is more economical than evaporation but not competitive with RO. However, high purity distillate can be obtain via MD since there is complete separation between feed and distillate and no entrainment. UF is a very popular membrane separation process for water clarification and disinfection. The process removes suspended solids and all micro-organisms from water. For medical and biotechnological field non-pyrogenic water is required. Pyrogen level can be reduced to below 0.05 ng/cm³ by combination of carbon adsorption, IX and UF.

MS can be used for a wide range of applications in Sri Lanka such as production of high purity water required for hospitals and pharmaceutical field, production of drinking water specially in the coastal areas where the water salinity levels are high. Seawater is proposed as the boiler feed water for the new coal power plant at Kalpitiya. Evaporation is suggested for purification of seawater for the plant, however RO also can be alternatively used [25].

UF and RO are the most widely used MS processes for the wastewater treatment. MF is sometimes used as a pre-treatment to other membrane separations to reduce suspended solids, which may block the UF or RO membrane. NF is also becoming popular in many applications such as pulp and paper industry. Application of MS techniques for the treatment of wastewater is advantageous compared to other processes such as coagulation, oxidation,

adsorption and IX since MS processes can be performed without degradation of valuable materials and without addition of new chemicals such as coagulants. Despite high capital cost of membrane separation processes recovery of valuable materials, energy, water and chemicals are so high the pay back period for installing MS system is only few months. (For example 18-30 months in textile industry [13]).

Pulp and paper, textile and dairy industries widely use MS processes for wastewater treatment since these processes not only treat wastewater but also recover valuable materials and recycle. Therefore such methods are profitable to use and can be tested for the Sri Lankan industry. Black liquor from the Embilipitiya paper mill cannot be treated by commonly used methods due to its high silica content. Hence storage of black liquor in lagoons costs over 9 million rupees [26]. ED has already been tested for treatment of black liquor [23] but other MS techniques can also be experimented. Further, the novel techniques such as Pervaporation (PV) can be used to remove traces of hazardous components from wastewater.

Membrane separation processes are preferable in food, bio chemical and medical fields because of low temperature operation, low energy requirements and high product quality. Dairy industry seems to be the largest membrane separation application in food industry. MF has been tested for the separation of oil from coconut water, waste from desiccated coconut industries, but not yet commercialised [28]. OD, is a comparatively new technique used for pre-concentration of many products such as fruit juice and reduce the water quantity before expensive freeze-drying.

Essential oil is exported from Sri Lanka in the raw form at low cost and the purified high-grade oils are imported at very high cost. Distillation is the commonly used technique for purification of essential oils. However, distillation is expensive due to the large number of stages required to obtain high purity products and removal of tracer components. Alternatively, PV can be used for purification of essential oils and high quality products can be achieved.

CONCLUSION

MF, UF, RO, ED and D are well-established processes. NF is becoming popular with the development of novel membranes. PV, OD and MD are relatively new operations and expensive compared to other membrane separation processes. However, such techniques are also used in many industries due to the advantage of low temperature operation. These methods are suitable for food, biochemical and pharmaceutical products, which deteriorate at high temperatures.

A wide range of membrane separation applications is possible in Sri Lanka for water treatment, wastewater treatment, and recovery of valuable materials and

energy from wastewater and for the separations in food and biotechnological industry.

Adoption of Membrane Technology for the Sri Lankan industry will not only assist in cleaner production, waste minimisation and environmentally friendly future but will also direct the industrialists for investigating new products.

ACKNOWLEDGEMENTS

The authors acknowledge with thanks the funds provided by the University Research Grant for the Research Assistantship of I.M.B.M. de Silva. We also wish to thank Mr. G.Jeyakumara for the support given in obtaining reference articles.

REFERENCES

1. Scott K., HandBook of Industrial Membranes, 1st edition, Elsevier Advanced Tech., Oxford, UK, 1995.
2. Williams R.A., Colloid and Surface Engineering: Applications in the process industries, Butterworth, Oxford, UK, 1992.
3. Scott K., Hughes R., Industrial Membrane Separation Technology, Chapman & Hall, UK, 1996.
4. Manttari M., Fouling management and retention in nanofiltration of integrated paper mill effluents, Lappeenranta teknillinen korkeakoulu, Monistamo, 1999.
5. Cheryan M., Ultra Filtration hand Book, Technomic Publishing Company, Inc, USA, 1986.
6. McGregor W C, Membrane Separations in Biotechnology, Marcel Dekker Inc. New York, 1990.
7. Tran T V, Advanced Membrane Filtration Process Treats Industrial Wastewater Efficiently, Chem. Eng. Progress, March 1985.
8. Mall I.D., Mishra A.K. and Upadhyay S.N., Membrane Separation Processes in Pulp and Paper Industry, IPPTA, Vol. 1, No 1, March 1989.
9. Paul R., Ramesh K. and Ram K, Effluent Treatment of Textile Waste Waters, Textile Dryer & Printer, Nov. 1995.
10. Sweeney M.J., Membrane-Based Liquid Separation Systems, Chem. Eng. Progress, Jan. 1985.
11. Diaper C., Correia V.M., Judd S.J., The Use of Membranes for the Recycling of Water and Chemicals from Dye house Effluents: an Economic Assessment, JDSC, Vol. 12, Oct 1996.
12. Hogan P.A. et. al., A New Option: Osmotic Distillation, Chem. Eng. Progress, July 1998.
13. Gaeta S.N., Separex S.P.A., Application of Membrane Processes to Textile Industry Development of Specific Membranes and Processes, Brite-Euram Seville Conference Proceedings, 1992.
14. Mansour O.Y., Nagaty A., El-Khatib M.M., Separation of Alkali from Silica Rich Black Liquor, Indian J. of Chemical Technology, Vol. 5, Jan. 1998.
15. Buckley C.A., Brouckaert C.J. & Kerr C.A., RO Application in Brackish Water Desalination and in the Treatment of Industrial Effluents, Reverse Osmosis 1993.
16. Dal-Cin M.M., et. al., Membrane performance with a pulp mill effluent: Relative contributions of fouling mechanisms, J of Membrane Science, 120, 1996.
17. Nuortila-Jokinen J., Kuparinen A., Nystrom M., Tailoring an Economical Membrane Process for internal Purification in the Paper Industry, Desalination, 119, 1998.

18. Zinkus G.A., Byers W.D., Identify Appropriate Water Reclamation Technologies, Chem Eng. Progress, May 1998.
19. McKetta J.J., Encyclopaedia of Chemical Processing and Design, Marcel Dekker Inc. New York, Vol. 59, 1997.
20. Nystrom M., Nuortila-Jokinen J., Current Trends in Membrane Technology, Reprints Kemia-Kemia, 23, 1996.
21. Porter M.C, Handbook of industrial membrane technology, Noyes pub., USA, 1990.
22. Ricci L., Separation techniques 1, Liquid-liquid systems, McGraw Hill publications, 1980.
23. Niranjala Sofalas M.E.L., Treatment and Chemical recovery of Embilipitiya Black Liquor by Electrodialysis, M.Phil. Thesis, 1999.
24. Grandison A.S. & Lewis M.J., Separation processes in the food and biotechnology industries, Woodhead Publications, 1996.
25. Study Report Phase 1, CEB - Coal Fired Thermal Development Project - West Coast, 1998.
26. Sunday Lankadeepa, 26th Sep. 1999.
27. Sunday Lankadeepa, 5th March 2000.
28. Somarasundra DHN et.al., Effect of protein on membrane separation of oil from coconut water, SLASS abstract, Sec B 86, 1999.

APPENDIX

QUESTIONNAIRE ON APPLICATIONS OF MEMBRANE SEPARATION PROCESSES IN SRI LANKAN INDUSTRIES

- i. Company :
 ii. Address :
 iii. Main Products :
 iv. Capacity :
 (Daily production)

1. Do you use **water purification** in your plant?

Yes	
No	

2. If water purification is done, please complete the table given below.

Technique	tick	Source of raw water	For what purpose the purified water is used	Capacity (m ³ /day)
Normal Filtration				
Ion Exchange				
Distillation				
Membrane Separation	Micro Filtration			
	Ultra Filtration			
	Nano Filtration			
	Reverse Osmosis			
	Dialysis			
	Electro Dialysis			
	Osmotic Distillation			
	Membrane Distillation			
	Pervaporation			
Other processes				

3. Do you have a **wastewater Treatment** plant?

Yes	
No	

4. If wastewater Treatment is done, Please complete the table given below.

Technique	Tick	Source of waste water*	Capacity/ Flow rate	Do you recover or recycle any material?	
				Yes/No	If so give details
Biological Treatment					
Chemical Treatment					
Membrane Separation	Micro Filtration				
	Ultra Filtration				
	Nano Filtration				
	Reverse Osmosis				
	Dialysis				
	Electro Dialysis				
Other process					

* Explain from which unit the waste water generated

5. Do you use Membrane Separation processes anywhere else in the plant other than mentioned above?

E.g. Concentration of Fruit Juice, Vegetable Juice
 Concentration of Proteins, Enzymes etc

Application	Membrane Separation process	Description

6. Any other comments

Name :

Designation :

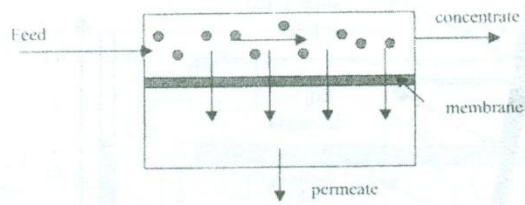
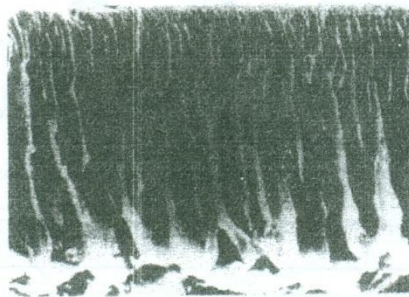
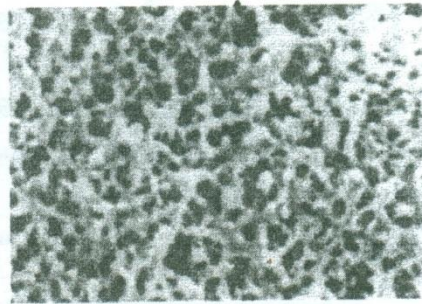


Fig 1: Schematic of a membrane separation

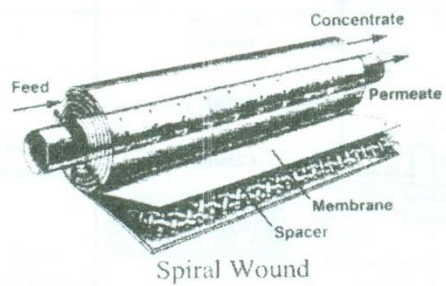


(a) Section through an asymmetric UF membrane

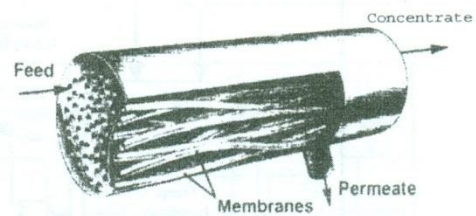


(b) PP membrane produced by stretching

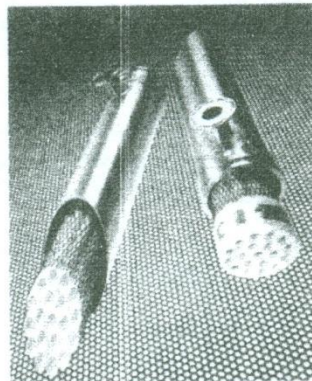
Fig. 2 : Electron micrographs of membranes



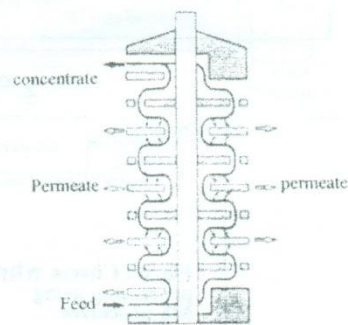
Spiral Wound



Hollow Fibre

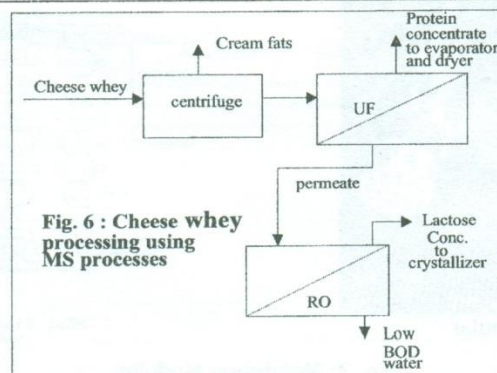
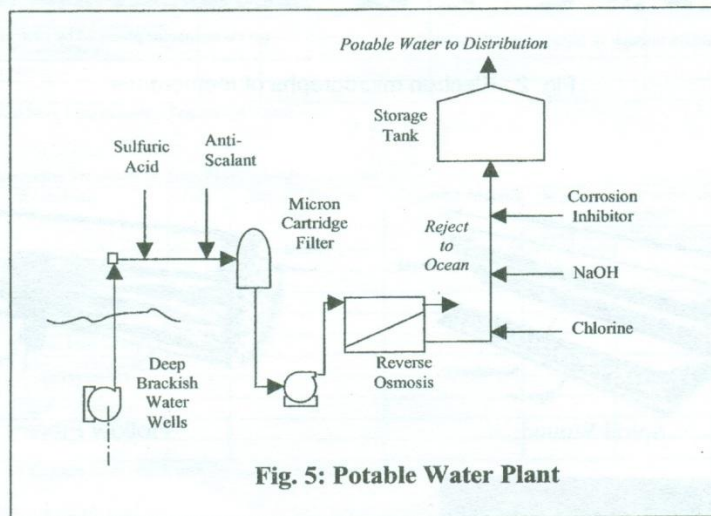
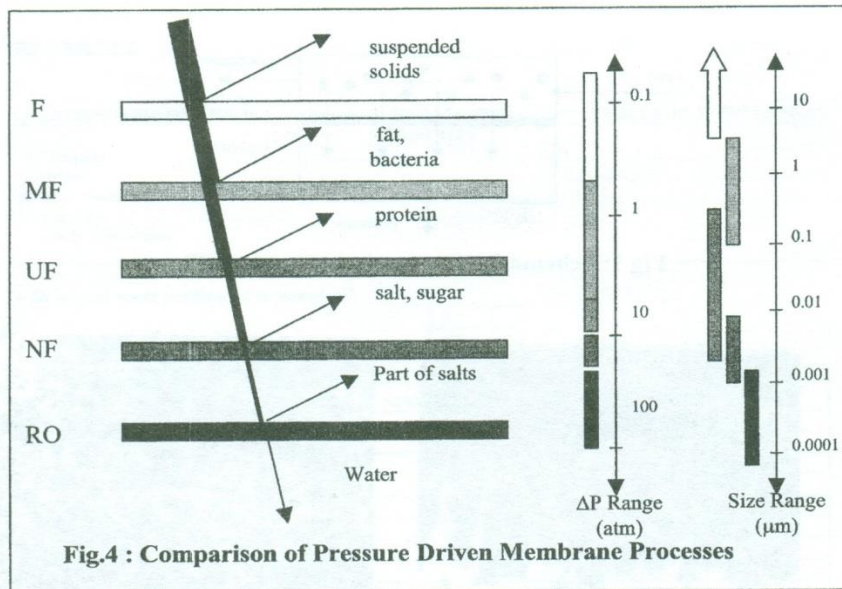


Tubular



Flat Plate

Fig. 3: Membrane Modules



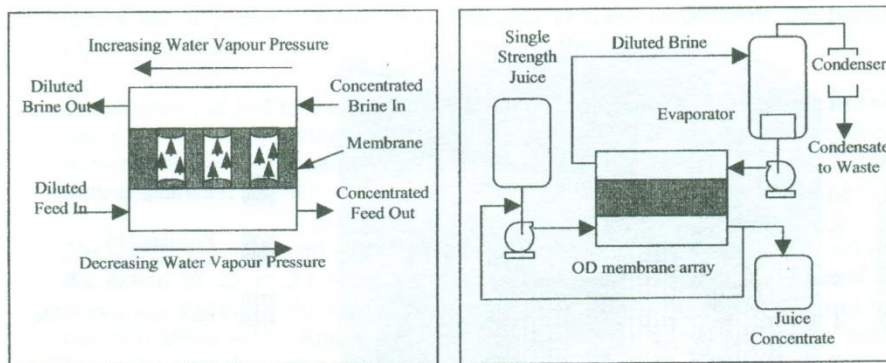
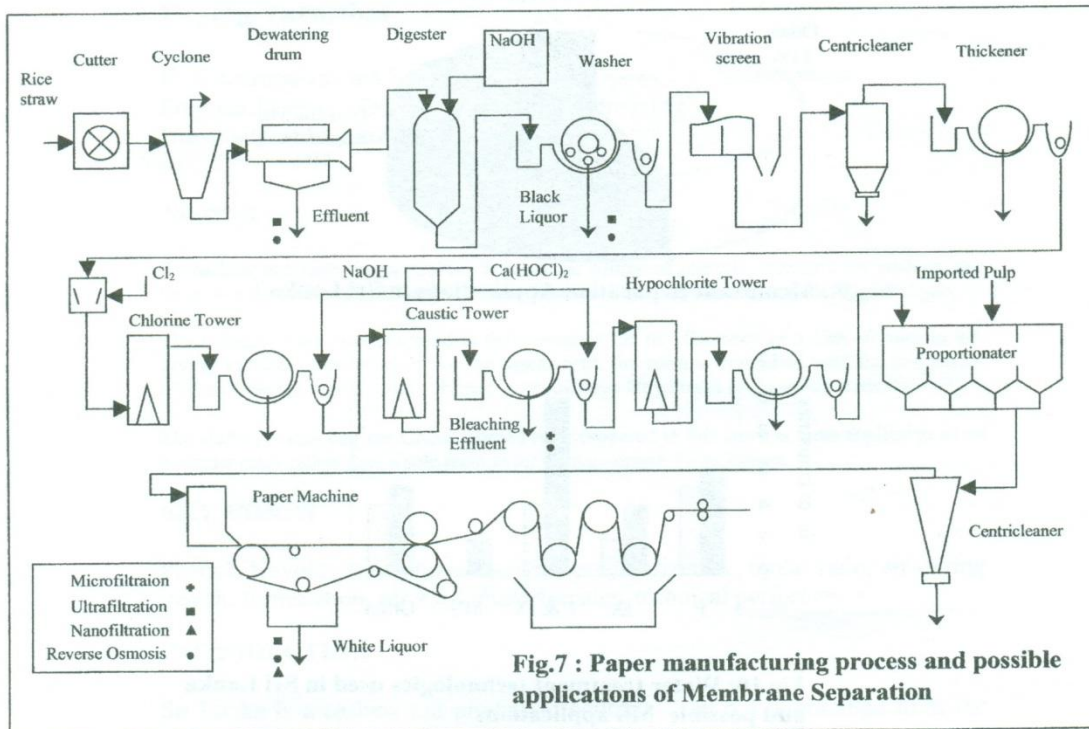


**Fig. 8: a) Mechanism of Osmotic Distillation
b) Concentration of fruit juice using osmotic**

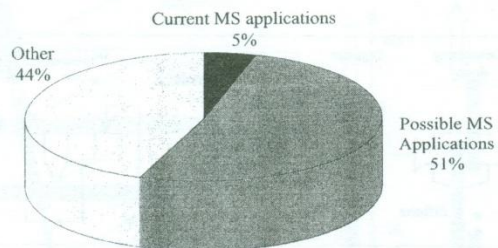


Fig.9 : Membrane Separation Applications in Sri Lanka

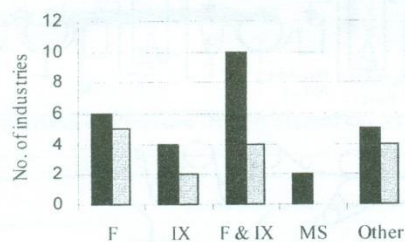


Fig 10: Water treatment technologies used in Sri Lanka and possible MS applications

■ - current application ▨ - possible MS applications

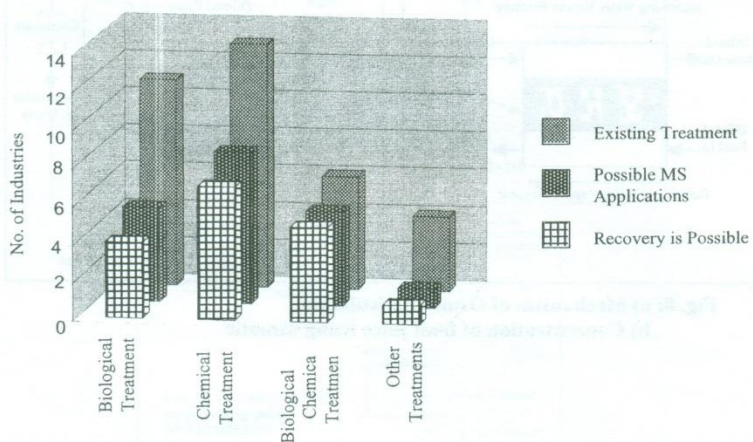


Fig.11 : Waste water treatment techniques used in Sri Lanka and Possible applications of MS

Cashew Nut Shell Liquid based Polymer Resin for making Air-Drying Varnishes

K. Subramaniam and Sunil Fernando
Polymer Division, Dept. of Chemical Engineering
University of Moratuwa

Cashew Nut Shell Liquid based Polymer Resin for making Air-Drying Varnishes

K. Subramaniam and Sunil Fernando
Polymer Division, Dept. of Chemical Engineering
University of Moratuwa

Abstract

As cashew nut shell liquid (CNSL) is a natural source of phenols, attempts are made in this work to prepare a synthetic polymer resin from the liquid, by treating it with formaldehyde.

The polymer resin thus prepared is then assessed for its efficiency as a film -former in air-drying varnish formulations. For the assessment, the resin is compared with the commonly used air - drying varnish film - former, short oil soya alkyd resin (60% solids content).

The studies reveal that the CNSL - based resin prepared in this work is most applicable as an extender resin rather than a sole resin in air drying varnish formulations.

KEYWORDS

Phenol, Novolac resin, formaldehyde, polymerization, molar ratio, air-drying varnish, formulation, physical characteristics, technical performance.

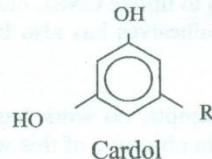
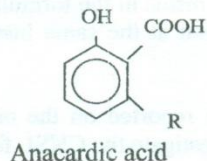
INTRODUCTION

Sri Lanka is a cashew nut producing country. The nut is obtained from the fruit of the tree '*Anacardium occidentale*'. The cashew fruit is sweet and nutritious and the nut with hard shell consists of a liquid, which is mainly composed of phenolic substances. Because of these constituents the liquid offers protection against insects which damage the cashew kernel.

The cashew nut is 2 to 4 cm long and kidney shaped and the shell of the nut is about 0.3 cm thick, having a soft leathery outer case and a thin hard inner case. Between these two cases, there is a honey comb cell which contains the cashew nut shell liquid.

The shell forms about 60 - 70 % of the raw cashew nut and CNSL is present to the extent of 25 to 30 % of the shell. CNSL consists of a mixture of a phenolic substances, the main components being anacardic acid and cardol in the ratio about 4:1¹. Anacardic acid is an aromatic hydroxy carboxylic acid having hydrocarbon (R) group in the benzene ring.

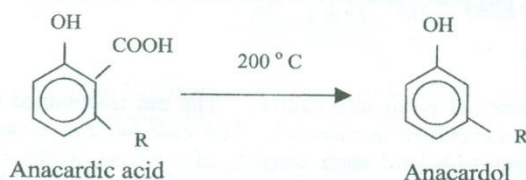
Cardol is a dihydroxy alkyl phenol. It has also a hydrocarbon group (R) in the benzene ring.



The hydrocarbon group (R) is identified as a long chain of 15 carbon atoms having various types of molecular structures ², as shown below:

Structure of Hydrocarbon group (R)	%
Mono olefinic constituents $-(CH_2)_7-CH=CH-(CH_2)_5-CH_3$	45.1
Di olefinic constituent $-(CH_2)_7-CH=CH-CH_2-CH=CH-(CH_2)_2-CH_3$	19.4
Tri olefinic constituent $-(CH_2)_7-CH=CH-CH_2-CH=CH-CH_2-CH=CH_2$	31.2
Saturated constituent $-(CH_2)_{14}-CH_3$	4.3

As raw CNSL is produced commercially by hot temperature boiling method (Ca. 200 °C), anacardic acid the main constituent in the liquid is decarboxylated in the method and converted into anacardol as shown below.



In consequence, the commercially available raw CNSL consists of only cardol and anacardol as its main constituents and is considered as a valuable source of phenols.

Although a wide range of products such as adhesives, surface coatings, waterproof sealing, dyestuff, pharmaceuticals etc. has been produced from CNSL in the developed countries³, limited work has been carried out regarding its utilisation in Sri Lanka.

Rajapakse *et al.* have conducted systematic work on the application of CNSL at Ceylon Institute of Industrial and Research, Sri Lanka and have been successful in finding a use of CNSL in natural rubber based tyre tread compounds as an anti-oxidant chemical⁴.

Further an evaluation to utilize CNSL based synthetic resins in the formulation of polychloroprene adhesives has also been undertaken at the same institute but with no success⁵.

Apart from these attempts, no work has so far been reported on the use of CNSL. Thus the main objective of this work is to investigate the CNSL for its

application in local industries, especially its use in surface coating manufacturing sectors.

Method of approach

As resin made from simple phenols are utilised as resin components in varnish formulations, attempts have been made in this work to produce CNSL - based synthetic resin, for the same purpose.

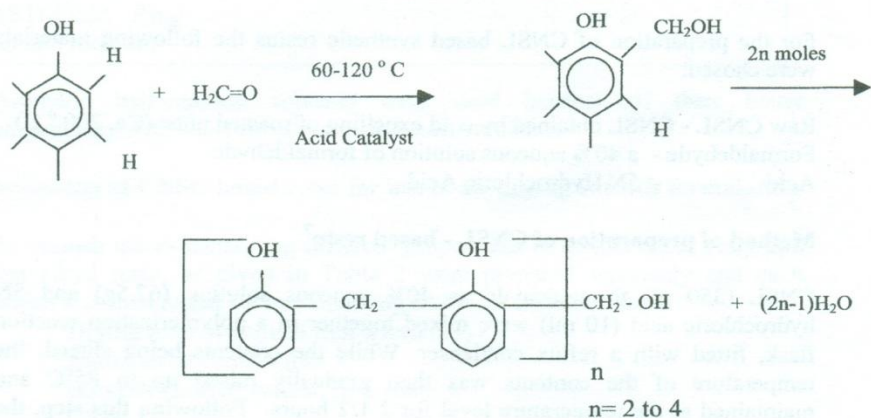
CNSL - based synthetic resin could be considered a better resin component than ordinary phenolic resin in varnish compositions because of its better UV (rays)-Screening effect and fungicidal properties.

Generally the phenolic resins produced from the reaction of phenols and formaldehyde are of two types namely novolac resin and resol resin. Acid conditions with a molar ratio of phenol to formaldehyde of more than 1:1 promote the formation of novolac resin, whereas alkaline conditions in conjunction with a molar ratio below 1:1 favour for the formation of resol resin.

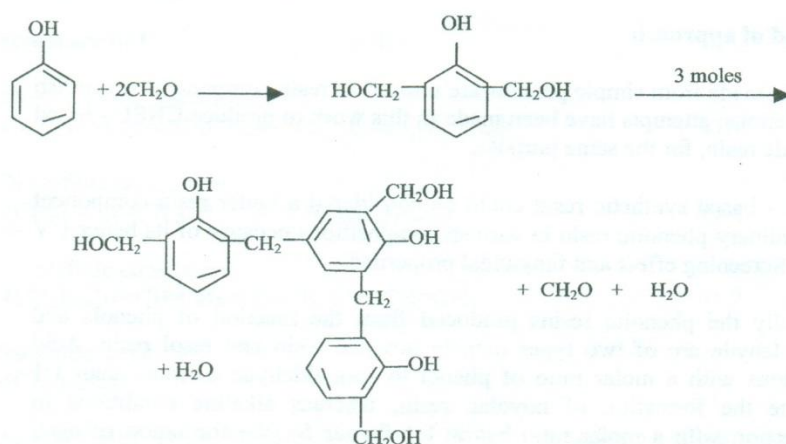
As the novolac resin formed in the reaction is almost inert and has linear molecules due to the absence of active methylol groups, the resin possesses better solubility than the resol resin, which contains branched and cross-linked molecules.

In view of this, preparation of novolac type resin from CNSL is attempted in this work to investigate its use in surface coatings.

Formation of novolac resin



Formation of resol resin



In the method of production CNSL - based resin, CNSL is treated with formaldehyde in the molar ratio 1:0.9 in acid medium. The resinous product formed in the reaction is then investigated for its suitability as a sole film forming resin as well as an extender resin in air - drying varnishes. Further in this work an air - drying varnish based on short oil alkyl resin (60 % solids content) was also prepared in parallel, for comparative studies.

MATERIALS AND METHODS

Preparation of CNSL - based synthetic resin

For the preparation of CNSL based synthetic resins the following materials were chosen:

Raw CNSL - CNSL obtained by cold expelling of roasted nuts (Ca. 200 ° C)

Formaldehyde - a 40% aqueous solution of formaldehyde

Acid - 5N Hydrochloric Acid

Method of preparation of CNSL - based resin⁷

CNSL (350 g), formaldehyde as 40% aqueous solution (67.5g) and 5N hydrochloric acid (10 ml) were mixed together in a polymerization reaction flask, fitted with a reflux condenser. While the contents being stirred, the temperature of the contents was then gradually raised up to 85°C and maintained at the temperature level for 2 1/2 hours. Following this step, the condensed water and the residual liquid contents were removed by distillation under vacuum. The resinous mass remaining in the flask was subsequently washed with water, dried and tested for its physical characteristics.

Characterization of CNSL - based resins

The following characteristics were determined for the CNSL based resin prepared by this method.

Colour
Solubility
Melting Point
Iodine Number

The results of these determinations together with the characterization of raw CNSL are presented in Table 1.

Table 1 - Characteristics of raw CNSL and CNSL - based resin

Characteristics	Raw CNSL	CNSL-based Synthetic resin
Colour (Visual inspection)	Dark Brown	Brownish black
Solubility	Alcohols Aliphatic and Aromatic hydrocarbons	Aromatic hydrocarbons* and alcohols
Iodine Number (Wij's Method)	280	272
Melting point (ASTM E28 - Ring and ball method)	-	95 - 97 °C

*Aromatic hydrocarbon solvents were used because of their better compatibility with short-oil alkyd resin based varnishes

Evaluation of CNSL-based resin for use in air drying varnish formulation

The varnish mixes containing different proportions of CNSL based resin and soya alkyd resin, as given in Table 2 were prepared separately and each varnish was then tested for the following technical characteristics.

Drying time of varnish film (Hard dry)
Hardness of varnish film
Bond strength of varnish film coating
Gloss

The test methods to assess these properties are summarized in Appendix 1⁸.

RESULTS AND DISCUSSION

Characterization of CNSL - based resins

The results of characterization tests carried out on the CNSL based resin prepared in this work (Table 1) indicate that the resin is brownish black with melting point. 95 - 97 °C and it is soluble in conventional aromatic solvents e.g xylene. These properties of resin are most desirable in local surface coating industry, because the resin can be prepared simply at low cost.

The results also show that the CNSL - based resin possesses high iodine value (Ca. 272) exhibiting greater unsaturation character and is not much changed from the iodine value of the raw CNSL (Ca. 280). This suggests that the unsaturated hydrocarbon groups (R) in raw CNSL phenol structures still remain unaltered in the polymer molecules of resinous product, to a great extent.

Table 2 - Varnish mix formulations and their technical properties

Component	Mix formulation					
	A	B	C	D	E	F
Film former short oil alkyd resin (60% solids content)	0	10	20	30	40	50
Resins: CNSL - based resin	50	40	30	20	10	0
Solvents: Xylene	46	46	46	46	46	46
Isopropyl alcohol	2.8	2.8	2.8	2.8	2.8	2.8
Dryers: 36% Cobolt Naphthenate	0.75	0.75	0.75	0.75	0.75	0.75
Anti skinning agent: Methyl ethyl Ketoxime	0.2	0.2	0.2	0.2	0.2	0.2
Technical properties						
Film drying time (hrs) (Hard dry)	4	4.5	5	5	5.5	6
Hardness (Pencil hardness)	4H	2H	H	H	H	HB
Gloss (%)	90	92	92	94	94	96
Bond strength (%Rating)	94	94	94	98	94	92

The same results (Table 2) also indicate that the bond strength values of varnish made with the blends of CNSL - based resin coatings and short oil

alkyd resin (60% solids content) are greater than the bond strength value obtained for varnish coating formed solely with short oil alkyd resin (60% solids content). The results are expected because CNSL-based polymer resin is physically hard and solid in nature when compared to the flexible type short oil alkyd resin (60% solids content). Consequently, the CNSL-based resin molecules could act as solid aggregates in the flexible alkyd resin molecular mass in the films of the blend of resins. Thus it is possible for these aggregates to reinforce and enhance the resistive force of the film coating (bond strength) when the coating is subjected to the force of separation from its substrate (metal plate), as in the method of bond strength test.

CONCLUSION

The results of our studies indicate that:

- i) the CNSL – based novolac type resin is most suitable to be used as an extender resin, rather than a sole resin in air - drying varnish formulations.

And

- ii) when the CNSL - based novolac type resin is added as an extender to short oil alkyd resin (60% solids content) varnish mix, in the range of weight from 20% to 80% by weight of the total resin content, it improves all the important properties (drying, strength and hardness) except the gloss of the varnish coating.

APPENDIX 1

- i. Assessment of film drying time (B. S. 3900 part C3)
A vertical steel plunger is tipped with rubber at the lower end. This rubber tip is capped with white drill, which is renewed for each test. The plunger assembly is loaded to a total weight of 4lbs. By an automatic device, the plunger is lowered gently on to the paint coating surface, rotated through 270 ° and then raised. A film is hard dry if the substrate is not exposed.
- ii. Assessment of Hardness (Pencil hardness test BS 3900 E2)
Pencil of decreasing hardness (6H, 5H, 4H, 3H, 2H, H, F, HB, B, 2B, 3B, 4B) are drawn across the surface until one is found which leaves a black line.
- iii. Assessment of bond strength (cross hatch test BS 3900 E3)
Using a sharp knife, a number of parallel cuts are made through the film to the substrate at 1mm intervals. These are crossed by a second series of making a number of 1mm-sided squares, and it is convenient to make 100 squares. If the adhesion is poor, some of these squares will fall out and the number can be expressed as a percentage. More often however, the severity of the test needs to be increased by

pressing a strip of adhesive tape across the squares followed by a quick pull off.

- iv. Measurement of gloss (BS 3900, part D5)
A film of uniform thickness is cast on a plane glass surface by means of 2mil steel shims and a doctor blade. The film is allowed to harden for 24 hours. The gloss determination is carried out using a gloss head connected to galvanometer.

ACKNOWLEDGEMENT

The authors wish to thank Mr. N. P. Hemachandra the laboratory technician, Polymer Division of the Department of Chemical Engineering, University of Moratuwa for technical assistance in this work.

REFERENCE

1. Tyman, J.H.P and Morris, H J.T. Chromatogr, 1967,27,287
2. Tyman, J.H.P and Jacob, N.J.Chromatogr, 1971,54,83
3. Prasad, T.R.N and Rangaraju, T.S. Resind, 1968, 13 pp 3,4
4. Rajapakse, R.A Gunasena, W.A.S, and Wijekoon, K.B Polymer, 1978,19, pp 205 - 210
5. Technical report on evaluation of resins synthesised from CNSL, CISIR, Sri Lanka 24th Feb., 1980.
6. Turner, G.P.A. Introduction to paint chemistry, 3rd edition, Chapman and hall Ltd, New york 1988, p 163
7. Stoye, D, Freitag, Resins for coating, Hanser/Gardner gardns Publications, Inc., Ohio, USA, 1996
8. Morgans, W.M., Outlines of paint technology, Volume 2, Charles Griffin & Co. Ltd., England, pp 174 - 190

Preparation and properties of starch xanthide encased powdered natural rubber

A. D. U. S. Amarasinghe, K. Subramaniam and S. Maduwage
Department of Chemical Engineering, University of Moratuwa

Preparation and properties of starch xanthide encased powdered natural rubber

A. D. U. S. Amarasinghe, K. Subramaniam and S. Maduwage
Department of Chemical Engineering, University of Moratuwa

ABSTRACT

Starch xanthide encased powdered natural rubber was produced by oxidatively co-precipitating the mixture of starch xanthate solution and natural rubber field latex under vigorous stirring. The resulting finely divided wet powdered rubber particles were separated by filtration and then converted to free-flowing powders by oven drying. The level of encapsulation as well as the properties of the resulting powder was highly dependent on the strength and the amount of the Starch Xanthate (SX) solution. The lower and the upper limits of Degree of Substitution (DS) of SX examined were 0.07 and 0.35 and the results suggested that the intermediate DS levels were more effective. The physical properties of the final vulcanizates were examined and found to be comparable with the rubbers available in the market.

INTRODUCTION

Rubber is the class of material, which has an ability to sustain large reversible extensions without rupture. Conversion of raw rubber to a useful product includes several processing stages such as compounding, shaping and vulcanizing. One way to bring about a fundamental change to the rubber industry is to alter the methods of compound mixing since all rubber compounds must pass through a mixing stage. The changes that could take place in mixing methods are directly dependent on the form in which raw rubber is available. The possible forms of rubber available in the market are bale, latex, liquid, crumb and powder. Bale form needs heavy machinery and hence high power consumption in processing and also it needs to be used in batch processing. If the raw rubber is available in free-flowing forms such as liquid, crumb and powder, it is possible to use automatic processing equipment and also to streamline the process of manufacture of rubber goods. However liquid and crumb rubbers have their inherent disadvantages in use as a raw rubber, compared to the powdered rubber. The most important feature of powdered rubber is that it can be mixed in existing equipment that are used to process bale rubber, with slight or no modifications.

Powdered rubber is the form of rubber having average particle sizes up to about 10 μ m. When the particle sizes are below 1 μ m, such powders are referred to as true powders. The use of powdered rubber has many advantages over the use of bale and other forms.¹ Some of them are high product quality, low processing costs at the secondary stage, low pollution mixing, less plant maintenance and faster dissolution cycles in adhesive and dough factories. The major disadvantages of powdered rubber are risk of agglomeration, non-development of the reinforcing potential of particulate fillers and the increase of the transportation and storage costs due to lower bulk density. It was also found difficult to add oils and plasticisers in liquid form into dry powder blends inside low shear blenders.

BACKGROUND

Rubber as a powder has been studied and reported in literature since the early 30's.¹ Although some had predicted that the powdered rubber usage would be of 10-15% of tyre rubber usage and 20-25% of non-tyre usage by 1980, that event has not yet occurred due to the lack of effort taken by raw material producers, equipment suppliers and rubber processors to meet each others' requirements.²

Uses of Powdered Rubber

The rubbers that generally available in powder form are natural rubber and synthetic rubbers such as acrylonitrile-butadiene rubber, styrene-butadiene rubber, polychloroprene rubber, ethylene-propylene-diene monomer and polyurethane. Powdered rubbers have been used in continuous feeding for extruders and injection moulding machines and also in batch processing to produce compression moulded articles either by using powder technology or by conventional vulcanized moulding^{3,4} and in preparing adhesives and making pastes for coating fabrics without using calendering process.¹ When available in powder form, rubber could be used as a direct additive in modifying bitumen, thermoplastic and thermosetting resins in order to improve their rubbery properties.^{5,6}

Manufacturing Methods

Several routes to manufacture powdered rubber have been reported in the literature.^{1,6,7,8,9} They were cryogenic grinding of bale rubber, latex spray drying, latex freeze drying and latex co-precipitation/encapsulation processes. The cryogenic grinding process consumed high energy, due to the raw material being used in solid form.¹ It also required a fairly high percentage of partitioning agents and produced uneven and coarse powders.⁸ Spray drying and latex freeze drying processes, too, consumed high energy for atomization of latex. Since they produced very fine particles, a high percentage of partitioning agents were required and also expensive equipment were needed.^{6,7} The equipment cost of both spray drying and freeze drying processes were relatively high. When compared with other processes, the encapsulation process is a simple process that does not require any specialized pieces of equipment for preparing powdered rubbers. By varying the process conditions in encapsulation process such as speed of stirring, process temperature, amount and rate of addition of protective agent the required particle can be produced in powder preparation.¹⁰

Role of Partitioning agents

Most grades of powdered rubbers will flow and fuse during transportation and storage. The re-agglomeration also takes place during filtration and drying operations of the powdered rubber forming process. Hence, all forms of powdered rubber, however prepared, contains 10-45% of partitioning agent and the amount of the partitioning agent is dependent on the physical properties required of the ultimate vulcanizate.¹⁰ The chemically attached

partitioning agents like encapsulating agents are more effective in retaining the free-flowing characteristics of the rubber than physically added partitioning agents.⁷ Some of such encapsulating agents are polymers containing carboxyl groups along the chain, sodium alginate,¹¹ regenerated cellulose¹² and starch/flour derivatives.¹³

Starch derivatives, zinc starch xanthate and starch xanthide, as encapsulation for synthetic rubber latices have been studied since the late '60 s. Although the type of starch did not show influence on the properties of the powdered rubber, the starch xanthide encasement showed better properties than that with zinc starch xanthate.^{3,10,13} The two important factors that govern the production of variable particle sizes are the Degree of substitution (DS) and the amount/loading of starch xanthate (SX).¹⁰

OBJECTIVES

Sri Lanka is a developing agricultural country, and hence the production of powdered natural rubber using the co-precipitation process is more viable. This is due to the simplicity and the low capital investment of the process and the availability of major raw materials, such as field latex and starch at low prices. The objective of the present work was to investigate the ability in producing a free-flowing powdered rubber with standard or improved properties, using natural rubber field latex, by encapsulation method, at a low cost.

MATERIALS AND METHODS

Materials

Major raw material used to prepare powdered natural rubber was ammonia preserved field latex (see Table 1). Field latex was first deammoniated, so that the alkalinity was dropped to 0.2 and it was then diluted with distilled water until the TSC was reduced to 10%.

Total solids content, TSC, weight percentage	– 43.5%
Dry rubber content, DRC, weight percentage	– 37.9%
Alkalinity, weight percentage of ammonia in latex	– 0.78%
Volatile fatty acid number	– 0.06

Table 1- Specifications* of field latex

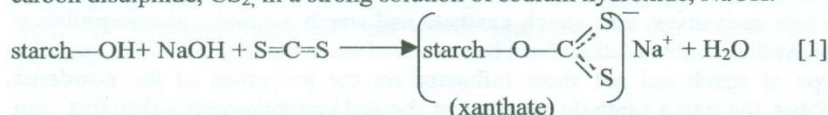
*According to Sri Lanka Standard Methods of testing Natural Rubber Latexes SLS 325:1974

Starch xanthate was used as the encapsulating agent. Unmodified tapioca starch, Carbon disulphide and Sodium hydroxide, were used in xanthation. Sodium nitrite (oxidizing agent) and Sulfuric acid (destabilizing agent) were used in co-precipitation. Zinc stearate was used as an anti-cake agent. Vulcanizing system consisted of sulphur as a vulcanizing agent, zinc oxide as an inorganic activator, stearic acid as an organic activator and MBTS as an accelerator. PBN was the antioxidant used in compounding. Except carbon disulphide, the other raw materials used were industrial grade chemicals.

Chemical Reactions

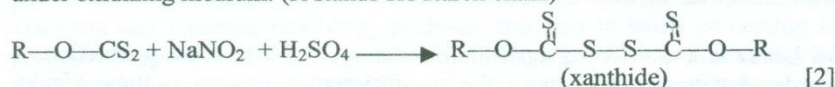
Xanthation

Sodium starch xanthate is formed when the starch hydroxyl group reacts with carbon disulphide, CS_2 , in a strong solution of sodium hydroxide, NaOH .



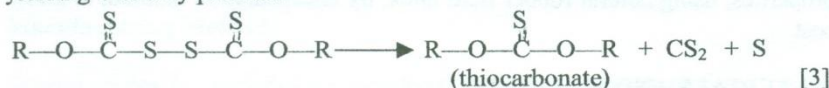
Conversion of xanthate to xanthide

Starch xanthide is formed from starch xanthate by acidification of the mixture under oxidizing medium. (R stands for starch chain)



Decomposition of xanthide

Starch xanthide is decomposed (about 70%) at 150°C within 10 minutes by yielding S as a by product.¹³



Methods

Xanthation

Initially, unmodified Tapioca starch (in dry form) was dispersed in distilled water to prepare 10wt.% concentrated sample and it was converted into gelatinous mass by adding the required amount of 40wt.% NaOH solution. Carbon disulphide was then added under vigorous stirring (at 333 rpm) at about 1 to 2 hours in a closed vessel. The amount of CS_2 is determined by the final degree of xanthation required (Xanthate degree of substitution, DS, is the average number of substituents CS_2 per D-glucose unit). Starch xanthate solution was kept inside a refrigerator at 5°C for the minimum period of 24 hours. Starch xanthates having DS values of 0.07, 0.28 and 0.35 were prepared according to the published procedure.^{3,10,14} The amount of reagents needed to prepare SX solutions are listed in Table 2.

Co-precipitation

The required amount of starch xanthate solution was added to NR latex of 10% TSC and was stirred at 333 rpm until the apparently homogeneous, viscous milky xanthate-latex mixture was obtained. The mixture was co-precipitated by adding 1.25 moles of sodium nitrite per 1 mole of xanthate group followed by slow addition of 1M sulfuric acid solution which

destabilized the latex and formed HNO_2 which in turn oxidatively cross-linked starch xanthate to starch xanthide. The mixture was then stirred at the same speed to facilitate the formation of small uniform curds and sulfuric acid was then added until the complete separation of wet curds were formed from the serum. Table 3 shows a list of samples having various DS and loading of starch xanthate used in the current work.

DS	0.07	0.28	0.35
10% starch solution, grams	162.0	71.2	178.0
40% NaOH solution, grams	20.0	16.0	49.0
CS_2 , ml	9.0	8.4	45.0

Table 2- Formulation for SX having different DS values

DS of SX	SX loading, in phr						
	15	20	30	40	60	80	100
0.07				D07/40	D07/60	D07/80	D07/100
0.28				D28/40	D28/60	D28/80	D28/100
0.35	D35/15	D35/20	D35/30	D35/40	D35/60		

Table 3-Samples of powdered rubber prepared with different DS and loading of SX

Separation and drying

Finely divided yellowish-white colour wet curds were separated by filtration through a normal funnel fitted with a piece of cheese cloth without applying any pressure. Filtered curds were washed with water to remove non-rubber substances, oxidizing agents, etc. Zinc stearate (4 phr), as an anti-cake agent was added to wet rubber curds using the same stirrer but attached with a ribbon type shaft under slow speed stirring at 33 rpm. The resulting curds were then dried in a hot air oven at 70°C .

Phase inversion

The literature review suggested that a phase inversion was taken place when oven dried hard friable crumbs were subjected to differential roll milling or grinding. In the present work, wet rubber curds were oven dried. During milling, SX encased rubber crumbs were broken into small, irregularly shaped pieces and then the rubber phase was coalesced to form a continuous phase. The process flow diagram for preparation of powdered natural rubber is given in Figure 1.

Properties of powdered natural rubber

Particle size analysis

Powdered natural rubber samples were ground for 5 minutes at 1500 rpm in a Jaipan economy model domestic grinder. They were then run through a series of U.S. standard testing sieves for 10 minutes on an Endecott test sieve shaker. Sieve aperture was varied from 500 to 5000 microns.

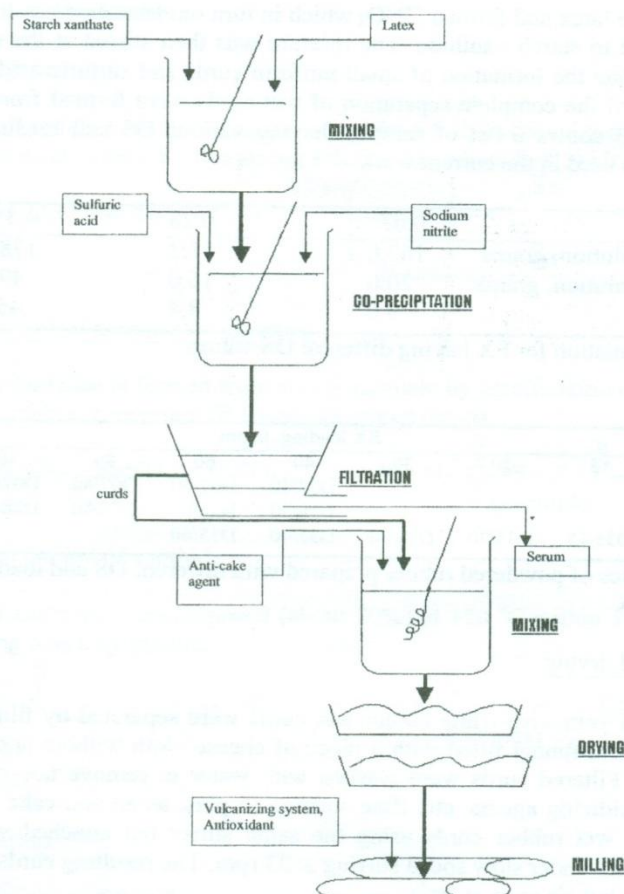


Figure 1-Process Flow Diagram for Manufacture of Powdered Natural Rubber

Cure characteristics

Powdered rubber samples that could be used for further processing, only, were selected to examine the properties and compared them with the control sample, which was a pure gum vulcanizate of RSS rubber. Test compounds were prepared according to the formulation given in Table 4, by milling on a water-cooled two-roll mill at about 10 passes. Cure characteristics of pure gum vulcanizates were studied in a Monsanto oscillating disc rheometer according to ASTM D275-68T method. Vulcanization was carried out for 20 to 30 minutes at 150 °C.

Physical properties

Standard size test specimens of different samples (for all tests carried out) were prepared with conventional compression moulding at the optimum cure times. The vulcanizing carried out at the temperature of 150°C and the

pressure of about 25 MN/m². Physical properties of the vulcanized samples were measured according to the standard test procedures given in Table 5.

Compounding ingredients	Amount, phr
Natural rubber*	100.0
Sulphar	2.5
Zinc Oxide	5.0
Stearic acid	1.0
Mercaptobenzothiazole, MBTS (accelerator)	1.0
Phenyl-beta-naphthylamine, PBN (antioxidant)	1.0

*Natural rubber in powder form except in control sample

Table 4-Dry formulation for rubber compounding

Property	Procedure	Equipment
Tensile properties	ASTM D412-83 method A (sections 9 - 13)	Pendulum type tensile strength tester
Hardness	ASTM D2240-86	Shore A Pencil Durometer
Reb. Resilience	ASTM - D2632-79	Bashore Rubber Resiliometer
Abrasion R.	DIN 53516-77	DIN Abrader
Compression Set	ASTM D395-85 Method B (sections 11-14)	Compression set apparatus
Flex cracking	ASTM D430-73	De-Mattia Flexing Machine
Crack growth	ASTM D813-59	

Table 5-Test Procedures to measure Physical Properties

RESULTS AND DISCUSSION

The effect of major factors on powder formation

A good powder was analyzed by examining both the appearance of wet curds and the serum and the free-flowing characteristics of dried crumbs. The results for different DS values and loading of SX on the powder formation are given in Table 6. The Table shows that the yellow colour of the serum decreases and the clarity of the serum increases, with the increase of DS and the loading of SX.

Since all samples having DS of 0.07 showed the difficulty in filtration through cheese cloth as they coagulated and made paste like wet cake, they are not suitable in mass production. SX having DS of 0.28 could be used to produce free-flowing powders with starch loading on or above 60 phr. If the starch loading was on or above 30 phr, SX having DS of 0.35 could be used to give free-flowing powdered natural rubbers. Although the samples of 40 phr with DS of 0.28 and 15 and 20 phr with DS of 0.35 could not be ground to give powders, they could be further processed, by milling. The level of co-precipitation is a direct function of the xanthate concentration in the sample solution and there may be a minimum concentration of SX for the co-precipitation to be completed. If the SX concentration is lower than this minimum level, the SX in the solution may be kept as unreacted.

The comparison of the yield values of different samples suggest that the yield is a direct function of the expensive raw material, carbon disulphide which is essential to increase either the DS or the loading of SX. Consequently the unit cost of production of powdered rubber increases with the increase of yield. Hence, these conflicting effects lead to an optimum combination of DS and loading of SX to produce a low cost free-flowing powder. Out of the combinations used in the research work, DS of 0.28 with starch loading of on or above 60 phr was more economical compared to the other samples.

Sample number.	1M H ₂ SO ₄ needed, ml	Appearance of wet curds	Appearance of serum	Observations on filtration	Appear. of dried crumbs	Observ. on grinding	Yield, grams	Cost, Rs./kg.
D07/40	120	V. fine/soft	Yellowish milky	a, e	H. elastic/h. tacky	h	78	144
D07/60	150	V. fine/soft	Yellowish milky	a, e	H. elastic/h. tacky	h	96	153
D07/80	230	Fine/hard	Light yellowish milky	b, e	Elastic/l. tacky	h	103	181
D07/100	270	Fine/hard	Off-white milky	c, e	Elastic/l. tacky	h	111	201
D28/40	135	Fine/soft	Yellowish slightly clear	b, f	Elastic/tacky	h	90	160
D28/60	145	Fine/hard	L. yellowish slightly clear	c, g	Non tacky/free-flow	i	103	174
D28/80	190	Fine/hard	Off-white slightly clear	d, g	Non tacky/free-flow	i	116	184
D28/100	235	Fine/hard	Off-white slightly clear	d, g	Non tacky/free-flow	i	125	200
D35/15	75	Fine/hard	Yellowish milky	a, c	H. elastic/ tacky	i	61	211
D35/20	85	V. fine/soft	L. yellowish slightly clear	c, f	Elastic/tacky	h	79	198
D35/30	106	Fine/hard	Off-white clear	d, g	Non tacky/free-flow	h	87	212
D35/40	160	Fine/hard	Off-white highly clear	d, g	Non tacky/free-flow	i	94	244
D35/60	225	Fine/hard	Off-white highly clear	d, g	Non tacky/free-flow	i	108	309

a- Very difficult to filter, b- Difficult to filter, c- possible to filter, d- easy to filter, e- agglomeration & makes a paste, f- some agglomeration on filtration, g- no agglomeration on filtration, h- could not be ground, i- could be ground

Table 6-Results on the powder formation for different samples

Properties of powdered natural rubber

Particle size distribution

Under-size cumulative weight percentage versus sieve aperture is illustrated in Figure 2. The results of the particle size analysis suggest that the particle size distribution of the natural rubber obtained from the co-precipitation method is highly dependent on the DS and the loading of SX. The increase of DS of SX increases the friability and the increase of loading of SX increases both friability and starch content in the sample, which also behaves as a partitioning agent.

Rheometric properties

Calculated rheometric properties are given in Table 7. The rheometric properties suggest that the optimum cure time with 20, 30 and 40 phr SX loading is less than the control sample and that may be due to the accelerator activity of xanthate. However, with higher SX loadings, the results were comparable with the control sample indicating the filler effect of starch. Results of the cure rate index, too, confirmed that the faster curing occurred at low SX loading. However, scorch time was independent from the effect of change of DS and loading of SX since none of the substances participate in the initialization of cross-link formation.

Physical Properties

The tensile test results given in Table 8 shows that the tensile strength is not a function of SX loading above 40 phr. However at low SX loadings (D 35/20 and D 35/30), the tensile strength values are between that for control sample and rest of the samples. This observation suggests that when starch is present excessively it acts as a filler and consequently the re-bonding during stretching is inhibited. The high difference of $E_b\%$ of test samples compared to control sample is due to the loss of elasticity as a result of the addition of SX into the oriented cross linked structure of natural rubber. This result is further confirmed by the observation of the decrease in $E_b\%$ with the increase in both DS and SX loading. Modulus which is a measure of the stiffness of the rubber compound increases with both DS and the SX loading as a result of loss of elasticity.

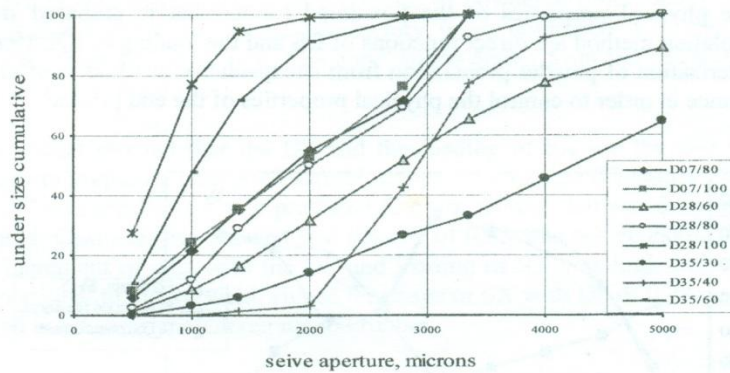


Figure 2-Particle size distribution

Sample.	Control	D28/40	D28/60	D28/80	D28/100	D35/20	D35/30	D35/40	D35/60
Scorch time*	2.4	2.8	2.5	4.8	2.5	2.5	3.25	2.5	2.5
Opt. cure time**	10	8.5	10.2	8.8	10.2	6	8.5	9.5	11.2
Cure rate index***	0.48	0.42	0.50	0.31	0.30	0.57	0.57	0.51	0.46

* Scorch time(in minutes): time taken to increase 3 units from the minimum torque

**Optimum cure time(in minutes): time required for the torque to increase to 90% of its total increment

***Cure rate index(in Nm/min): the average slope of the cure rate curve

Table 7-Rheometric properties of gum vulcanizates

Sample	Control	D28/40	D28/60	D28/80	D28/100	D35/20	D35/30	D35/40	D35/60
T/S	28.91	5.98	7.76	7.64	8.26	21.45	15.59	6.65	7.26
300% Modulus	0.88	-	-	-	-	5.5	7.9	-	-
100% Modulus	-	3.6	5.17	5.73	-	-	-	4.75	6.5
$E_b\%$	1100	180	170	130	60	550	400	160	150

Table 8-Tensile properties of powdered natural rubber samples prepared with different DS and loading of SX (All units in MPa)

The results of the other physical properties, hardness, rebound resilience, compression set and abrasion resistance are given in Figure 3 (i), (ii) and the results of flex cracking and crack growth are given in Table 9. In general the difference between the results of control sample and the other test samples are significant. Hardness increases with the increase of both DS and loading of SX while rebound resilience, and abrasion resistance decreases. These variations may be due to the disturbance of highly elastic character of natural rubber with the presence of starch as a filler and also with the formation of more cross-links by SX. Compression set gradually increases with the increase of SX loading only for low SX loading. As the SX loading reaches a limiting value compression set seems to reach to a plateau indicating that the variation of compression set by changing the SX loading is limited. Both crack initiation and crack growth occur more quickly with the increase of SX loading due to the loss of elasticity by incorporation of SX into rubber. These results suggest that the physical properties of the powdered rubber that is prepared from encapsulation method are direct functions of DS and the loading of SX. Hence characterization of powder preparation from encapsulation method is of great importance in order to control the physical properties of the end product.

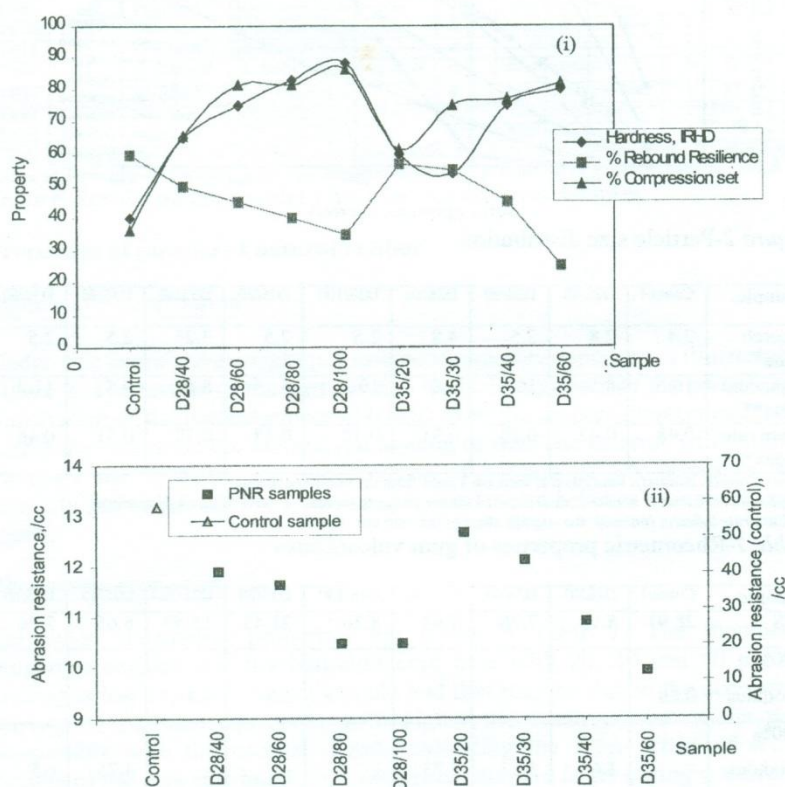


Figure 3-Results of powdered natural rubber samples prepared with different DS and loading of SX (i) Hardness, Rebound resilience and Compression set (ii) Abrasion resistance

Sample	Control	D28/40	D28/60	D28/80	D28/100	D35/20	D35/30	D35/40	D35/60
Crack initiation, cycles	33540	700	10	-	-	14223	11000	-	-
Rate of crack growth, mm/cycles	0.001	0.03	0.8	-	-	0.003	0.008	-	-

Table 9-Flex cracking and crack-growth of powdered natural rubber samples prepared with different DS and loading of SX

CONCLUSIONS

Powdered natural rubber was successfully prepared by co-precipitation technique, using starch xanthate, SX, as the encapsulating agent. The effects of degree of substitution and the loading of SX on the powder formation were examined. SX was co-precipitated with natural rubber latex and was permitted to give powdered products. The properties of powdered rubber samples were investigated and found to be satisfactory when compared with the ribbed smoked sheet (RSS) sample. The conclusions drawn from the research work are summarized below.

The results showed that the DS and the loading of SX are the two critical factors in preparing powdered natural rubber. Of the three DS values used, DS of 0.07 was insufficient as it produced fine wet powder that was difficult to be filtered. Cost analysis showed that the DS of 0.35 was not economical since the increment of cost with the DS and loading of SX was high and was not proportional to that of yield. Hence the usage of SX with DS of 0.28 was more suited in preparing powdered natural rubber.

Natural rubber powders with different particle sizes could be produced by the co-precipitation method, according to the specified application, by changing the DS and loading of SX. The ease of grinding and the particle size distribution were improved with the increase of SX loading and with the high DS values due to the decrease of rubber to starch weight ratio. Starch facilitated grinding by behaving as a partitioning agent.

Powdered natural rubber could be formulated by short period milling cycles, avoiding high-shear mastication procedures required for bale rubbers. There was a progressive difficulty in milling with the increase of SX loading due to high stiffness. Optimum cure time was reduced with low SX loading due to the accelerator activity of xanthates. However, increase in SX loading increased optimum cure time, thus ruling out the possibility of controlling cure by extra xanthates, providing an optimum level of SX for this phenomenon. The optimum level of SX of the research work was 20 phr with DS of 0.35, within which the values of DS of 0.28 and 0.35 and the loading of SX range 20-100 phr. Scorch time was independent on effect of change of either DS or loading of SX. Cure rate index, which was directly proportional to the rate of cure was reduced with the increase of SX loading by confirming the observations obtained on cure time.

The physical properties of powdered natural rubber gum vulcanizates prepared with low SX loading were comparable with the properties of RSS sample. The results showed that the tensile strength decreased with the increase of both DS

and loading of SX. Best tensile properties occurred at 20 phr of SX having DS of 0.35. Thus a low SX loading has the advantages of giving maximum reinforcing value from the starch and allowing more freedom for addition of conventional fillers and reinforcing agents. Stiffness, hence modulus and hardness increased and elongation at break and rebound resilience decreased with the increase of both DS and loading of SX due to the loss of inherent rubbery properties of natural rubber by incorporation of SX. Abrasion resistance dropped and compression set raised drastically with the addition of SX and both were independent on the DS and the content of SX. These observations suggest that the required properties could be achieved by varying the combinations of DS and loading of SX.

ACKNOWLEDGEMENTS

Our thanks are due to the Head and all other staff members of Department of Chemical Engineering, University of Moratuwa, to the officers of both Rubber Research Institute, Ratmalana and Industrial Development board, Peliyagoda.

REFERENCES

- 1 Evans, C.W. Powdered & particulate rubber technology Applied Science publishers Ltd., London, 1978
- 2 Capelle, G. and Hunziker, P. Powdered rubber technology an equipment concept Rubber world 1992:July.94
- 3 Buchanann, R.A., Katz, H.C., Russell, C.A. and Rist C.E. Powdered elastomers from starch-encased latex particles Rubber Journal 1971:October.55
- 4 Reed, D. and Rudy, S. Powdered rubber progresses European Rubber Journal 1984:May.21
- 5 Burford, R. P. and Pittolo, M. Characterization and performance of powdered rubber Rubber Chemistry and Technology 1982:55.5.1233
- 6 Widmer, H. and Milner, P. W. Powdered Rubber Rubber Age 1974:106.11.41
- 7 Lau Chee Mun Spay Drying of Natural Rubber Latices Journal of RRIM 1977:25.3rd part.119
- 8 Blackley, D.C. Synthetic rubbers -Their Chemistry & Technology Applied Science publishers Ltd., London, 1983:345-347
- 9 Bleyie, P.L. Influence of morphology and particle size of powdered rubber on mill processing Rubber Chemistry and Technology 1975:48.254
- 10 Abbott, T.P., James C., Doane, W.M. and Russell, C.R. Elastomer encased in a little starch could put starch in powdered rubber mart Rubber World 1974: March.40
- 11 Coomaraswamy, A., De Silva, K.G.K., and Wijesinghe, U.P. Preparation of free-flowing granular natural rubber Journal of RRISL 1981: 58.58
- 12 Mano, E.B. and Nunes, R.C.R. Regenerated cellulose elastomer compounds European polymer journal 1983: 19.10/11.919
- 13 Karunaratne, S.W. and Tharmalingam, R. Powdered natural rubber Journal of RRIM 1977: 54.2nd part.605
- 14 Lanchaster, E.B., Black, L.T., Conway, H.F. and Griffin E.L. Alkali starch xanthate solution Industrial starches by Ronald W. James, Noyes Data Corporation, London, 1974:p221

DEVELOPMENT AND EVALUATION OF THE AESTHETICS OF STRUCTURAL FORM

C. Kulasuriya, W.P.S. Dias and M.T.P. Hettiarachchi.
Department of Civil Engineering, University of Moratuwa.

DEVELOPMENT AND EVALUATION OF THE AESTHETICS OF STRUCTURAL FORM

C. Kulasuriya, W.P.S. Dias and M.T.P. Hettiarachchi.
Department of Civil Engineering, University of Moratuwa.

ABSTRACT

This Paper demonstrates that the aesthetic concepts of engineering design do not just arise; but that they are derived from various models of aesthetics. It also presents various Proportioning Systems and their application in Structures, through case studies, notably the use of the Golden Proportion.

The Paper then describes the investigation of the aesthetic perception of two sets of respondents and also the optimisation of a simple structure. The preference for equality and for the Golden Ratio is discovered from the experiments on aesthetic perception. The study also deals with the optimisation of simple structure.

Finally, it also describes the possibility of making initial design decisions relating to dimensions, using the plots of optimisation and plots of aesthetic preferences.

1. INTRODUCTION

The main purpose of designing a structure is to satisfy certain functional needs. However, designing a structure involves many considerations, in addition to the functional requirements. They are, topography, site forces, character of the place, technical requirements, etc. Therefore aesthetics of a structure is an outcome of the synthesis of all these considerations with the creativity of the designer.

Whatever the structure is, it can only be realised if the total cost of the structure falls within the allocated budget. The cost of a structure depends on many factors. Among them 'scale and proportion' is one of the most influential factors, which is also linked with aesthetics as well. Therefore, it would be useful to study the variation of cost with respect to scale and proportion of a particular structure.

If the designer has the above information, then, he would be able to design structures with the required aesthetic qualities within the allocated budget. This study attempts to find the above information.

'Engineering' and 'Aesthetics' are not pure, definite or isolated disciplines. They have links with many other disciplines as well. Therefore, a study related to 'Engineering and Aesthetics' can not be done in isolation. Hence, this study is also integrated with Art, Architecture, Philosophy and Sociology.

However the scope is limited to the following objectives.

2. OBJECTIVES

The main objectives of this study are:

1. To study basic aesthetic concepts and proportioning systems used in design.
2. To examine the application of proportioning systems in structures.
3. To investigate the perception of proportions and of the perception of aesthetics of simple structures.
4. To optimise a simple structure, using simple measures.
5. To identify ranges of dimensions that a designer should work with, in order to be within the allocated budget.

3. METHODOLOGY

In order to achieve the above objectives, the following methodologies were adopted.

1. A literature review was carried out to determine the basic aesthetic concepts and proportioning systems used in design.
2. Case studies were used to examine the application of proportioning systems in structures.
3. Social surveys were carried out to investigate the perception of proportions and perception of the aesthetics of a three span bridge.
4. A simplified approach was used to find the optimisation curve for a given structure.
5. The optimisation curve was used to identify the ranges of dimensions that a designer should work with, in order to be within the allocated budget.

4. AESTHETICS IN DESIGN

The word 'aesthetics' had been derived from the Greek word '*aisthesis*', meaning sensory perception. It was regarded as a branch of philosophy concerned with the understanding of beauty and its manifestation in art and nature.¹ However it is extremely difficult to give a precise definition for aesthetics.

Aesthetic consciousness covers special sentiments, tastes, interests, concepts, ideals, views and theories². Therefore, for any aesthetically conscious designer, it is useful to study the theories of aesthetics.

However, adherence to any such theory may reduce creativity. Hence, what is important is not the blind application of any such theory, but the intelligent and intuitive understanding of aesthetic concepts and their application in design creatively.

4.1 Models of Aesthetics

Aesthetic concepts do not just arise. They are derived from various models of aesthetics. Therefore for any designer, it is important to be aware of the various models of aesthetics, which have been developed through the centuries.

In the course of its development, aesthetics has evolved five major theoretical models.³

Model 1 (Objective Idealism):

The aesthetic appears when God or the Ideal spiritualizes the world.

Model 2 (Subjective Idealism):

The aesthetic appears when the individual's inner wealth is superimposed on life, which is aesthetically neutral.

Model 3 (Dualism):

The aesthetic is produced by a union of the objective and the subjective.

Model 4 (Metaphysical Naturalism):

Regards aesthetic characteristics as the natural properties of objects like, say weight symmetric composition, colour or shape.

Model 5 (Dialectical Materialism):

Treats the aesthetic as an objective property of phenomena and objects which is a result of their relations with the life of society and mankind.

4.2 Aesthetic Concepts in Structural Design

As mentioned above, aesthetic concepts are derived from various aesthetic models. Some basic aesthetic concepts are given below.

1. *"Structures should harmonise with nature"* – this is derived from the model of metaphysical naturalism.
e.g.- Clustered water tanks at Alençon, France,⁴ look like trees in nature. (Figure 1a)
2. *"Structures need not necessarily harmonise with nature, the conflict between the structure and the environment may create new progressive aesthetic values"* – this is derived from the model of dialectical materialism.
e.g.- Eiffel Tower in Paris⁵ contradicted with the environment and the contemporary society, when it was erected. However, later it was able to create new aesthetic values and become the Semiotic Symbol of France. (Figure 1b)
3. *"Structures should subjectively be related with the consumer or the user"* – this is derived from the model of subjective idealism.

e.g.- Water Tower at Fisons Fertilizer Factory, UK,⁶ is subjectively related with the factory workers and expresses the feeling of sharing the work. (Figure 1c)

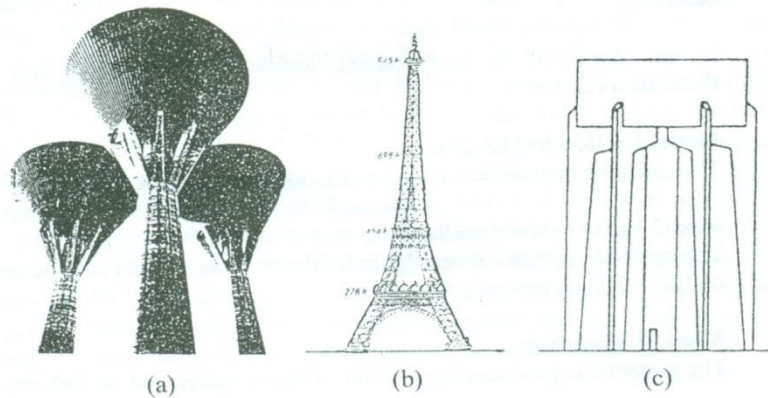


Fig. 1 – Aesthetic Concepts and their application in Structures^{4, 5, 6}

In addition to the above-mentioned historical aesthetic models, new models can be created. Based on these new models, new aesthetic concepts too can be derived.

Aesthetic concepts in design are always linked with the visual aspect. It is not sufficient that the object or structure functions satisfactorily; its appearance must be visually satisfactory. Indeed, appearance may be an essential part of purpose or use.⁴

Appearance of any object is linked with scale, size, volume, proportion, styling, light and shade, optical illusions, etc. Among these, 'Proportion' is one of the major factors that influence the appearance of an object. Therefore this study concentrates on aesthetic beauty and proportions.

4.3 Aesthetic Beauty and Proportions

Proportions play an essential part in aesthetic beauty. Certain arrangements in the proportion of shape and form result in pleasurable sensations. Lack of it leads to a reaction of indifference, discomfort or even revulsion.

The early Greek philosophers tried to define aesthetic beauty through the geometrical laws of proportion.⁷ They believed that beauty is harmony and that harmony is due to the observation of proportions.

Throughout history, artifacts and buildings, which have been universally recognised as good examples of aesthetic beauty, have used proportion as the foundation of their designs.⁸

4.4 Proportioning Systems

A number of proportional theories have been put forward in the search for aesthetic beauty, each gaining favour from time to time.

From the ancients, we have two mathematical systems that can bring a sense of proportion to the world of design.⁹

1. Commensurable (or rational) system of proportion.
2. Incommensurable (or irrational) system of proportion.

4.4.1 Commensurable System of Proportions

Since the Renaissance, and perhaps since Greek and Roman times, history seems to have favoured the commensurable system of proportions and its simple ratios like 1:2, 2:3 and 3:4. In music these numbers are connected to what we hear and understand to be harmony and consonance.⁹ The ratios 1:2, 2:3 and 3:4 in the harmonic series are related with the major scale of western music. The ratio 1:2 of the harmonic series is designated as the 8th or the *octave*. Similarly ratios 2:3 and 3:4 are designated as *fifth* and *fourth* respectively. The somewhat hollow-sounding 4th, 5th and 8th of the major scale are called *Perfect Intervals*. They possess what we may perhaps call a 'purity' distinguishing them from other intervals. When spaces or objects are organised and designed around these simple whole-number ratios, they convey a sense of musical harmony.⁹

4.4.2 Incommensurable System of Proportions

While the Vitruvian Canon reflects a desire for musical harmony that is very much in keeping with the human anatomy, another ancient system of proportions offered a different, perhaps even richer, method of finding harmony between the parts and the whole. This is done not through whole-number ratios that produce the harmonics in music, but through incommensurable ratios, like $1:\sqrt{2}$, $1:\sqrt{3}$, and $1:\phi$ (or the Golden Mean). These are the very same numbers that appear in simple geometric shapes, such as the square, the triangle and the pentagon.⁹ (Figure 2)

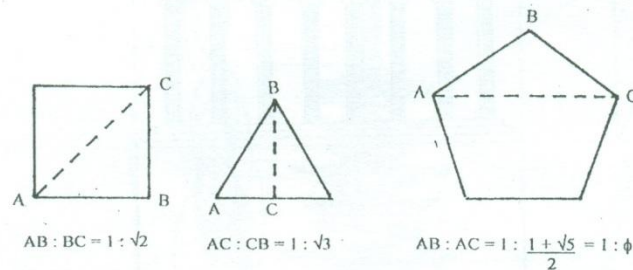


Fig. 2 – Incommensurable ratios of simple geometric shapes

Of all the incommensurable proportions, the most elegant and efficient way to achieve harmony is the Golden Mean. The Golden Mean Proportion appears in nature constantly, from sunflowers, apple blossoms, and daisies in the plant world to spiral shells beneath the seas. The spirals of pinecones exhibit this proportion, as do artichokes, pussy willows, and pine apple husks. Many of the proportions of the human body also conform to the Golden Mean. The Golden Ratio is found when a line is divided into two unequal lengths so that the shorter relates to the longer as the longer relates to the whole. The ratio is identified by the Greek letter ϕ , and it translates numerically to a ratio of $1: (1 + \sqrt{5}) / 2$ or 1: 1.618.⁹

5. APPLICATION OF GOLDEN PROPORTION IN STRUCTURES

Throughout the history and prehistory of architecture, the Golden Mean has consistently brought a sense of harmony to design, not to mention a spiritual and even a physical sense of well-being. A number of examples could be cited, including Stonehenge and the Great Pyramids in Egypt; classical temples of Greece; Gothic Cathedrals; and modern buildings.⁹ Some of these structures are given below.

5.1 Parthenon in Athens, Greece

Even from the time of the early Greeks, a rectangle whose sides are in the "Golden Proportion" has been known. This rectangle is supposed to appear in many of the proportions of that famous ancient Greek temple, the Parthenon, in Athens, Greece, built around 400 BC.¹⁰(Figure 3)

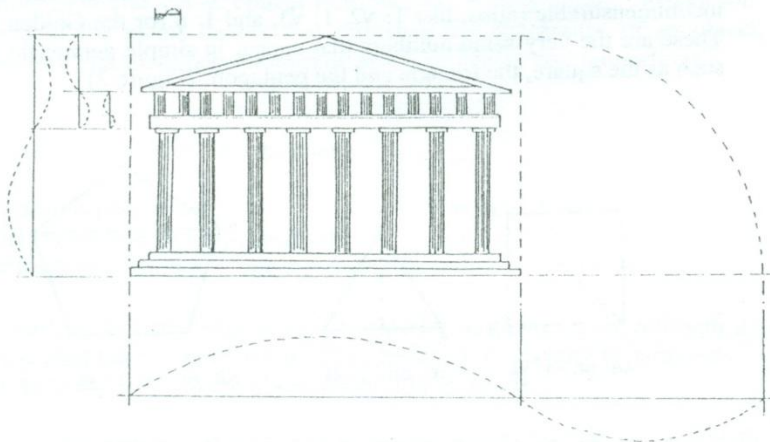


Fig. 3 - Golden Proportions of Parthenon, Greece.

5.2 Cistercian Abbey, Fontenay

The Golden proportion can also be identified in nature and be developed from basic forms and shapes of spatial order, to music and even to a sense of time. Through this development, the Abbeys of St. Bernard and Le Corbusier's La Tourette Monastery achieved not only simplicity and visual beauty but also through the reverberation of sound within the church, they transformed human chanting and singing into supposedly celestial music.⁷ (Figure 4)

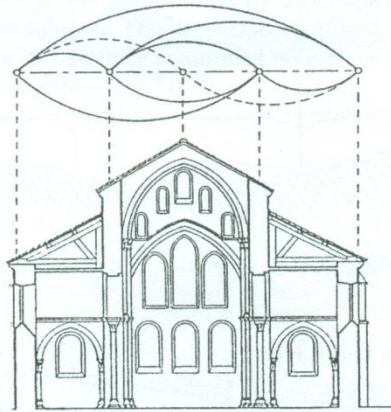


Fig. 4 - Golden Proportions of Cistercian Abbey, Fontenay⁷

5.3 Yakushiji Temple

The use of the golden proportion is not exclusive to Western culture for there is evidence of its use in both the art and architecture of the East. In Japan, for example, the Pagoda of the Yakushiji Temple, which is known for its soaring grace and ingenious structural strength employs the golden section to define the heights and dimensions of its six roofs.⁷ (Figure 5)

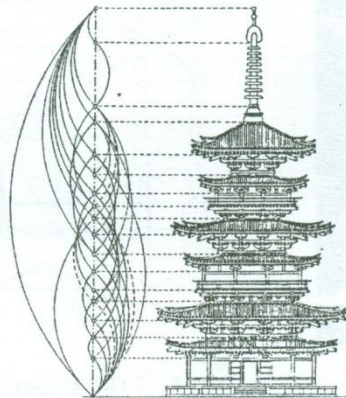


Fig. 5 - Golden Proportions of Yakushiji Temple Pagoda, Japan⁷

5.4 Redheugh bridge in Newcastle

Redheugh Bridge in Newcastle is a Three-span bridge. The Golden Mean has been employed to decide the lengths of the three spans.⁸ (Figure 6)

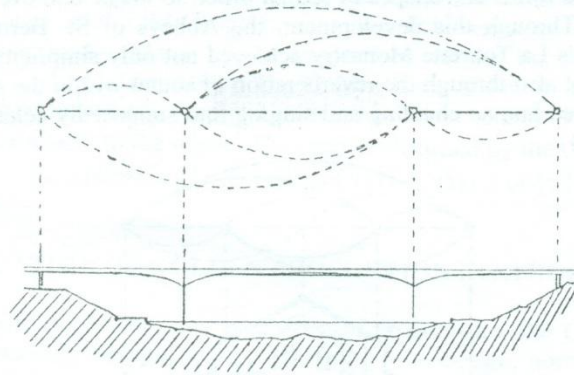


Fig. 6 - Golden Proportions of Redheugh bridge⁸

5.5 Ting Kau Bridge, Hong Kong

The arrangement conceived for the cable-stayed solution of the Ting Kau Bridge in Hong Kong involved a twin span triple towered pylon. The central tower, while it mirrored the outer two, had to be structurally much stiffer and therefore became the focus for the composition. In order to make the whole composition visually attractive the golden proportion was fully integrated into the design.⁷ (Figures 7 and 8)

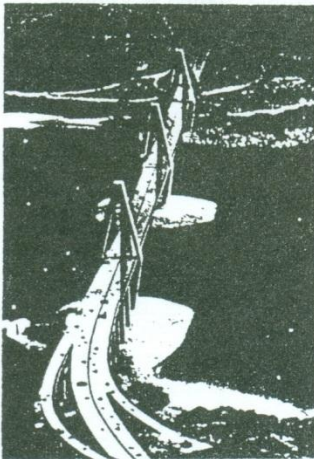


Fig. 7 Ting Kau Bridge⁷

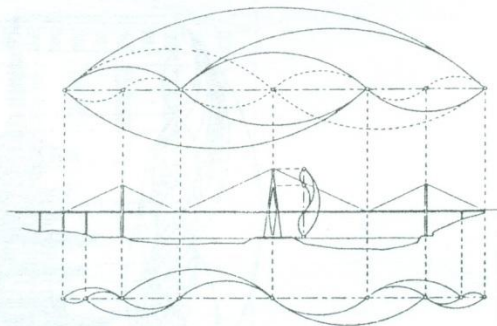


Fig. 8- Golden Proportions of the Ting Kau Bridge composition⁷

5.6 Vasco da Gama bridge, Portugal

The pylons for the second Tagus road crossing in Portugal are conceived as pure sculpted elements, as if carved from a single piece. All the surfaces flow smoothly one into another with uncomplicated simple lines. The pylon's legs are cranked to allow vertical cable profiles and a sense of the concentration of the forces is expressed by the subtle taper in the legs below the change in angle. The omissions of a cross beam immediately below the deck at the pylons visually articulates the fact that the deck is suspended throughout. The tie beam, required to withstand lateral and seismic forces, is carefully positioned according to golden proportions and completes the composition.⁸ (Figures 9 and 10)

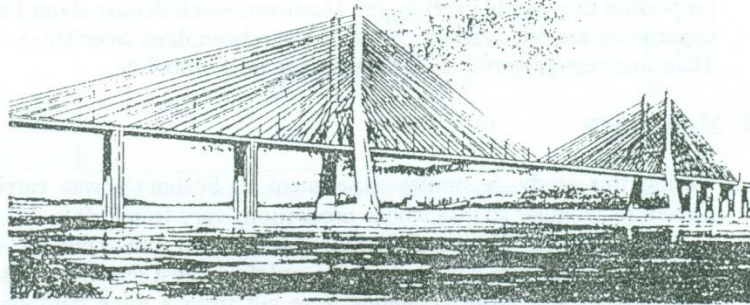


Fig. 9- Twin-towered Vasco da Gama bridges.⁸

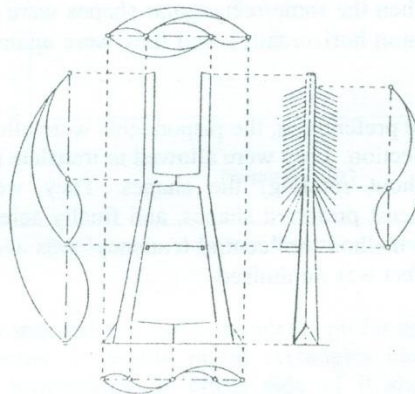


Fig. 10 - Golden Proportions of the Pylon of the Vasco da Gama Bridge.⁸

6 EVALUATION OF AESTHETICS

6.1 Perception of Proportions

6.1.1 Introduction

It is possible that some people are quite unaware of proportions in the physical aspects of things. Just as some people are colour blind, so some may be oblivious to the sensory stimuli of shape and form. However it is probably more reasonable to assume that people unaware of proportions are rare. It is more likely that they have an underdeveloped perception of proportions.

Georg Th. Fechner, in his laboratory experiments, studied the aesthetic preferences of common people with no aesthetic training. Fechner's experiments in 1876 were extensive, showing that over 75% of a large, randomly selected sample group preferred rectangles in the golden proportion to any other rectangle⁸. However, much details about Fechner's experiment are not available. Further it has been done over 100 years ago. Therefore repeating of his experiment can be worthwhile.

6.1.2 Methodology

During this study, a similar experiment to Fechner's was carried out. Eleven rectangular shapes whose proportions vary from 1.0 to 2.0 in steps of 0.1 were used. Here one unit was taken as 40 mm. Thus the smallest rectangle was 40 mm x 40 mm in size and the largest rectangle was 40 mm x 80 mm in size. The rectangles were cut from a thick cardboard. The colour of the rectangle was white. These eleven rectangles were kept randomly on a large brown colour board and the respondents were asked to select their preferences.

The rectangular shapes were first placed horizontally (i.e. shorter dimension vertically), and the respondents were asked to select their preferences. Then the same rectangular shapes were placed vertically (i.e. shorter dimension horizontally), and they were again asked to select their preferences.

In selecting the preferences, the respondents were allowed to use their own methods of selection. They were allowed to translate (move horizontally or vertically without rotating) the shapes. They were also allowed to eliminate the least preferred shapes, and finally select the most preferred shape. By this method the 'central tendency' was avoided and the 'lost in the shapes' effect was minimised.

6.1.3 Results

In the above study 100 randomly selected people were interviewed. Only four of them expressed their inability to identify the most preferred shape.

One had an idea that any shape would be pleasing. The other three had a view that there was no significant perceptual difference between the shapes. However 96 respondents out of 100 were able to select their preferences. The summary of results is shown in Figures 11 and 12. (where α = longer dimension of the rectangle / shorter dimension of the rectangle)

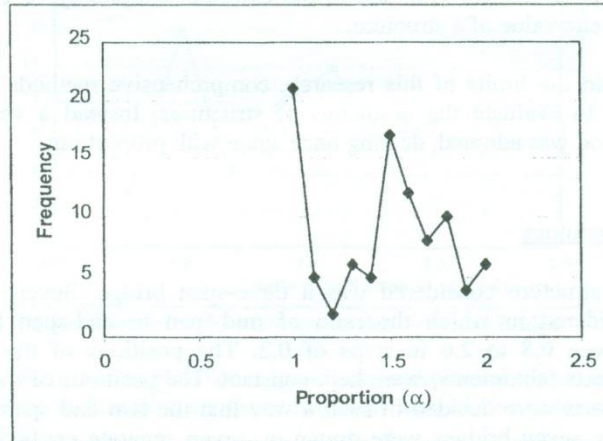


Fig. 11 – Preferences when shorter dimension is vertical

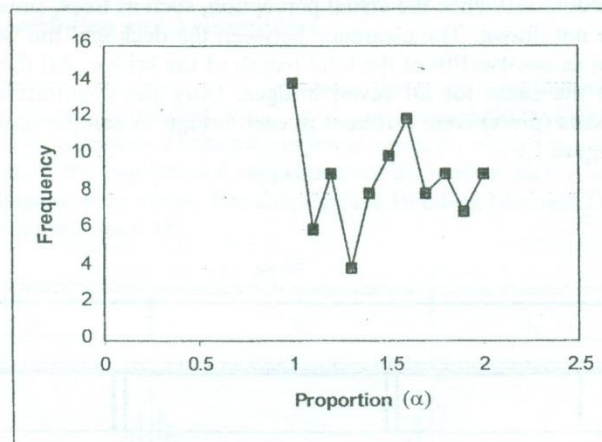


Fig. 12 – Preferences when shorter dimension is horizontal

The results show that most of the respondents prefer squares. After that a considerable number of people prefer rectangles close to the Golden Rectangle, with proportions on either side of it showing diminishing preferences.

6.2 Perception of Aesthetics of Structures

6.2.1 Introduction

In the true sense, the aesthetic value of a structure depends on many factors such as scale, size, proportion, hollow and volume, colour, light and shade, styling, optical illusions, compatibility, integrity, rhythm, harmony, balance, unity, etc. In addition aesthetic taste is a highly subjective matter. This shows the extreme complexity of evaluating the aesthetic value of a structure.

Within the limits of this research, comprehensive methods could not be used to evaluate the aesthetics of structures. Instead a very simplified method was adopted, dealing once again with proportions.

6.2.2 Methodology

The structure considered was a three-span bridge. Seven bridges were considered in which the ratio of mid-span to end-span length varied between 0.8 to 2.0 in steps of 0.2. The positions of the two exterior supports (abutments) were kept constant. The positions of the two interior supports were decided in such a way that the two end spans were equal. These seven bridges were drawn on seven separate cards. The size of a card was 150 mm x 30 mm. The bridges were drawn in black on white background. Only the bridge deck together with a simple railing, abutments, piers and the water level was shown. Other surrounding objects that could influence the visual perception, such as trees, flow of water, etc. were not drawn. The clearance between the deck and the water level was taken as one-twelfth of the total length of the bridge. All the above factors were the same for all seven bridges. Only the positions of the interior supports (piers) were different in each bridge. A sample drawing is shown in Figure 13.

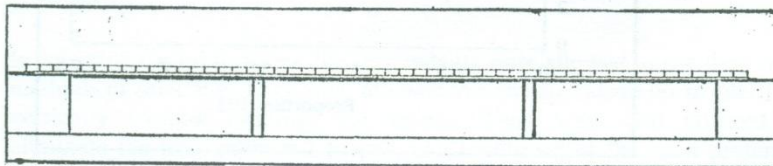


Fig. 13 - Sample drawing of a Three-span Bridge

These cards were kept randomly on the table and respondents were asked to select their preferences as explained in the previous experiment.

6.2.3 Results

As the above mentioned diagrams were technical in nature, only Civil Engineers were interviewed. In selecting preferences the respondents were advised to consider only the aesthetic appearance, but not the stability, economy, etc. The size of the sample was 50. The summary of the results is shown in Figure 14. (where α = length of mid span / length of end span)

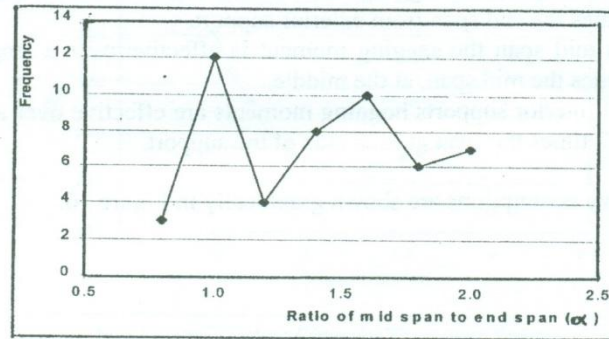


Fig.14 – Respondents' Preferences for the Three-span Bridge

The results show that most of the respondents prefer equal span continuous bridges. There is however another maximum around the golden section proportion.

7 OPTIMISATION OF SIMPLE STRUCTURES

7.1 Problem Description and Assumptions

For the purpose of analysis, a 30 unit long three-span continuous beam with a uniformly distributed load of 1 unit weight/unit length was considered. The positions of the two exterior supports were kept constant. The positions of the two interior supports were decided in such a way that the two end spans were equal. The shape of the Bending Moment Diagram is as shown in the Figure 15.

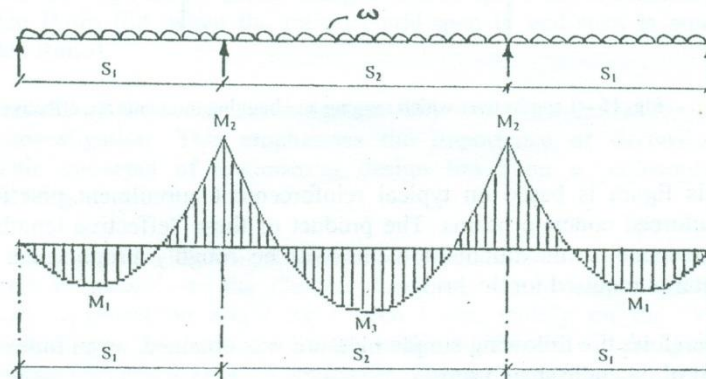


Fig.15 - Bending Moments in the Three-span Beam

The ratio of the mid-span to the end-span (i.e. $\alpha = S_2/S_1$) was varied between 0.5 to 2.0 in steps of 0.1, and the whole family of beams were analysed.

For the purpose of optimisation a simple measure was defined. This measure was based on certain assumptions.

1. In end spans the sagging moments are effective over a length of 0.8 times the end span from exterior support.
2. In mid span the sagging moment is effective over a length of 0.6 times the mid span, at the middle.
3. At interior supports hogging moments are effective over a length of 0.2 times the span at each side of the support.

The above assumptions are shown graphically in Figure 16.

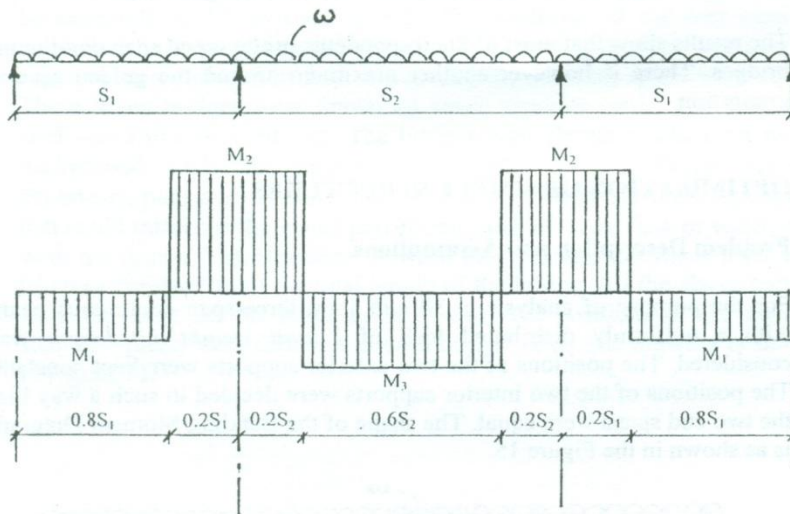


Fig. 16 – Lengths over which sagging and hogging moments are effective.

This figure is based on typical reinforcement curtailment practices for reinforced concrete beams. The product of these “effective lengths” and corresponding maximum moments will be roughly proportional to the material required for the bridge.

Therefore, the following simple measure was obtained, as an index for the cost of the three span beam.

$$f(M) = 2S_1 \{ 0.8 |M_1| + 0.2 |M_2| \} + S_2 \{ 0.6 |M_3| + 0.4 |M_2| \}$$

7.2 Results

The variation of the above measure with respect to α is shown in Figure 17. (where α = length of mid span / length of end span)

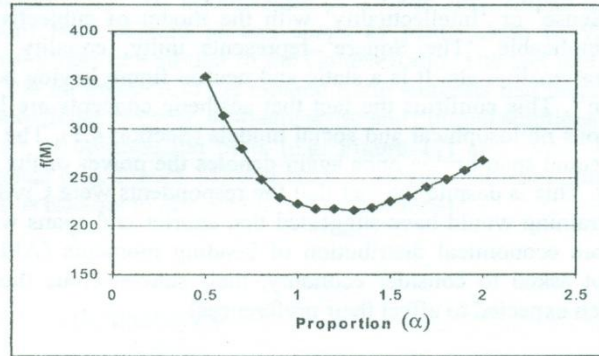


Fig. 17- Optimisation Curve for Three-span Beam

It shows a minimum (though not a very marked one) at a proportion around 1.4, a value close to $\sqrt{2}$.

8. DISCUSSION

In the investigation on 'Perception of Rectangular Shapes' it was found that most respondents prefer rectangles of equal side (i.e. square shapes). After that a considerable number of respondents prefer rectangles close to the Golden Rectangle.

The second investigation was about the perception of span lengths of a 'three-span bridge'. Here it was found that most of the respondents prefer a three-span bridge having equal spans. Secondly, once again a reasonable number of respondents prefer bridges whose spans are decided by the Golden Ratio (i.e. when the ratio of mid-span to end-span is equal to Golden Ratio).

The results of the second investigation tally well with the results of the first investigation. This emphasises the importance of derivation of aesthetic concepts of engineering design based on a philosophy of proportions.

The desire for the Golden Rectangle or Ratio may be linked with an 'interest in nature', as the Golden Ratio appears in nature. Here the aesthetic appreciation might have been based mainly on the 'Visual Perception' or the 'Surface Sense' with the model of metaphysical naturalism (Section 4.1) being applicable. This desire for the Golden Ratio was evident in the structures shown in a previous section as well (Section

5). The ratio was evident in both facades and longitudinal views of both buildings and bridges, in both horizontal and vertical directions.

However, the most significant result is the desire for the Square. This cannot be explained merely by the 'Visual Perception' or the 'Surface Sense'. Perhaps, the 'Square' might have addressed the respondent's 'Inner Sense' or 'Intellectuality' with the model of subjective idealism being applicable. 'The Square' represents unity, equality, simplicity, purify, rationality, etc. It is a static and neutral figure having no preferred direction¹¹. This confirms the fact that aesthetic concepts are linked with the various philosophical and social models (Section 4.1). The preference for the equal span bridge once again denotes the power of the concept of equality. This is despite the fact that the respondents were Civil Engineers whose training would have suggested that shorter end spans would result in a more economical distribution of bending moments (Although they were not asked to consider economy, their subconscious thoughts may have been expected to affect their preferences).

The optimisation curve has a minimum value close to $\alpha = \sqrt{2}$, i.e. when the ratio of mid-span to end-span is around $\sqrt{2}$. Although the structure selected was an ideal structure and only the simplest loading case (i.e. a uniformly distributed load) was considered for the purpose of analysis, there is nevertheless a well known value of $\sqrt{2}$ that is obtained as the optimum proportion. This is not too far away from the Golden Ratio either. Hence there may be some correspondence between aesthetic sense and optimal solutions.

The plots of optimisation and plots of aesthetic preferences will enable designers to make initial design-decisions relating to dimensions (or proportions). If there are plateaus (or inverted plateaus), in both or either of the plots, then the designer would be able to work within a wide range without adversely affecting the economy.

9 CONCLUSION

This study leads to the following conclusions.

1. Aesthetic concepts in engineering design can be derived from the models of aesthetics.
2. The golden ratio was evident in the proportions of existing structures, both buildings and bridges, in both facades and longitudinal views, in both horizontal and vertical direction.
3. The experiments on perception indicated that the concept of equality was a very strong aesthetic principle, reflected in choices for the square (among other rectangles) and a three span bridge with equal spans (compared to other bridges of varying mid-span to end-span ratios).
4. The above experiments indicated that the Golden Ratio also received considerable support, whether in the form of a Golden Rectangle or in

the ratio of mid to end spans of a three span bridge being close to the Golden Ratio.

5. The preference for equality could be an application of the aesthetic model of subjective idealism, while that for the Golden Ratio an application of the aesthetic model of metaphysical naturalism.
6. The albeit simplified optimisation of a three span bridge yielded the optimum ratio of mid to end spans as being close to $\sqrt{2}$, another classical proportion similar to the Golden Ratio. The fact that this value is not too far away from the Golden Ratio suggests that there may be a correspondence between aesthetic sense and optimal solutions.
7. The use of optimisation plots (e.g. Figure 17) and plots of aesthetic preference (e.g. Figure 14) will enable designers to make initial design decisions relating to dimensions (or proportions).

10 ACKNOWLEDGEMENTS

We wish to thank all the respondents who participated in the experiments on perception.

11 REFERENCES

1. Encyclopedia, Britannica –Vol. 1, Encyclopedia, Britannica, Inc., USA, 1995.
2. Syusyukalov, B.I and Yakovleva, L.A : A Handbook of Philosophy, Progress Publishers, Moscow, 1988.
3. Borev, Yuri : Aesthetics – a text book, Progress Publishers, Moscow, 1985.
4. Reekie, R. Fraser : Design in the Built Environment, Edward Arnold Publishes Ltd., London, 1972.
5. Salvadori, Mario : Structure in Architecture, Prentice-Hall, Inc., New Jersey, 1963.
6. Gray, W.S and Manning, G.P. : Concrete Water Towers, Bunkers, Silos and other Elevated Structures, Cement and Concrete Association, 1973.
7. Bennett, David : The Architecture of Bridge Design, Thomas Telford Publishing, U.K, 1997.
8. Yee, R : The Golden Proportion and its use in the aesthetic design of bridges, Proceedings of Institution of Civil Engineers, 1997.
9. Fletcher, Rachel : The Human Side - Improving Design with Human Proportions, http://web.uprr.pr/conner/body_symetry.html.
10. Knott, Ron : The Golden Section in Art, Architecture and Music, <http://www.mcs.surrey.ac.uk/Personal/R.Knott/Fibonacci/fibInArt.html>.
11. Ching, Francis, D.K. : Architecture – Form, Space and Order, Van Nostrand Reinhold Company, Inc., New York, 1979.
12. Stevens, Garry : The Reasoning Architect – Mathematics and Science in Design, McGraw-hill Publishing Company, Singapore, 1990.

PASSIVE CONCEPTS FOR IMPROVEMENT OF THERMAL AND VISUAL COMFORT IN HOUSES IN SRI LANKA

A I Jayawardane, Research Assistant, Department of Civil Engineering, University of
Moratuwa

Dr M T R Jayasinghe, Senior Lecturer, Department of Civil Engineering, University of
Moratuwa

Dr R A Attalage, Senior Lecturer, Department of Mechanical Engineering, University of
Moratuwa.

PASSIVE CONCEPTS FOR IMPROVEMENT OF THERMAL AND VISUAL COMFORT IN HOUSES IN SRI LANKA

A I Jayawardane, Research Assistant, Department of Civil Engineering, University of Moratuwa

Dr M T R Jayasinghe, Senior Lecturer, Department of Civil Engineering, University of Moratuwa

Dr R A Attalage, Senior Lecturer, Department of Mechanical Engineering, University of Moratuwa.

ABSTRACT: One of the primary requirements of houses constructed in hot humid climatic conditions such as those prevailing in Sri Lanka is that those should be thermally comfortable for the occupants throughout the day and around the year. Most of the single and two storey houses constructed in Sri Lanka have failed to fulfill this requirement. Therefore, a critical review was undertaken to develop passive concepts that can be incorporated in the future houses. It is shown with a detailed study that three storey houses can perform much better than single and two storey houses not only with respect to thermal comfort, but also with respect to visual comfort, functionality, minimisation of flash floods, creation of a desirable micro climate etc. It is also shown that the cost of three storey houses can be in the range of that of the single and two storey houses, when the traditional construction materials are used in an efficient manner. The use of these concepts for houses built in the future in Sri Lanka will be extremely important in order to minimise the electrical energy required for operation of houses; this will be quite useful since the electrical energy sources available for Sri Lanka are limited.

INTRODUCTION

Man needs shelter from various natural forces such as intense sunlight, blinding glare, nasty winds and driving rain. Over the years, his shelter has developed from the primitive cave to the built environment, or the house. Mohsen (1979) views a house as an intermediate object between the natural environment and man, its function being the control of natural environment in favour of the man. This means, the built environment should create an environment which is considered comfortable to its occupants, especially with respect to thermal and visual comfort.

In Sri Lanka, there are many houses that are uncomfortable, both thermally and visually, to their occupants. Indoors are hot, not only during daytime but at night too, and are gloomy during daytime. The solutions adopted to counter hot indoors are forced ventilation (eg: ceiling fans) and sometimes even active based air conditioning. To counter gloomy indoors during daytime, artificial lighting is used to supplement the daylighting.

According to a recent questionnaire survey conducted among a predominantly employed population, three out of four say that at least two fans are usually used in their houses to inhibit the thermal discomfort experienced. Moreover, one out of three say that at least one room of their house is gloomy during the daytime even when all its windows are open ; of them, 95% resort to artificial lighting when they have work to do in such a room.

The use of such active means is not prudent both with respect to the energy scenario of Sri Lanka and the cost of running the building. The energy prospects of Sri Lanka are not positive as they stand today. The total hydropower potential of Sri Lanka is about 2000 MW (Kariyawasam, 1999). Of this, nearly 1200 MW has already been harnessed (Fernando & Ratnasiri, 1997). Many other sites are being developed. The shortfall in power generation

has to be met with thermal power plants which consume imported fossil fuels. Since Sri Lanka does not have its own petroleum resources, any world petroleum crisis could adversely affect the electricity prices. Thus, if houses with better energy performance could be planned by incorporating passive techniques, the limited power generated can be used for more productive activities like manufacturing and value addition rather than for providing thermal and visual comfort in houses

Sri Lanka is a tropical island blessed with a desirable warm humid climate. Even during the early afternoons, the outdoors can be thermally comfortable at well shaded places with sufficient natural ventilation. When the built environments are thermally uncomfortable, the fault usually lies not with the climate, but with the incompatibility of the built environment with the climate. This paper critically evaluates the ways and means of achieving thermal and visual comfort in built environments by strategic use of passive solar concepts to minimise the adverse effects of the surrounding environment. In order to show the passive performance of multi-storey houses and single storey houses, a case study is presented, which includes three comparable houses of single, two and three storeys. The other advantages of using multi-storey houses with passive elements are also been highlighted.

OBJECTIVES

The main objectives of the research presented in this paper can be highlighted as:

1. to identify the passive concepts and techniques that can be used for planning of houses with a view of minimising the energy required for thermal comfort,
2. to determine the means of incorporating them for houses in the future,
3. to compare the passive performance of various house types; single, two and three storey, and
4. to evaluate the benefits of promoting three storey houses.

In order to achieve the above objectives, the following methodology was adopted:

1. Passive strategies that are appropriate to houses constructed in a warm humid climate to achieve thermal and visual comfort are listed and evaluated.
2. The best ways of incorporating the above strategies are determined by means of a detailed case study involving single, two and three storey houses.
3. A questionnaire survey has been conducted among a predominantly employed population of 142 (male 55%, female 45%), resident in the Western Province, Galle District or Matara District, in order to determine if they will appreciate the new concepts presented in this research.
4. Other beneficial effects of three storey houses are critically evaluated.

THERMAL COMFORT

One of the primary objectives of the building designer should be to ensure that the built environment is thermally comfortable to its occupants, possibly throughout the day and around the year. According to Mathews et al. (1992), this should receive sufficient attention from the very beginning as the foundation for a good thermal design is laid during the sketch design stage.

Thermal comfort is a sensation of complete physical and mental well being; it is a subjective quantity resulting from internal environmental variables such as dry bulb temperature, mean radiative temperature, humidity and air velocity. It is also affected by personal variables such as activity level and clothing level of the occupants. The thermally comfortable conditions for Sri Lankans involved in sedentary activities such as desk work can be presented as shown in Figure 1 for various internal air velocities (Jayasinghe & Attalage, 1999a). It can be seen that Sri Lankans can be thermally comfortable at elevated temperatures like 30° C, when sufficient internal air velocities are available.

In low altitudes of Sri Lanka (i.e. below 300 m), where the climate is warm and humid, the designers should aim to minimise the *heat gains* while maximising the *natural ventilation* and *structural cooling* (Jayasinghe & Attalage, 1999b). Very distinct seasonal changes do not occur in Sri Lanka since it is located close to the equator. The general requirement throughout the year is cooling, which has to be achieved with careful planning.

The heat gains into a building are basically of two types; external and internal. The external gains occur through the building envelope, namely, roof, external walls and external windows. The internal gains are, however, generated within indoors. Therefore the strategy should be to resist solar gains, resist conductive heat gains and minimise internal heat gains.

The internal heat gains are primarily due to various electrical appliances used within the house. The use of electric bulbs to supplement the daylighting can be a contributory factor.

These strategies can be put into work by incorporating various passive concepts and techniques such as:

1. Selection of appropriate orientation of walls and windows.
2. Minimising the area of undesirable building elements such as roof.
3. Selection of appropriate colour for external and internal surfaces.
4. Shading of windows and walls.
5. Creation of a desirable micro-climate around the houses.

Minimisation of heat gains

Heat gains occur through the building envelope, which consists of roof, external walls and external windows; they depend on the orientation, the materials used, shading available, etc. A comparison of materials can be done by using the thermal conductance. This is generally called the U value which has units of W/m²K. The time lag represents the delay that a certain material can cause for the heat transfer. Thermal conductance values are compared in Table 1.

Table 1: Thermal properties of various elements of a house (Szokolay, 1991)

Element	Material	U value (W/m ² K)	Time lag (hours)
Roof	Asbestos	4.9	0.0
External wall	Brickwork with plaster (225mm)	2.2	6.5
Window	Wood framed plane glass	4.3	0.0

The roof and the windows can be very weak against solar radiation since they allow almost instantaneous heat transmittance. The walls, on the other hand, can give a considerable time lag, which can be particularly helpful not only in delaying, but also in reducing the total heat flow into a building.

Since Sri Lanka is located close to the equator with a latitude between 5° to 9° north, there can be direct solar radiation on both north facing and south facing walls for about five months of the year, at different times. Everyday, the walls facing east and west will be subjected to direct solar radiation for about half a day. Therefore, any unshaded window can be undesirable on any of these directions with respect to minimising the direct solar gains. However, for windows on north and south facing walls, direct solar gains can be reduced by using overhang type shading devices. It is shown by Jayasinghe & Attalage (1999b) with the aid of cylindrical sun charts developed for Sri Lanka that an overhang which makes an angle of about 60° with the horizontal as shown in Figure 2 can provide adequate shading throughout the year. However, such overhangs are not so effective on east facing windows and can be almost useless on windows facing west; such windows can allow large amounts of direct solar radiation irrespective of the presence of shading devices, as the sun sets when the external temperatures are high.

Overhangs should be of very light colours. A dark overhang can absorb heat and then in turn emit infrared radiation into the building through the window which is now protected from direct solar radiation. Since shading devices are less effective on east and west facing openings, strategically located trees could be used to protect such windows.

Since the roof is also very weak in resisting the transfer of heat, attempt should be made to minimise the roof area. Since the total area required for a house is determined on the basis of the functional needs, the roof area can be minimised only by adopting multi-storey construction. In order to determine the effects of constructing multi-storey buildings on the variation of temperature and humidity, thermal surveys were carried out. The measurements were taken indoors and outdoors of a three storey hostel building of 24 m x 17 m of plan area at University of Moratuwa, during a month of March when extremely warm and humid conditions prevailed in the Western Province. The results of temperature measurements taken at the ground floor, the first floor and the second floor are given along with the outdoor temperature in Chart 1. The variation of relative humidity is given in Chart 2.

It can be seen from Chart 1 that the minimum surrounding temperature recorded was 27°C and the maximum was 33°C . The 2nd floor with a roof followed a temperature pattern with a temperature fluctuation of about 3°C , which may be due to thermal gains through the roof. The ground floor recorded a temperature fluctuation of 2°C which can be attributed to thermal gains due to ground reflected components during the day time. The first floor, which is sheltered better than ground and second floors, recorded a temperature fluctuation of only 1.5°C . This indicates that it is possible to maintain well sheltered floors of multi-storey buildings with minimum fluctuations of temperature provided the external heat gains can be minimised and there is a sufficient drop of temperature during the night time. It can be seen from Chart 2 that these readings have been taken during extremely humid days where outside relative humidity has reached 100% around 5.30 a.m.

Unlike direct solar radiation, controlling the gains due to diffused and ground reflected radiation is difficult. However, their intensities are much lower. The reflected radiation follow the rule that angles of reflectance and incidence are equal. Therefore, man-made surfaces such as paved areas and roads should be avoided as much as possible and vegetation should be promoted around houses (Watson & Labs, 1983). For example, a concrete surface reflects about 25-35% of incident solar radiation, a grass surface, only 10-15% (Mohan, 1989). According to Watson & Labs (1983), an irregular or rough surface with plenty of trees can further reduce the ground reflected component.

The colour of the external fabric also plays an important role in determining the extent of the heat gained through the walls. According to Bansal et al. (1992), the colour of the outside surface of a building envelope is expected to influence the thermal performance of a building significantly as it determines the amount of absorbed solar radiation, and therefore, its inward transmission into the building. Buildings with light shades will always possess a better thermal performance than those with dark shades (Bansal et al., 1992). In this respect the prevailing condition in Sri Lanka is satisfactory; 70% of those surveyed have light colour external walls in their houses.

The solar radiation absorbed by a house can be further reduced by minimising the difference between the outdoor and the indoor temperatures. Thus, the thermal comfort indoors can be improved by lowering the outdoor air temperature. For this purpose, trees can be used. Trees are good solar radiation absorbers; they can provide evaporative cooling effect. Due to evapotranspiration, vegetation can convert large amounts of solar radiation into latent heat, which does not cause the air temperature to rise (Takatura et al., 2000). Thus, by providing vegetation in abundance around the structure, a more desirable micro climate can be achieved. Lack of evapotranspiration surface can be a reason for the temperature in big cities to be higher than those of rural vicinities.

Therefore, the minimisation of heat gains can be achieved in a better way by using multi-storey houses with less roof area for the same total floor area. Since the front of the houses will need more glazed openings for aesthetics, it is advisable to have them facing either north or south, where the openings can be adequately shaded. This can be achieved only if land is subdivided with this in mind. Since multi-storey houses can leave more open area around a house, such spaces can be used to create a desirable micro-climate with sufficient number of strategically located trees. Such houses are more likely to be thermally comfortable, and therefore will need less active means for thermal comfort. Thus, multi-storey houses can be very useful in developing better houses which utilise less energy for operation.

Maximisation of ventilation

An effective distribution of fresh air within an occupied space is of considerable importance in securing thermal comfort and good indoor air quality. A well designed natural ventilation system is not only energy efficient, but also provides a healthy indoor environment (Gan, 2000). The importance of maintaining adequate ventilation with a sufficient air velocity can be seen from Figure 1. As the air velocity increases, the comfort zone becomes larger, capturing more points on the psychrometric chart.

Ventilation is of two types; cross ventilation and stack ventilation. The former is due to wind which is created due to difference in pressure between two places. The latter is due to a difference in air density, which usually occurs vertically as the height increases.

For improved cross ventilation, the inlet should face the general wind direction. It is stated by Watson & Labs (1983) that cross ventilation can be improved further by having both the inlet and outlet located on exterior walls. However, if multi-storey houses are constructed with the same floor area, more rooms will be able to have exterior walls, thus allowing more openings on them as indicated in Figures 3,4 and 5. This is a particular advantage that multi-storey houses can offer. For single storey houses, this is not easy to achieve as indicated in Figure 6, where a number of rooms are provided with windows only on one wall.

Single storey houses constructed close to each other will also suffer because the breeze tends to blow over them (Mohan, 1989). On the other hand, a multi-storey house can act as a barrier to wind, which effectively increases the surface air pressure, thus forcing the air through the building. This can be further improved by having a recess for the windward face of the building thus trapping more wind (Figure 4). According to Chand et al. (1989), the provision of small openings facing the main wind direction can allow considerable amount of fresh air into a building.

In both single and multi-storey houses, the courtyards can enhance the natural ventilation. Multi-storey houses can offer better use of the courtyard since the same courtyard can be shared at many different levels as shown in Figure 3. The courtyards are of particular use since the windows can be kept open without any security threat. The concepts for the proper planning of courtyards for houses built in Sri Lanka are given by Jayasinghe and Attalage (1999 b), and can be highlighted as shown in Figure 7.

These concepts show that a multi-storey building with sufficient open spaces on the windward side can improve natural ventilation. These will also allow more openings to be placed on the external walls. Thus, multi-storey houses can be very useful in providing improved thermal comfort.

VISUAL COMFORT

A key variable for visual comfort is the quantity of sunlight penetrating into a room; it is mainly determined by the depth of penetration rather than by the intensity of direct sunlight. By increasing the amount of diffused radiation entering a room, the depth of penetration can be maximised (Neeman, 1977).

Since allowing too much diffused radiation can also affect the thermal comfort, the window orientation and sizes should be carefully selected. For example, for houses in Sri Lanka, shading devices can be used to intercept direct solar radiation for windows facing north or south. Provision of a sufficient number of shaded windows on these two faces can allow a sufficient amount of diffused radiation. For windows facing west, shading devices are almost ineffective. Thus, such windows should be avoided or very short windows should be provided, where direct solar radiation can be limited to that just before sunset by using shading devices. Since multi-storey houses allow more external walls for each occupied space, a wider choice is available to select windows with desirable orientation, as shown in

Figures 3 and 4. A single storey house may not offer this flexibility since it might have some rooms having the external wall facing west (Figure 6).

By making diffused radiation inside a room to reflect, visual comfort can be further enhanced. For this light colour interior surfaces are desirable. The survey reveals that 73% have light colours for interior wall surfaces; however, the corresponding figure for the floor is only 9% because people tend to avoid light colours due to difficulty in cleaning.

Another major problem for allowing adequate natural light to the interior is the use of blind walls. When single storey houses are constructed in small blocks of land, blind walls may be attractive to increase the lot coverage. However, this will prevent provision of windows on such walls. When three storey construction is used, blind walls can be avoided as indicated in Figure 3 and 4, or even when one is provided, it will be possible to have an adequate number of windows to allow sufficient daylight

INCORPORATION OF PASSIVE TECHNIQUES TO NEW HOUSES

It is clear that passive techniques can be incorporated more easily into multi-storey houses than into single-storey houses. Moreover, the passive performance of the 3-storey house is better than that of an equivalent 2-storey one. Therefore, two layouts of 3-storey passive houses were developed: one of total floor area around 160 m²; the other, 125 m² (Figures 3 and 4). The latter consists of a courtyard too.

Three-storey passive houses can be planned this way. The ground floor, which would be sheltered during the day time , can accommodate utility areas such as living, dining and pantry. If the house is large, these spaces can be planned at the ground floor level around a courtyard, which can serve all floors (as shown in Figure 3). It will promote ventilation and somewhat improve the visual comfort in the spaces around it. However, in plan, it need not be as large as those dictated by the building regulations because alternative windows can be provided on the external walls of the spaces concerned (Figure 3).

The first floor is sheltered both from the solar radiation from above and from the ground reflected radiation. It is therefore the most desirable floor level. For best thermal comfort, bedrooms and the study room can be located there. In a large house as that shown in Figure 3, bedrooms can be planned around a courtyard so that bedroom windows can open into it without privacy or security problems. Even in a 3-storey house without a courtyard (Figure 4), keeping windows open day and night will not be a problem as serious as in the case of a single-storey house.

The second floor is the least desirable, and therefore it should be employed to house spaces that are occasionally occupied, such as visitors bedroom, utility room and balcony.

As shown above, 3-storey houses offer various options to achieve thermal comfort : strategic locations of bedrooms and study rooms, sheltered floors, sharing the same courtyard at different floor levels, planning spaces around a courtyard and so on. Single-storey and 2-storey houses however do not offer such flexibility in planning houses with respect to thermal and visual comfort.

CASE STUDY: COMPARISON OF SINGLE AND MULTI-STOREY HOUSES

In order to compare the advantages of three storey houses with single and two storey ones, a case study was conducted for the houses given in Figures 4, 5 and 6. It is considered that all these houses will be constructed on a block of land of extent 11.5 perch (17x17 m²). A comparison for these houses based on centre line dimensions can be presented as given in Table 2.

Table 2 : Comparison of alternative types of houses

	3-storey	2-storey	Sinlge-storey
Total usable floor	100.44 m2	116.64	101.34
Total floor	126.36 m2	144.72	131.40
Usable /Total floor	0.795	0.806	0.771
Plot extent	289 m2 (11.5 perches)	289	289
Plan area of ground floor(with courtyard)	43.20 m2	72.36	140.40
Plan area of roof (with 1 m eaves)	72.24 m2	111.76	190.80
Roof /Total floor	0.572 (100%)	0.772 (135%)	1.452 (254%)
Roof /Plot area	0.250 (100%)	0.387 (155%)	0.660 (264%)
Exposed area /plot area	0.750 (100%)	0.613 (82%)	0.340 (45%)
Gross external wall area for windows	200.88 m2	156.33	119.88
Gross ext wall area for windows/Served floor	2.268 (100%)	1.492 (66%)	1.183 (52%)

It can be seen that the usable area to total area in both three and two-storey houses are comparable. Single-storey houses may need more area for circulation, thus resulting in a lower ratio for usable to total area. The roof area of the three-storey house is the least as expected. This will be particularly useful in reducing heat gains. The lower lot coverage of three storey houses will give larger garden area, thus facilitating the creation of a desirable micro climate.

The use of three storey instead of single storey houses can have a number of additional benefits as well. Those are given below.

Reduction of flash floods

One out of four of those surveyed reveals that, following a heavy rain, their street or house gets flooded. Such flash floods occur in urban and suburban areas mainly due to two reasons; inadequate exposed surface area for infiltration of storm water and inadequate capacity of the drainage system which now has to handle a much larger amount of storm water. For example, for a rainfall intensity of 25 mm/hour lasting for one hour, the total volume of runoff due to roof is about $72.24 \times 0.025 = 1.806 \text{ m}^3$ for the three storey house in Figure 4. It is about 2.794 m^3 for the two storey house in Figure 5, and for the single storey house in Figure 6, it is about 4.770 m^3 . Thus, the runoff from the roof of a three storey house will be only about 40% of the runoff from a single storey house of similar total floor area. Another main advantage of lower lot coverage of three storey houses is that there will be sufficient vacant space on the land for the construction of detention ponds (Wijesekera, 1999) than in other two types. The effect of constructing these ponds on the foundations of the house also could be minimised by locating them away from the house. These ponds will be helpful to increase the ground water recharge, which in turn will sustain the growth of trees. Trees will reduce the speed of runoff thus reducing the soil erosion and siltation of drains.

Improved functionality

In a single storey house, all activity spaces are located at ground floor level, resulting in some problems associated with privacy. The three storey houses shown in Figures 3 and 4 provide three different levels for space allocation. The ground floor can be occupied by the family members and visitors during the daytime comfortably. The first floor can be occupied by the family members. The second floor bed rooms can be allocated for infrequent use such as visitors bed rooms, and the balcony can be used for sleeping in hot nights or for drying of clothes during daytime.

In three storey houses, activity spaces can be arranged around the staircase as shown in Figures 3 and 4, minimising the circulation space. The space beneath the staircase at ground floor can be used for a storage area. The water tank can be located at the roof level above the staircase or bathrooms.

All the external windows in a single storey house are located at the ground floor level. Therefore, keeping the bed room windows open until late into the night, although desirable in terms of thermal comfort, is difficult due to safety reasons. The survey reveals that, even when the night is hot, 56% do not keep the bedroom windows open; 21% keep them open until late night. The concern of the former is security (87%), followed by mosquito menace (47%) and privacy (18%). In a multi-storey house, on the other hand, bedrooms can be easily located upstairs.

Cost aspects

Despite these advantages, the general public is reluctant to consider three storey houses as a possible alternative due to the misconception that three storey houses can cost much more than single or two storey houses. It is shown by Jayasinghe & Jayawardane (2000) that loadbearing brickwork can be safely used in three storey house construction while achieving substantial cost savings with respect to reinforced concrete framed structures.

In order to compare the likely costs of two storey and three storey houses, a comparison is made for different types of gross surface areas of the houses given in Figure 4, 5 and 6. The results are given in Table 3.

Table 3 : Comparison of gross surface areas of alternative types of houses

		3-storey	2-storey	1-storey
Vertical surfaces	Total	327.24 m ²	326.43	268.92
	Total surface/ Total floor	2.590 (100%)	2.256 (87%)	2.047 (79%)
Non-vertical surfaces	Earth fill area	43.20 m ²	72.36	131.40
	RC slab area (incl. Stair slab)	85.14 m ²	73.08	0
	Roof (plan area)	72.24 m ²	111.76	190.80
	Total	200.58 m ²	257.20	322.20
	Total surface/ Total floor	1.587 (100%)	1.777 (120%)	2.452 (155%)

It can be seen that three storey house needs only two thirds of non vertical surface area of that of the single-storey house. A reason, for example, is that the first floor slab serves both as the floor of the first-storey and the roof of the ground-storey. Thus, better use of structural materials such as loadbearing brickwork would be able to keep the cost per unit area for two and three storey houses approximately the same.

In order to compare the actual costs of the three types of houses, a detailed cost study was carried out by Subashi et al (2000). They have assumed that the houses are provided with basic finishes such as asbestos sheet roofs, asbestos ceilings and cement rendered floors etc but not tiles, bathroom fittings etc. All three houses have loadbearing brickwork and rubble foundations. The techniques of using these two materials for proper multi-storey house construction is described in detail by Jayasinghe & Jayawardane (2000). The rates used are those specified for the local authority contracts by the Western Provincial Organization for the year 1999. These results are given in Table 4. It can be seen that the construction cost per unit area is in the same region.

Table 4: Comparison of cost of construction for single, two and three storey houses

	Three storey	Two storey	Single storey
Total cost (Rs)	1002,164/=	949,915/=	904,392/=
Total floor area (m²)	139.86	144.72	132.66
Cost per unit area (Rs/m²)	7165.50	6563.80	6817.40

CONCLUSIONS

It is shown that three storey houses can perform better than single and two storey houses with respect to providing thermal comfort throughout the day, around the year. The advantages of three storey houses such as ability to provide visual comfort, better arrangement of functional spaces, minimisation of circulation spaces and minimisation of land usage are described with suitable case studies. It is also shown that the construction cost of a three-storey house is not substantially higher, a finding contrary to the general belief. Moreover, its operational cost will be lower due to its less dependence on active techniques for thermal comfort. These findings are extremely important for Sri Lanka since its electrical energy generation capacity is limited and has to rely to a certain extent on non-renewable sources.

It is also shown that the use of three storey houses allows the creation of a much desirable micro climate with increased vegetation. Two out of three surveyed consider environmental pollution as a "serious problem threatening the future"; 18% consider it as "just one out of many problems." Moreover, 88% express their willingness to grow trees if garden space is available; 8% cannot decide for the time being. Therefore it is clear that the majority of the people have not only realised the severity of the problem, but also are willing to act to solve it. The best solution is maximising the greenery, but this requires vacant land, which is becoming scarce in urban and suburban areas. Therefore, 3-storey houses should be encouraged in such areas for a sustainable environment.

The low plot coverage of three storey houses also will allow the construction of detention ponds to minimise the runoffs from the roofs. This will help to minimise the changes to the drainage patterns, minimising the possibility of flash floods, which often occur after heavy rains.

People have been more inclined towards lateral development rather than vertical development, even in urban areas. For example, of the total floor space of 13.5 million m² available in Colombo City in 1996, ground floor and first floor accounted for 86% (City of Colombo Development Plan 1999: Vol 1). However, the current trend with respect to houses is towards vertical development. For example, of those surveyed, 67% live in single-storey houses; 29% in 2-storey houses. However, only 37% prefer to live in single-storey houses; 53% favour 2-storey houses. Three-storey house is a new concept. With the trend of residential buildings preferring vertical development, people will appreciate it especially when they realise the string of benefits it can offer, long term as well as short term.

When such passive solar concepts are adopted, for its success, the occupants should understand and appreciate the importance of all the concepts associated with it. They also should be prepared to work for the creation and maintenance of a much desirable micro climate in the entire neighbourhood since that can bring more benefits than creating such an environment around one or two houses.

References

- Bansal, N.K., Gary, S.N., Kothari, S (1992), "Effects of exterior surface colour on the thermal performance of buildings", *Building and Environment*, Vol. 27, No. 1, pp 31-37.
- Chand, I., Sharma, V.K., Krishak, N.L.V. (1989), "Ventilation survey of typical airy buildings - A few case studies in hot dry and hot humid zones of India", *Building and Environment*, Vol. 24, No. 3, pp 229-238.
- City of Colombo Development Plan (1999), Vol:1, Urban Development Authority, Ministry of Urban Development, Housing and Construction
- Fernando, W.J.N., Ratnasiri, J., (1997), "Green house emissions from the energy sector and options for mitigation", *OUR Engineering Technology*, Volume 3-#1, March, pp 77 - 83.
- Gan, G.(2000), "Effective depth of fresh air distribution in rooms with single sided natural ventilation", *Energy and Buildings*, Vol 31, No 1, pp 65 - 72.
- Jayasinghe, M. T. R., Attalage, R. A. (1999 a), "Comfort conditions for built environments in Sri Lanka", *Engineer, Journal of Institution of Engineers, Sri Lanka*, Vol: xxix, No 1, pp 12-23.
- Jayasinghe, M. T. R., Attalage, R. A. (1999 b), "Passive techniques for residential buildings in low altitudes of Sri Lanka", *Engineer, Journal of Institution of Engineers, Sri Lanka*, Vol: xxx, No 2, pp 18-27.
- Jayasinghe, M. T. R., Jayawardane, A. I. (2000), *Use of loadbearing brickwork for three storey houses in Sri Lanka*, Research Monograph, Department of Civil Engineering, University of Moratuwa, 48 p.
- Kariyawasam P. L. G. (1999), "Wind power to generate electricity", *Sri Lanka Engineering News*, IESL, Vol 1, No 34, p 1,8.
- Mathews, E. H., Etizion, Y. Erell, E., Richards, P.G. (1992), "Simplified analysis of naturally ventilated desert buildings", *Building and Environment*, Vol. 27, No. 4, pp 423-432.
- Mohan, I. (1989), *Environment and Habitat*, Ashish Publishing House, New Delhi, India.
- Mohsen, M.A. (1979), "Solar radiation and courtyard house forms - 1: A mathematical model", *Building and Environment*, Vol. 14, pp 89-106.
- Neeman E. (1977), "Sunlight requirements in buildings II – visit of an assessment team and experiments in a controlled room", *Building and Environment*, Vol 12, pp 147-157
- Subashi G.H.M.J., Rangana B.D.A., Batepola B.A.C. (2000), *Passive solar techniques for Sri Lanka*, Undergraduate Research Report, Department of Civil Engineering, University of Moratuwa

Szokolay, S.V. (1991), *Heating and Cooling of Buildings - Handbook of Architectural Technology*, Ed. Cowan, H. J., Van Nostrand Reinhold, New York, pp 323-365.

Takatura, T, Kitade, S., Goto, E. (2000), "Cooling effect of greenery cover over a building", *Energy and buildings*, Vol 31, No 1, pp 1-6.

Watson, D., Labs, K. (1983), *Climatic design*, McGraw Hill Book Co., USA.

Wijesekera, N. T. S. (1999), "Surface water drainage systems to manage environmental consequences of development: An application to industrial estate development in Sri Lanka", *Engineer, Journal of the Institution of Engineers*, Sri Lanka, Vol: xxx, September, No 3.

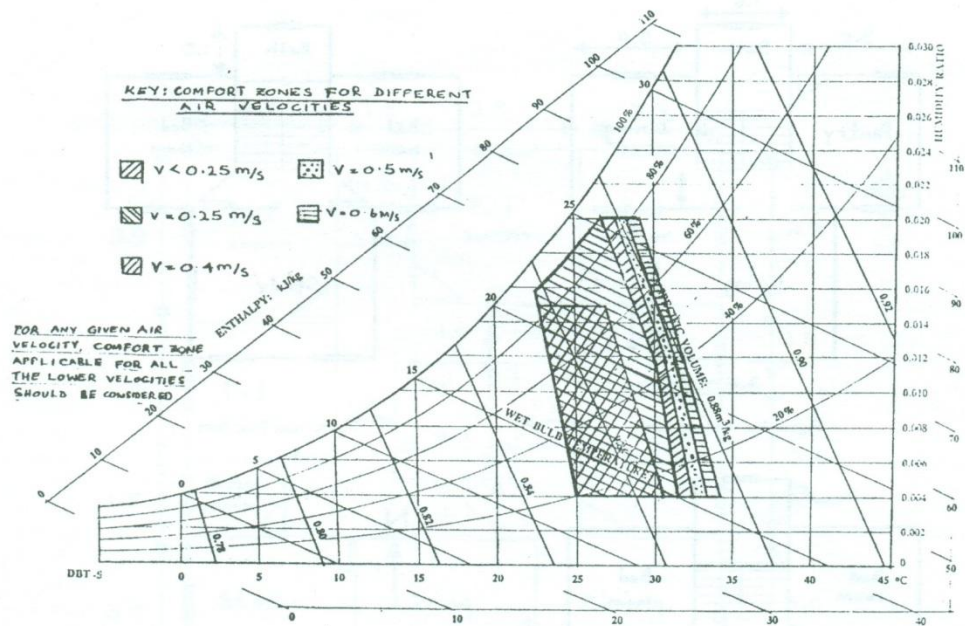


Figure 1: Psychrometric chart giving modified comfort zones taking account of physiological effects of cooling

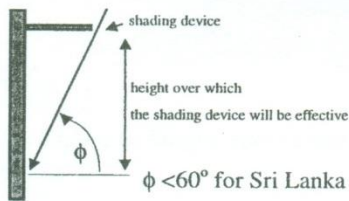


Figure 2: Effectiveness of shading devices

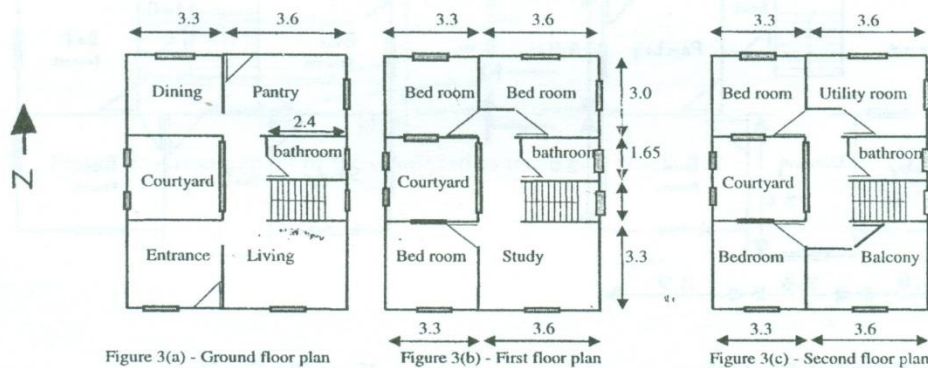


Figure 3: Three storey courtyard house of a total floor area 160m²

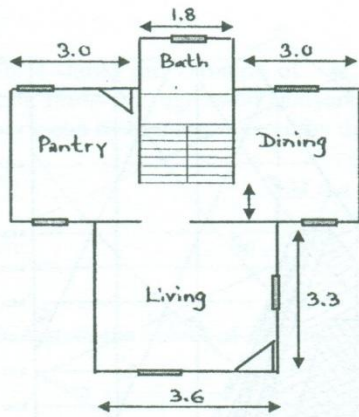


Figure 4(a): Ground floor

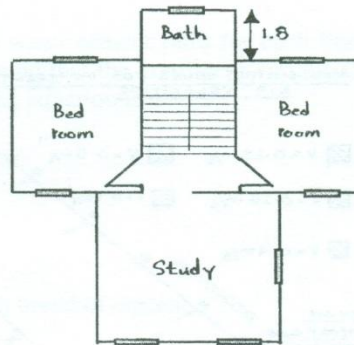


Figure 4(b): First floor

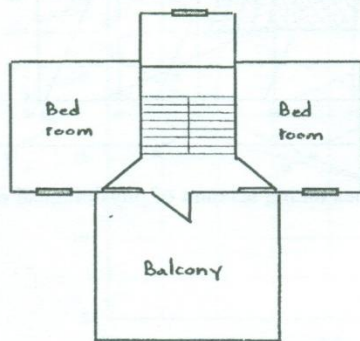


Figure 4(c): Second floor

Figure 4: Three storey house of a total area 125 m²

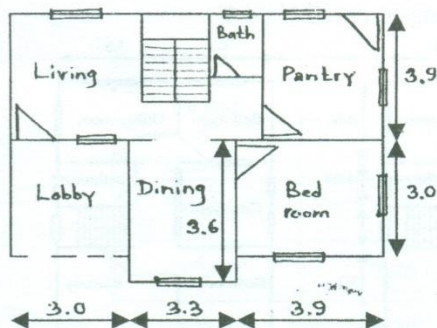


Figure 5(a): Ground Floor

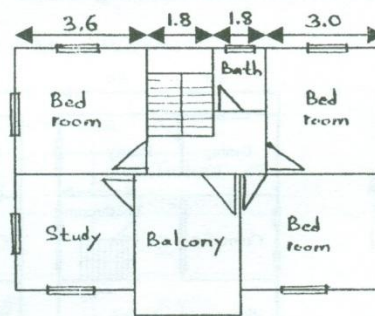


Figure 5(b): First Floor

Figure 5: Two storey house of a total floor area 140 m²

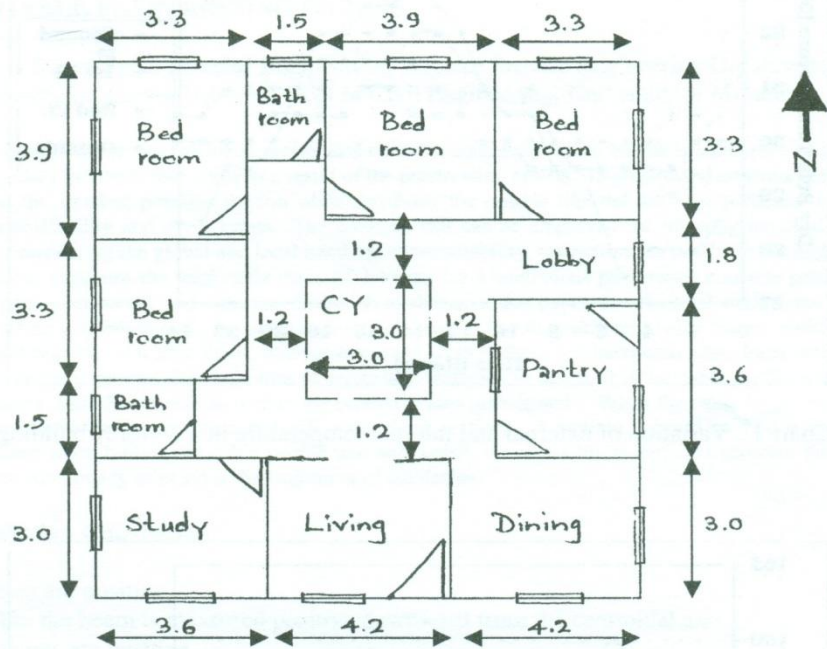


Figure 6: Single storey courtyard house of total floor area 130 m²

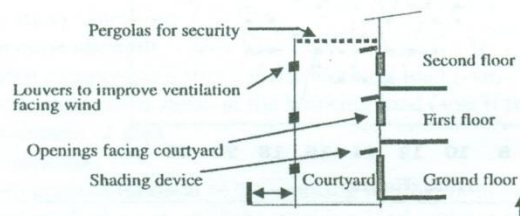


Figure 7: Arrangement of the courtyard to maximise ventilation

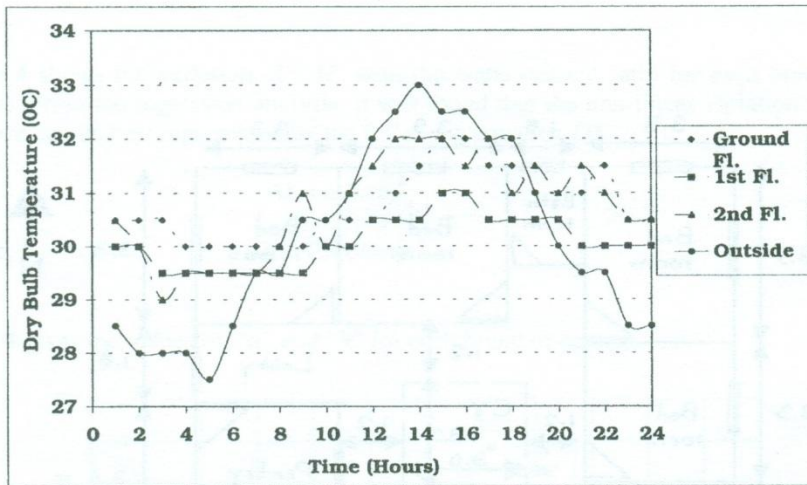


Chart 1 : Variation of external and internal temperature in a 3-storey building

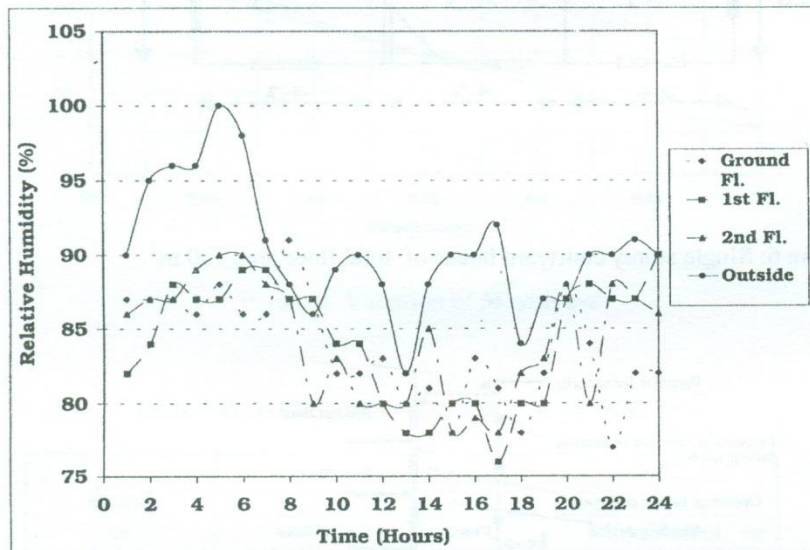


Chart 2 : Variation of Relative Humidity in a 3-storey building

**DESIGN OF CONTINUOUS PRISMATIC PRESTRESSED
CONCRETE SPINE BEAMS
WITH VARIABLE PRESTRESSING FORCES**

Eng W M D N Ranasinghe, Director Engineering, Western Province Engineering Organisation
Dr M T R Jayasinghe, Senior Lecturer, Dept of Civil Engineering, University of Moratuwa.

DESIGN OF CONTINUOUS PRISMATIC PRESTRESSED CONCRETE SPINE BEAMS WITH VARIABLE PRESTRESSING FORCES

Eng W M D N Ranasinghe, Director Engineering, Western Province Engineering Organisation
Dr M T R Jayasinghe, Senior Lecturer, Dept of Civil Engineering, University of Moratuwa.

Abstract: Design of continuous prismatic prestressed concrete continuous spine beams is a complex task, primarily due to the secondary moments that occur as a result of the prestressing effects. In prestressed concrete members, it is useful to select the smallest possible section while satisfying the criteria like the use of a particular construction technique, constructability and stress limits. The methods that can be employed for selecting the smallest section dimensions by considering the global and local bending, constructability, restrictions on depth etc are highlighted. It is advantageous to minimise the total cable force (JPs) used for a continuous prestressed concrete prismatic spine beam with respect to economy and constructability. It is shown in this paper that the total cable force can not be minimised by using a constant cable force throughout the length. For that, different cable forces could be used in span and support regions. It is also shown that for any given section, there is a maximum cable force that should not be exceeded over the supports. The selection of secondary moments to ensure that the cable profile zone resulting from the minimum cable forces will lie within the section is also highlighted. When the cable force changes, there will be point moments and point forces that will act at those sections. A straight forward method is presented for dealing with these when finding the cable profile that will satisfy the stress limits and also generate the secondary moment distribution already selected at the beginning of the design.

Notation and Sign Convention

Tensile stresses are positive

Position within the beam is measured positive downward from the centroidal axis.

Sagging moments are positive.

A	Total cross-sectional area
c	Cover from edge of concrete to centre of tendon
d	Overall depth of beam
e	Tendon eccentricity
e_{max}	Maximum eccentricity at which tendon can be placed ($y_2 - c$)
e_{min}	Minimum eccentricity at which tendon can be placed ($y_1 + c$)
$e_{sn(i)}$	Eccentricity of new cable at i^{th} change point
f	Limiting stress condition
f_{cu}	Concrete cube strength
f_{cw}	Permissible compressive stress at the working load (-ve)
f_{tw}	Permissible maximum stress at the working load (+ve if tensile)
I	Second moment of area
M	Applied moment
$M_{a(act)}$	Maximum applied moment at the working load without secondary moments
$M_{b(act)}$	Maximum applied moment at the working load without secondary moments
M_a	Maximum applied moment at the working load with secondary moments
M_b	Maximum applied moment at the working load with secondary moments
M_2	Secondary moment
$(M_2)_j$	Secondary moment at internal support j
P	Prestressing force in cable at transfer
P_B	Cable force corresponding to point B of Magnel diagram
P_i	Forces acting on i^{th} system
$P_{n(i)}$	Cable force in the new cable at the i^{th} cable force change point
$P_{r(i)}$	Cable force in the running cable at i^{th} cable force change point
R	Loss ratio

R_{ik}	Reactions due to loading on beams
y_1	Position of top fibre (-ve)
y_2	Position of bottom fibre (+ve)
Z_1	Elastic section modulus of top fibre (I/y_1) (-ve)
Z_2	Elastic section modulus of bottom fibre (I/y_2) (+ve)
$\alpha_{n(i)}$	Inclination of the anchor for new cable
$\alpha_{r(i)}$	Inclination of the running cable at force change point I
β_j	Distribution coefficient for M_2
$\beta_{ll(i)}$	Inclination of lower bound of cable profile at left hand side of i^{th} cable force change point
$\beta_{ur(i)}$	Inclination of the upper bound of the cable profile at right hand side of the i^{th} cable force change point
Δ_i	Displacements of the i^{th} system

INTRODUCTION

Box girder bridges are often used in the span range of 30-200 m (Swann, 1972). They are quite popular due to the inherent torsional rigidity that gives good load sharing characteristics. A box girder consists of single or multiple cells with cantilever overhangs on either side at the top flange. Since these structures are generally constructed as continuous over the supports, the design process becomes a complicated task. This is due to the secondary moments that are induced as a result of prestressing effects. Such secondary moments can alter the bending moments due to dead and live loads thus leading to many iterations in the design calculations.

A design method that can be followed as a logically evolving process by the design engineer to produce an optimum design was presented by Ranasinghe & Jayasinghe (1998). This method was presented for a constant prestressing force. In this paper, the above method was further refined to deal with variable prestressing forces. When the cable forces vary, there are additional constraints on the cable due to the location of anchor blocks. A straight forward method is presented which allows the designer to select the location of anchor blocks. It also gives a simple method to find an appropriate cable profile that generates the secondary moments selected earlier. With this rational design method, now it will be possible for any design engineer to produce continuous spine beam bridges which are very close to the optimum solutions that can be achieved with respect to the smallest cross section.

METHODOLOGY

The following methodology was used for the research work presented:

1. The design principles were developed to select minimum variable cable forces that would be needed for the continuous cable.
2. A design method was developed to select suitable secondary moments.
3. A straight forward design method was presented to find a suitable cable profile that will generate the above selected secondary moments and also fit within the limits on the cable profile.

THE DESIGN METHOD

The design method suggested can be presented as follows:

1. Selection of the smallest practically possible cross section.
2. Determination of minimum cable forces that can be used for the above section.
3. Selection of suitable secondary moments so that the smallest practically possible section can be used with the minimum cable forces.
4. Determination of the cable profile so that the secondary moments generated are quite close to those selected.

SELECTION OF SECTION DIMENSIONS

The selection of the smallest possible section based on construction aspects and other practical considerations is described in detail by Ranasinghe & Jayasinghe (1998). In order to clarify the design process, a design example is also presented along with the design method and principles. The box girder used for the design example is as follows. The box girder bridge consist of three spans of 40m, 50 m and 40 m. This bridge will carry a two lane highway of lane width 3.5 m and two walkways of width 1.5 m on either side. Thus the total top flange width is 10.0 m. It will be constructed using span by span construction technique. The section dimensions selected for the design example are presented in Table 1 highlighting the underlying principles. The section selected is shown in Figure 1.

The other useful design information are as follows:

1. Grade of concrete (f_{cu})= Grade 40 = 40 N/mm²
2. Allowable stress in compression (f_{cw}) (BS 5400/4)= -16,000 kN/m²
3. Allowable stress in tension (f_{tw}) (BS 5400/4)= 0.0 kN/mm²
4. Allowable stress in compression used for calculations = -15,000 kN/m²
5. Allowable stress in tension used for calculation = -1000 kN/m²

It should be noted that the allowable stresses used for calculations have a certain allowance for any effects that cannot be taken into account accurately at the preliminary design stage.

As soon as the trial section is selected, it is necessary to check whether it can satisfy the minimum section required. This must ensure adequate behaviour at both the working loads and ultimate loads. Thus, a bending moment envelope should be developed taking account of dead, superimposed dead and live loads. For the bending moments due to dead loads, it is necessary to consider both as built and monolithic bending moment diagrams. As soon as the bridge is built, the dead load bending moments are given by the as-built bending moment diagram. However, this changes towards the monolithic (built at once) bending moment diagram due to long term creep defromations in concrete (Neville et al., 1981). Thus, a dead load bending moment envelope should be considered with as built and monolithic conditions as boundaries.

The resultant bending moment envelope for various loading conditions can be obtained by using a suitable method such as grillage analogy. For the design example, a shear flexible griallge, as shown in Figure 1, having two longitudinal beams representing the two webs and the associated flanges are used (Jaeger & Bakht, 1982). These are connected by using transverse members at 5.0 m intervals.

It is also considered that the bridge will be constructed by span by span construction technique with one span and 10m length of the next span being constructed in one operation. This can be illustrated as given in Figure 2. When the bending moment envelope is available, the global bending behaviour at working loads can be used to determine the section size required (lines 19 and 20 of the spread sheet).

Table 1: Dimensions selected for the box girder and the reasons for the selection

Dimension	Reason
Width of top flange = 10 m	To accommodate two lanes of width 3.5 m and two walkways of width 1.5 m.
Depth of the section = 2.1 m	A final depth of 2.1 which gives a span/depth ratio of 23.8 for the internal span
No of webs = 2	Two webs to minimise the number of webs (Podolny & Muller, 1982)
Width of webs = 0.35 m	A width of 0.35 m to anchoring of cables (Podolny & Muller, 1982)
Spacing of webs = 4.65 m	A centre to centre spacing of 5.0 m which gives a cantilever overhang of 2.325 m
Width of the bottom flange = 5.35 m	5.35 m with vertical webs
Thickness of bottom flange = 0.175 m	A thickness of 0.175 m which is the minimum to prevent horizontal cracks due to horizontal shear flow (Podolny & Muller, 1982)

In prestressed concrete beams, it is necessary to ensure that a Magnel diagram exist at all sections. Figure 3 shows a typical Magnel diagram for a beam subjected to a range of bending moments. Two pairs of lines originate from each of the Kern points ($e = -Z_1/A$ and $e = -Z_2/A$). One of each pair of lines relates to tensile stresses in the relevant extreme fibre, the other relates to compressive stresses in that fibre.

For the feasible region to exist, there must be a positive separation of the two bound lines emanating from each Kern points. This is equivalent to saying that the section must have elastic section moduli sufficiently large that the range of stresses caused by the range of applied moments are less than the range of stresses that the concrete can resist.

They can thus be expressed in the form:

$$Z_1 \leq \frac{M_b - M_a}{f_{tw} - f_{cw}} \quad (Z_1 \text{ is -ve}); \quad Z_2 \geq \frac{M_a - M_b}{f_{cw} - f_{tw}} \quad \text{eq -1, eq -2}$$

These expressions assume that the working load moments range govern the design, which is the case for the span by span construction technique considered in this paper. Therefore, the Z values required can be calculated as soon as the bending moment envelope is obtained. In a box girder, there are many ways of achieving the required Z values such as adjusting either the depth of the section or the thickness of the bottom flange or the width of the webs or the thickness of the top flange. The best option should give the required value of Z with the smallest cross sectional area. This is most likely to be the adjusting of the depth of the section. However, it is advisable to carry out a parametric study.

For the design example, the required value of Z_1 and Z_2 are -0.978 and 0.978 (eq. 1 and eq. 2), respectively at the most critical section, which is at the second internal support (lines 21 and 22 of the spread sheet). The minimum section selected with a depth of 2.0 m on the basis of guidelines explained in this paper gave Z_1 and Z_2 of -1.94 and 0.954. Thus, the initial section is not sufficient. A parametric study can be carried out as given in Table 2 in order to find the smallest possible section that gives the required section moduli. It can be seen that increasing the depth of the section to 2.1 m will give the smallest cross section while achieving the required Z values.

When the depth of the section is increased, there can be additional costs incurred by access roads resulting from more fill materials etc. If the depth is restricted and cannot be increased, then increasing the thickness of the bottom flange or the webs can be considered. In this particular example, depth is increased. Since the new section has a higher area than the initial section, the dead load bending moment envelope has to be re-evaluated. However, this is unlikely to affect the moment range drastically since it is primarily determined by the live loads.

Table 2: The results of parametric study for a spine beam having a top flange width of 10.0m and vertical webs.

Depth of section (m)	Thickness of a web (m)	Thickness of bottom flange (m)	Thickness of top flange (m)	Area of half section (m ²)	Z_1	Z_2
2.0	0.35	0.175	0.30	2.471	-1.940	0.953
2.0	0.35	0.200	0.30	2.525	-1.970	1.020
2.0	0.40	0.175	0.30	2.704	-1.945	0.982
2.0	0.35	0.175	0.35	2.540	-2.066	0.951
2.1	0.35	0.175	0.30	2.506	-2.079	1.025
2.1	0.35	0.200	0.30	2.560	-2.113	1.101
2.1	0.40	0.175	0.30	2.580	-2.085	1.050
2.1	0.35	0.175	0.35	2.738	-2.221	1.023

CRITERIA FOR THE SELECTION OF CABLE FORCES

Once the section is selected, an appropriate set of cable forces has to be selected. The cable forces can be either constant throughout the length of the beam or vary as appropriate. In both cases, it is advantageous to select the minimum cable force both in terms of cost and the need to accommodate all the ducts within the limited space available in the section.

When the cable forces are selected, whether constant or variable, it is possible to determine the line of thrust zone (e_p) along the beam. This also can be transformed to obtain the corresponding cable profile zone (e_s), when secondary moments (M_2) are known. The secondary moments should be selected so that the cable profile zone will lie within the section throughout the length. The relationship $e_s - e_p = \frac{M_2}{RP}$ can be used to find e_s when e_p , M_2 and P are known.

Any cable profile that fits within a line of thrust zone should be concordant; it should generate zero secondary moments. There is a unique condition for the existence of a concordant profile within a line of thrust zone (Burgoyne, 1987 (a)). This condition is valid irrespective of the type of cable forces; whether constant or variable. When a cable is fitted along the upper boundary of a line of thrust zone, it should generate hogging secondary moments. If a cable is fitted along the lower

boundary of the line of thrust zone, it should generate sagging secondary moments. It is only then that a profile can exist that will generate zero secondary moments.

The minimum cable force corresponds to the case where the cable at the upper boundary of the line of thrust zone generates zero secondary moments over all supports. This can be achieved for practical cases only if variable cable forces are used. The use of a constant prestressing force is most likely to make the secondary moments zero only at one internal support.

Determination of secondary moments

It is possible to determine the secondary moments in a beam once the cable profile and the cable forces are known by using the generalised Clark Maxwell's theorem as described by Burgoyne (1987 a). This theorem states that when two force systems act on a linear elastic structure, the work done by the forces of first system on the displacements of second system is equal to the work done by the forces of the second system on the displacements of the first system ($\sum P_i \Delta_{ii} = \sum P_{ii} \Delta_i$).

The first system consist of a set of fictitious moment system and associated reactions as shown in Figure 4 with one system at each internal support. The reactions R_{ik} are unknown, but need not be determined since they do not appear in the equations. The second system consist of the cable forces, corresponding secondary moments and associated reactions at the internal supports as shown in Figure 5. Due to cable forces and secondary moments, there is a curvature at each section given by $(\sum (\beta M_2)_j - RPe)/EI$. The support reactions resulting from cable forces are R_{jk} , but those need not be calculated since they appear at the supports where the displacements are zero in the first system. The application of the generalised Clark Maxwell's theorem results in Equation 3 from which $(M_2)_i$ can be canceled from the equation without loosing the generality, thus resulting in Equation 4.

$$\int \beta_i (M_2)_i \left(\sum_j \beta_j (M_2)_j - Pe \right) \frac{1}{EI} dx = 0 \quad \text{for } i = 2, 3, \dots, n-1 \quad \text{eq-3}$$

$$\sum_j (M_2)_j \int \frac{\beta_i \beta_j}{EI} dx = \int \frac{\beta_i Pe}{EI} dx \quad \text{for } i = 2, 3, \dots, n-1 \quad \text{eq-4}$$

The equations form a set of linear equations consisting of unknown secondary moments $(M_2)_j$. The cable profile, e , appears on the right hand side of the equations, and the coefficients of the $(M_2)_j$ terms are integrals of products of the β functions, many of which are zero since β_i is non zero only on either side of the support under consideration. The integration $\int \beta_i \beta_j dx$ results in simple expressions as indicated in the left hand side of the matrix notation given in equation 5 for a

prismatic section. The integral $\int \frac{\beta_i RPe dx}{EI}$ can be determined using numerical integration, preferably using the Simpson's rule, since the cable profile is known as a set of eccentricities with parabolic segments in between. In the spreadsheet given in Appendix A, the values of β factors and the Simpson's rule coefficients (s) have been indicated in lines 37, 38 and 39 of the spread sheet given in Appendix A. For each of the β coefficients, a row of $\beta.RP e.s$, have been prepared and then summed to give the totals shown at the end of the row. These values should be multiplied by $h/3$ as generally done in Simpson's rule summations where h is the interval considered for the cable eccentricities (5.0 m in this case). The matrix can now be inverted to obtain the unknown secondary moments.

$$\frac{1}{6} \begin{bmatrix} 2(L_1 + L_2) & L_2 & 0 & - \\ L_2 & 2(L_2 + L_3) & L_3 & - \\ 0 & L_3 & 2(L_3 + L_4) & - \\ - & - & - & - \end{bmatrix} \begin{bmatrix} (M_2)_2 \\ (M_2)_3 \\ (M_2)_4 \\ - \end{bmatrix} = \begin{bmatrix} \int \frac{\beta_2 R P e}{EI} \\ \int \frac{\beta_3 R P e}{EI} \\ \int \frac{\beta_4 R P e}{EI} \\ - \end{bmatrix} \quad \text{eq-5}$$

SELECTION OF MINIMUM CABLE FORCES

If the cable profile is concordant, the secondary moment at each support, (M_2) , should be zero. It is both a necessary and sufficient condition for this that the terms in the right hand side of equation 4 are all separately zero. Thus, a cable profile is concordant if

$$\int \frac{\beta_i P e dx}{EI} = 0 \quad \text{for all } i. \quad \text{eq-6}$$

In order to determine the minimum cable forces, this condition can be used. When the cable is fitted along the upper boundary, the cable position is given by the following equations with respect to the prestressing force P_B shown on the Magnel diagram given in Figure 3 :

When $P \leq P_B$

$$e_{p-\min} = \frac{-Z_2}{A} - \frac{Z_2 f_{tw}}{RP} + \frac{M_b}{RP} \quad \text{eq-7}$$

When $P \geq P_B$

$$e_{p-\min} = \frac{-Z_1}{A} - \frac{Z_1 f_{cw}}{RP} + \frac{M_a}{RP} \quad \text{eq-8}$$

Hence, the choice of governing equations for $e_{p-\min}$ depends only on the magnitude of the cable force in each region. It is shown later that there is no point in using a prestressing force greater than P_B . Hence, only equation 7 will determine the location of the cable at upper limits of e_p . It should be noted that these conditions are valid only if the secondary moments selected are large enough to ensure that the upper boundary of the cable profile zone will lie within the physical limits imposed by the dimensions (depth) of the concrete section.

The total cable force along a beam can be determined by $\int P ds$ where s is measured along the cable profile. In order to minimise the value of $\int P ds$, the following strategy can be adopted. It can be seen from equation 6 that the condition for zero secondary moment involve the function β which varies from zero to 1.0 and then to zero over a given support from either side. Therefore, it would be reasonable to suggest that the integral $\int \frac{\beta_i P e dx}{EI}$ is dominated by the value of P close to the support.

This can be exploited in the following manner to find suitable minimum cable forces along the beam. It is considered that cable forces will be changed on either side of an internal support.

In order to minimise the total prestress, the cable forces over supports should be maximised and those in the span regions should be minimised. However, this should be done while satisfying the condition that a valid cable profile zone exist in the span regions. Thus, the minimum cable force that can ensure that there is a sufficient cable profile zone at the span critical section can be first found for each span region. Then, the corresponding prestressing forces should be found over the internal supports. If those values are less than P_B , then it is satisfactory. If the required prestressing cannot be provided with values below that given by P_B , then select a value close to P_B over the supports. Then adjust the prestressing forces in span regions until the condition for the existence of a concordant profile is satisfied. In either way, the cable forces selected will represent the least values that can be selected with the given number of cable force change points, thus leading to lowest for $\int Pds$.

This method of selecting cable forces is valid only if the upper boundary of the cable profile zone will lie within the physical limits imposed by the depth of the section. Otherwise the method explained by Jayasinghe (1992) has to be used.

In the design example, $P_B = 37145$ kN. The cable forces selected above first and second internal supports are 30,000 kN and 37000 kN respectively. At the second internal support, it was found that a cable force should be close to P_B . At the first internal support, the cable forces selected for the span regions on either side to allow a sufficient cable profile zone, allowed the use of a lower value than P_B of 30,000 kN. The corresponding cable forces in the span regions are 20,000 kN, 26,000 kN and 23,000 kN. The latter two values are not the lowest that can be used for those two spans, but have been appropriately increased to ensure the existence of a concordant profile. The secondary moments caused by these forces with the cable at upper limit of the line of thrust zone are -137.0 kNm and -6.0 kNm; these are sufficiently close to zero. This results in $\int Pds$ of 3,417,615. When this value is divided by the length of the beam, the corresponding average prestress can be determined. It is $3,417,615/130.0 = 26,289$ kN. If a constant prestressing force is used, the minimum cable force that can be used is 31000 kN. This will result in $\int Pds$ value of 4,035,260. The corresponding average value is 31,040 kN. Thus, the use of variable cable forces can lead to a reduction of about 15% for the total prestressing force in this particular design example.

Importance of P_B for the existence of a cable profile

In order to show the importance of P_B , a closer look at the function, $P \times e$, (cable force \times eccentricity) can be taken. For the existence of a cable profile, $\int \frac{\beta_i P e dx}{EI}$ should be zero at each support. Since the cable is draped below the neutral axis in the span region, this function is positive. Thus, over the supports, this function should be as small as possible. The variation of $P \times e$ can be evaluated as follows:

When $P \leq P_B$

$$e_{p-\min} = \frac{-Z_2}{A} - \frac{Z_2 f_{tw}}{RP} + \frac{M_b}{RP} \quad \text{eq. 9}$$

$$\frac{d(Pe_{p-\min})}{dP} = \frac{-Z_2}{A}; \text{ as } P \text{ increases, } Pe_{p-\min} \text{ decreases (since } Z_2 > 0)$$

When $P \geq P_B$

$$e_{p-\min} = \frac{-Z_1}{A} - \frac{Z_1 f_{cw}}{RP} + \frac{M_a}{RP} \quad \text{eq. 10}$$

$$\frac{d(Pe_{p-\min})}{dP} = \frac{-Z_1}{A}; \text{ as } P \text{ increases, } Pe_{p-\min} \text{ increases (since } Z_1 < 0)$$

This means that there is no point in increasing the value of P beyond P_B , since the function increases. This is in contrary to the requirement. Thus, P_B , which is a unique value for a given prismatic section irrespective of the moments acting on it, can be considered as a maximum value when selecting the cable forces over the supports.

SELECTION OF SECONDARY MOMENTS

After selecting the minimum section on the basis of global bending behaviour, Magnel diagrams can be drawn along the beam. If the line of thrust zone given by Magnel diagram over critical sections (in this case the support sections) lies outside the physical limits imposed by the need for cover to the cable with the selected prestressing forces, there are two options available for the designer. He can either use the secondary moments to change the location of the Magnel diagram (lower it over the supports) so that it will lie below the physical limits. On the other hand, he can go for a larger section. The first option is better since the minimum section already selected can be used. The magnitude of the secondary moments can be selected as a percentage of the as built dead load moments. Any value between 0% and 90% could be feasible. A higher secondary moment will give a greater clearance over the supports for the cable profile zone and also ensure that the minimum cable force calculated as described above is valid.

Tests by Mattock et al. (1971) and Cohn & Frostig (1983) have shown that for all practical purposes, the beam acts as though secondary moments are present right up to failure. It is therefore valid to include secondary moments when determining the required ultimate moment capacity. This is particularly of importance when considering the resistance to hogging moments over the piers, since secondary moments are normally sagging, and they reduce the required ultimate moment capacity.

CABLE PROFILE FOR VARYING CABLE FORCES

If a constant prestressing force is used, it is quite straight forward to find a cable profile that will generate the assumed secondary moments. This can be achieved in the following way:

1. Find the line of thrust zone corresponding to the cable profile zone by using the relationship $e_p = e_s - M_2/(RP)$.
2. Fit a concordant profile into the line of thrust zone. Then transfer the concordant profile back into the cable profile zone using the relationship $e_s = e_p + M_2/RP$. This will not only fit within the bounds of the cable profile zone, but will also generate the assumed secondary moments.

Thus, the main task of finding the appropriate cable profile will be the determination of a concordant profile which fit within the bounds of a line of thrust zone; for this, use is made of an important property of concordant profiles. Any bending moment diagram due to a set of loads acting on the beam can be scaled to form a concordant profile. Hence the determination of a concordant profile is a matter of finding an appropriate distribution of 'notional loads', which give rise to a suitable bending moment. It is shown by Burgoyne (1987 b) that this process can be automated, if necessary, when a constant cable force is acting.

When the cable forces vary, there is an additional set of forces and moments that will act at the cable force change points. When a cable starts at a given point away from the centroid of a section with an inclination, it can give rise to a point force and a moment. When selecting the location of anchor blocks, the designer has to ensure that the centroid of the new cable and the running cable should lie within the bounds of the cable profile zone. Thus, it would be worthwhile to determine the limits on eccentricity for the new cables prior to selecting the actual locations. This method is explained later.

When the cable forces vary, the concordant profile should be a result of two sets of loads. Those are the 'notional loads' and a set of known forces and moments at sections that the cable forces change. Since it will be cumbersome to combine these two, there is an easy alternative. That is to modify the line of thrust zone using the bending moment diagram that results due to the known point forces and bending moments. Thus, the design process can be presented as follows:

1. Select the location of anchor blocks and the inclination of new cables.
2. Obtain a force x eccentricity ($RP \times e$) zone by multiplying the limits of line of thrust zone by the cable force in each region.
3. Modify this by using the inverse of the bending moment diagram that results due to point forces and moments that act at the change over points.
4. Find a set of 'notional loads' that will give a bending moment diagram which fits within the modified force eccentricity zone.
5. Modify this bending moment diagram with the bending moment diagram due to point forces and moments. Transform this into the cable profile zone.

The resulting cable profile will not only satisfy the bounds on the cable profile, but also generate the assumed secondary moments. This process can be illustrated by using the design example.

Figure 6 shows the cable profile zone corresponding to the cable forces selected along with the actual cable profile selected. It can be seen that it is discontinuous at the places where the cable forces change. The corresponding force eccentricity zone is shown in Figure 7. This has discontinuities at cable force change points. Only the discontinuity at a chainage of 100 m is not allowing a continuous smooth cable. This means that only this point will need some adjustment for the moment.

The eccentricities selected and the corresponding vertical forces and point moments are given in Table 3. These will result in a bending moment diagram of the shape shown in Figure 8. Figure 9 shows the modified force eccentricity zone with the bending moment diagram resulting due to a set of notional loads. This can be transformed back into the actual cable profile as shown in Figure 6.

Table 4 gives a comparison of the assumed secondary moments and those generated. The loss ratio is 0.7.

Table 3: Vertical forces and point moments at cable force change points

Cable force change point	1	2	3	4
Chainage (m)	30	50	80	100
Force in new cable (kN)	10,000 x 0.7	4000 x 0.7	11,000 x 0.7	14,000 x 0.7
Eccentricity (m)	0	0	0	-0.2
Angle with horizontal	2°	2°	2°	2°
Point force (kN) ↑	244	97	268	341
Moment(anticlockwise +)	0	0	0	1960

Table 4: Secondary moments selected and those which actually occur

Location	Selected secondary moments (kNm)	Actual secondary moments due to the cable selected (kNm)
First internal support	7967	7976
Second internal support	7114	7136

FORCES AND MOMENTS AT CABLE FORCE CHANGE POINTS

The situation at a point where the cable force changes due to start of a new cable can be visualised as shown in Figure 10. If $P_{r(i)}$ is the force in the running cable, $P_{n(i)}$ is the force in the new cable, then on the left of i^{th} change point, the cable force is $P_{r(i)}$ and on the right, it is $P_{r(i)} + P_{n(i)}$. The centroid of total $P_{r(i)} + P_{n(i)}$ will represent the location of the resultant cable profile. This situation is equivalent to the application of a point moment equal to $P_{n(i)} e_{sn(i)}$ and a vertical force equal to $P_{n(i)} \sin \alpha_{n(i)}$ at the location where a new cable starts. The quantities $e_{sn(i)}$ (positive downwards) is the eccentricity of the new cable and $\alpha_{n(i)}$ is the inclination at which the new cable is started.

Limits on eccentricity

Since the cable forces have already been selected, the anchors cannot be placed at any eccentricity within the section. There are maximum and minimum eccentricities that are imposed by the shape that the cable profile can possibly take at the change points. These shapes can be visualised in terms of the force eccentricity zone and the bending moment diagram which fits into it as shown in Figures 11 and 12.

Figure 11 shows that the cable is placed at $e_{p-\min}$ to the left of anchor point and $e_{p-\max}$ to the right of it, which gives a maximum moment. Maximum moment that can act at this point is $[P_{r(i)} + P_{n(i)}]e_{p-\max} - P_{r(i)} e_{p-\min}$. The corresponding maximum eccentricity at this point is $\{[P_{r(i)} + P_{n(i)}]e_{p-\max} - P_{r(i)} e_{p-\min}\}/P_{n(i)}$. The inclination of the cable is ignored.

Figure 12 shows that the cable is placed at $e_{p-\max}$ to the left of anchor point and $e_{p-\min}$ to the right of it. This gives rise to a minimum moment. Minimum moment that can act at this point is $[P_{r(i)} + P_{n(i)}]e_{p-\min} - P_{r(i)} e_{p-\max}$. The corresponding maximum eccentricity at this point is $\{[P_{r(i)} + P_{n(i)}]e_{p-\min} - P_{r(i)} e_{p-\max}\}/P_{n(i)}$. The inclination of the cable is ignored. When the location of anchors are selected, the point moments should be in between these two minimum and maximum values.

CONCLUSIONS

A design method, that guides the designer with a logically evolving series of design decisions is presented. The main advantage of this design method is that the designer has the opportunity to select the section dimensions of the box girder by considering the governing criterion for each component such as top flange, webs and the bottom flange. A simple parametric study can be used to determine the smallest section that can be used.

It is shown that there is a unique criterion to satisfy the existence of a concordant profile within the line of thrust zone. This condition can be used to determine the minimum cable force that can be used. Then, the designer will be able to select suitable secondary moments that will ensure that the cable profile zone will lie inside the section throughout the length of the beam.

The use of minimum total cable forces for a prismatic beam is advantageous with respect to minimising the cost of construction. It is shown that when variable cable forces are used, the cable force over the support should not exceed a maximum value that can be derived for a given section. It is also necessary to ensure that the selected cable forces will ensure the existence of a cable profile zone at each cross section. A simple design method that can be easily followed by the designer to satisfy all the above conditions is presented. This allows the selection of a suitable set of cable forces that can lead to a minimum total cable force.

Once the cable forces are selected, a suitable cable profile should be found. This should not only satisfy the stress limits, but also should generate the secondary moments selected earlier in the design process. When the cable forces vary, there are additional constraints due to point loads and moments due to cable anchorages. It is shown that the designer can modify the force eccentricity zone by using the effects of point loads and point moments acting at the cable force change points. Then a concordant cable profile can be fitted to this modified force eccentricity zone by using a suitable set of notional loads.

Thus, this design method allows the designer to use the smallest possible cross section with minimum prestressing force, while satisfying other criteria like constructability, long term behaviour and stress limits. The design method given for selecting the minimum cable force can be used for any section which is larger than the smallest given by the moment range. Therefore, this method can be used for generating a number of alternative solutions, for which the best can be selected on the basis of an overall cost analysis. This is of particular advantage in competitive bidding where the optimum designs are most likely to be successful. It is shown with a design example that all these calculations can be carried out using a suitable structural analysis program and a simple spreadsheet that can be prepared by the designer himself.

REFERENCES

- BS 5400/2 (1978), Code of practice for Design of Concrete Bridge, British Standards Institution, BS 5400, Part 2, London.
- BS 5400/4, (1984), Code of practice for Design of Concrete Bridge, British Standards Institution, BS 5400, Part 4, London.
- Burgoyne, C.J. (1987 a), "Cable design for continuous prestressed concrete bridges", Proc. Instn. Civ. Engrs., Part 2, Vol 85, pp. 161-184.

Burgoyne, C.J. (1987 b), "Automated determination of concordant profiles", Proc. Instn. Civ. Engrs., Part 2, Vol 85, pp. 333-352.

Cohn, M. Z., Frostig, Y. (1983), Nonlinear analysis of continuous prestressed concrete beams, Procs, Int. Symp. on Nonlinearity and Continuity in Prestressed Concrete, Vol 2: Hyperstatic structures: Nonlinear analysis, 45-76, Waterloo, Ontario, Canada.

Gee, A.F. (1987), "Bridge winners and losers", The Structural Engineer, Vol 65A, No. 4, pp 141-145.

Jaeger, L.G. & Bakht, B. (1982), "The grillage analogy in bridge analysis", Canadian Journal of Civil Engineering, Vol 9, No. 2, June, pp 224-235.

Jayasinghe, M. T. R. (1992), "Rationalisation of prestressed concrete spine beam design philosophy for expert systems", Ph.D. Thesis, Department of Engineering, University of Cambridge, United Kingdom, p 234.

Mattock, A. H., Yamazaki, J & Kattula, B. T. (1971), "Comparative study of prestressed concrete beams, with and without bond", ACI Journal, 68/2, 116-125.

Neville, A.M., Dilger, W.H., Brooks, J.J. (1983), *Creep of plain and structural concrete*, Construction press, London.

Podolny, W. & Muller, J.M. (1982), *Construction and design of prestressed concrete segmental bridges*, John Wiley & Sons, New York.

Ranasinghe, W. M. D. N., Jayasinghe, M. T. R. (1998), "A design method for prismatic prestressed continuous box girder bridges", Proc. Research for Industry - 1998, University of Moratuwa, Sri Lanka, pp 52-68.

Swann, R.A. (1972), "A feature survey of concrete box spine-beam bridges", Technical Report 469, Cement and Concrete Association, London, 1972.

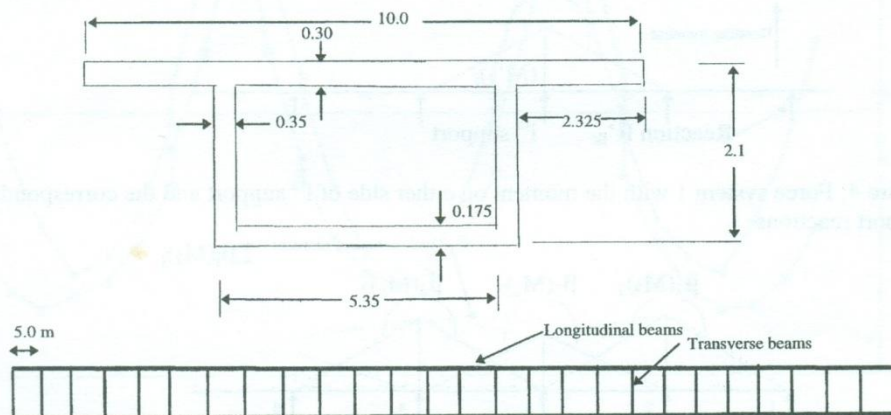


Figure 1: Cross section used for the design example and the grillage model used

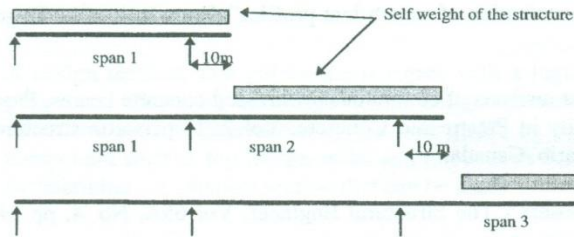


Figure 2: Loading due to self weight at as built condition

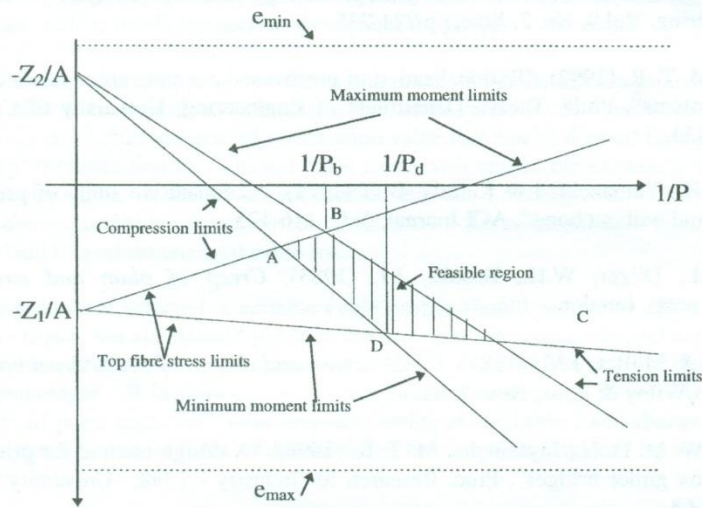


Figure 3: Magnel diagram showing governing conditions and the corresponding prestressing forces

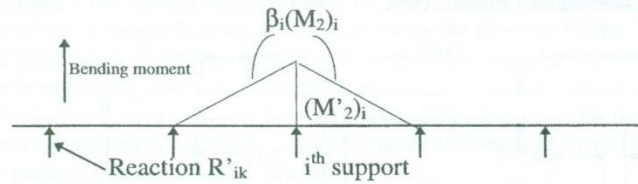


Figure 4: Force system 1 with the moment on either side of i^{th} support and the corresponding support reactions

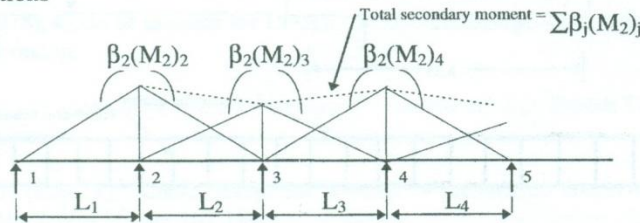


Figure 5: Force system 2 - Secondary moment at j^{th} support

Figure 6: Cable profile with varying prestressing forces and the upper and lower bounds of cable profile zone

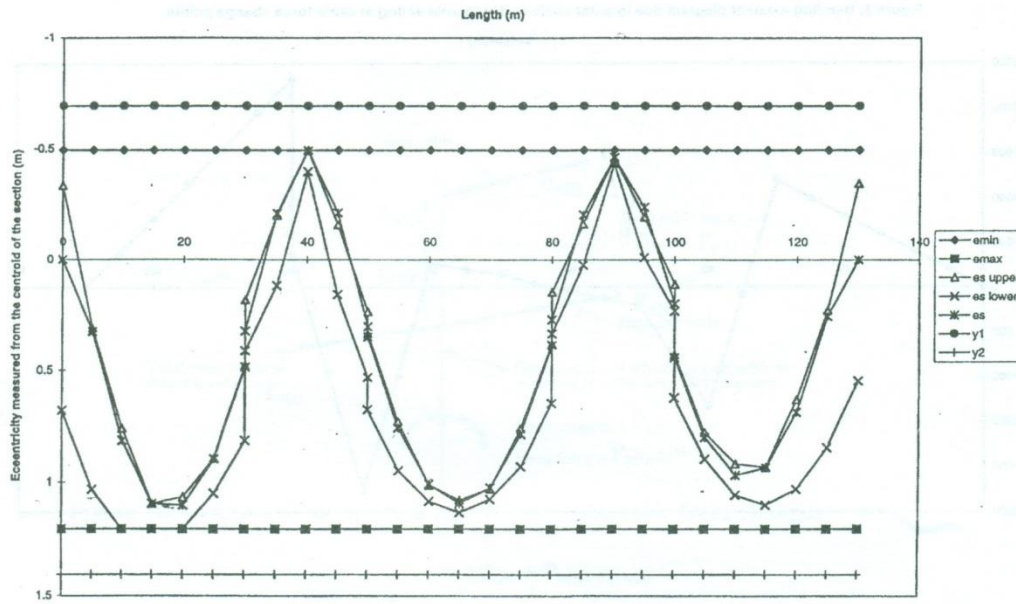


Figure 7: Force eccentricity zone due to force x eccentricity (ep)

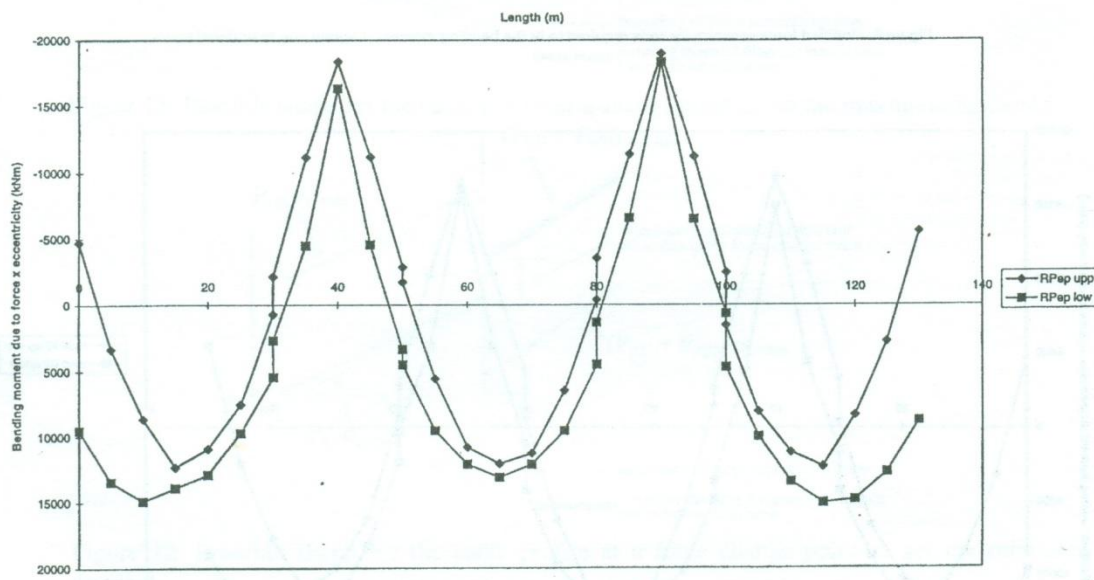


Figure 8: Bending moment diagram due to point loads and moments acting at cable force change points

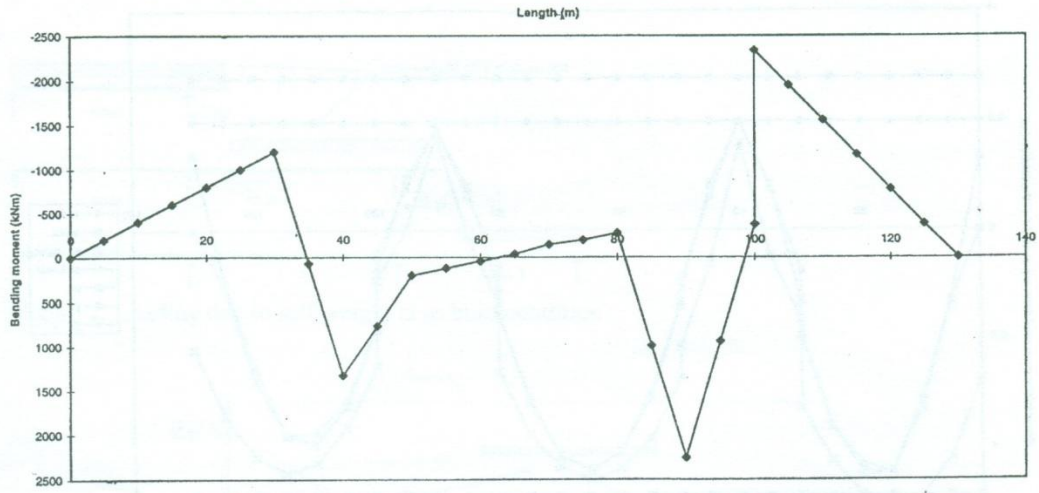
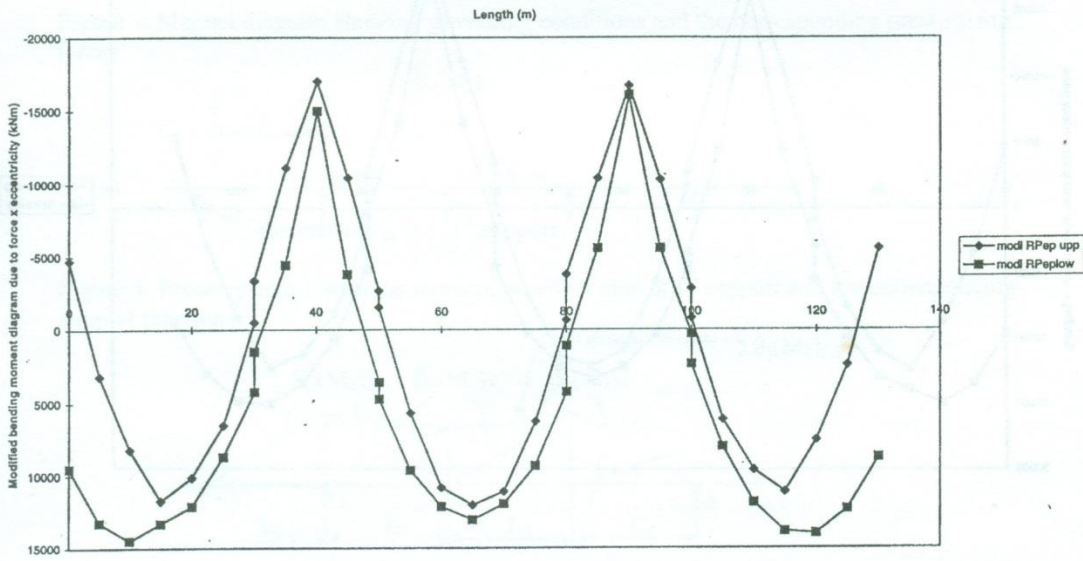


Figure 9: Modified force eccentricity zone required to fit the bending moment diagram due to notional loads



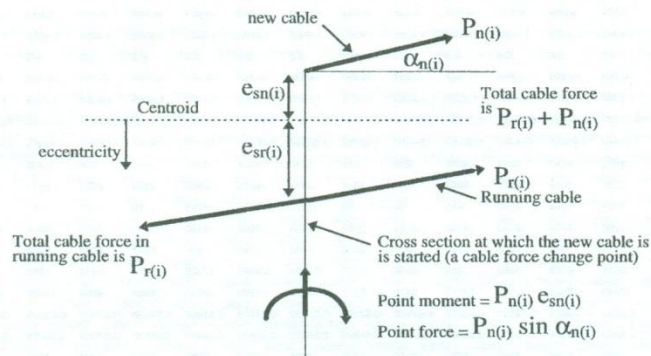


Figure 10: Forces and moments at a point where the cable force changes

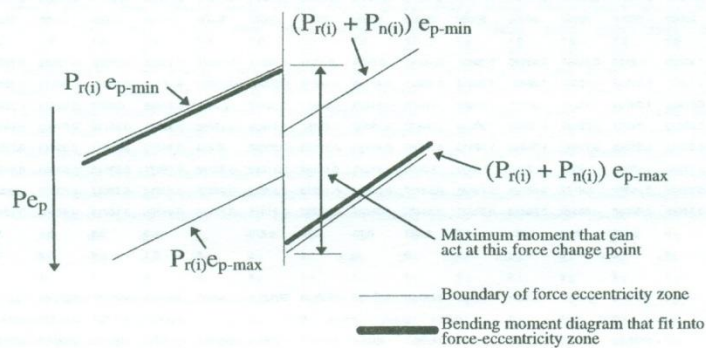


Figure 11: Possible shape for the cable profile at a change point to get the maximum moment

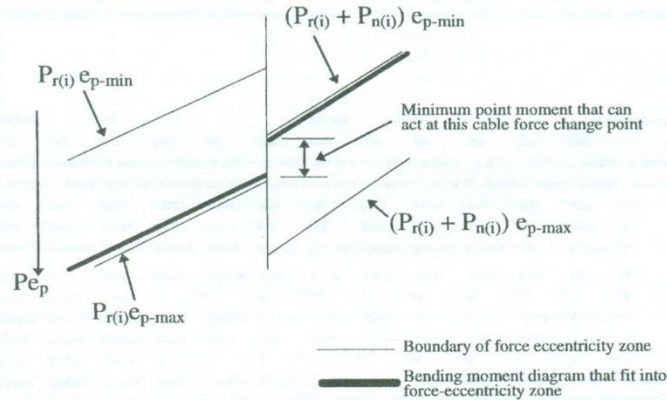


Figure 12: Possible shape for the cable profile at a force change point to get the minimum moment

1	chainage	0	5	10	15	20	25	30	30	35	40	45	50	50	55	60
2	f _{0w}	-15000	-15000	-15000	-15000	-15000	-15000	-15000	-15000	-15000	-15000	-15000	-15000	-15000	-15000	-15000
3	f _{1w}	-1000	-1000	-1000	-1000	-1000	-1000	-1000	-1000	-1000	-1000	-1000	-1000	-1000	-1000	-1000
4	l ₀	1.44	1.44	1.44	1.44	1.44	1.44	1.44	1.44	1.44	1.44	1.44	1.44	1.44	1.44	1.44
5	A ₀	2.5063	2.5063	2.5063	2.5063	2.5063	2.5063	2.5063	2.5063	2.5063	2.5063	2.5063	2.5063	2.5063	2.5063	2.5063
6	depth of sec	2.1	2.1	2.1	2.1	2.1	2.1	2.1	2.1	2.1	2.1	2.1	2.1	2.1	2.1	2.1
7	y ₁	-0.694	-0.694	-0.694	-0.694	-0.694	-0.694	-0.694	-0.694	-0.694	-0.694	-0.694	-0.694	-0.694	-0.694	-0.694
8	y ₂	1.4065	1.4065	1.4065	1.4065	1.4065	1.4065	1.4065	1.4065	1.4065	1.4065	1.4065	1.4065	1.4065	1.4065	1.4065
9	cover	0.2	0.2	0.2	0.2	0.2	0.2	0.2	0.2	0.2	0.2	0.2	0.2	0.2	0.2	0.2
10	emin	-0.494	-0.494	-0.494	-0.494	-0.494	-0.494	-0.494	-0.494	-0.494	-0.494	-0.494	-0.494	-0.494	-0.494	-0.494
11	emax	1.2065	1.2065	1.2065	1.2065	1.2065	1.2065	1.2065	1.2065	1.2065	1.2065	1.2065	1.2065	1.2065	1.2065	1.2065
12	z ₁	-2.07493	-2.07493	-2.07493	-2.07493	-2.07493	-2.07493	-2.07493	-2.07493	-2.07493	-2.07493	-2.07493	-2.07493	-2.07493	-2.07493	-2.07493
13	z ₂	1.02382	1.02382	1.02382	1.02382	1.02382	1.02382	1.02382	1.02382	1.02382	1.02382	1.02382	1.02382	1.02382	1.02382	1.02382
14	M monoi	0	3718	5933	6644	5851	2555	-245	-245	-5549	-12357	-5590	-326	-326	3432	5688
15	M as built	0	4018	6532	7543	7050	5053	1551	1551	-3453	-9959	-2966	2523	2523	6510	8992
16	M sup dead	0	853	1361	1524	1342	815	-56	-56	-1273	-2835	-1282	-75	-75	787	1305
17	M live min	0	-633	-1266	-1900	-2533	-3166	-3799	-3799	-4433	-7905	-4456	-3015	-3015	-2604	-2803
18	M live max	0	3183	5450	7962	7235	6349	3915	3915	1102	1125	607	2247	2247	4668	6920
19	Ma(aci)	0	3938	8028	6268	4660	204	-4100	-4100	-11255	-23097	-11328	-3416	-3416	1615	4190
20	Mb(aci)	0	8054	13343	17029	15627	12217	5410	5410	-3624	-11669	-3641	4695	4695	11965	17217
21	Z1 required	0	-0.294	-0.5225	-0.76864	-0.78336	-0.85807	-0.67929	-0.67929	-0.54507	-0.81629	-0.54907	-0.57936	-0.57936	-0.73929	-0.9305
22	Z2 required	0	0.294	0.5225	0.76864	0.78336	0.85807	0.67929	0.67929	0.54507	0.81629	0.54907	0.57936	0.57936	0.73929	0.9305
23	M2	0	995	1991	2987	3980	4975	5970	5970	6965	7967	7882	7797	7797	7712	7627
24	Ma	0	4933	8019	9255	8640	5179	1870	1870	-4290	-15130	-3446	4381	4381	9327	11817
25	Mb	0	9049	15334	20016	19607	17192	11380	11380	3341	-3702	4241	12492	12492	19677	24844
26	Pmax allow	37144.9	37144.9	37144.9	37144.9	37144.9	37144.9	37144.9	37144.9	37144.9	37144.9	37144.9	37144.9	37144.9	37144.9	37144.9
27	Ptrial	20000	20000	20000	20000	20000	20000	20000	20000	30000	30000	30000	30000	30000	26000	26000
28	R	0.7	0.7	0.7	0.7	0.7	0.7	0.7	0.7	0.7	0.7	0.7	0.7	0.7	0.7	0.7
29	es upper 1	-1.38525	-0.7489	-0.29997	0.03446	0.00525	-0.16725	-0.5824	-0.1123	-0.49511	-0.83049	-0.45225	-0.05935	-0.19585	0.19693	0.48283
30	as upper 2	-0.33537	0.31099	0.75992	1.09435	1.06513	0.89263	0.47749	0.18216	-0.20065	-0.53603	-0.15779	0.23511	0.33413	0.72891	1.01281
31	es lower 1	0.67968	1.03203	1.25246	1.34075	1.29682	1.0496	0.81325	0.81813	0.52479	0.0086	0.56498	0.9377	0.96459	1.22635	1.36316
32	es lower 2	0.68845	1.04081	1.26124	1.34952	1.30559	1.06838	0.82202	0.41185	0.11852	-0.39768	0.15871	0.53142	0.67602	0.94778	1.08459
33	es upper	-0.33537	0.31099	0.75992	1.09435	1.06513	0.89263	0.47749	0.18216	-0.20065	-0.494	-0.15779	0.23511	0.33413	0.72891	1.01281
34	es lower	0.67968	1.03203	1.2065	1.2065	1.0496	0.81325	0.41185	0.11852	-0.39768	0.15871	0.53142	0.67602	0.94778	1.08459	1.08459
35	ep upper	-0.33537	0.32992	0.6177	0.88099	0.78085	0.53727	0.05106	-0.10213	-0.53232	-0.87338	-0.53313	-0.13617	-0.09428	0.30517	0.59374
36	ep lower	0.67968	0.96096	1.06429	0.99314	0.92221	0.69425	0.38682	0.12756	-0.21315	-0.77706	-0.21663	0.16013	0.24762	0.52404	0.66553
37	beta1	0	0.125	0.25	0.375	0.5	0.625	0.75	0.75	0.875	1	0.9	0.8	0.8	0.7	0.6
38	beta2	0	0	0	0	0	0	0	0	0	0	0.1	0.2	0.2	0.3	0.4
39	s	1	4	2	4	2	4	1	1	4	2	4	1	1	4	2
40	beta1ep up	0	1679.42	432.92	18500.8	10931.8	18804.6	536.137	-1608.48	-39125.2	-36682	-40304.3	-2287.71	-1372.67	15551.6	12967.4
41	beta2ep up	0	0	0	0	0	0	0	0	0	0	-4478.25	-571.927	-343.188	6664.99	8644.93
42	beta1ep lo	0	6726.73	7450	20856	12911	24298.7	4061.6	2009.11	-15666.6	-32638.4	-16377.1	2690.25	3605.29	28705.3	14535.1
43	beta2ep lo	0	0	0	0	0	0	0	0	0	0	-1819.67	672.563	901.322	11445.1	9690.09
44	RPep upp	-4695.15	3358.65	8647.85	12333.8	10931.8	7521.85	714.849	-2144.64	-11178.6	-18341	-11195.6	-2858.64	-1715.84	5554.16	10806.2
45	RPep low	9515.46	13453.5	14900	13904	12911	9719.48	5415.46	2578.82	-4476.18	-16318.2	-4549.18	3362.82	4506.61	9537.61	12112.6
46	min mom to be applied							0							0	
47	corres eccentricity							0							0	
48	Eccentricity selected							0							0	
49	corresponding moment							0							0	
50	corres vert force with 2 deg incl to horizontal							244.173							97.6691	
51	mom pol io,mo	0	-200	-400	-600	-800	-1000	-1200	-1200	69	1330	770	201	201	122	43
52	modi RPep up	-4695.15	3158.65	8247.85	11733.8	10131.8	6521.85	-485.151	-3344.64	-11109.6	-17011	-10425.6	-2658.64	-1514.84	5676.16	10849.2
53	modi RPep lo	9515.46	13253.5	14500	13304	12111	8719.46	4215.46	1478.82	-4407.18	-14988.2	-3779.18	3563.82	4707.61	9559.61	12155.6
54	concord	0	3366	9008	11738	10643	6572	-386	-386	-11294	-16990	-11558	-1238	-1238	6206	10763
55	RPep actual	0	3596	9408	12338	11443	7572	814	814	-11363	-18320	-12328	-1439	-1439	6084	10720
56	epactual	0	0.25471	0.672	0.88129	0.81736	0.54086	0.05814	0.03876	-0.5411	-0.87238	-0.58705	-0.06852	-0.07907	0.33429	0.58901
57	beta1ep RPs	0	1783	4704	18507	11443	18930	610.5	610.5	-39770.5	-36640	-44380.8	-1151.2	-1151.2	17035.2	12864
58	beta2ep RPs	0	0	0	0	0	0	0	0	0	0	-4931.2	-287.8	-287.8	7300.8	8578
59	es actual	0	0.32579	0.81421	1.09464	1.10164	0.89621	0.48457	0.32305	-0.20943	-0.493	-0.21171	0.30276	0.34934	0.75802	1.00808
60	beta1es	0	2280.5	5699.5	22987.5	15423	31367.5	5088	5088	-15393	-20706	-16005.6	5086.4	5086.4	38628.8	22016.4
61	beta2es	0	0	0	0	0	0	0	0	0	0	-1778.4	1271.6	1271.6	16555.2	14677.8
62	f _{1w} >	-5585.92	-1202.33	-1742.47	-1004.05	-1499.26	-1048.98	-1096.84	-3889.81	-819.924	-1882.61	106.021	-2387.59	-1270.4	-1517.52	-915.846
63	f _{1w} >	-5585.92	-5755.21	-3956.95	-2660.52	-2316.89	-2034.96	-3217.65	-6010.61	-8430.94	-6076.64	-8860.83	-7426.08	-6308.9	-5107.89	-4114.6
64	f _{1w} <	-5585.92	-7748.89	-7482.37	-7846.72	-7602.38	-7824.58	-7800.94	-10583.9	-12108.7	-11584.3	-12565.5	-11335.1	-10217.9	-10096	-10392.9
65	f _{1w} <	-5585.92	-5222.58	-8887.29	-11514.7	-12211.1	-12782.5	-10385.6	-13178.6	-8273.4	-13044.8	-7402.15	-10309.9	-9192.71	-11626.7	-13639.8
66	f _{1w} max	-5585.92	-1202.33	-1742.47	-1004.05	-1499.26	-1048.98	-1096.84	-3889.81	-819.924	-1882.61	106.021	-2387.59	-1270.4	-1517.52	-915.846
67	f _{1w} min	-5585.92	-7748.89	-7482.37	-7846.72	-7602.38	-7824.58	-7800.94	-10583.9	-12108.7	-11584.3	-12565.5	-11335.1	-10217.9	-10096	-10392.9
68	total prestre		100212	100476	100157	100000	100064	100338		150848	150241	150237	150792		130434	130162
69																
70	M22 UPP=	-136.753		M22 LOWER =		4960.11										
71	M23 UPP=	-6.44172		M23 LOWER =		3561.86										
72																
73	M22 actual	7976.26		M22 selected		7967										
74	M23 actual	7135.96		M23 selected		7114										

115

PREDICTION OF COMPRESSIVE STRENGTH OF CONCRETE

S.M.A. Nanayakkara

Dept. of Civil Engineering, University of Moratuwa

PREDICTION OF COMPRESSIVE STRENGTH OF CONCRETE

S.M.A. Nanayakkara

Dept. of Civil Engineering, University of Moratuwa

ABSTRACT

This report presents a method of predicting the compressive strength of concrete. The approach is based on experimental investigation of compressive strength development of four mix proportions with three different brands of cement. The criterion used for the prediction of strength involves the determination of equivalent age of concrete, which depends on curing temperature and age of concrete. It was found that the compressive strength of concrete varies linearly with respect to the logarithmic value of the equivalent age. Furthermore, it was observed that the rate of change of strength with respect to logarithmic value of equivalent age varies non-linearly with respect to w/c ratio. This variation was not the same for all cement brands tested. Expressions were derived for compressive strength for each brand of cement with respect to w/c ratio, age and curing temperature. Based on these expressions, a chart was developed to establish the relationship between strength and w/c ratio for a range of strength grades. This chart can be used in mix design of concrete using local materials. Since it was not possible to develop a unique expression for the prediction of compressive strength of concrete in terms of mix design parameters such as w/c for any cement brand, the identified behaviour of the strength development of concrete with respect to equivalent age was used in predicting strength of concrete. In the proposed method, the 28-day strength can be predicted with strength results at two ages such as 1-day and 3-day strengths. Good agreement with the predicted and experimental results have been obtained not only for test results obtained under this study but also for other published test data.

INTRODUCTION

The strength developed by concrete made with given materials and given proportions increases for many months under favourable conditions, but in the majority of specifications the strength is specified at the age of 28 days. It is a common practice to continue construction during this 28-day period and by the time the 28-day strength is known, a considerable amount of construction may have been carried out. If the 28-day strength of concrete does not meet the specified strength then the remedial actions will be extremely difficult and costly due to progress of construction work. In such situations, prediction of compressive strength of concrete, specially the 28-day strength is very important to detect first sign of change in the 28-day strength and to make necessary changes to the mix proportion to restore the expected 28-day strength. Early prediction of the 28-day strength can save lot of money if concrete strength does not meet the required strength. On the other hand, prediction of concrete strength will also help the contractor to make decisions such as when the concrete is strong enough for the removal of formwork, when slabs can be used without damage, and when the construction load can be applied. Furthermore, it would be useful for quality control purposes at ready-mixed concrete plants.

Many researchers have investigated methods of predicting concrete strength using various testing procedures and conducting laboratory experiments [1,2,3,4]. Some investigators used properties of fresh concrete to predict early age strength based on

statistical analysis [2]. In addition, several attempts have been made to relate concrete strength to its age and curing temperature [3,4].

The main objective of this research is to predict the 28-day compressive strength of concrete in terms of early age strength of concrete, which is easily measurable in the field.

EXPERIMENTAL INVESTIGATION

Based on the literature survey[1,2,3,4], it was decided to investigate the strength development of concrete for a period of 28 days for different grades of concrete under different curing temperatures. Also the effect of source of cement (brand of cement) on strength development of concrete was also investigated.

Concrete Mixes

The physical properties of aggregates were determined in accordance with relevant BS specifications[5] and given in Table 1. Concrete mixes for four different grades (i.e. Grade 20, 25, 30, and 50) were designed based on DoE method[6]. Table 2 gives the mix proportion for all mixes. Three OPC cement brands available in the local market were selected for this study. This selection was based on the fact that these brands have been widely used in the local construction industry.

Table 1 Physical properties of aggregates

Aggregate	Property		
	Relative Density (SSD)	Bulk density (kg/m ³)	Water absorption (%)
Fine	2.65	1636	0.52
Coarse	2.76	1608	0.19

Table 2 Mix Proportions (per 1m³)

Mix No.	Grade	Cement (kg)	Water (kg)	Fine Aggregate (kg)	Coarse Aggregate (kg)	W/C
1	20	282.33	181.03	834.53	1176.67	0.64
2	25	316.67	183.64	747.00	1129.40	0.58
3	30	380.00	183.67	731.42	1176.12	0.48
4	50	423.70	184.28	675.71	1165.70	0.43

Testing Procedure

Twelve test cubes of 150mm×150mm×150 mm were cast from each mix proportion and for each cement brand to obtain compressive strength at the ages 1 day, 3 days, 7 days and 28 days. The slump and the compacting factor were determined for each

batch in accordance with BS specifications [7]. This procedure was repeated for all three cement brands and the four mix proportions. Thus a total of 144 cubes were cast.

The cubes were tested in accordance with BS 1881: Part 4: 1970 after curing under laboratory conditions for the required period. The temperature of the curing tank was recorded daily.

ANALYSIS OF RESULTS

Test results

The results of the Cube Tests are given in Table 3. The slump was always around 25 mm while the compacting factor was almost 0.85 for all the batches. The minimum and the maximum values of the ambient temperature in the curing tank were found to be 26 °C and 28 °C respectively during the entire period.

Equivalent Age concept

The strength development of concrete made with all types of Portland cement depends on the temperature and humidity condition during curing. Concrete gains strength more rapidly at higher temperatures due to the increase in speed of the chemical reaction. There are two terms, namely Maturity and Equivalent age, to express a relationship between strength, time and temperature so that the strength of a particular concrete after any particular time and temperature cycle can be established from the knowledge of its strength after any other time and temperature cycle.

Maturity is the age of a particular concrete expressed as degree-hour, i.e. as the area under a temperature-time curve.

The Equivalent Age is the age at which a particular concrete would attain its current strength and degree of hydration, if maintained at a nominated standard temperature. It can be expressed by the following equation [8].

$$EA = \sum \left(t e^{-q \left(\frac{1}{T_a} - \frac{1}{T_s} \right)} \right) \quad (1)$$

Where,

EA = Equivalent Age (hours)

q = Activation Energy / Universal Gas Constant

T_a = Temperature (actual) for the time interval 't' (K)

T_s = Standard (reference) temperature (K)

t = Time spent at temperature 'T_a' (hours)

Table 2 Summary of test results

Brand Of Cement		“CSN”		“CME”		“CRH”	
Mix No.	Age (days)	Average* Ambient Temp. ($^{\circ}\text{C}$)	Average Cube Strength (N/mm^2)	Average* Ambient Temp. ($^{\circ}\text{C}$)	Average Cube Strength (N/mm^2)	Average* Ambient Temp. ($^{\circ}\text{C}$)	Average Cube Strength (N/mm^2)
1	1	26.00	5.17	27.50	6.98	27.00	7.35
	3	26.00	9.36	-	-	27.25	12.17
	4	-	-	27.33	16.32	-	-
	7	26.50	12.18	27.00	18.37	27.33	15.54
	28	27.33	18.54	27.28	28.07	27.14	21.82
2	1	28.00	6.30	26.50	7.44	27.00	9.02
	3	28.00	10.16	26.88	15.21	27.50	14.64
	7	27.83	14.34	26.92	21.06	27.42	19.62
	28	27.40	23.20	27.22	30.11	27.14	25.86
3	1	28.00	7.73	26.75	11.23	28.00	12.57
	3	27.75	12.54	26.75	23.43	-	-
	4	-	-	-	-	27.67	22.67
	7	27.83	17.09	26.75	31.26	27.58	25.83
	28	27.45	28.43	27.25	42.18	27.14	34.30
4	1	28.00	9.59	27.25	16.67	27.25	12.70
	3	28.00	17.07	-	-	27.38	23.24
	4	-	-	27.17	34.26	-	-
	7	-	-	27.25	39.46	27.58	28.40
	8	27.75	24.92	-	-	-	-
	28	27.38	38.42	27.26	53.05	27.01	38.11

* This denotes the average daily ambient temperature in the curing tank during a particular period of curing.

In this study, T_a denotes the average ambient temperature of the curing medium. For local conditions, T_s is taken as 27°C (300K). Generally, the value of ‘q’ is 4200.

Since the equivalent age concept is more accurate [9], it was used to analyze the strength data.

Compressive strength development

Figures 1,2 & 3 show the variation of strength with Equivalent Age (EA) for “CSN”, “CME” and “CRH” cement respectively. It can be seen that the variation of strength with $\text{Log}(\text{EA})$ is almost linear for all three brands of cement and for all four mix proportions.

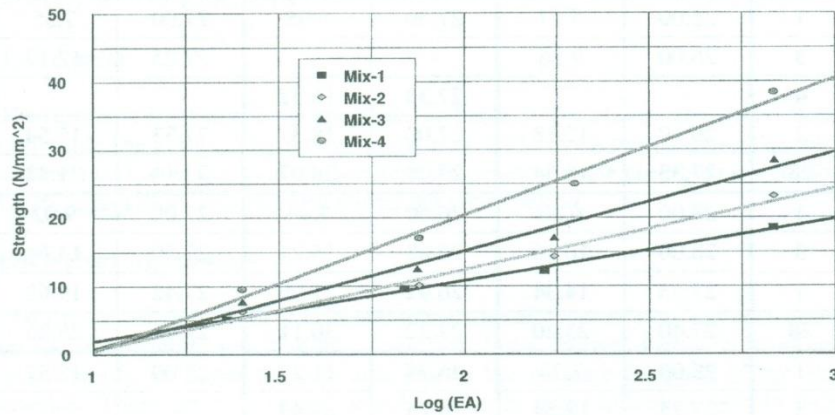


Figure 1 Variation of Strength with $\text{Log}(\text{EA})$ for “CSN”

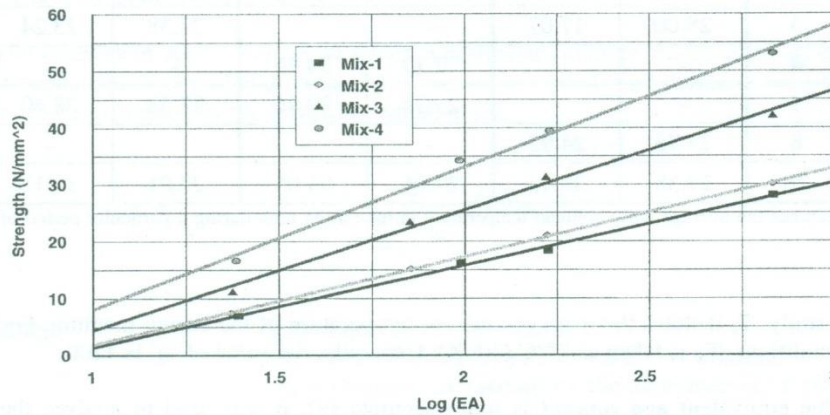


Figure 2 Variation of Strength with $\text{Log}(\text{EA})$ for “CME” cement

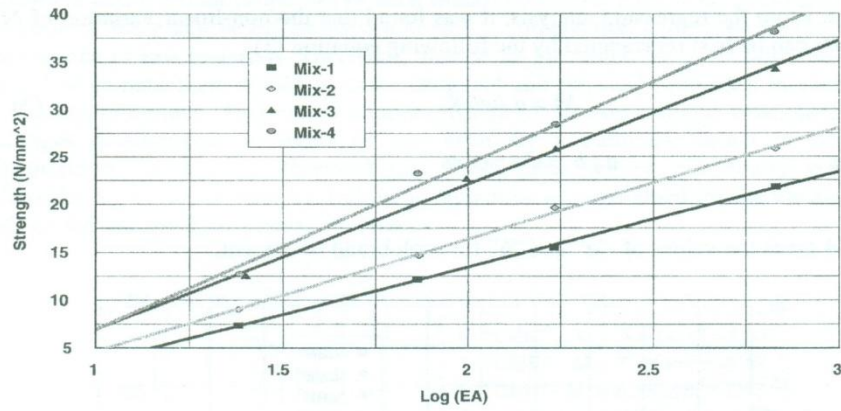


Figure 3 Variation of Strength with Log(EA) for “CRH”

Thus, for a particular concrete mix, the strength ‘ F_{cu} ’ at age ‘ t ’ can be expressed as follows.

$$(F_{cu})_t = M \text{ Log}(EA)_t + C \quad (2)$$

Where,

M = Gradient of “Strength vs. Log(EA)”

C = Y - intercept

Table 3 gives the summary of regression curves for each mix shown in Figures 1,2 & 3.

Table 3 Summary of regression curves in Figures 1, 2 & 3

Mix	w/c	Cement brand								
		“CSN”			“CME”			“CRH”		
		M	C	R*	M	C	R*	M	C	R*
1	0.64	9.02	-7.29	0.99	14.50	-13.13	0.99	9.93	-6.39	0.999
2	0.58	11.83	-11.22	0.98	15.52	-13.64	0.99	11.73	-7.08	0.997
3	0.48	14.38	-13.58	0.98	21.20	-16.86	0.99	15.14	-8.22	0.997
4	0.43	19.98	-19.56	0.99	24.97	-16.69	0.99	17.20	-10.13	0.991

* Coefficient of correlation

Figure 4 shows the variation of ' M ' with the water-cement ratio for each brand of cement. From the regression analysis, it was found that the non-linear variation of M with w/c can be best represented by the following equation (3).

$$M = a (w/c)^b \quad (3)$$

Where, a, b = Constants

Table 4 gives the values of " a " and " b " for each brand of cement.

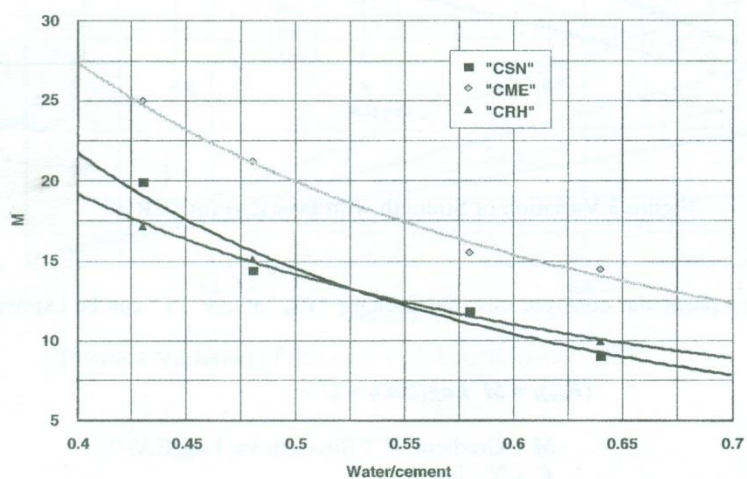


Figure 4 Variation of M with w/c

Table 4 Power Regression Data of "M vs. W/C"

Brand of Cement	Regression curve data		
	a	b	Coefficient of correlation R
"CSN"	4.11	-1.82	0.958
"CME"	7.46	-1.42	0.986
"CRH"	5.46	-1.37	0.996

It is clear from Figure 5, that the strength development is different for the same mix proportion with different brands of cement. This can be due to the difference in chemical and physical properties of each brand of cement. Even with the same brand of cement, there can be differences in chemical composition depending on the batch and source of raw materials. Therefore, there is no guarantee that even with the same brand of cement there would be same chemical and physical properties in each and every bag of cement. This makes it more difficult to develop a unique relationship for strength development in terms of w/c even for a particular brand of cement. Furthermore, it can be observed that these three curves are nearly parallel. Considering this behaviour, the following equations were obtained for the variation of M and w/c for the three brands of cements.

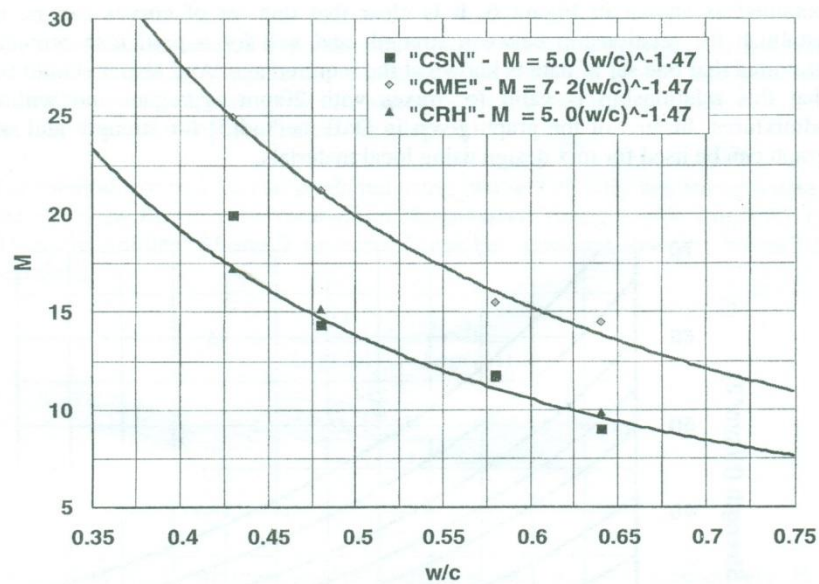


Figure 5 M vs. w/c for all brands of cement

For "CSN" Cement - $M = 5.0(w/c)^{-1.47}$ (4.a)
For "CME" Cement - $M = 7.2(w/c)^{-1.47}$ (4.b)
For "CRH" Cement - $M = 5.0(w/c)^{-1.47}$ (4.c)

Table 6 Summary of C/M

Mix	w/c	Brand of cement					
		"CSN"		"CME"		"CRH"	
		C/M	Average	C/M	Average	C/M	Average
1	0.64	0.808	0.919	0.905	0.812	0.643	0.594
2	0.58	0.948		0.879		0.603	
3	0.48	0.944		0.795		0.543	
4	0.43	0.978		0.668		0.588	

In addition, it can be seen from Table 6, that the C/M ratio for three brands of cement is approximately constant for each brand of cement. Therefore, the following equations can be derived for the strength of concrete in terms of w/c for the three brands of cement.

$$\text{For "CSN"} \quad (F_{cu})_t = 5.0(w/c)^{-1.47} (\log(EA)_t - 0.92) \quad (5.a)$$

$$\text{For "CME"} \quad (F_{cu})_t = 7.2(w/c)^{-1.47} (\log(EA)_t - 0.81) \quad (5.b)$$

$$\text{For "CRH"} \quad (F_{cu})_t = 5.0(w/c)^{-1.47} (\log(EA)_t - 0.59) \quad (5.c)$$

Based on the above equations, the strength variation with w/c for different ages can be obtained as shown in Figure 6. It is clear that this set of curves can be used to establish the relationship between strength and w/c for a particular cement brand provided that one set of data is known at the required age. And also it should be noted that this relationship is valid for mixes with 20mm aggregate and without any admixtures. Instead of the graph given in DoE method[5] for strength and w/c, this graph can be used for mix design using local materials.

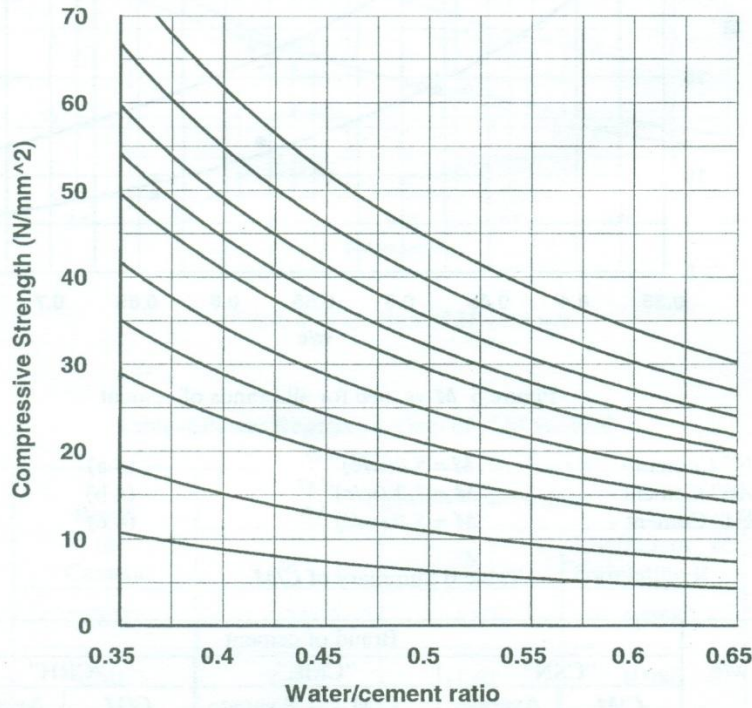


Figure 6 Relationship between compressive strength and w/c ratio

The above three equations (5.a),(5.b) & (5.c) can be written in the general form as follows.

$$(F_{cu})_t = m(w/c)^{-1.47} (\log(EA)_t - k)$$

Taking the average value of k for three brands of cement, compressive strength of concrete can be approximately represented by the following equation.

$$(F_{cu})_t = m(w/c)^{-1.47} (\log(EA)_t - 0.77)$$

The above equation can be used to predict strength of concrete if the w/c ratio and one set of strength data at known age are available. Therefore the 28-day compressive strength can be predicted with early age strength data. If the mix proportion is not available, then the following method can be adopted.

Under this method, strength can be predicted using two sets of early age strength data. This is based on the fact that the variation of compressive strength with $\log(EA)$ is linear. Thus, the gradient M and Y intercept C can be calculated from the following two expressions.

$$M = \frac{(F_{cu})_{t1} - (F_{cu})_{t2}}{\log(EA)_{t1} - \log(EA)_{t2}}$$

$$C = \frac{\log(EA)_{t1}(F_{cu})_{t2} - \log(EA)_{t2}(F_{cu})_{t1}}{\log(EA)_{t1} - \log(EA)_{t2}}$$

Where $(F_{cu})_{t1}$ and $(F_{cu})_{t2}$ are compressive strength at ages t_1 and t_2 respectively. By substituting this M and C values in Equation (2), strength can be predicted up to 28 days irrespective of brand of cement and w/c ratio.

PREDICTION OF COMPRESSIVE STRENGTH

Prediction was done for the 28 day compressive strength of each mix (i.e. $t=28$ days). The earliest age at which the strength data were available was used as ' t_0 '. Also, the Equivalent Age for 28 days (EA_{28}) was calculated based on the average ambient temperature for the period ' t_0 '. Tables 7 gives the predicted 28-day strength for strength data given in Table 2. Since the real test of any relation is its ability to fit data other than data from which it has been derived, the proposed relation was applied to data from other sources. Table 8 shows the predicted 28-day strength based on 3-day and 7-day strength data from other sources which shows the proposed equation correlates the test data with a significant accuracy. It should be noted that, when the ambient temperature was not available, it was assumed to be same as the reference temperature.

Table 7 Prediction of 28-day Strength using 3-day and 7-day strengths given in Table 2

Brand of cement	W/c	Actual strength (N/mm ²)	Predicted strength* (N/mm ²)	Variation (%)	Predicted strength** (N/mm ²)	Variation (%)
"CSN"	0.64	18.54	17.88	3.55	16.79	9.4
	0.58	23.20	18.01	22.3	21.18	8.7
	0.48	28.43	22.32	21.5	24.53	13.7
	0.43	38.42	32.28	16.0	34.95	9.0
"CME"	0.64	28.07	29.43	4.8	23.45	16.4
	0.58	30.11	31.01	3.0	30.63	1.7
	0.48	42.18	48.23	14.3	44.33	5.1
	0.43	53.05	58.95	11.1	52.34	1.3
"CRH"	0.64	21.82	21.97	0.7	21.05	3.5
	0.58	25.86	26.07	0.8	27.77	7.4
	0.48	34.30	36.85	7.4	33.66	1.9
	0.43	38.11	44.67	17.2	36.84	3.3
Average (Std. dev.)				10.22 (7.89)		6.80 (4.87)

* Predicted strength using 1 day and 3 days (or 4 days) strength data

** Predicted strength using 3 days and 7 days (or 8 days) strength data

Table 8 Predicted 28-day Strength for test data from other sources

Source	Measured strength (N/mm ²)		28-day strength (N/mm ²)		% error
	3 days	7 days	Measured	Predicted	
[5]	27.0	36.0	49.0	50.7	+3.47
[10]	24.5	31.6	39.4	43.1	+9.39
	35.5	40.6	49.7	48.8	-1.81
	21.5	26.7	35.9	35.1	-2.22
[11]	24.8	33.9	46.1	48.8	+5.85
Average					4.55

CONCLUSIONS

According to the results, 60% to 75% of the 28-day strength of concrete is achieved in the first 7 days. It was found that the variation of compressive strength varies linearly with respect to the logarithmic value of Equivalent age of concrete. Furthermore, it was found that the gradient of "Strength vs. Log(EA)" is a function of the water-cement ratio. In addition, it was found that the strength development was different for the same mix proportion with different cement brands. Three equations were derived for prediction of strength in terms of w/c ratio and equivalent age for the three brands of cement used. Based on these equations, a series of curves were developed for the relationship between strength and water-cement ratio. These sets of curves can be used in mix design of concrete using local materials.

The following general form of the relationship between strength and equivalent age was proposed to predict the 28-day strength from two sets of early age strength data.

$$(F_{cu})_t = M \text{Log}(EA)_t + C$$

Thus, the gradient (M) and Y intercept C can be calculated from the following two expressions.

$$C = \frac{\text{Log}(EA)_{t1}(F_{cu})_{t2} - \text{Log}(EA)_{t2}(F_{cu})_{t1}}{\text{Log}(EA)_{t1} - \text{Log}(EA)_{t2}}$$

$$M = \frac{(F_{cu})_{t1} - (F_{cu})_{t2}}{\text{Log}(EA)_{t1} - \text{Log}(EA)_{t2}}$$

Where $(F_{cu})_{t_1}$ and $(F_{cu})_{t_2}$ are compressive strengths at ages t_1 and t_2 respectively. It was found that with 3-day and 7-day strength data, the 28-day strength could be predicted with a significant accuracy.

ACKNOWLEDGEMENTS

The author would like to acknowledge the University of Moratuwa for funding this research project. The contributions of the Research Assistant Mr. W.S.A. De Silva, Technical Officer Mr. S.L. Kapuruge and the laboratory staff in the Building Materials Laboratory are gratefully acknowledged.

REFERENCES

1. Nasser, K.W., Malhotra, V.M., "Accelerated Testing of Concrete: Evaluation of the K-5 Method", ACI Materials Journal, Nov.-Dec. 1990, pp. 588-593.
2. Snell, Luke M., Roekel, Jacob Van, and Wallace, Norval D., "Predicting Early Concrete Strength," Concrete International, Dec. 1989, pp. 43-47.
3. Parsons, Thomas J., and Naik, Tarun R., "Early Age Concrete Strength Determination by Maturity," Concrete International, Feb. 1985, pp. 37-43.
4. Oluokun, F.A., Burdette, E.G., and Deatherage, J.H., "Early-Age Concrete Strength Prediction by Maturity- Another Look, ACI Materials Journal, Nov.-Dec. 1990, pp. 565-567.
5. "Methods for Sampling and Testing of Mineral Aggregates, Sands and Fillers," (BS 812), British Standards Institution, 1975, Part1 and Part2.
6. Teychenne, D. C., Franklin, R.E., and Erntroy, H.C., "Design of Normal Concrete Mixes," Department of Environment, Building Research Establishment, 1988.
7. "Methods of Testing Concrete," (BS 1881), British Standards Institution, 1970, Part2, Part3 and Part4.
8. Bazant, Zdenek P., and Carol, Ignacio, "Creep and Shrinkage of Concrete," E & FN Spon, An imprint of Chapman & Hall, 1993.
9. Day, Ken W., Concrete Mix design, Quality Control and Specifications, E & FN Spon, An imprint of Chapman & Hall, 1995.
10. Dias, W.P.S., Nanayakkara, S.M.A., "Properties of PFA Blended Cement in Concrete", International Symposium on Asian Concrete Model Code, Colombo, 2000.
11. Nanayakkara, S.M.A, "Mix design for Grade 35A concrete", Test Report CE/ST/96, Dept. of Civil Eng. University of Moratuwa.

AN EXPERIMENTAL METHOD TO DETERMINE THE THERMAL CONDUCTIVITY OF CONCRETE

S.M.A. Nanayakkara
Dept. of Civil Engineering, University of Moratuwa

AN EXPERIMENTAL METHOD TO DETERMINE THE THERMAL CONDUCTIVITY OF CONCRETE

S.M.A. Nanayakkara

Dept. of Civil Engineering, University of Moratuwa

ABSTRACT

This paper reports an experimental method developed to measure the thermal conductivity of concrete. This method involves the measurement of steady state temperature distribution across a cylindrical specimen of concrete under known heat flux supplied at the centre of the specimen by a heating coil. It was observed that the thermal conductivity of concrete varies across the section of the specimen and also with the age of concrete. The variation of conductivity across the section may be due to the non-uniform distribution of free water and hydrated products. This idea was verified by conducting the test with a dry mixture of cement, sand and aggregate. It was observed that the thermal conductivity of the dry mix was very low and it did not vary across the section as the composition of the materials was uniform across the section.

INTRODUCTION

Thermal conductivity is an important property of concrete for calculation of thermal stresses due to heat of hydration of cement or external heat transfer such as solar radiation. Since concrete is a multiphase material, thermal conductivity may vary depending on the composition of constitutive materials of concrete[1]. Knowledge of thermal properties of various types of concrete can be a useful tool to control heat generation within large concrete structures and also to develop accurate models for heat of hydration [2].

Thermal conductivity of concrete used in these models has been based on properties of aggregate or the hardened concrete, with a single value being assumed irrespective of the composition. This does not represent the actual condition and thermal conductivity varies due to change in composition with the progress of hydration and also with mix proportion. The use of more accurate values of thermal conductivity increases the validity of such models used to determine the thermal profiles within the concrete structure.

The most widely used method to determine the thermal conductivity of solids of rather low thermal conductivity like concrete is the guarded hot plate method [3]. In this method it is necessary to use two slabs of the specimen in the apparatus where a guard heater, cooling system and thermocouples are installed. One of the disadvantages of this method is that the properties of concrete, especially the moisture content of concrete may vary in the process of preparing the required size of sample to be tested in this apparatus. Recently another method known as thermal probe method was developed to measure the thermal conductivity in both semi-liquid and solid state of concrete [4]. But the thermal

conductivity of concrete with large aggregate size cannot be measured directly using this method. The aggregate size should be less than half the size of the probe (i.e. 30mm). Since the volume of sample being involved in the test is $5 \times 10^{-6} \text{ m}^3$ and the length of the probe is 64mm, it measures the thermal conductivity of a very thin layer (approximately 5mm) of the material. Therefore, for a non-homogeneous material like concrete, this method is not very suitable.

This paper describes a simple test method to measure the thermal conductivity of concrete using an undisturbed concrete sample. This method can also be used to measure thermal conductivity of any granular material.

THEORETICAL BACKGROUND

Conduction through thick walled pipes is a common heat transfer problem and may be treated one – dimensionally if surface temperatures are uniform [5]. Then the heat flow is in the radial direction only; Fig. 1 illustrates the situation for a single layer. Fourier's law may be applied to a cylindrical layer at radius r as

$$Q = -kA \frac{dT}{dr}$$

where A is the surface area at radius r and k is the thermal conductivity. By considering a unit length of the cylinder, radial heat transfer Q is given by

$$Q = -k(2\pi r) \frac{dT}{dr}$$

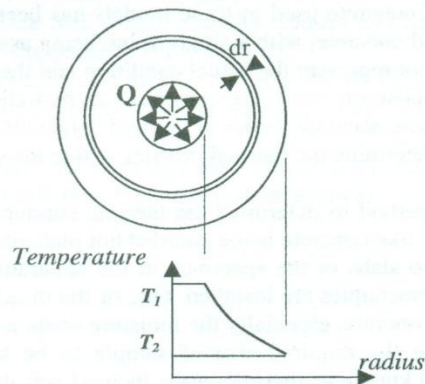


Fig. 1 Heat flow in cylindrical layers

Since the same quantity of heat Q is flowing through a steadily increasing cylindrical area, the temperature gradient must decrease with increasing radius. Integrating the above equation, the following equation can be obtained.

$$Q = \frac{2\pi k(T_2 - T_1)}{\ln r_2/r_1}$$

This provides the basis to develop an experimental method for measuring thermal conductivity by obtaining steady state temperature profile of a cylindrical specimen under known heat flux.

EXPERIMENTAL INVESTIGATION

In order to obtain the temperature distribution across a cylindrical specimen under known heat supply, a test method was developed. Fig. 2 shows the basic set up used in this test method. A cylindrical formwork made out of hard board with inner surface coated with non-absorbing material was used to cast the cylindrical specimen of 300mm in diameter and 500mm in length. Heating of concrete was done by supplying DC current through a Ni-Cr wire embedded at the center of the concrete cylinder. Since the heating wire was inside the specimen, heat generated in the wire was entirely transferred to concrete. Before casting concrete, Ni-Cr wire was fixed at the center of the cylindrical formwork with the help of a frame attached to the formwork.

Table 1 Mix proportion of concrete(per m³)

Water (kg)	Cement(kg)	Sand (kg)	Coarse Agg. (kg)	Superplasticizer (kg)
174	550	857	827	1.5% of Cement

The mix proportion of the concrete used is given in Table 1. This particular mix proportion was used by Maekawa et al [2] in the test series to verify a heat of hydration model incorporating the thermal properties of concrete; the values given in Table 2 were assumed for thermal properties of concrete for the mix proportion given in Table 1 in the temperature analysis.

Table 2 Thermal properties of concrete used in analysis [2]

Thermal conductivity	41 kcal/m/day/°C
Heat transfer coefficient	18 kcal/m/day/°C

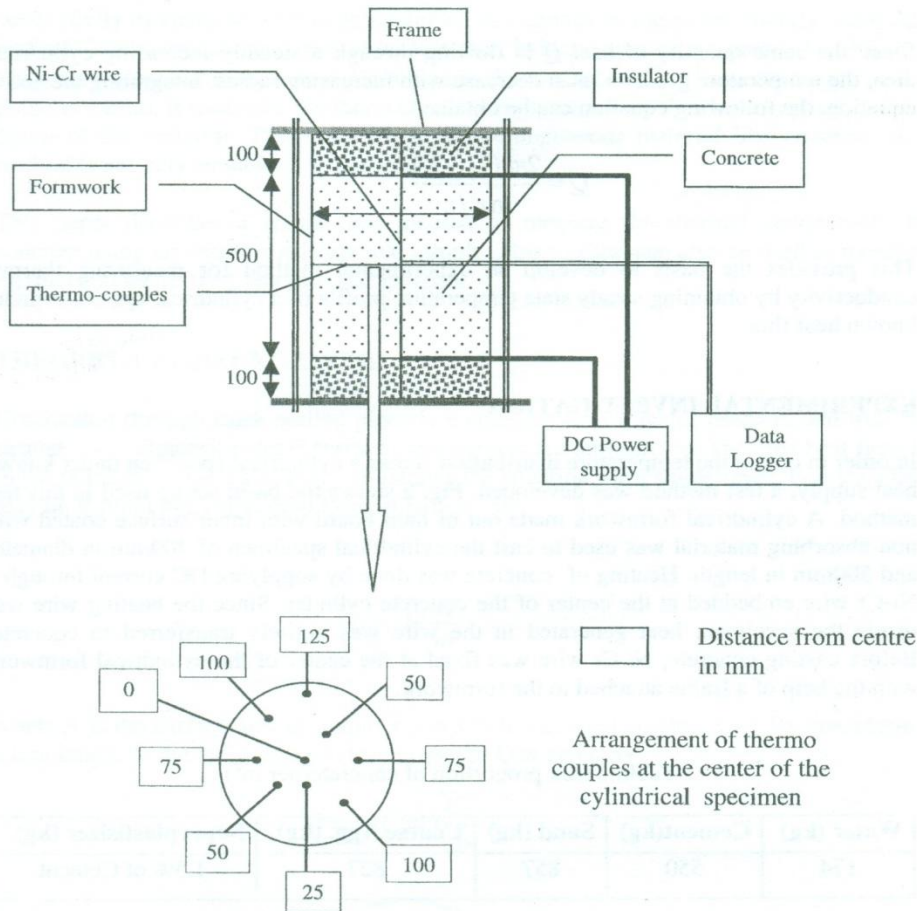


Fig. 2 Experimental setup

After placing concrete to a depth of 250mm, thermo-couples were placed radially as shown in Fig. 2. Thermo-couples were inserted to measure temperature at the centre and at distances of 25mm, 50mm, 75mm, 100mm and 125mm from the center. And also a thermo-couple was used to monitor the environmental temperature as well.

Precautions were taken to not displace the thermo-couples while concreting the upper half of the cylinder. The top and bottom sides of the specimen were insulated to prevent any loss of heat from top and bottom. Monitoring of the temperature was started as soon as the concreting was completed. Once the temperature of concrete had dropped to the

ambient temperature after temperature rise due to heat of hydration, heating was started by supplying electric current (DC) through the Ni-Cr wire. The amperage was maintained at 4 Amp. and the voltage across the two ends was measured using a digital multimeter. The heating was continued until the steady state temperature distribution was reached. The procedure was repeated at 3 days and 7 days after casting concrete. In order to find out the effect of hydrated products and free water on thermal conductivity of concrete, another test was carried out with a dry mix, which was a mixture of cement, sand and gravel. The same ratio of cement, sand and coarse agg. of the concrete mix given in Table 1 was used for the dry mix.

TEST RESULTS

Fig. 3 shows the temperature rise at the centre of the specimen due to heat of hydration and it can be seen that the inside temperature reached the ambient temperature after 2 days.

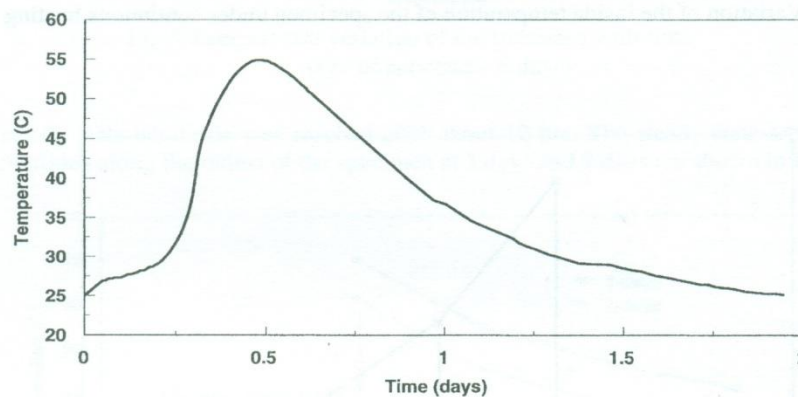


Fig.3 Temperature variation at the centre due to heat of hydration

Heating of the specimen was started after reaching the ambient temperature and the temperature variation at various points inside the specimen with time is shown in Fig. 4. It can be seen that after about one day of heating, the temperature distribution cross the section has stabilized and variation of temperature during the next 24 hrs was in the order of 0.1 °C. Fig. 5 shows the steady state temperature distribution across the specimen.

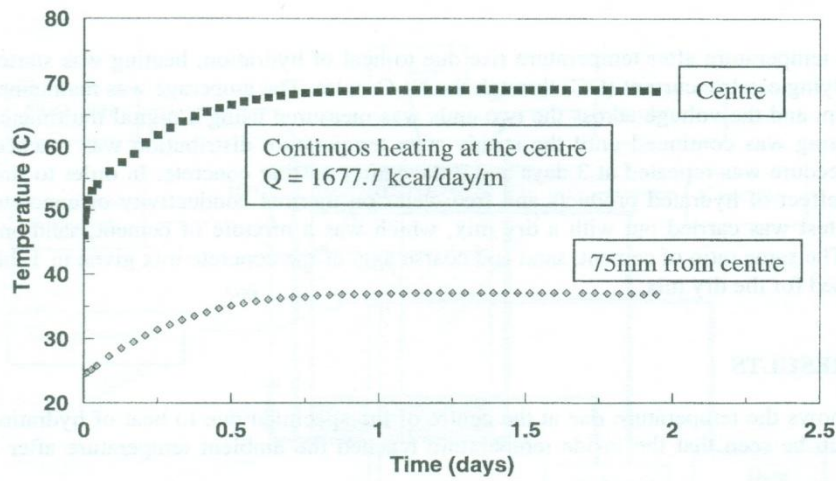


Fig. 4 Variation of the inside temperature of the specimen under continuous heating

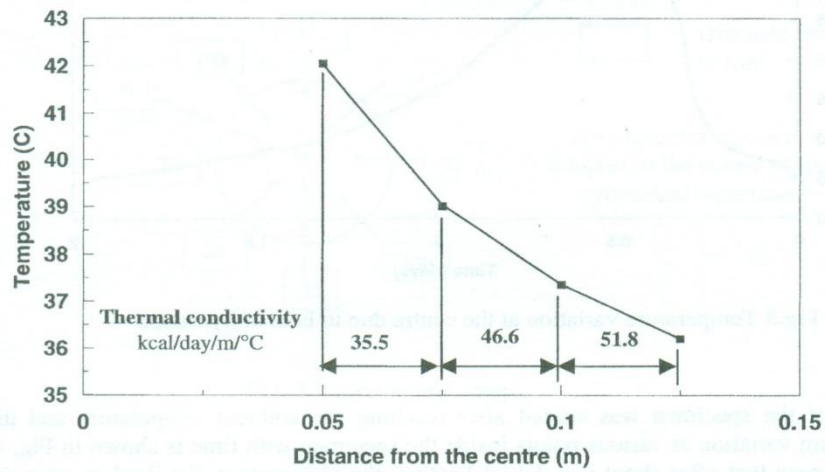


Fig. 5 Temperature variation across the section under steady state condition

Based on the above temperature distribution, the calculated thermal conductivities along the radius are also given in Fig. 5. As it can be seen from Fig. 5, the thermal conductivity

is decreasing towards the center of the cylinder. Further heating was carried out after 6 days and the temperature variation with time is shown in Fig. 6 and

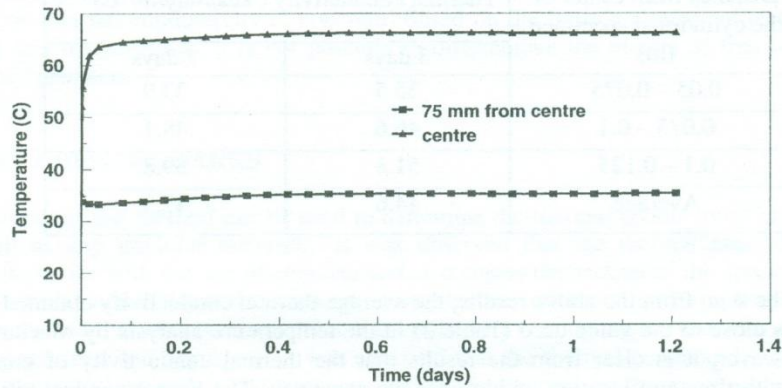


Fig.6 Temperature variation of the specimen with time
(age of concrete – 6 days)

the steady state condition was reached after about 12 hrs. The steady state temperature distributions along the radius of the specimen at 3 days and 7 days are shown in Fig.7.

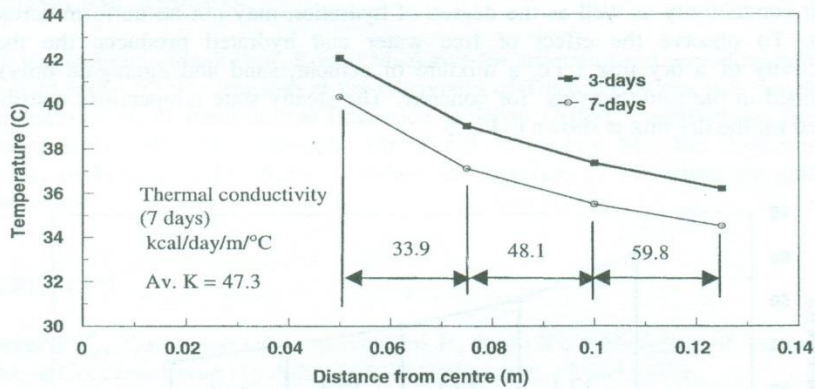


Fig. 7 Temperature distribution along the radius under steady state condition

Based on the steady state temperature distribution, the calculated thermal conductivity values are given in Table 3.

Table 3. Thermal conductivity of concrete

Distance from center of the cylindrical specimen (m)	Thermal conductivity (kcal/day/m/°C)	
	3 days	7 days
0.05 – 0.075	35.5	33.9
0.075 – 0.1	46.6	48.1
0.1 – 0.125	51.8	59.8
Average	44.6	47.3

As it can be seen from the above results, the average thermal conductivity obtained from this test is close to the value used (Table 2) in the temperature analysis by Maekawa et al[2]. However, it is clear from the results that the thermal conductivity of concrete changes with time and location within concrete specimen. The lowest conductivity was recorded close to the centre and the highest conductivity was at outer surface. The change in thermal conductivity with time can be due to the progress of hydration of cement and it was high at the outer layer of the cylinder. Due to high temperature at the center (60 °C), free water may dissipate towards the outer surface of the cylinder and therefore, there may be sufficient water at the outer layer to continue hydration but not at the central portion. Due to non-uniform distribution of free water across the section of the cylinder, thermal conductivity as well as the degree of hydration may not be uniform across the section. To observe the effect of free water and hydrated products, the thermal conductivity of a dry mix (i.e. a mixture of cement, sand and aggregate only) was determined in the same way as for concrete. The steady state temperature distribution obtained for the dry mix is shown in Fig.8.

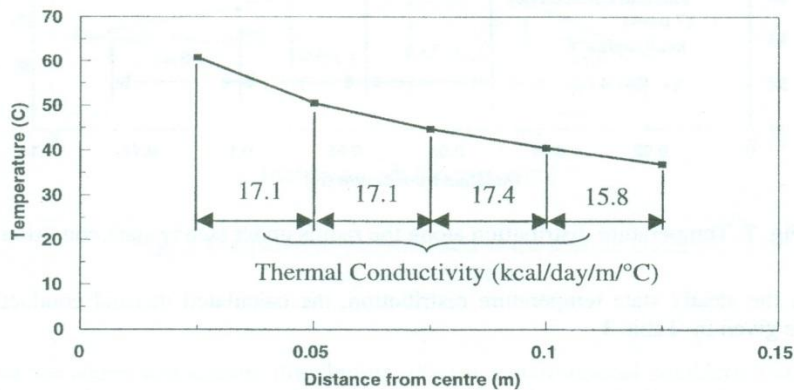


Fig.8 Temperature distribution along the radius of the specimen for the dry mix

It can be clearly seen from Fig. 8 that the thermal conductivity of the dry mix does not vary much across the section when compared with the concrete specimen. The average thermal conductivity was around 17 kcal/day/m/°C, which is very much lower than the conductivity of concrete. This clearly indicates the effect of hydrated products and free water on thermal conductivity of concrete. Based on the limited number of tests carried out in this investigation, it is not possible to differentiate the effects of free water and hydrated products.

CONCLUDING REMARKS

The proposed test method can be used to determine the thermal conductivity of concrete as well as any granular material. It was observed that the thermal conductivity of concrete varies with the age of concrete and also across the section of the specimen. The variation of conductivity across the section may be due to the non-uniform distribution of free water and hydrated products. This was verified by conducting the test with a dry mix of cement, sand and aggregate. It was observed that the thermal conductivity of the dry mix was very low and it did not vary across the section as the composition of the materials was uniform across the section. Using this test method, it is possible to investigate the thermal conductivity of individual materials such as un-hydrated cement, sand and aggregate. However, further investigation is necessary to propose a complete model for thermal conductivity of concrete.

ACKNOWLEDGEMENTS

Author would like to thank Prof. Koichi Maekawa for arranging and providing necessary facilities to carry out this research at the University of Tokyo. This research was funded by the Association of International Education in Japan (AIEJ). Contributions from Dr. Toshiharu Kishi, Mr. Akira Hosoda, Mr. Kouji Kinomura, Mr. Kei Yoshimura of University of Tokyo and Dr. Rahula Attalage of University of Moratuwa are gratefully acknowledged.

REFERENCES

1. Sarker P.K., Tantermsirikul S., Jitvutikrai P., Kishi T., " Modeling of Temperature Rise in Concrete Using Fly Ash", IABSE Colloquium, Phuket, 1999.
2. Maekawa K., Rajesh C., Kishi, T., " Modelling of Concrete Performance", E& FN Spon, 1999.
3. Holman, J.P., Gajda W.J., " Experimental Methods for Engineers", McGraw-Hill, 1988.
4. Gibbon G. J., Baallim Y., " Determination of thermal conductivity of Concrete during the early age stage of hydration" , Magazine of Concrete Research, 1998, Vol.50, No.3, September, pp. 229-235.
5. Simonson, J.R., "Engineering Heat Transfer", Macmillan Education Ltd, 1988.

PERFORMANCE ANALYSIS OF PEDESTAL FANS AN EXPERIMENTAL INVESTIGATION

A. G. T. Sugathapala and P.B.I. Somarathne
Dept. Mechanical Engineering, University of Moratuwa.

PERFORMANCE ANALYSIS OF PEDESTAL FANS: AN EXPERIMENTAL INVESTIGATION

A. G. T. Sugathapala and P.B.I. Somarathne
Dept. Mechanical Engineering, University of Moratuwa.

ABSTRACT

Performances of pedestal fans were analysed through experimental measurements of the induced flow field (velocity distribution) and the power consumption by two different types of fans. A test rig was constructed to facilitate the measurement of axial flow velocities in the three dimensional space. In order to predict the jet pattern produced by the fan, axial velocity distributions on sufficient number of planes were measured. These data were used to calculate the jet diameter, flow rate, kinetic energy and the linear momentum of the flow at different planes from the rotor. The power consumption and the angular speed of the rotor for each regulator setting were also measured.

The velocity distributions measured on different planes from the rotor clearly illustrate the general characteristics of the flow generated by free flow fans, including the reverse flow near the rotor plane, jet entrainment and diffusion. The results show that the overall energy efficiency of a fan depends critically on its speed (i.e. regulator setting); efficiency increases with the speed. The results also indicate that the service factor defined by the flow rate at a specified section divided by the power consumption is not a suitable performance index for free-flow fans. Even with a similar axial velocity profile generated by two different fans could result in two different jet developments leading to completely different flow characteristics and performances. The results of the present study indicate the complexity of the jet development and the necessity for detailed experimental measurements of the flow velocity distribution including the swirl components in predicting performance of free-flow fans.

INTRODUCTION

Free-flow fans are commonly used in buildings to achieve the necessary thermal comfort levels. The flow generated by a fan provides the required circulation and velocity for comfort. Further, steady and uniform temperature conditions in the space could be maintained. The overall performance of a free-flow fan is determined by the aerodynamic design of the rotor blades together with the correct matching of the electric motor characteristics at different speeds (i.e. at different regulator settings). The characteristics of the air-jet generated by the fan, especially the velocity profile at the rotor plane and jet swirl, determine the extent of the comfort region in space developed by the fan. Another factor that affects the effectiveness of the fan is the presence of solid boundaries, such as walls and furniture in the vicinity of the fan rotor and the air jet. There are a number of different brands of free-flow fans available in the market with different design features (i.e. different blade shapes, sizes, number of blades etc.). In general, performance characteristics of air-circulating fans are not provided to the customer. In some cases, wide variations in the performance could be observed among the fans even with the same design and brand. These observations indicate the difficulty of drawing a general conclusion on the relative performances of different types of free-flow fans and recognize the need for performance testing of each brand and design.

Among the available types of free flow fans pedestal and table fans are the most common types used in domestic sector. Generally these design has some notable advantages such as flexibility in placing, wider coverage through rotor swing facility, etc. These fans have high solidity rotors with propeller type blades, where the chord length and blade angle vary continuously for maximum performance.

The flow field generated by a free-flow fan is very complex and difficult to predict theoretically as well as experimentally. Thus the prediction of the performance is not an easy task. Modern experimental techniques, such as laser doppler velocimetry and wide-field shadowgraphy, could be used to obtain data necessary for detailed study. However, these experimental setups are expensive and the testing is difficult to perform (Conlisk 1997). Further, theoretical methods such as free vortex techniques and three-dimensional Navier-Stokes computations are computationally intensive (see Ahmad & Duque 1996 for applications in helicopter rotors). Therefore, the only alternative available would be to have less detailed study based on experimental investigation using basic instruments. Such a method is presented in the SL Standards for fan testing (SLS 814 - Part 1), where the axial velocity distribution on a specified plane from the fan rotor is to be measured to calculate the flow rate at different regulator settings. Then the performance of the fan is evaluated by the ratio between this flow rate and the electric power consumption, which is known as service factor. Previous investigations based on testing of ceiling fans showed the limitations of the service factor as a performance index for air-circulating fans (Sugathapala 1997).

The present study is carried out to investigate further the performance of free-flow fans through testing of pedestal fans. A number of fans are tested and results of two similar fans of different brands are presented and analyzed in this paper. The measurements include jet development pattern, velocity distributions and power consumption at different regulator settings. These results too clearly show the ineffectiveness of the service factor as a performance index of free-flow fans. The present study is also aimed at introducing an alternative method for fan testing which will be more useful in selecting fan(s) for particular application.

BASIC CHARACTERISTICS OF PEDESTAL FANS

Geometric Characteristics

Pedestal fans have propeller type rotors with three blades (most common) with continuously varying chord lengths and blade angles. Blades are made out of plastic or sheet metal with a circular arc profile. Usually the rotor has high solidity (i.e. ratio of blade area to rotor area) compared with ceiling fans.

Pattern of Flow

The mechanical energy generated by the electric motor is converted into fluid energy through a hydrodynamic action of the fan rotor, in the form of flow rate through the rotor together with a pressure rise across it. As a result, the fan discharges a jet of air possessing a free boundary (see Figure 1). Since the fan is operating in a common, unrestricted space, it is fed principally by air that has returned to the inlet side of the fan by the medium of a converging stream of reverse flow outside the jet. Even in front of the rotor, the streamlines of the jet converge rapidly and become parallel within a short distance. While the surrounding air in contact with the jet is accelerated due to the transfer of momentum through the action of shear forces, and more and more air is entered to the jet. This process of entrainment continues as the air stream moves further away from the fan and the jet expands owing to the increase in flow rate. Finally, the momentum of the jet reaches zero and entrainment ceases, and there is a net loss of air through the boundaries as the kinetic energy of the jet is steadily

converted into kinetic energy of turbulence, which decays through viscous shear (see Figure 2). The buffer region between the diverging jet and the reverse flow is one of large-scale random turbulence except in the near vicinity of the fan (Wallis 1983). The rotation of the blades also imparts a swirl to the jet flow, which determines the rate of jet diffusion (Rajaratnam 1976) and therefore the amount of jet penetration.

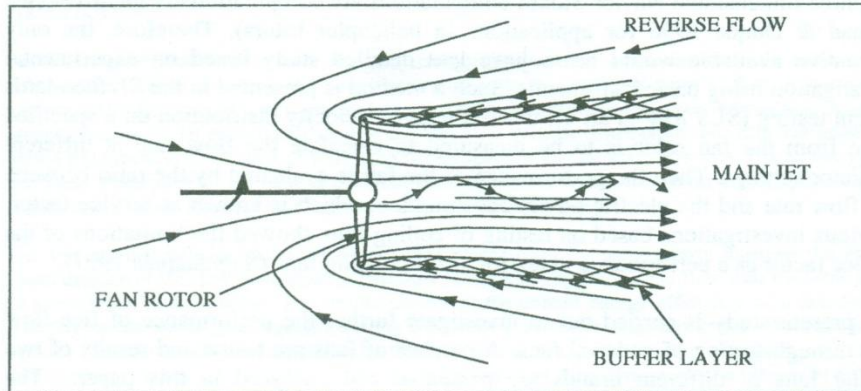


Figure 1: Pattern of flow in the near vicinity of the rotor

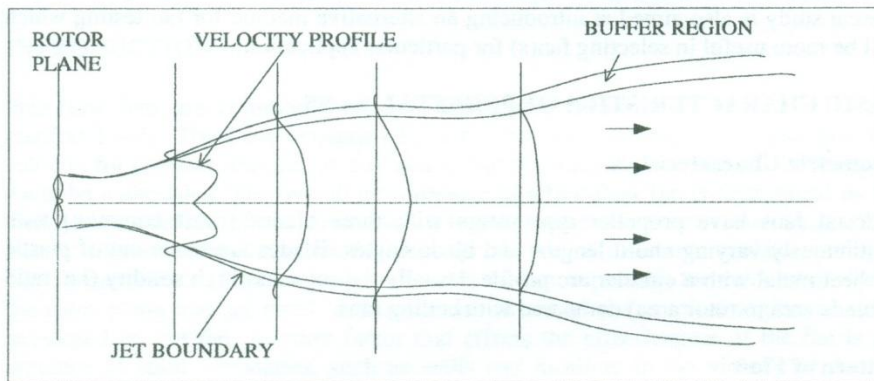


Figure 2: Jet development

EXPERIMENTAL SETUP

The air velocity was measured by using a rotating vane digital anemometer with a resolution of 0.01 m/s. It was mounted on the test grid, which has a facility to move the anemometer to any point in the three-dimensional space within the required limits, as shown in Figure 3. The energy was measured by means of digital wattmeter with a resolution of 0.5 W. The angular velocity of rotor measured by using a stroboscope.

The axial velocity distributions generated by a fan were measured on different planes from the fan along two diametrical directions, one horizontal and one vertical, and the power consumption by the fan at each case was also measured. These data were

collected at different regulator settings for two pedestal fans of same rotor size but different brands.

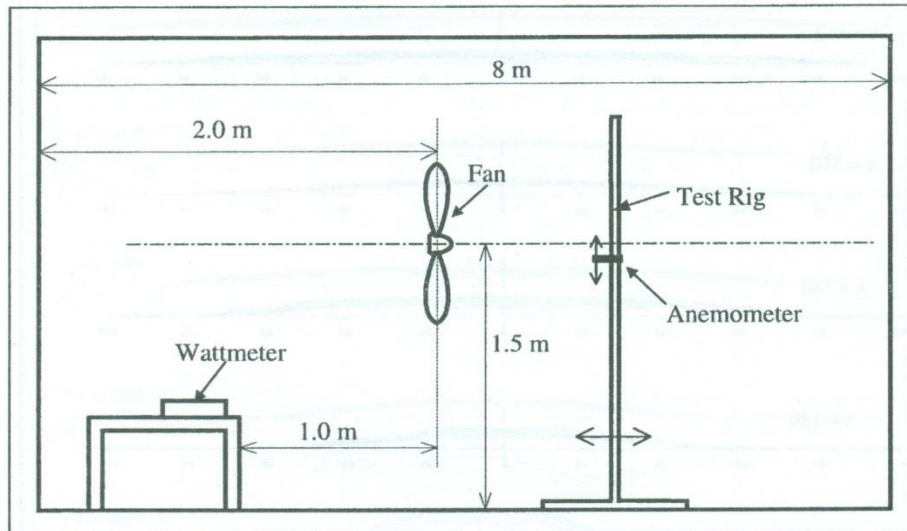


Figure 3: Experimental setup

MEASUREMENTS

The measured data for the two pedestal fans are summarized below:

Power Consumption and Rotational Speeds

Fan Model	Parameter	Regulator Position		
		1	2	3
Pedestal Fan Brand - A	Rotational Speed (rpm)	734	957	1178
	Power Consumption (W)	45	51	57
Pedestal Fan Brand - B	Rotational Speed (rpm)	877	1005	1166
	Power Consumption (W)	41	44	46

Table 1: Power consumption and rotational speeds at different regulator positions.

Velocity Distributions

Velocity distribution at one plane of the pedestal fan - A is given in the Appendix. Similar set of readings was taken for eight more planes for each regulator position. The procedure was repeated for other regulator positions for each fan. Therefore, there are altogether 54 set of such reading. These data are not provided with this paper, but presented graphically here.

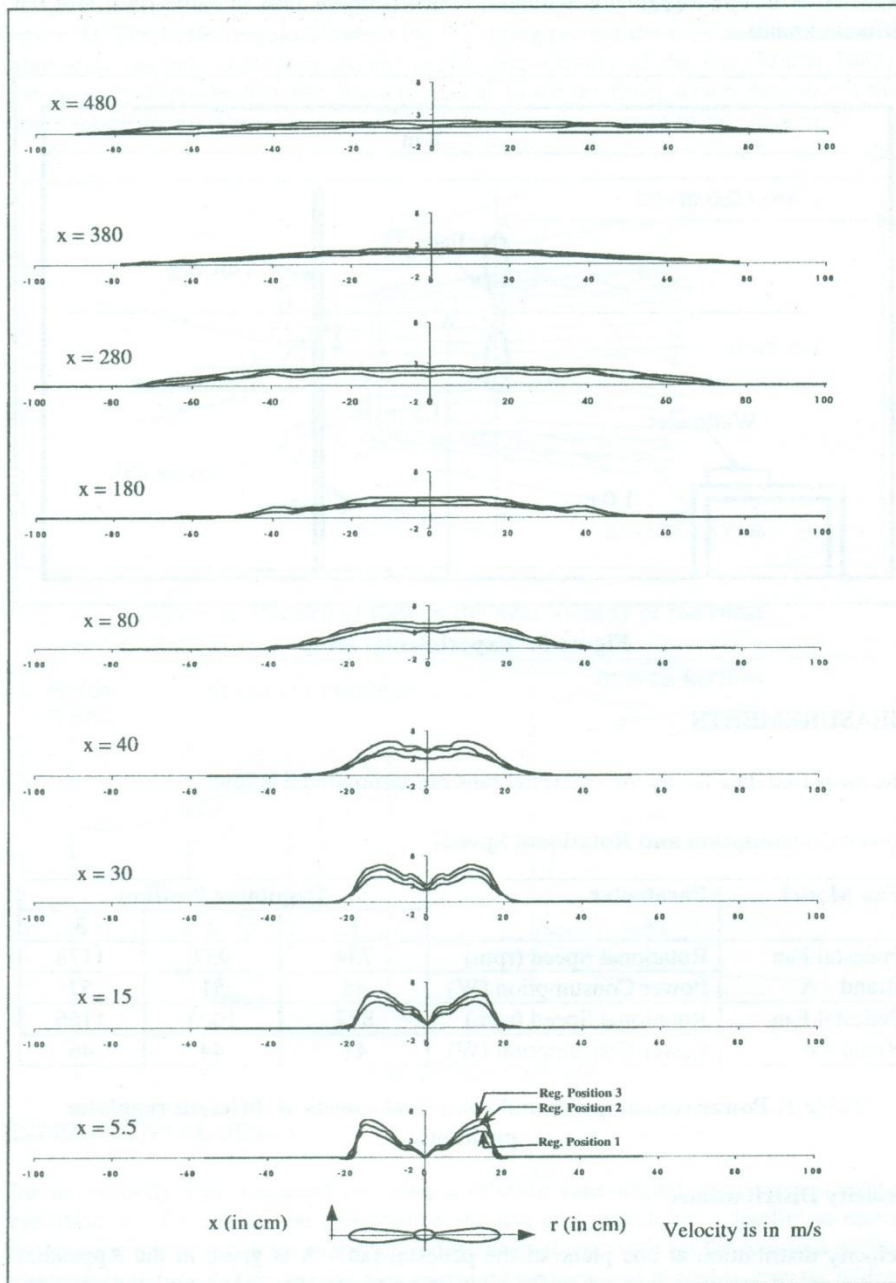


Figure 4: Axial velocity distribution generated by Fan-A at different regulator positions

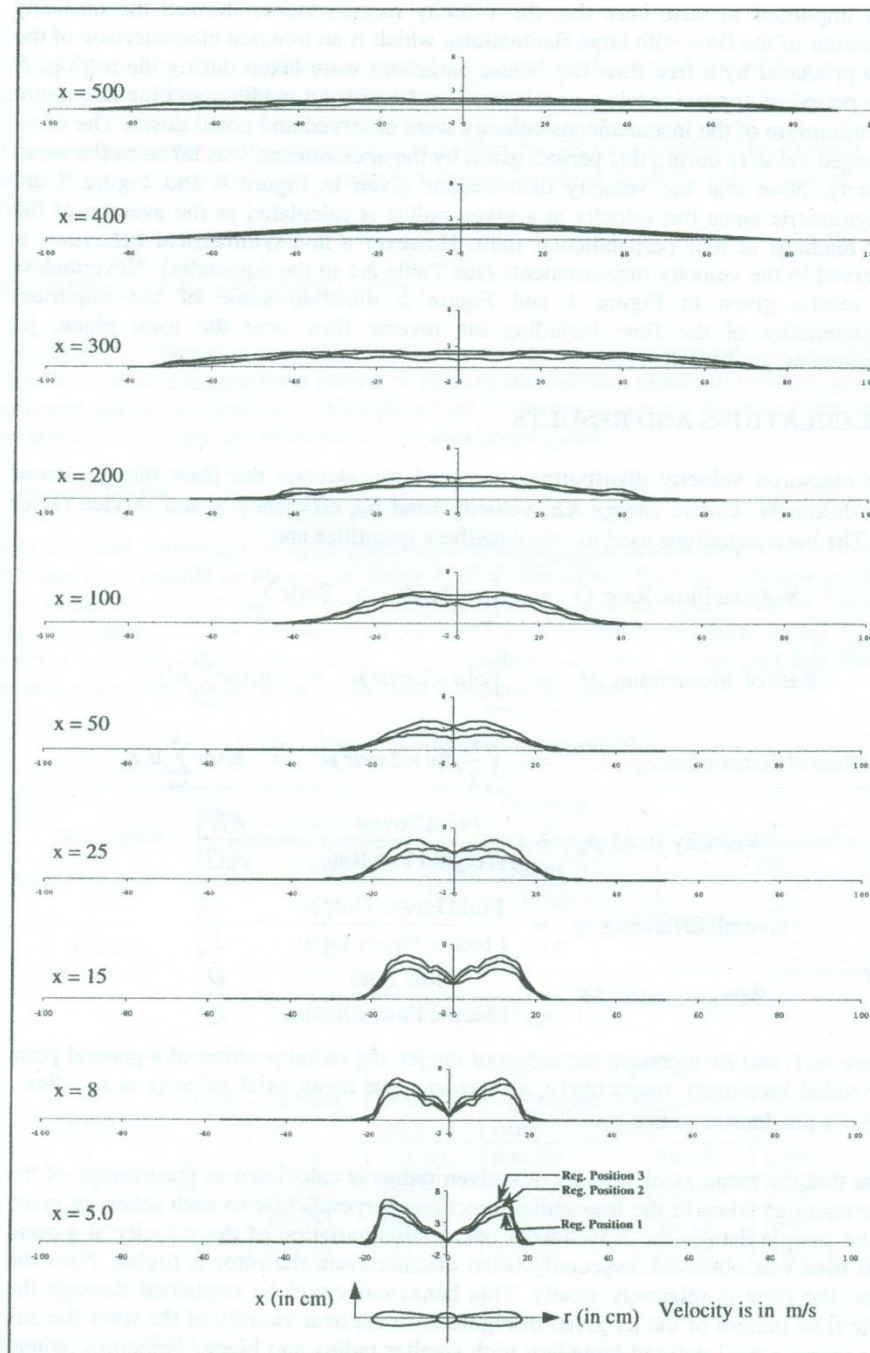


Figure 5: Axial velocity distribution generated by Fan-B at different regulator positions

It is important to state here that the velocity measurements showed the unsteady behaviour of the flow with large fluctuations, which is an inherent characteristic of the flow produced by a free-flow fan. These variations were taken during the testing. A time period of approximately two minutes was taken for a reading, and the maximum and minimum of the instantaneous velocity were observed and noted down. The time-averaged velocity during this period, given by the anemometer, was taken as the mean velocity. Note that the velocity distributions given in Figure 4 and Figure 5 are axisymmetric since the velocity at a given radius is calculated as the average of the four readings at four perpendicular radii. However a non-symmetrical behaviour is observed in the velocity measurements (see Table A1 in the Appendix). Nevertheless the results given in Figure 4 and Figure 5 illustrate some of the important characteristics of the flow including the reverse flow near the rotor plane, jet entrainment, jet diffusion, etc.

CALCULATIONS AND RESULTS

The measured velocity distributions are used to calculate the flow rate Q , linear momentum M , kinetic energy KE , velocity head h_v , efficiency η and service factor SF . The basic equations used to calculate these quantities are:

$$\text{Volume Flow Rate } \dot{Q} = \int_{r=0}^{r_0} u \times 2\pi r dr = 2\pi \Delta r \sum_{i=1}^n u_i r_i$$

$$\text{Rate of Momentum } \dot{M} = \int_{r=0}^{r_0} \rho(u \times 2\pi r dr)u = 2\pi \rho \Delta r \sum_{i=1}^n u_i^2 r_i$$

$$\text{Rate of Kinetic Energy } \dot{KE} = \int_{r=0}^{r_0} \frac{1}{2} \rho(u \times 2\pi r dr)u^2 = \pi \rho \Delta r \sum_{i=1}^n u_i^3 r_i$$

$$\text{Velocity Head } h_v = \frac{\text{Fluid Power}}{\text{Weight Flow Rate}} = \frac{\dot{KE}}{\rho g \dot{Q}}$$

$$\text{Overall Efficiency } \eta = \frac{\text{Fluid Power Output}}{\text{Electric Power Input}} = \frac{\dot{KE}}{P_{in}}$$

and

$$\text{Service Factor } SF = \frac{\text{Flow Rate}}{\text{Electric Power Input}} = \frac{\dot{Q}}{P_{in}},$$

where r_0 , r , and Δr represent the radius of the jet, the radial position of a general point and radial increment, respectively, u represents the mean axial velocity at a radius r and ρ is the density of air.

Note that the mean axial velocity at a given radius is calculated as the average of the four readings taken in the four radial directions perpendicular to each other, as given in the sample data in the Appendix. Considerable variation of the velocity at a point with time was observed, especially when distance from the rotor is higher. Near the rotor, the flow is relatively steady. This behaviour could be explained through the basic flow pattern of the jet given in Figure 2. In the near vicinity of the rotor the air-jet possess a well defined boundary with smaller radius and higher velocities, where the buffer layer is limited to very thin layer. In this region, the flow is well controlled by the momentum of the jet imparted by the rotor. However, on the planes further away from the rotor the jet expands, flow rate increases, mean velocity decreases and

the buffer layer developed to a thicker regime. As the momentum of the jet becomes much smaller, the jet gets more susceptible to external disturbances and therefore becomes unsteady. These fluctuations are usually governed by the size of the room and the furniture and other solid boundaries present in the room.

The calculated results are presented in Table 2, Table 3, Table 4 and Table 5. The variations of the basic flow parameters along the air-jet of the two fans are given in Table 2 and Table 3.

Fan Type	Parameter	Regulator Position	Axial Distance (in number of rotor diameters)								
			0.14	0.38	0.75	1.00	2.00	4.50	7.00	9.50	12.00
Type - A	Flow Rate (m ³ /s)	1	0.35	0.37	0.41	0.44	0.66	0.84	1.43	1.13	1.09
		2	0.39	0.49	0.52	0.57	0.96	0.89	2.09	1.47	1.91
		3	0.48	0.55	0.61	0.68	1.12	1.34	2.68	1.82	2.68
	Rate of Momentum (N)	1	1.50	1.59	1.72	1.45	1.83	1.43	2.00	1.23	0.94
		2	2.21	2.62	2.73	2.24	3.36	1.72	3.75	1.98	2.25
		3	3.10	3.33	3.75	3.54	4.44	3.44	5.84	3.08	3.83
	Rate of Kinetic Energy (W)	1	2.85	3.11	3.27	2.27	2.46	1.17	1.28	0.66	0.36
		2	5.41	6.45	6.52	4.42	5.84	1.69	3.16	1.33	1.22
		3	8.91	9.29	10.42	8.95	8.75	4.37	5.79	2.57	2.58
	Velocity Head (m)	1	0.69	0.72	0.67	0.44	0.32	0.12	0.08	0.05	0.03
		2	1.17	1.11	1.06	0.66	0.52	0.16	0.13	0.08	0.05
		3	1.57	1.44	1.45	1.12	0.67	0.28	0.18	0.12	0.08

Table 2: Variations of the flow parameters along the air-jet of Fan A.

Fan Type	Parameter	Regulator Position	Axial Distance (in number of rotor diameters)							
			0.20	0.38	0.63	1.25	2.50	5.00	7.50	10.00
Type - B	Flow Rate (m ³ /s)	1	0.27	0.33	0.34	0.30	0.26	0.36	0.30	0.22
		2	0.32	0.36	0.38	0.33	0.31	0.42	0.39	0.31
		3	0.29	0.39	0.43	0.38	0.35	0.48	0.44	0.36
	Rate of Momentum (N)	1	1.18	1.30	1.27	0.62	0.24	0.26	0.16	0.06
		2	1.54	1.58	1.56	0.75	0.31	0.35	0.24	0.12
		3	1.32	1.89	1.98	0.93	0.39	0.41	0.31	0.14
	Rate of Kinetic Energy (W)	1	2.30	2.48	2.31	0.59	0.11	0.09	0.04	0.01
		2	3.42	3.32	3.06	0.79	0.15	0.13	0.07	0.02
		3	2.77	4.37	4.38	1.06	0.20	0.16	0.10	0.03
	Velocity Head (m)	1	0.71	0.64	0.58	0.17	0.04	0.02	0.01	0.00
		2	0.91	0.79	0.68	0.20	0.04	0.03	0.02	0.01
		3	0.80	0.95	0.86	0.24	0.05	0.03	0.02	0.01

Table 3: Variations of the flow parameters along the air-jet of Fan B.

The graphical representations of these variations are given in Figure 6 to Figure 13. The flow rate variation generated by Fan-A given in Figure 6 shows a continuous increase illustrating the jet entrainment process due to viscous shear. Flow rate becomes a maximum of about 4 to 6 times the flow rate near the rotor at about a distance of 7 rotor diameters downstream. Then further downstream the flow rate tends to decrease as a result of turbulent diffusion. The characteristic of the jet generated by Fan-B shows much inferior performance than that of Fan-A as the jet entrainment appears to be much weaker (see Figure 7). The jet entrainment

predominantly takes place up to about 0.6 rotor diameters downstream, where the flow rates become approximately 20 - 50% higher than that of at the rotor. Then the jet entrainment as well as diffusion takes place resulting fluctuating characteristics. The flow rates again reach a maximum at about 5 rotor diameters downstream, where the flow rates are approximately 30 - 60% higher than that near the rotor. Further downstream, jet diffusion becomes predominant and there is a continuous decrease in the flow rates. Note that there are large fluctuations in the flow rates, especially on the planes far downstream from the rotor. On these planes, the thickness of the buffer layer is considerably higher, where the flow velocity shows considerable fluctuations and therefore difficult to measure. As the flow rate in this regime can be considerable due to larger flow area, the calculated flow rates (as well as momentum) can exhibit large fluctuations.

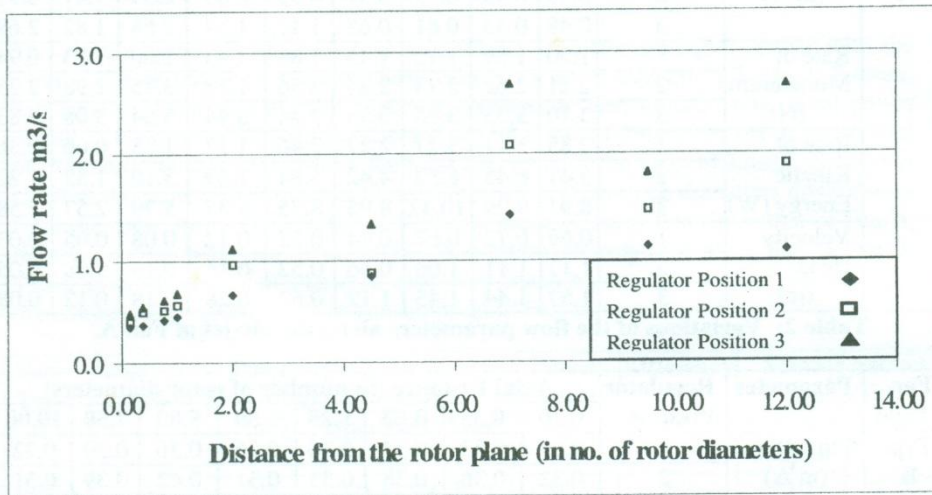


Figure 6: Variation of the volume flow rate along the air-jet of Fan-A.

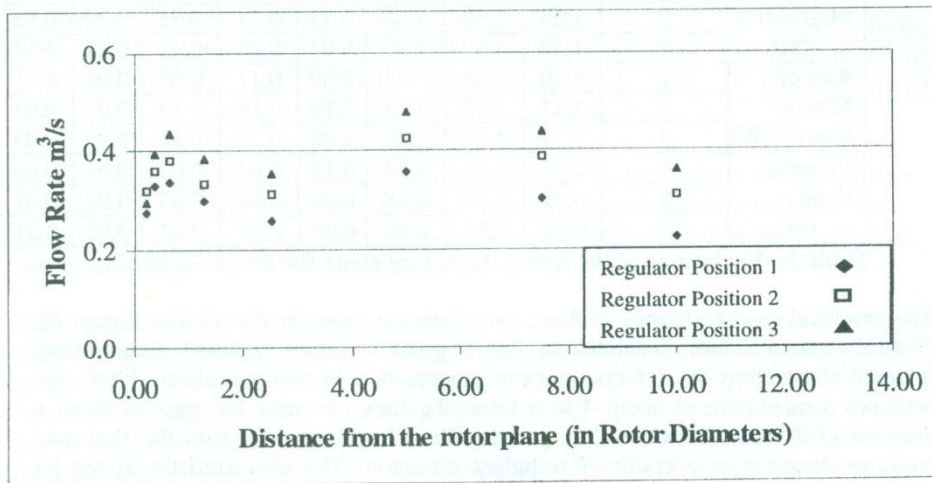


Figure 7: Variation of the volume flow rate along the air-jet of Fan-B.

The difference between the above characteristics of the two fans is difficult to explain with the existing data. One possible reason could be the level of swirl generated by the fan torque. A jet with a higher swirl diffuses more rapidly than that with a lower swirl component (Rajaratnam 1976). Another possibility is that the Fan-B generates higher turbulence level resulting higher rate of diffusion. In order to have a better understanding about these behaviors, the variations of the axial momentum of the jet of the two fans are plotted in Figure 8 and Figure 9.

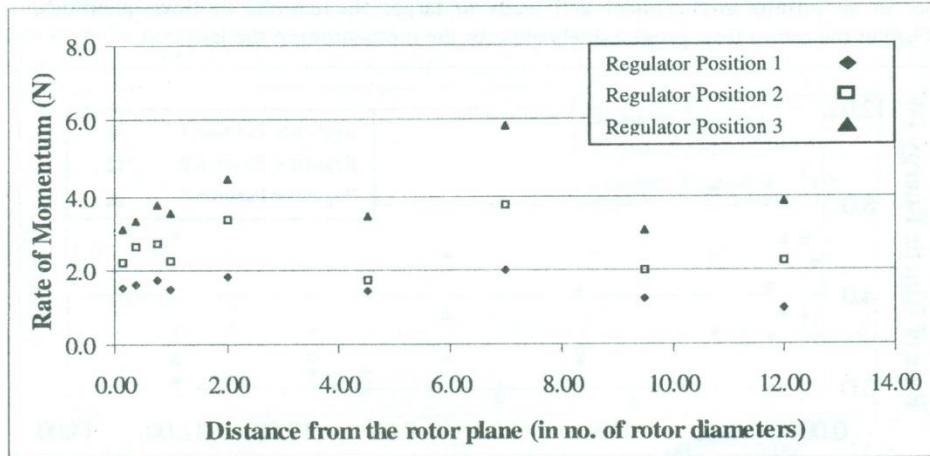


Figure 8: Variation of the rate of momentum along the air-jet of Fan-A

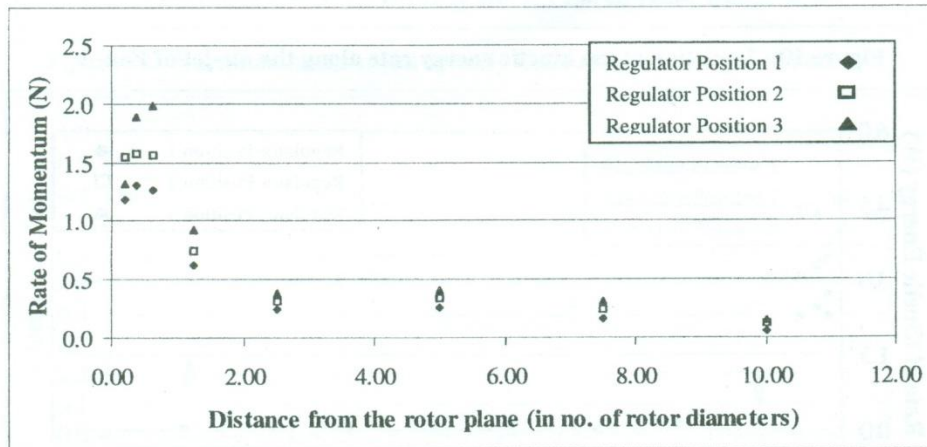


Figure 9: Variation of the rate of momentum along the air-jet of Fan-B

Both figures show a continuous increase in the axial momentum up to about a distance less than one rotor diameter. Axial momentum of Fan-B decreases rapidly indicating a strong diffusion of the jet, while that of Fan-A fluctuates but shows a slight decrease in trend indicating a higher penetrating capacity. The initial increase in the axial momentum of the jet is obvious because, as the jet converges, the pressure generated by the fan is converted into axial momentum. The resultant momentum reaches a maximum at the section with a minimum jet diameter. Therefore it could be concluded that the minimum jet diameter occurs at a distance less than one rotor

diameter (according to the present results, 0.75 diameters for Fan-A and 0.6 diameters for Fan-B). This is more apparent according to the variation of the kinetic energy (based on the axial velocity), as given in Figure 10 and Figure 11. It is important to state here that the jet flow generated by the fans is not an ideal jet in the sense that it is in a finite environment. For such confined flows, conservation of mass demands that a return flow be set up between the jet and the outer boundaries, which increases with the downstream distance. This behaviour results in a thicker buffer layer than that of a jet in an infinite environment and leads to larger fluctuations in flow quantities. Further the return flow progressively absorbs the momentum of the jet.

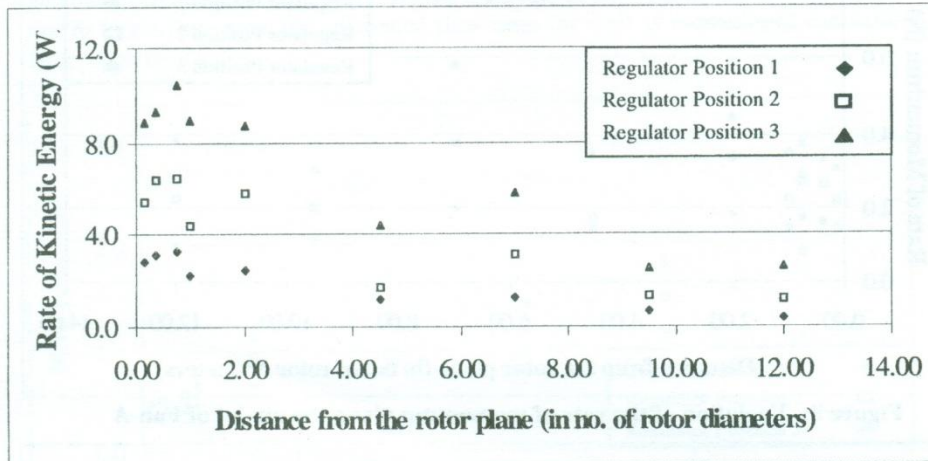


Figure 10: Variation of the kinetic energy rate along the air-jet of Fan-A

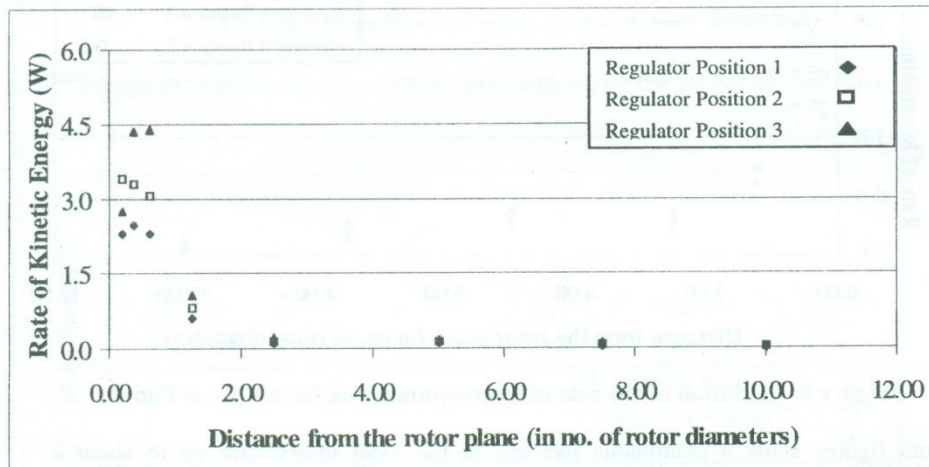


Figure 11: Variation of the kinetic energy rate along the air-jet of Fan-B

In both fans, the total rate of kinetic energy of the jet increases due to conversion of pressure energy to kinetic energy till the minimum jet diameter is reached, where the pressure energy becomes zero. Further downstream the kinetic energy of the jet decreases rapidly due to jet diffusion. The rate of diffusion is much higher for Fan-B

than that of Fan-A resulting in lower performance. The relative effects of the jet diffusion and pressure energy to kinetic energy conversion could be analyzed by evaluating a mean value for the velocity head of the fluid.

In the case of Fan-A, the mean velocity head remains approximately constant in the near vicinity of the rotor, where the pressure energy to kinetic energy conversion takes place. Therefore it could be concluded that this conversion rate is of the same order as the rate of jet diffusion. While the results of Fan-B indicate a higher diffusion rate than the pressure energy to kinetic energy conversion rate.

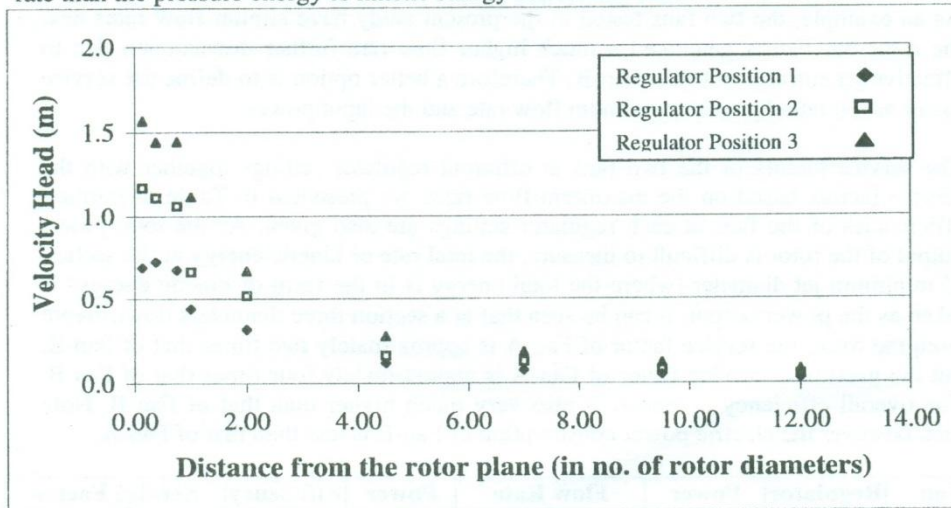


Figure 12: Variation of the mean velocity head along the air-jet of Fan-A

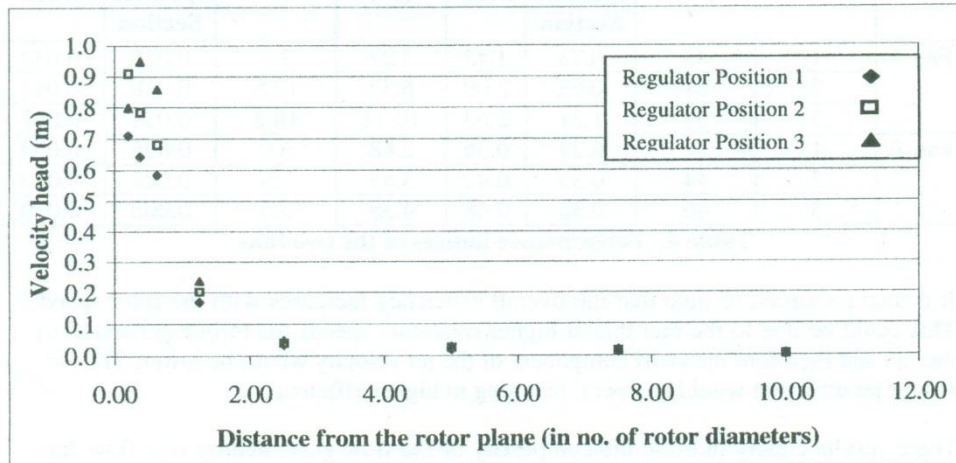


Figure 13: Variation of the mean velocity head along the air-jet of Fan-B

One of the prime objective of the present study is to identify a performance index to represent the overall performance of a given free-flow fan. The most commonly used parameter in fluid machinery is the overall efficiency, that is the output power to input power ratio. However for free-flow fans this quantity is difficult to predict as the output energy of the air (which includes both the pressure energy and the kinetic

energy) is difficult to measure. Further the energy of the fluid is in little use for the customer, what is important is the flow velocity generated by the fan. Therefore another performance index is defined for air-circulating fans, so called service factor, which is the ratio between the flow rate at a specified section from the rotor plane (three rotor diameters in the case of pedestal and table fans) to the electric power input to the fan (SLS 814 - Part 1). However, no specific values for the service factor have been defined to identify whether the performance of a given fan is satisfactory or not. Another disadvantage of the use of service factor as a performance index is that the flow rate at a specified section would not reflect the overall performance of the jet. As an example, the two fans tested in the present study have similar flow rates near the rotor but Fan-A generated a much higher flow rate further downstream due to effective jet entrainment than Fan-B. Therefore a better option is to define the service factor as the ratio between maximum flow rate and the input power.

The service factors of the two fans at different regulator settings together with the service factors based on the maximum flow rates are presented in Table 4. Further, efficiencies of the fans at each regulator settings are also given. As the total power output of the rotor is difficult to measure, the total rate of kinetic energy at the section of minimum jet diameter (where the total energy is in the form of kinetic energy) is taken as the power output. It can be seen that at a section three diameters downstream from the rotor, the service factor of Fan-A is approximately two times that of Fan-B, but the maximum service factor of Fan-A is approximately four times that of Fan-B. The overall efficiency of Fan-A is also very much higher than that of Fan-B. Note that, however the electric power consumption of Fan-B is less than that of Fan-A.

Fan Type	Regulator Position	Power Consump. (W)	Flow Rate (m^3/s)		Power Output (W)	Efficiency (%)	Service Factor ($\text{m}^3/\text{s}/\text{W}$)	
			Specified Section	Max			Specified Section	Max.
Fan-A	1	45	0.73	1.43	3.27	7.3	0.016	0.032
	2	51	0.93	2.09	6.52	12.8	0.018	0.041
	3	57	1.21	2.68	10.42	18.3	0.021	0.047
Fan-B	1	41	0.27	0.36	2.48	6.0	0.006	0.009
	2	44	0.33	0.42	3.42	7.8	0.008	0.010
	3	46	0.38	0.48	4.38	9.5	0.008	0.010

Table 4: Performance indices of the two fans

It is also important to note that the overall efficiency increases with the rotor speed. This could be due to the fact that at higher rotational speeds the torque generated by the fan and therefore the swirl component of the jet velocity would be lower. Thus the rate of jet diffusion would be lower, resulting in higher efficiencies.

These results clearly indicate the complexity of the flow generated by free-flow fans and difficulty of predicting the overall performance. Both the fans considered in the present study generated a similar axial velocity distribution at the rotor, but different behaviour of the overall jet developments leading to a vast difference in the performances. As an example, the velocity distributions at the near vicinity of the rotor of Fan-A at the regulator position 2 and that of Fan-B at the regulator position 3 are plotted in Figure 14. It can be seen that the two velocity distributions are quite similar, resulting volume flow rates of $0.392 \text{ m}^3/\text{s}$ and $0.394 \text{ m}^3/\text{s}$, respectively.

However, as shown in Figure 15 the jet development behaviour of the two cases are not similar; one jet shows a strong entrainment with considerable increase in the flow rate in downstream direction, while the other jet shows very little increase in the flow rate indicating higher diffusion.

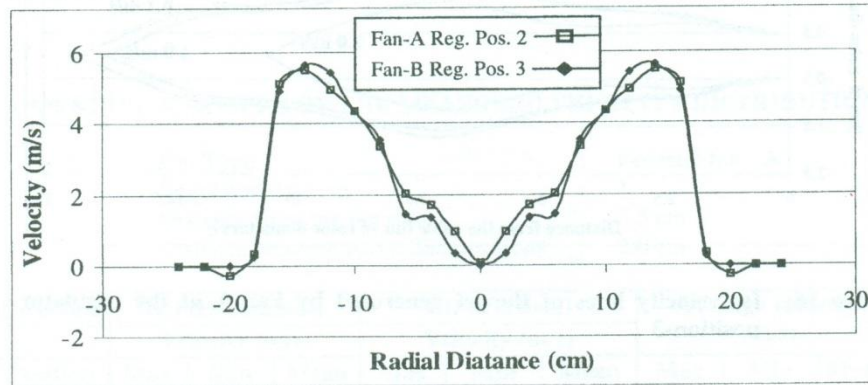


Figure 14: Velocity profiles at the near vicinity of the rotors of the two fans

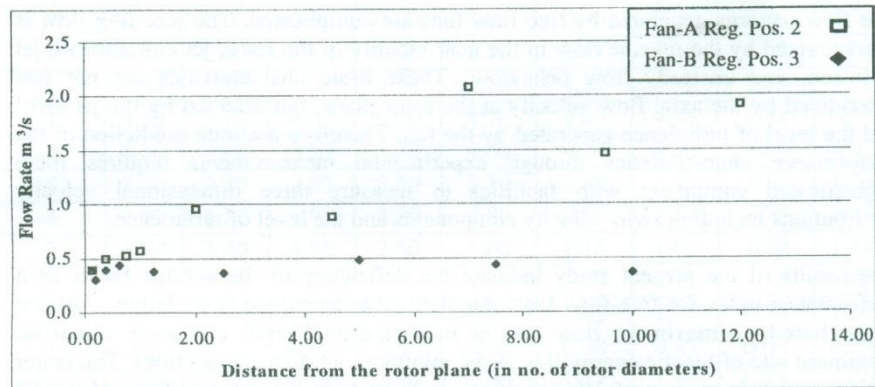


Figure 15: Comparison of the jet development behaviours of the two fans

The above results also indicate the limitations of the service factor as a performance index for free-flow fans. However, both the overall efficiency based on the rate of kinetic energy at the minimum jet diameter section and the service factor based on the maximum flow rate illustrate clearly the relative performances of the two fans. Therefore, these two indices would be more appropriate for performance evaluation of free-flow fans.

Further, as free-flow fans are widely used for air circulation and comfort, it would be more appropriate to define a comfort region that a fan could cover at each regulator setting. This is achieved by forming iso-velocity lines based on the axial velocity distribution generated by a given fan. As an example, iso-velocity lines for Fan-A at the regulator position 3 are illustrated in Figure 16.

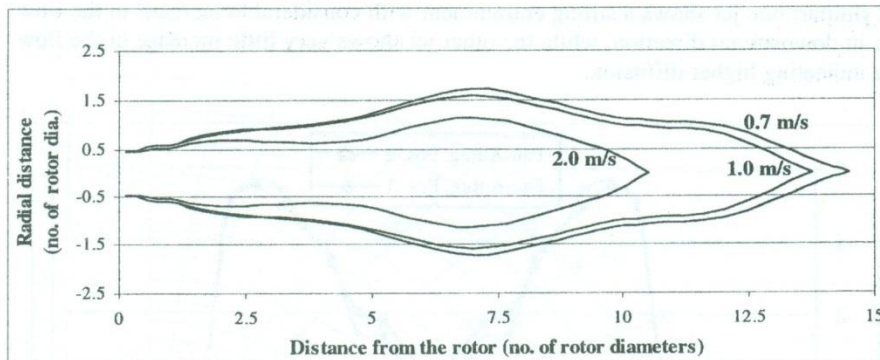


Figure 16: Iso-velocity lines of the jet generated by Fan-A at the regulator position-3

CONCLUSIONS

The flow patterns generated by free-flow fans are complicated. The resulting flow is characterized by the reverse flow in the near vicinity of the rotor, jet entrainment, jet diffusion, and unsteady flow behaviour. These basic characteristics are not just determined by the axial flow velocity at the rotor plane, but affected by the jet swirl and the level of turbulence generated by the fan. Therefore accurate prediction of the performance characteristics through experimental measurements requires more sophisticated equipment with facilities to measure three dimensional velocity distributions including swirl velocity components and the level of turbulence.

The results of the present study indicate the deficiency of the service factor as a performance index for free-flow fans. An alternative technique is to define a service factor based on maximum flow rate or to define an overall efficiency based on maximum rate of kinetic energy (i.e. at the minimum jet diameter section). The better option, which is more useful for the user, is to provide iso-velocity lines of the jet generated by the fan at each regulator setting together with the power consumption by the fan.

REFERENCES

- AHMAD, J. & DUQUE, E.P.N. 1996. Helicopter rotor blade computation in unsteady flows using moving embedded grids. *J. Aircraft*, 33, pp. 54-60.
- CONLISK, A.T. 1997. Modern Helicopter Aerodynamics. *Ann. Rev. Fluid Mech.*, 29, pp. 515-567.
- RAJARATNAM, N, 1976. Turbulent jets. Elsevier Scientific Publishing Company.
- SLS 814 - Part 1. SRI LANKA STANDARD, Specification for electric fans and regulators - Part 1 - Performance.

SUGATHAPALA, A.G.T. 1997. Performance analysis of free-flow fans: A theoretical and experimental study. Seminar on Contribution to the Energy Scenario in Sri Lanka, SLAAS, Colombo 07, Sri Lanka, 26th November 1997 (unpublished).

WALLIS, R.A. 1983. Axial flow fans and ducts. John Wiley & Sons Inc.

APPENDIX: A SAMPLE OF THE MEASURED VELOCITY DISTRIBUTION

Fan Type : Pedestal fan - A
 Regulator Position : 1
 Distance from the fan rotor : 5.5 cm
 Distance between two radial positions : 2.0 cm

Direction	AB (Horizontal)			CD (Vertical)			Average velocity		
	Velocity (m/s)			Velocity (m/s)			(m/s)		
Position	Max	Min	Mean	Max	Min	Mean	Max	Min	Mean
-12	0.00	0.00	0.00	0.00	0.00	0.00	0.00	0.00	0.00
-11	0.00	0.00	0.00	0.00	0.00	0.00	0.00	0.00	0.00
-10	0.00	0.00	0.00	0.00	0.00	0.00	-0.20	0.00	-0.04
-9	0.50	0.00	0.10	2.60	1.70	2.17	2.15	1.68	1.87
-8	1.44	0.70	1.04	4.70	4.10	4.32	4.33	3.83	4.11
-7	4.40	3.90	4.05	5.00	4.70	4.89	4.58	4.35	4.45
-6	4.10	3.80	3.89	4.50	4.00	4.29	4.20	3.88	4.02
-5	3.20	2.80	2.82	3.50	3.10	3.39	3.48	3.18	3.29
-4	2.20	1.80	1.96	3.30	2.80	2.99	2.83	2.55	2.67
-3	1.90	1.40	1.82	2.50	1.80	2.16	1.65	1.30	1.48
-2	1.40	0.10	1.06	1.50	1.10	1.25	1.70	1.10	1.45
-1	0.80	0.00	0.61	1.10	0.90	1.02	1.10	0.78	1.01
0	0.04	0.00	0.09	0.50	0.00	0.08	0.27	0.00	0.09
1	1.40	1.20	1.22	1.10	1.00	1.17	1.10	0.78	1.01
2	1.60	1.40	1.43	2.30	1.80	2.06	1.70	1.10	1.45
3	1.60	1.50	1.35	3.10	2.80	2.92	1.65	1.30	1.48
4	2.20	2.10	2.18	3.60	3.50	3.55	2.83	2.55	2.67
5	2.90	2.70	2.76	4.30	4.10	4.20	3.48	3.18	3.29
6	3.60	3.20	3.36	4.60	4.50	4.53	4.20	3.88	4.02
7	4.10	4.00	4.04	4.80	4.80	4.80	4.58	4.35	4.45
8	4.40	4.30	4.44	3.90	3.10	3.57	4.33	3.83	4.11
9	4.90	4.50	4.67	0.60	0.50	0.55	2.15	1.68	1.87
10	-0.40	0.00	-0.14	-0.40	0.00	-0.01	-0.20	0.00	-0.04
11	0.00	0.00	0.00	0.00	0.00	0.00	0.00	0.00	0.00
12	0.00	0.00	0.00	0.00	0.00	0.00	0.00	0.00	0.00

Table A1: Axial velocity distribution of the jet at different planes from the rotor

Influence of Linings on Stress and Deformation in Rock Around Tunnels

U.G.A. Puswewala (1), I.R.P. Gunatilaka (2), C.L. Hapuarachchi (3) and
R.M. Nandasena (4)

(1) Senior Lecturer, University of Moratuwa

(2) Civil Engineer, Central Engineering Consultancy Bureau

(3) Captain, Sri Lanka Army

(4) Civil Engineer, Road Construction & Design Company

Influence of Linings on Stress and Deformation in Rock Around Tunnels

U.G.A. Puswewala⁽¹⁾, I.R.P. Gunatilaka⁽²⁾, C.L. Hapuarachchi⁽³⁾ and
R.M. Nandasena⁽⁴⁾

(1) Senior Lecturer, University of Moratuwa

(2) Civil Engineer, Central Engineering Consultancy Bureau

(3) Captain, Sri Lanka Army

(4) Civil Engineer, Road Construction & Design Company

ABSTRACT

Stress distribution and deformation in rock around lined tunnel openings subjected to internal pressure are investigated by using plane strain finite element analysis. Two typical tunnel cross-sections, in the forms of an elliptical and a horse-shoe shaped tunnel, are considered with varying thicknesses of concrete linings; material behavior is assumed to be isotropic linear elastic, and analyses are done using typical elastic material parameters to represent a particular type of rock and the concrete. Variation of major and minor principal stresses in the rock medium with increasing liner thickness and distance from the tunnel face is presented for both tunnel shapes. The influence of the lining thickness on the deformation (displacement) characteristics at selected locations in the rock medium is illustrated. The results show the general trend that stresses and deformations in the rock medium decrease with increasing liner thickness, but the effect of the liner thickness depends on the stress or displacement quantity being investigated as well as the shape of the tunnel. Thus an optimal liner thickness has to be estimated as a compromise between economy and effectiveness.

INTRODUCTION

Stress and deformation fields in rock surrounding tunnel excavations are of considerable importance in tunnel engineering. The stress fields set up due to different load systems that may be imposed on the tunnel walls can be used to determine potential failure regions in the surrounding rock. Many instances arise when stresses transmitted to the surrounding rock need to be reduced by some appropriate means; an example for this is the tensile normal tangential stress set up in rock surrounding a circular or elliptical tunnel conveying water under pressure. A concrete lining is often introduced to tunnels to prevent generation of high stresses in the surrounding rock mass, in addition to other potential purposes such as protecting the exposed rock surface from weathering/ erosion, controlling seepage of water and preventing rock falls.

This paper illustrates the effect of tunnel lining on the stress distribution and deformation behaviour in the surrounding rock mass for two typical tunnel shapes. The two tunnel shapes considered are an elliptical shape and a horse-shoe shape (Szechy 1973). Concrete linings of different thickness are considered, and numerical analyses of the problems are conducted by using the Finite Element Method. It is assumed that material behaviour for both the rock-mass and concrete is isotropic linear elastic, and that conditions of plane strain prevail in all cases considered.

Scope of the analysis is limited to demonstrative purposes only; thus, only a limited parametric study is conducted, by selecting a single set of typical material parameters for rock and concrete, and a particular geometry for each of the two tunnel shapes. However, a range of tunnel lining thicknesses is considered.

TUNNEL SHAPES AND BOUNDARY CONDITIONS

The two tunnel shapes considered for study are an elliptical tunnel and a horse-shoe shaped tunnel. Typical dimensions were selected to define each of the two tunnel cross-sections (Szechy, 1973); the plane strain domains considered for the two tunnel shapes are as shown in Figure 1 (elliptical tunnel) and Figure 2 (horse-shoe shaped tunnel).

Since the scope of the current analyses is limited to demonstrative purposes, the loading is taken as a uniform pressure applied by a fluid (water) under pressure inside the tunnel; this loading and tunnel geometry permitted symmetry of the system to be utilised. Consequently, double symmetry exists in the elliptical tunnel, requiring only one fourth of the domain to be analysed; and symmetry about the vertical central axis in the horse-shoe shaped tunnel enables only half the domain to be considered. The far boundaries of the domains were selected at a sufficient distance from the tunnel wall so that effects of forces at the tunnel walls will be negligible at these boundaries. Therefore the far boundaries of the domains were fixed against any movement.

FINITE ELEMENT MODELLING

The two finite element meshes along with the displacement boundary conditions applied on the boundaries are shown in Figure 1 (elliptical tunnel) and Figure 2 (horse-shoe tunnel), referred to earlier. Four noded finite elements were used to discretise the material domains. Memory limitations of the personal computer used to analyse these problems meant that meshes could not be made much finer than shown in the figures. Figures 3(a) and (b) show the concrete liner introduced to each tunnel shape in the respective finite element mesh.

The constitutive behaviour of rock domain and concrete in liners are assumed to be according to isotropic linear elasticity. Typical material properties selected to represent the assumed behaviour of rock and concrete are as given below (Selvadurai, 1979):

Material	Young's Modulus (kN/m ²)	Poisson's Ratio
Rock	0.21×10^7	0.30
Concrete	0.21×10^8	0.20

Thus a ratio of Young's Moduli of the concrete to rock of 10 is considered. The uniform fluid pressure applied on internal tunnel surface is assumed as 1000

kN/m^2 . The rock mass is assumed to have reached equilibrium under gravity before the imposed pressure is applied, and only the stress field set up by the imposed pressure on the tunnel walls is investigated here. Plane strain conditions are assumed to prevail, which would be the case if the tunnel axis is a straight line with uniform cross-sectional dimensions in homogeneous rock. Analyses were conducted by varying the thickness of concrete liner from 0 m (unlined case) to 1 m, in increments of 0.2 m, for both tunnel shapes.

NUMERICAL RESULTS

Influence Of Liner Thickness On Stress In Rock Around The Elliptical Tunnel

A limited parametric study by finite element analysis was conducted for both tunnel shapes by considering the range of liner thicknesses mentioned above.

For the elliptical tunnel, principal stresses were investigated along three radial lines AB, CD and EF, shown in Figure 4 radiating from the center of the tunnel. Variation of the major principal stress along the radial line CD for different liner thicknesses is shown in Figure 5, and the variation of the minor principal stress along the same line for different liner thicknesses is shown in Figure 6. The major principal stresses in Figure 5 are tensile, and the minor principal stresses in Figure 6 are compressive.

Variation of the major principal stress (tensile) along the radial line AB for different liner thicknesses is shown in Figure 7, and the variation of the minor principal stress (compressive) along the same line for different liner thicknesses is shown in Figure 8. Corresponding results for the radial line EF are shown in Figure 9 (tensile stresses) and Figure 10 (compressive stresses), respectively.

Note that the Figures 5 to 10 indicate the variation of stresses commencing from a point within the rock mass, which is actually located beyond the maximum thickness of the concrete lining considered here (1.0 m).

The numerical results, and the comparison of Figures 5, 7 and 9, show that the line EF is the critical line along which maximum tensile stresses occur. Figure 9 shows that a concrete lining of thickness 0.2 m causes the tensile stresses at point E to reduce by about 25% as compared to the magnitudes that existed in the case of an unlined tunnel; for a lining thickness of 0.4 m, this reduction is 49% and for a thickness of 1.0 m, it is 69.5%.

In the case of line CD (Figure 5), tensile stresses at point C reduce by 28.3% when a liner of thickness 0.2 m is introduced, as compared to the stresses in the case of an unlined tunnel; the corresponding reductions are 40% for a liner of 0.4 m thickness, and 55% for a liner of 1.0 m thickness.

In the case of line AB (Figure 7), tensile stresses at point A reduce by 20.4% when a liner of thickness 0.2 m is introduced, as compared to the stresses in the case of an unlined tunnel; the corresponding reductions are 38.9% for a liner of 0.4 m thickness, and 65.5% for a liner of 1.0 m thickness.

Figures 6, 8 and 10 show the influence of concrete liner thickness on the compressive principal stress around the elliptical tunnel. According to Figure 8, the compressive principal stress at point A reduces by 16.5% when a 0.2 m thick concrete is introduced to the originally unlined tunnel; this reduction is 26% for a 0.4 m thick liner and 40.8% for a 1.0 m thick liner. Figure 6 shows similar behaviour of the compressive principal stress along the line CD.

Figure 10 shows that large percentile stress reductions occur in the case of the compressive principal stress along line EF. This stress reduces at point E by 52.5% when a 0.2 m thick liner is introduced to the unlined tunnel; the corresponding reduction is 79.2% for a 0.4 m thick liner, and 91.1% for a 1.0 m thick liner.

Figure 11 shows the variation of principal tensile stress along an elliptical (circumferential) line of a shape similar to that of the tunnel opening, but at some distance inside the rock mass from the tunnel face, as the liner thickness is increased.

Influence Of Liner Thickness On Deformation In Rock Around The Elliptical Tunnel

For the elliptical tunnel, influence of the concrete liner on displacement at points inside the rock mass are illustrated by Figures 12 and 13, which show displacements at points located along an elliptical (circumferential) line inside the rock mass, similar to that considered in Figure 11 earlier. According to these results, the percentage reduction of x-displacement and y-displacement over the rock domain varies with the location. Figure 12 shows relatively large percentage reductions in the x-displacement at the x-axis as the tunnel liner thickness is increased (this is 43% when a 0.2 m thick liner is introduced on the unlined tunnel; and 94.5% for a 1.0 m thick liner).

Influence Of Liner Thickness On Stress In Rock Around The Horse-shoe Shaped Tunnel

Figure 14 shows three lines A'B', C'D' and E'F' in the analysis domain of the horse-shoe shaped tunnel. Principal tensile and compressive stress variations as the liner thickness is varied were considered along these lines, as well as (circumferential) lines traced around the shape of the tunnel opening. For brevity, only selected results are illustrated here.

Figure 15 shows the variation of the tensile principal stress along line A'B', as the liner thickness is varied. This stress at the point A' reduces by 46.8% when a liner of thickness 0.2 m is introduced; this reduction is 63% for a 0.4 m thick liner and 82.4% for a 1.0 m thick liner.

Figure 16 shows the variation of the tensile principal stress along line C'D', and has a behaviour similar to that seen in Figure 15 above. Figure 17 shows the variation of tensile principal stress along the line E'F' as the liner thickness is varied; the percentile stress reductions are comparatively less along this direction, with a 39.7% reduction in the stress at point C' for a liner of 1.0 m thickness.

The numerical results further indicated similar behaviour for compressive principal stresses, these being reduced in general as the liner thickness is increased.

Influence Of Liner Thickness On Deformation In Rock Around The Horse-shoe Shaped Tunnel

Figure 18 shows the reduction of the displacement in the x-direction along a (circumferential) line traced around the shape of the tunnel opening. It shows a considerable reduction in the displacement for a liner of 0.2 m thickness, as compared to the case of an unlined tunnel.

Figure 19 shows the variation of the displacement in the y-direction along the identical line; it can be seen that the percentile reduction in the y-displacement at points along this line is relatively small, and that some points experience increases in the latter displacement as the tunnel liner thickness is increased. Thus the effect of liner thickness is not pronounced on the y-displacement of points in the rock mass, while this has a distinct effect on the x-displacements.

Discussion Of Numerical Results

Stress distributions depicted in Figures 5-11 and 15-17 demonstrate the general trend of reduction of stress magnitude in the rock mass as a concrete liner is introduced to the unlined tunnel; this trend in stress behaviour for elliptical and horse-shoe shaped tunnels is in general confirmation with the trend that can be analytically predicted for circular tunnels (Jaeger, 1979), whereby the stress levels in rock mass decrease as liner thickness increases.

It is also seen that the percentage reduction in stress levels (considering the stress that existed for the unlined tunnel as the datum) at points in the rock mass does not show uniformity, but depends on the location of the point and the stress component being considered.

Reduction of deformation with the introduction of the concrete liners is illustrated in Figures 12, 13, 18 and 19. As in the case of stresses, the percentage reductions

in displacements depend on the location of the point and the displacement quantity being considered. For tunnels of elliptical shape, increasing liner thicknesses reduce both x-displacement and y-displacement at points within the rock mass, while for the horse-shoe shaped tunnel considered, the liner thickness has an influence on the x-displacement, but has very little effect on the y-displacement.

The present study illustrates the stress and deformation behaviour in the rock mass as the liner thickness is varied. These criteria, specially the stresses, may determine the thickness of the concrete liner to be used. It is also seen here that there is no major benefit in using liners of very large thickness for the purpose of reduction of stress or deformation in the rock mass. Therefore, a balance of economy and efficiency will have to be worked out in a practical situation.

CONCLUSION

The analyses show that introduction of liners contribute in general to reduction of stress levels and deformations in the rock mass surrounding tunnels, and an optimum liner thickness could be arrived at in practical situations. The actual reduction in stress magnitudes and displacements at points inside the rock mass depends on the tunnel shape, location of the point, and the stress or displacement quantity being considered. This type of finite element analysis offers the tunnel engineers the tools to arrive at an optimum linear thickness for different tunnel shapes, by striking a balance between cost and efficiency.

Acknowledgement: The authors acknowledge the support received from Mr. N. Kodagoda and Mr. V. Somaratne of the Computer Laboratory, University of Moratuwa, for this work.

REFERENCES:

Jaeger, C. (1979), Rock Mechanics and Engineering, Second Edition, Cambridge University Press.

Selvedurai, A.P.S. (1979), Elastic Analysis of Soil-Foundation Interaction, Developments in Geotechnical Engineering, Vol. 17, Elsevier Scientific Publishing Co., Netherlands.

Szechy, Karoly, (1973), The Art of Tunnelling, Second English Edition, Akademiai Kiado, Budapest.

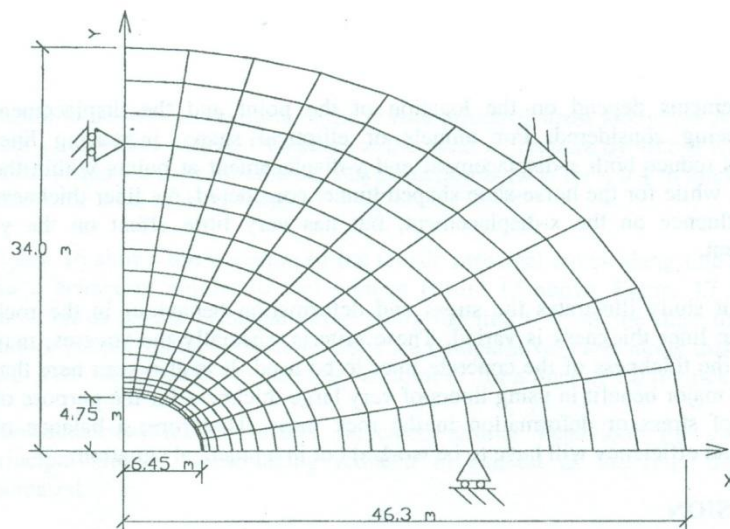


Figure 1. The domain and finite element mesh for the elliptical tunnel

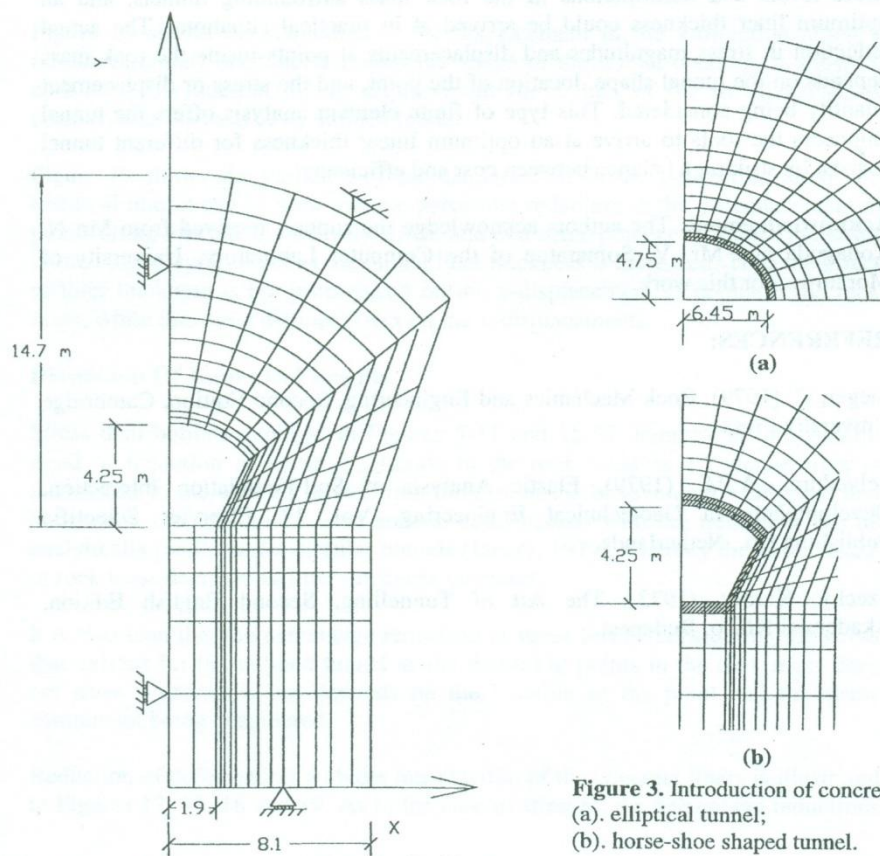


Figure 2. The domain and finite element mesh for the horse-shoe shaped tunnel

Figure 3. Introduction of concrete liner to
(a). elliptical tunnel;
(b). horse-shoe shaped tunnel.

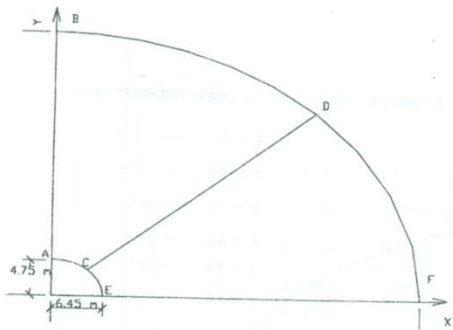


Figure 4. The elliptical tunnel domain showing three radial lines AB, CD and EF.

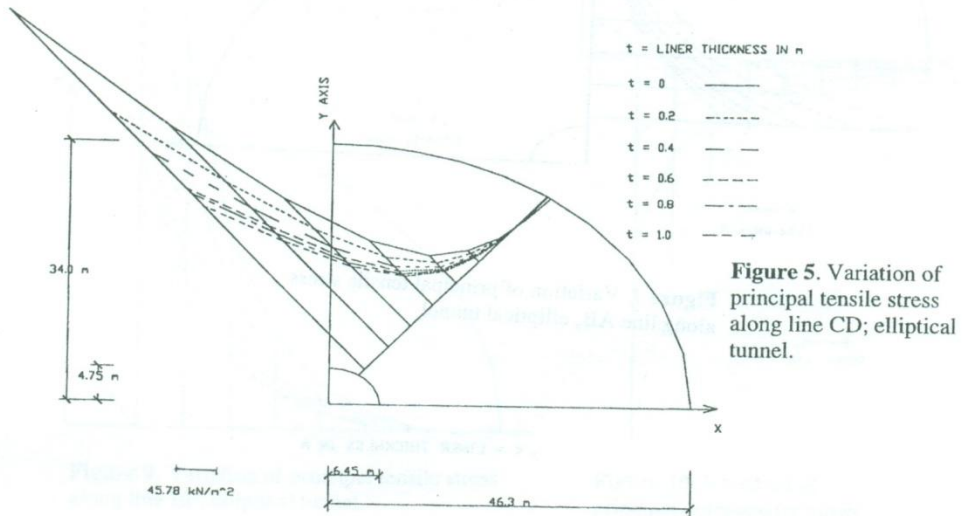


Figure 5. Variation of principal tensile stress along line CD; elliptical tunnel.

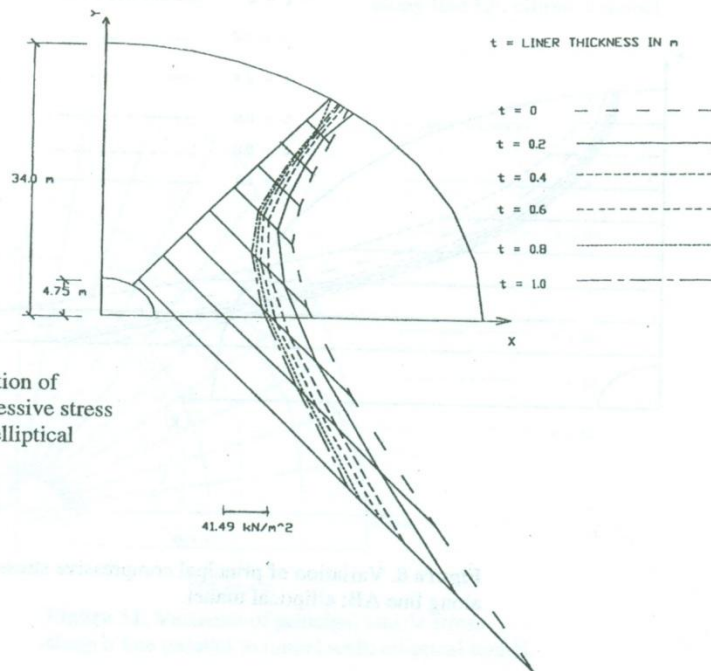


Figure 6. Variation of principal compressive stress along line CD; elliptical tunnel.

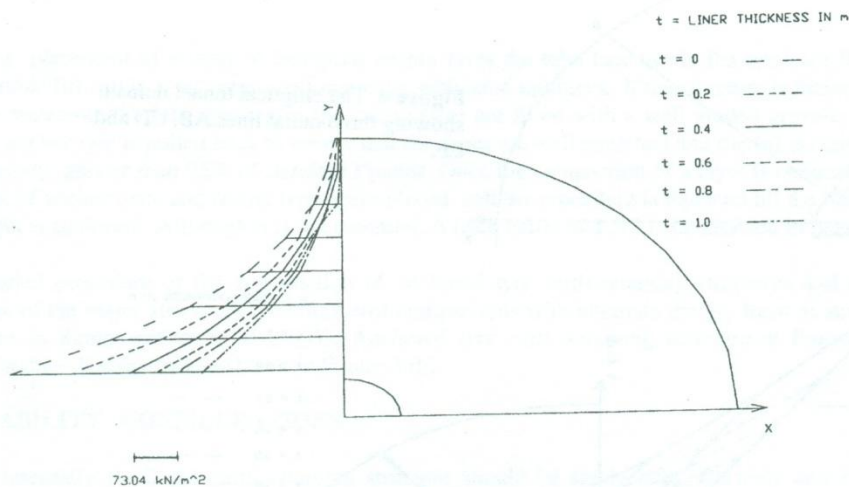


Figure 7. Variation of principal tensile stress along line AB; elliptical tunnel.

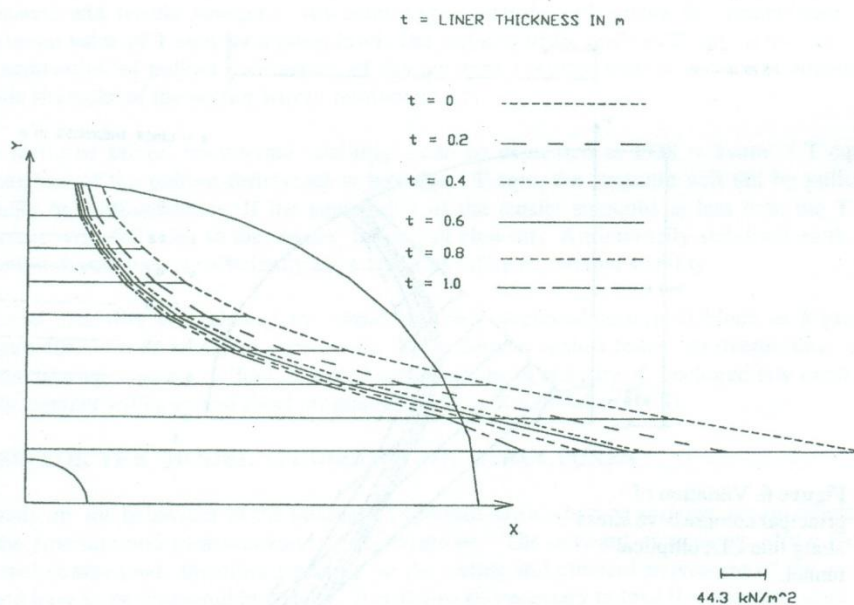


Figure 8. Variation of principal compressive stress along line AB; elliptical tunnel.

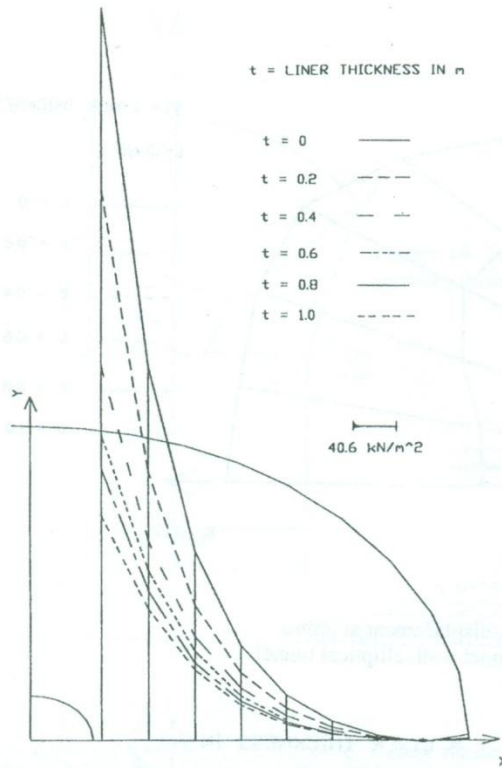


Figure 9. Variation of principal tensile stress along line EF; elliptical tunnel.

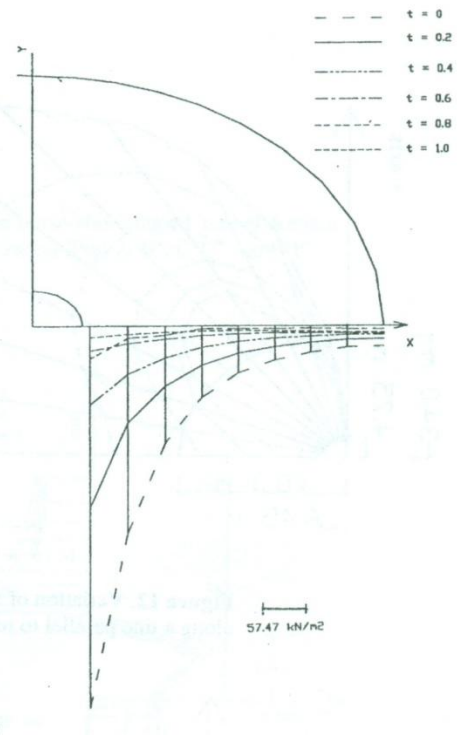


Figure 10. Variation of principal compressive stress along line EF; elliptical tunnel.

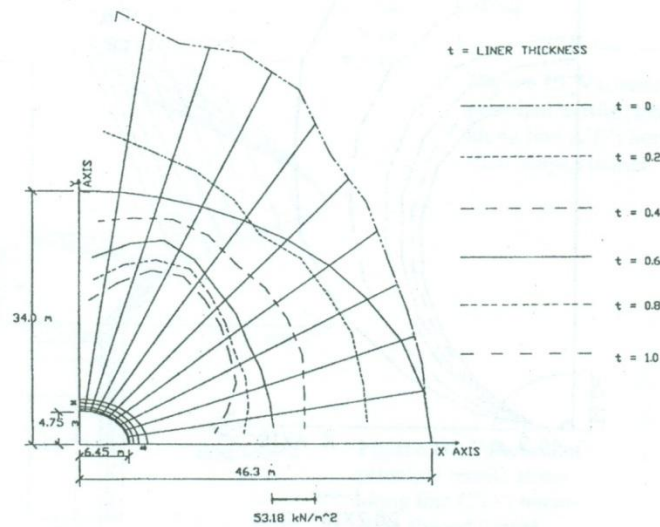


Figure 11. Variation of principal tensile stress along a line parallel to tunnel wall; elliptical tunnel.

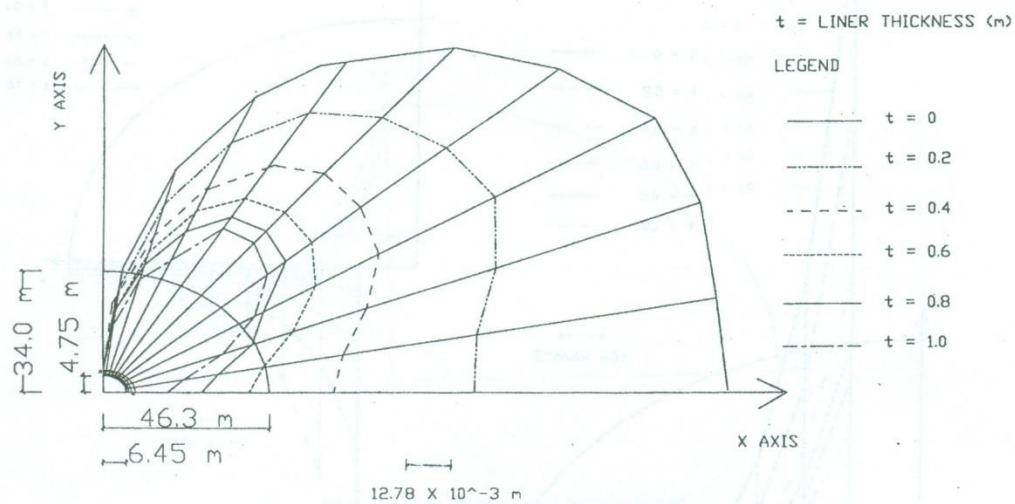


Figure 12. Variation of x-displacement at points along a line parallel to tunnel wall; elliptical tunnel.

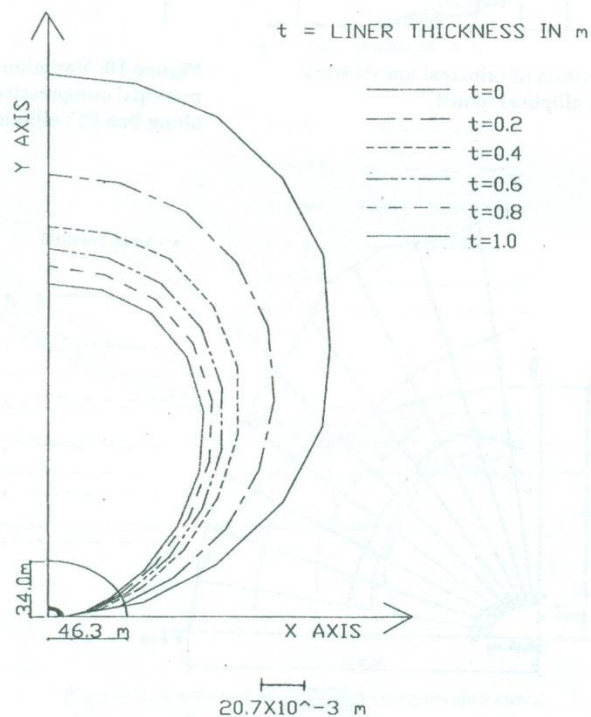


Figure 13. Variation of y-displacement at points along a line parallel to tunnel wall; elliptical tunnel.

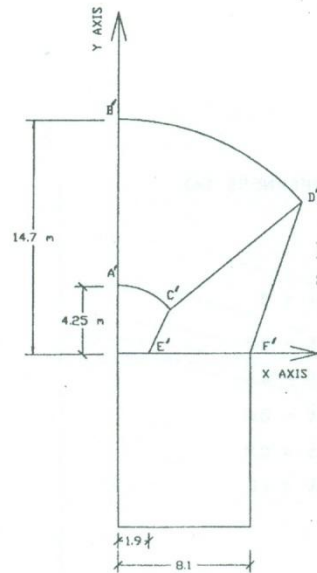


Figure 14. The horse-shoe shaped tunnel domain showing three radial lines A'B', C'D' and E'F'.

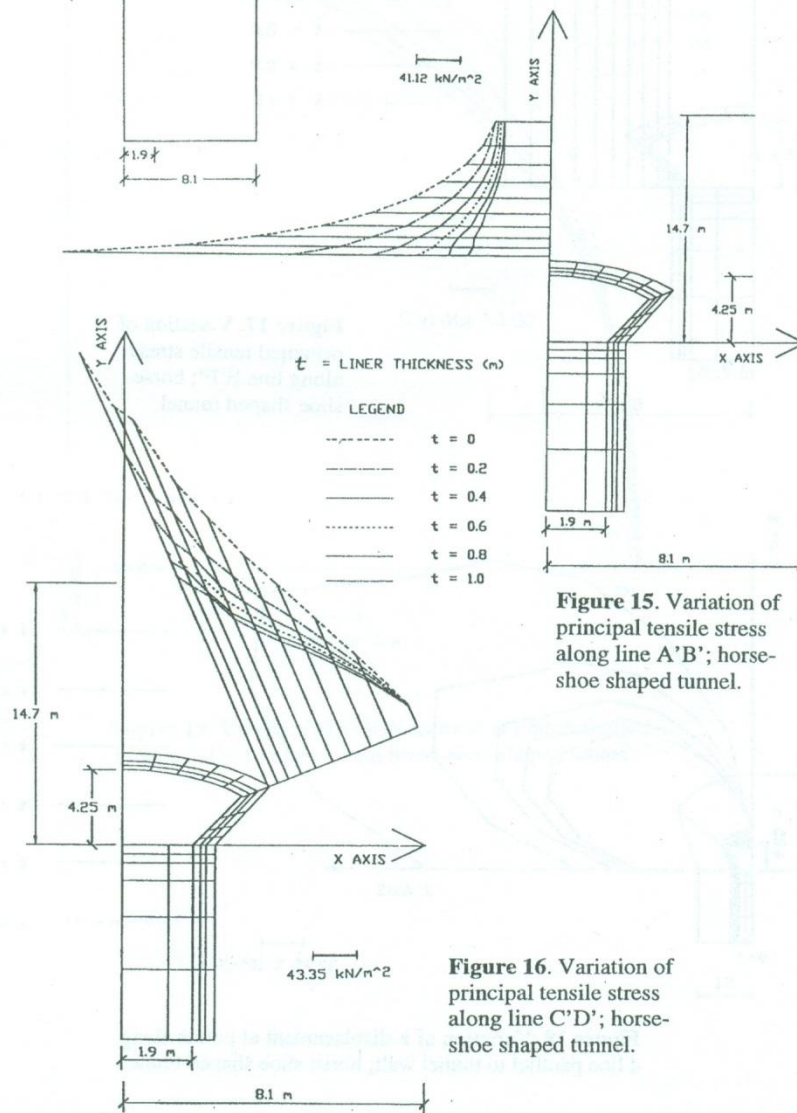


Figure 15. Variation of principal tensile stress along line A'B'; horse-shoe shaped tunnel.

Figure 16. Variation of principal tensile stress along line C'D'; horse-shoe shaped tunnel.

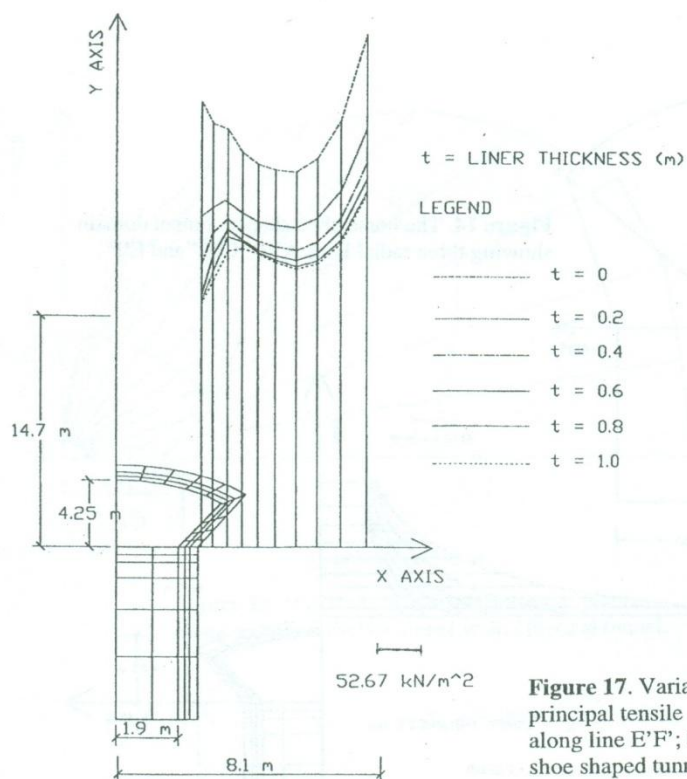


Figure 17. Variation of principal tensile stress along line E'F'; horse-shoe shaped tunnel.

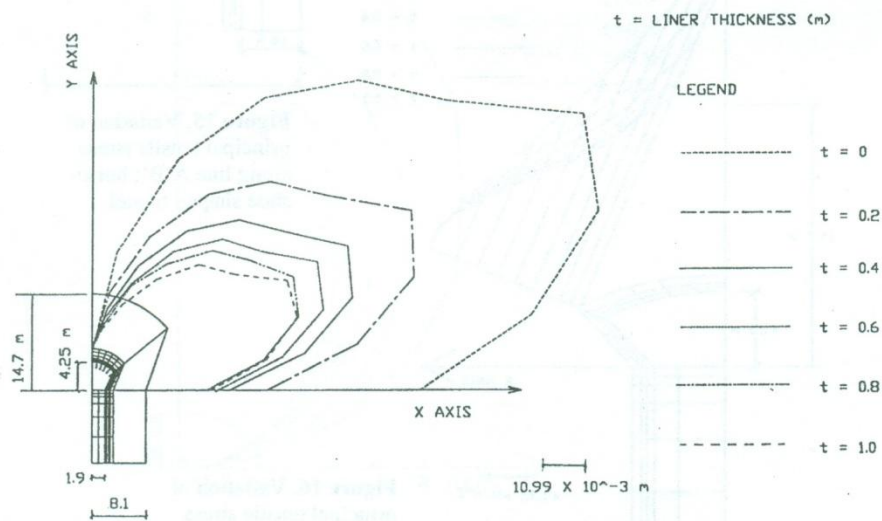


Figure 18. Variation of x-displacement at points along a line parallel to tunnel wall; horse-shoe shaped tunnel.

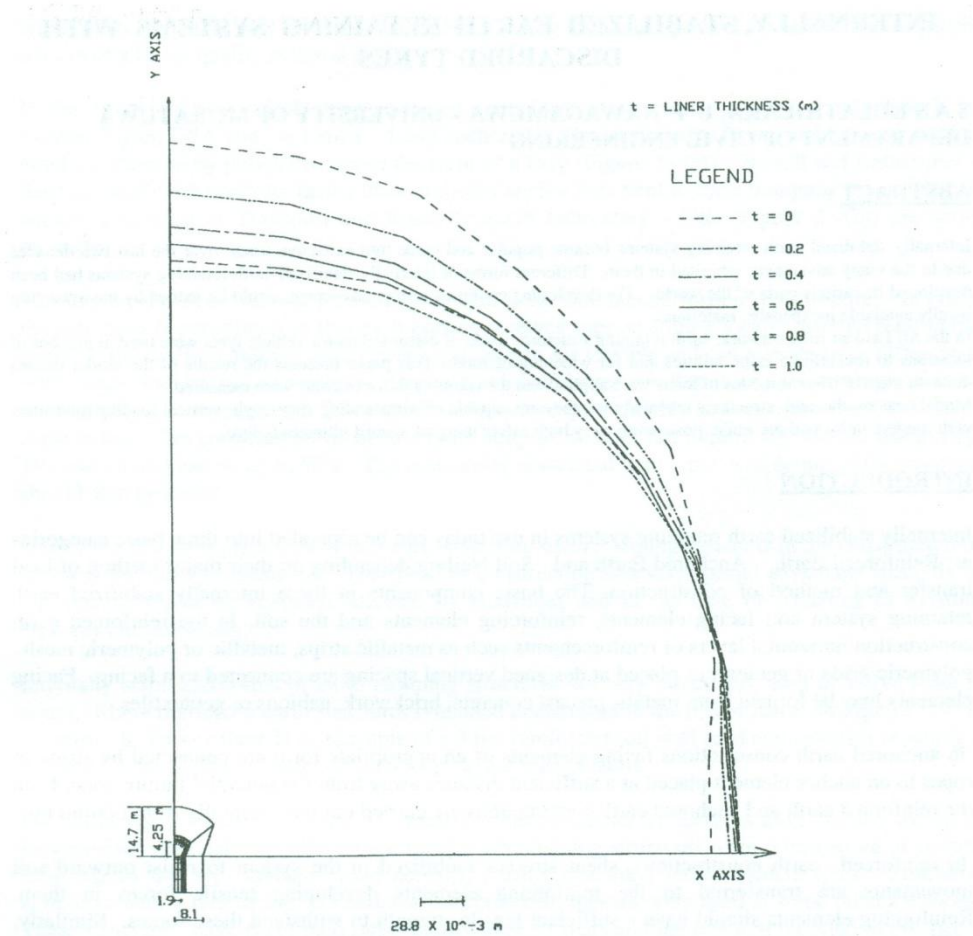


Figure 19. Variation of y-displacement at points along a line parallel to tunnel wall; horse-shoe shaped tunnel.

INTERNALLY, STABILIZED EARTH RETAINING SYSTEMS WITH DISCARDED TYRES

S A S Kulathilaka, U P Nawagamuwa - University Of Moratuwa
Department Of Civil Engineering

INTERNALLY, STABILIZED EARTH RETAINING SYSTEMS WITH DISCARDED TYRES

**S A S KULATHILAKA, U P NAWAGAMUWA – UNIVERSITY OF MORATUWA
DEPARTMENT OF CIVIL ENGINEERING**

ABSTRACT :

Internally stabilized earth retaining systems became popular and came into extensive usage over the last two decades due to the many advantages inherited in them. Different forms of internally stabilized earth retaining systems had been developed in various parts of the world. For developing countries further advantages could be gained by incorporating locally available inexpensive materials.

In the Sri Lankan road network, earth retaining structures made of discarded motor vehicle tyres were used at number of locations to rehabilitate slope failures and for widening of roads. This paper presents the results of the model studies done on them. Different modes of loads were applied and the resulting deformations were measured.

Model tests on the said structures revealed that they are capable of withstanding very high vertical loading intensities with limited deformations while possessing very high safety margins against ultimate failure.

INTRODUCTION

Internally stabilized earth retaining systems in use today can be separated into three basic categories as: Reinforced Earth, Anchored Earth and Soil Nailing depending on their major method of load transfer and method of construction. The basic components in these internally stabilized earth retaining system are; facing elements, reinforcing elements and the soil. In the reinforced earth construction horizontal layers of reinforcements such as metallic strips, metallic or polymeric mesh, polymeric grids or geotextiles placed at designed vertical spacing are connected to a facing. Facing elements may be formed from metals, precast concrete, brickwork, gabions or geotextiles.

In anchored earth constructions facing elements of an appropriate form are connected by strips or ropes to an anchor element placed at a sufficient distance away from the potential failure zone. Both the reinforced earth and anchored earth constructions are carried out incrementally from bottom up.

In reinforced earth constructions, shear stresses mobilized in the system to resist outward soil movements are transferred to the reinforcing elements developing tensile forces in them. Reinforcing elements should have a sufficient tensile strength to withstand these forces. Similarly, pulling out of the reinforcements should be prevented by embedding them over a sufficient length in the resistant zone (Figure 1 (a)). The closely spaced reinforcements and the soil behaves as one structural unit. A facing is used simply to prevent local ravelling, erosion and deterioration. It does not carry any significant structural load.

In anchored earth retaining systems (Figure 1 (b)), forces exerted on the facing elements by the outward moving soils are transferred to the anchor elements through the connecting strip or rod. Stability of the system depends on the pullout resistance of the anchor blocks and/or the tensile strength of the connecting wire/rod. The pullout resistance of an anchor block will depend on its shape, overburden stress and the shear strength parameters of the fill and is developed mainly through the formation of a plastic failure mechanism in front of the anchor element. The resistance developing via interface friction of the strip and top and bottom surfaces of the anchor is much smaller in magnitude. Anchored earth has an advantage over the reinforced earth in relation to the location of the anchor block. In reinforced earth constructions the reinforcing strip should be continued to a sufficient distance beyond the potential failure zone to develop the necessary pullout resistance. However, with anchored earth constructions anchors can be placed just outside the failure zone leaving space for the formation of the plastic collapse mechanism. Thus the necessary

width of the structure will be somewhat reduced. Also the higher passive resistance values permit the use of a lesser quality material as fill.

In the 1980's techniques of using anchored earth form of structures evolved simultaneously in Europe, Japan, USA and Sri Lanka. Loop anchored wall with concrete facing and concrete anchor blocks connected by polymeric ties in the form of a loop (Figure 2 -(a)) – Brandl and Dalmatiner – Austria, wall with concrete facing units and steel anchor bars bent to form triangular wedge shaped anchor developed at Transport and Road Research Laboratory - UK. (Figure 2 -(b)) are some examples.

The key aspect of an internally stabilized system is its incremental form of construction. In effect the soil mass is partitioned so that each portion receives support from a locally inserted reinforcing element. Internally stabilized earth retaining structures are flexible and can tolerate large differential settlements and lateral movements. Hence good foundation conditions or special preparation of founding soils is not essential. They can be constructed quite quickly and are operational as soon as constructed. The construction process is quite simple and does not require any special machinery. The cost saving can be up to 50%. The cost saving associated with rapid completion of the structure should also be added.

One of the largest applications of internally stabilized earth retaining system is in the construction of highway and bridge abutments. The speed of construction is a very special advantage specially in the case of repair of highways affected by landslides and in the case of widening of existing highway embankments.

Internally stabilized forms of earth retaining structures are very effectively used in active seismic zones. Many reinforced earth structures remained undamaged in the recent Kobe earthquake (1994) in Japan. In Turkey there is an example of a 3 tier reinforced soil wall road embankment retaining a height of 50 m from foundation to road in an active seismic zone.

For developing countries further advantages could be gained by incorporating locally available inexpensive material. Number of anchored earth retaining structures were constructed at several locations in the Sri Lankan road network, using discarded motor vehicle tyres. Similarly, structures with a tyre facing and bamboo reinforcement meshes were used at some other locations. These structures have performed satisfactorily over 10 years and the research reported in this paper was carried out to study their behaviour and to develop efficient design procedures.

ANCHORED TYRE EARTH RETAINING STRUCTURES IN THE SRI LANKAN ROAD NETWORK

Anchored tyre earth retaining structures can be constructed under any ground conditions if the necessary width is available. As the structure is flexible sound founding conditions are not essential. Facing tyres are placed on the founding soil along the desired alignment, with each tyre being connected to its neighbour using nylon wires of diameter 8 to 10 mm. Alternate facing tyres are then tied to anchor tyres kept at a sufficient distance away from the facing. Maximum of four facing tyres are connected to one anchor tyre. Facing tyres that are not connected to the anchor tyres are kept slightly behind the connected ones to have an interlocking effect. The anchor tyres are kept in the resistant zone and this is ensured by keeping them behind the 45 deg line. Therefore, at a height H from the base, the anchor tyre is kept at a distance of $H+1$ m from the facing (Figure 3 (a)).

After placement of a layer of facing an anchor tyres the tube face inside the tyres are filled with lateritic fill and is well compacted manually with hand rammers. If the structure is facing a stream or a waterway the tube spacing in the facing tyres are filled with a well graded gravelly material. The anchor tyre is pulled back to ensure that the ropes are well stretched and the fill is compacted to a density greater than 95% of standard Proctor. Once the compaction of a layer is completed a new layer of anchor tyres and facing tyres were placed and the procedure is repeated till the desired wall height is achieved. Although it is not essential. A back batter of 1 :12 is maintained in the structure.

Detailed procedure of the construction of anchored tyre earth retaining structures and details of some of the major structures including cost comparisons with alternate gravity form of structures is given in Sumanarathna et al (1997). Anchored tyre earth retaining structure at Ranwala along Colombo – Kandy road is shown in Figure 3 (b).

STABILITY CONSIDERATIONS

An internally stabilized earth retaining structure should be stable both internally and externally. Internally, it should be stable against pull out of anchor or reinforcing elements and tensile failure of these members. Externally the reinforced block should be stable against sliding, overturning or bearing failure just as in the case of a gravity retaining structure. Internal stability can be evaluated through a tie back wedge analysis done at different levels of the structure. At any given level of the structure the potential failure surface can be considered to be of the shape of a wedge (Figure 4 (a)). A trial wedge considered will be in equilibrium under the forces W , T , S and T_{eqm} . The force T_{eqm} is provided by the anchors / reinforcements intercepted by the wedge through their pullout resistance and tensile strength. An equilibrium analysis will enable the computation of the maximum value of T_{eqm} for a given level. The capacity of the anchors T_{sum} is the lower value of the summation of pullout resistances of the anchors / reinforcements and the summation of the tensile strengths of the anchor wires / reinforcements.

The factor of safety on internal stability can be expressed as $FOS = T_{sum} / T_{eqm}$. If the summation of the pullout resistances is less than T_{eqm} , the structure will fail by pullout of the anchors or reinforcements. If the summation of the tensile strengths is less than the T_{eqm} the structure will fail due to the tensile failure of elements. An internally stabilised earth retaining structure should have a sufficiently large factor of safety on internal stability.

External stability is evaluated by considering the anchored/reinforced block as a gravity wall (Figure 4(b)). Factor of safety expressions can be derived against failure by overturning, sliding or for the bearing capacity failure. Detailed computations of stability of anchored tyre earth retaining walls together with a spread sheet program is given in Kulathilaka (1998).

BASIS FOR THE MODEL STUDIES ON THE STRUCTURES

A study on the behaviour of the internally stabilized earth retaining systems would require loading of the structure and measurement of deformations. The outward movements of the facing, the internal strains (and therefore stresses) in the wires and outward movement of the anchors etc. would have to be measured in a study. It will also be necessary to load the structure until failure to identify possible failure mechanisms. The difficulties in attaching strain gauges to nylon wires and bamboos and likely experimental errors, and imposing the large surcharge loads on the real size structures were recognized. Hence it was decided to carry out the study through model tests.

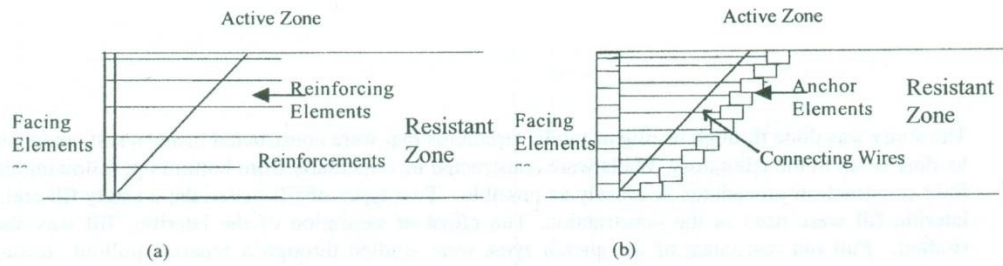
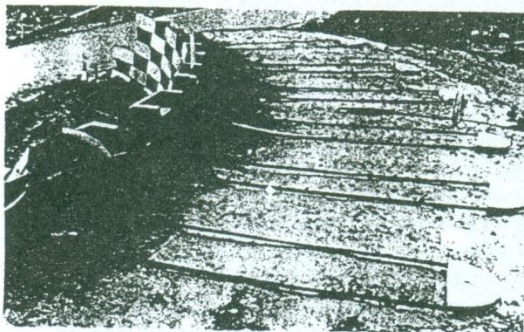
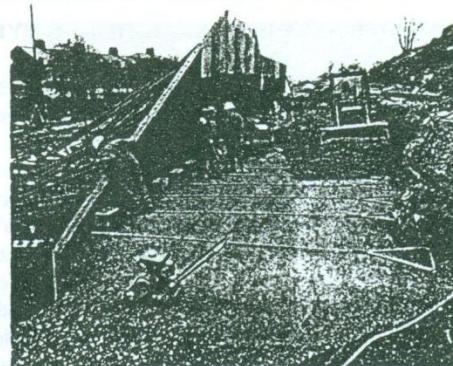


Figure 01-Reinforced Earth and Anchored Earth Concept



Loon Anchored Wall



TRRL – Anchored Wall

Figure 02- Different types of Anchored Earth Structures



(a) Placement of Anchor Tyres and Facing tyres



(b) Completed Anchored Tyre Structure at Ranwala

Figure 03 – Anchored Tyre Earth Retaining Structures in Sri Lanka

The study was done through testing of model structures that were constructed inside a self contained loading setup in the laboratory. Walls were constructed incrementally from bottom up, following the field construction procedures as closely as possible. Two types of fill materials; a sandy fill and a lateritic fill were used in the construction. The effect of saturation of the lateritic fill was also studied. Pull out resistance of the anchor tyres were studied through a separate pullout testing arrangement.

Two types of loading conditions; a vertical load within the anchor or reinforced and a vertical load behind the said zone, were applied simulating the different types of loads a prototype structures could be subjected in its life.

MODEL STUDIES ON ANCHORED TYRE EARTH RETAINING STRUCTURES

A model tyre – a reinforced rubber ring of external diameter 55 mm, internal diameter 35 mm and thickness 15 mm, was used in this construction as both facing elements and anchor elements. In the construction of a anchored tyre wall in the field, soil or rubble is filled inside the tube space and well compacted to form a stiff ring. Hence modeling the tyre with a stiff reinforced rubber ring could be justified. Facing tyres were connected to each other by nylon wires and the same type of wires were used to connect the facing tyres to the anchor tyre. The basic unit used in the model structure consisted of three facing tyres connected to an anchor tyre. Adjacent tyres are connected to each other and the two outer ones are connected to the anchor tyre. The distance between the facing tyres and the anchor tyres was varied to ensure that the anchor tyre is kept in the resistant zone. The construction of the model was done incrementally inside a Perspex box. The box was fabricated with slotted angle sections and the Perspex sheets were used in three vertical sides to observe the failure patterns. No Perspex sheet was used in the side of the wall facing. The wall was loaded by jacking it against the self contained loading set up. The outward movement of the wall facing with the increasing load was measured at three vertical sections along the length of the wall. In one vertical section five points were selected and the measurements were done using a vernier caliper with reference to an independent measuring frame.

Model Studies With A Sandy Fill

A well graded sandy soil where particles of sizes greater than 3.35 mm were removed, was used for the study. It was necessary to find a way of ensuring that the sand is placed at a controlled density as the model is incrementally constructed. The sand was found to have a good workable moisture content of 10 % by trial and error. The construction of the model was done layer by layer. The basic units corresponding to a particular layer is taken and facing tyres were kept along the desired alignment. The wire connecting the facing tyres to the anchor tyre was stretched by applying a small tension and the sand was filled in between. Thereafter sand was placed behind the anchor covering the plan area upto the back wall of the perspex box. Moist sand was placed in this manner over the full length of the wall and was compacted by taking a steel roller of weight 2.9 kg, length 190 mm and diameter 50 mm on the sand placed. In order to maintain a uniform density of the structure throughout, the same weight of sand was used for the construction of each layer. Within a layer also sand was placed carefully to ensure a uniform condition. Construction stages of a model retaining structure constructed inside the Perspex box in the self contained loading set up is depicted in Figure 5. The alternate sand layers were coloured in the models to facilitate the identification of failure patterns. The sand had a bulk density of 1740 kg/m^3 and Direct shear tests conducted on sand compacted to the same density yielded shear strength parameters of zero cohesion and $\phi = 34 \text{ deg.}$

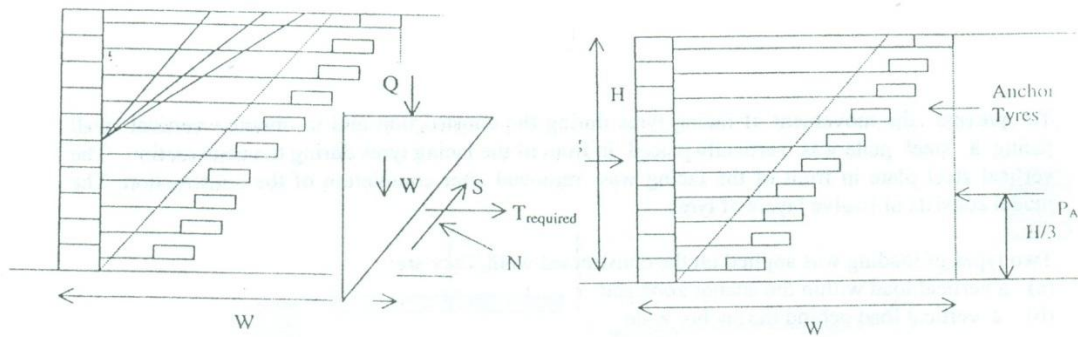
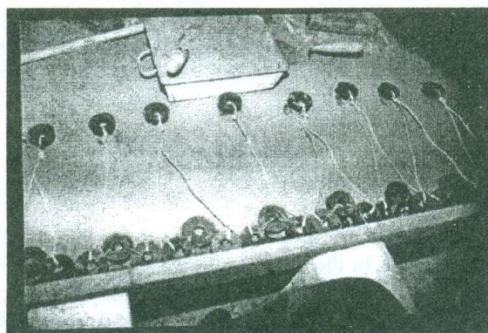
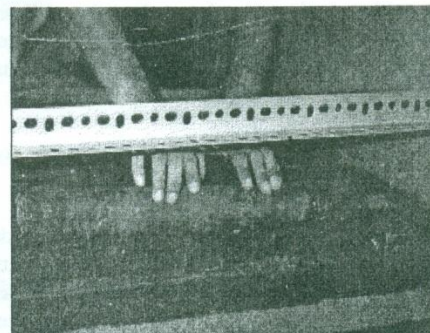


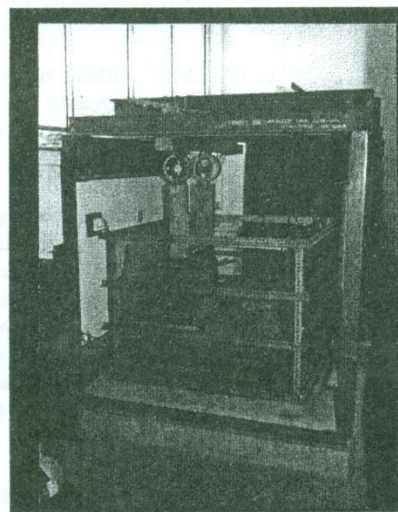
Figure 04 – Stability Criteria for Internally Stabilised Earth Retaining Structures



(a) General Layout of Model Tyres



(b) Compaction Process



(c) Completed wall in the loading Setup

Figure 05 – Construction of Model Tyre Wall inside the Perspex Box under the Loading Frame

To prevent the movement of facing tyres during the construction and to obtain a vertical wall facing a steel plate was vertically placed in front of the facing tyres during the construction. The vertical steel plate in front of the facing was removed after completion of the construction. The model consists of twelve layers of tyres.

Two types of loading was applied on the constructed wall. They are:

- (a) a vertical load within the anchor zone and
- (b) a vertical load behind the anchor zone.

An anchored earth or reinforced earth structure forming a highway abutment where the main load is applied vertically on top is simulated by the application of a vertical load within the anchor or reinforced zone. An anchored earth or reinforced earth structure constructed at the foot of a slope to provide stability can be simulated by applying a vertical load behind the anchor zone (Figure 6). The deformations of the structure were measured with the incremental application of the load and failure modes (if any) were noted.

Loading of the Model within the Anchor Zone

Model Constructed with Nylon Wires

Initial tests were done with a smaller model of length 300 mm and width (in cross section) 250 mm. Once the wall was constructed to the necessary height in the Perspex box, a number of timber planks were placed on the horizontal surface of the model to ensure an uniform application of the load. Thereafter a hydraulic jack was placed along with a proving ring and the model was loaded vertically by jacking up against the loading frame. The vertical load was applied in increments of 25 kN/m² and the resulting outward movements of the wall were measured with reference to a measuring frame. Also a close eye was kept on the sides of the Perspex box to identify the possible formation of any failure surface.

Loading intensity could be increased to 175 kN/m² without any indication of a catastrophic failure. Increased outward movement of the wall with the increased load is presented in Figure 7. At the loading intensity of 175 kN/m² the uneven settlement of the surface caused the loading system to slip and the model could not be loaded any further.

When the vertical load is applied on top of the anchors it could only be subjected to an internal instability either by the pullout of the anchors or by the tensile failure of the connecting wires. The vertical load applied on top of the anchor tyres have increased its pullout resistance preventing that mode of failure. However, this has led to the mobilization of a reasonably high tensile force in the connecting wires. Unfortunately the tensile force on the nylon wires could not be measured due to the unavailability of appropriate type of strain gauges. The nylon connecting wires have extended up to a maximum of 20 mm showing an outward movement of the wall facing. Nevertheless, these tensile stresses are not large enough to cause tensile failure of the nylon wire and a catastrophic failure of the model was thus prevented.

Therefore, in an attempt to induce failure another series of tests were carried out where the connection of facing tyres to the anchor tyre was done with threads used in sewing work. The average tensile capacity was found to be around 13.3 N.

Model Constructed with Sewing Threads

The model was constructed in the same manner with the exception that anchor tyres and facing tyres being connected by sewing threads. However the facing tyres were connected with each other

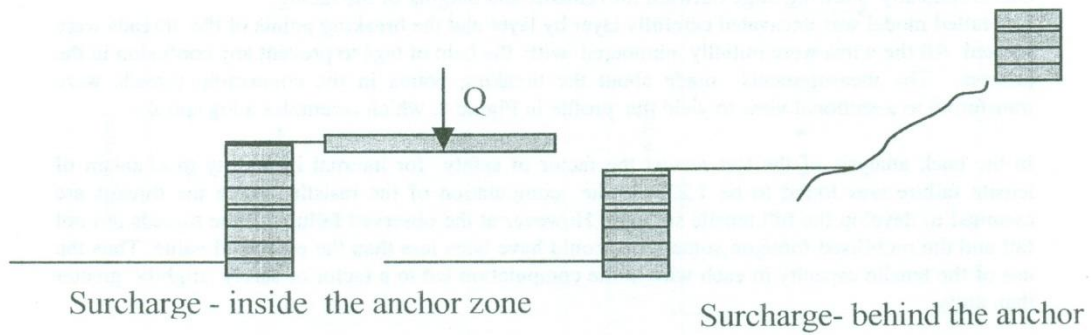


Figure 06- Different types of Loading Conditions

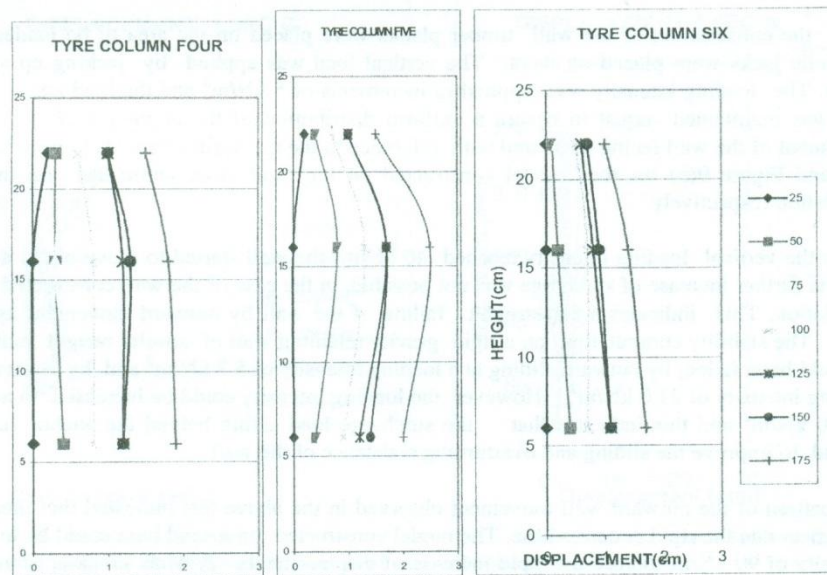


Figure 07- Outward Movement of wall facing with the incremental loading
Small Model - Sandy Fill - Load within the anchor zone

with nylon wires as before. When the loading intensity just exceeded 50 kN/m^2 , the structure failed catastrophically showing large outward movements and bulging of the facing.

The failed model was excavated carefully layer by layer and the breaking points of the threads were located. All the wires were initially numbered with the help of tags to prevent any confusion in the process. The measurements made about the breaking points in the connecting threads were transferred to a sectional view to yield the profile in Figure 8, which resembles a log spiral.

In the back analysis of the test results the factor of safety for internal instability mechanism of tensile failure was found to be 1.23. In the computation of the resisting force the threads are assumed to develop the full tensile strength. However at the observed failure all the threads did not fail and the mobilised force on some wires could have been less than the estimated value. Thus the use of the tensile capacity in each wire in the computation led to a factor of safety slightly greater than unity.

Loading of the Model Behind the Anchor Zone

Anchored earth retaining structures may be subjected to a condition of loading where the major load is applied behind the anchor zone as in the case of a wall constructed at the foot of a slope. Under such conditions, the wall behaves effectively as a gravity wall. Thus the external stability criteria were checked by the application of a vertical load behind the anchor zone. Two types of model tests were done, namely ; a wall constructed on a rigid foundation and a wall constructed on compressible soil. The wall on a rigid foundation was simulated by the construction of the model wall directly on the concrete base of the loading setup. A sand fill with same density was placed to a thickness of 200 mm to simulate a compressible base in the other series.

After the construction of the wall timber planks were placed on the area to be loaded and two hydraulic jacks were placed on them. The vertical load was applied by jacking up against the frame. The loading intensity was applied in increments of 5 kN/m^2 and the load applied by each jack was maintained equal to ensure a uniform distribution of the applied load. The outward movement of the wall facing measured with reference to the measuring frame is presented in Figure 9(a) and Figure 9(b) for the model constructed on the rigid foundation and on the flexible foundation respectively.

When the vertical loading intensity reached 40 kN/m^2 the wall started to move out at a rapid rate and the further increase of surcharge was not possible, in the case of the wall constructed on a rigid foundation. This indicates a catastrophic failure of the wall by outward movement as a gravity wall. The stability computation on a rigid gravity retaining wall of similar weight indicated that it would have failed; by outward sliding at a loading intensity of 5.7 kN/m^2 and by overturning at a loading intensity of 21.0 kN/m^2 . However the loading intensity could be increased to an intensity of 40 kN/m^2 and this indicates that the surcharge load acting behind the anchor zone is also helpful to improve the sliding and overturning resistance of the wall.

The pattern of the outward wall movement observed in the above test indicated that there is some influence due the rigid concrete base. The model constructed on a sand base could be loaded to an intensity of 90 kN/m^2 before the rapid increase of displacements. A wide crack appeared behind the anchors and wall unit was seen to separate out from the fill as depicted in Figure 10.

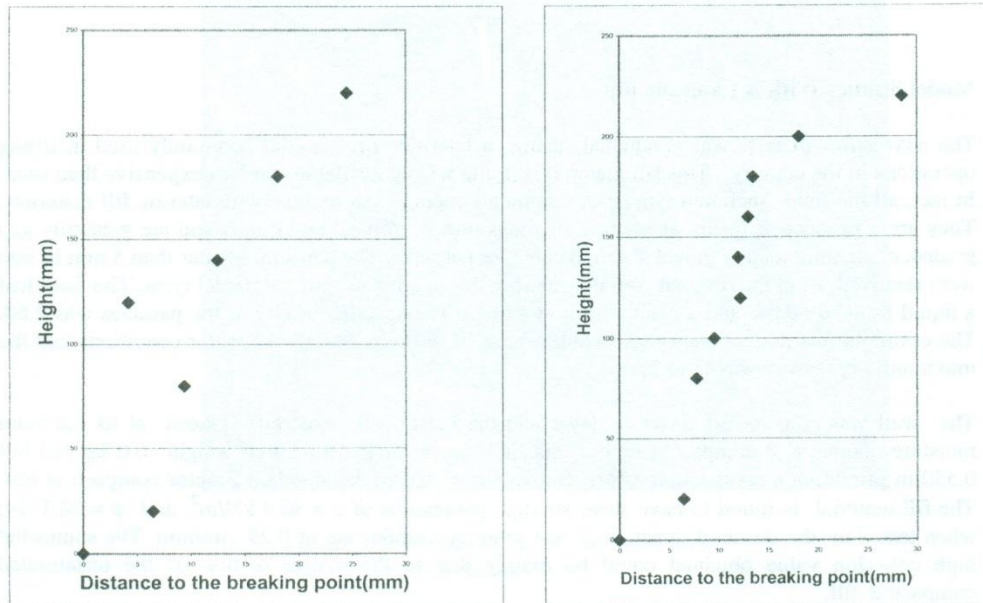
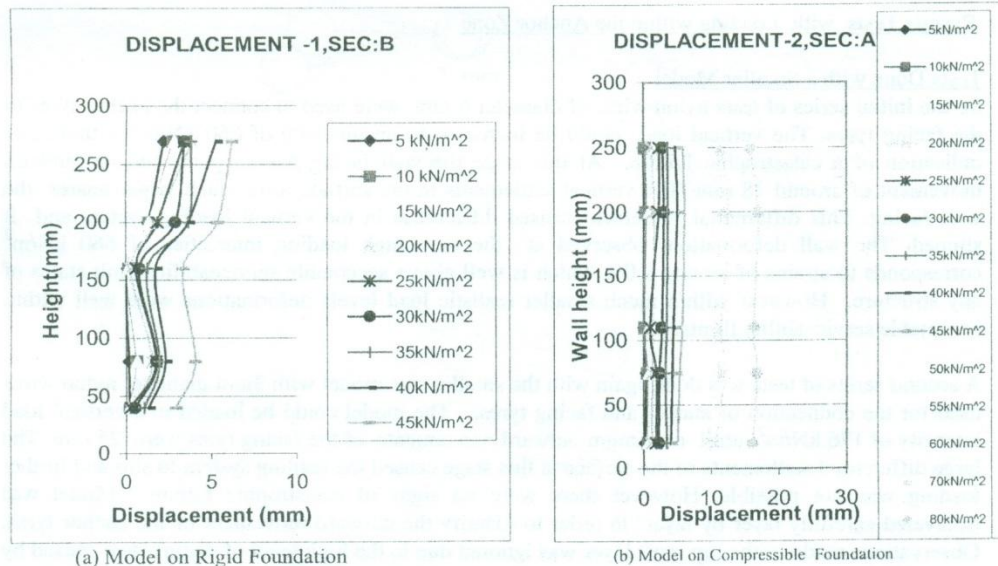


Figure 08 - Failure Profiles of Connecting Sewing Threads



(a) Model on Rigid Foundation

(b) Model on Compressible Foundation

Figure 09 -Outward Movement of Wall Facing- Sandy Fill
Loading Behind the Anchor Zone

Model Studies With A Lateritic Fill

The next series of tests was conducted using a lateritic fill material commonly used in filling operations in the country. This fill material is quite widely available and less expensive than sand. In fact, all the field anchored tyre earth retaining structures were done with lateritic fill materials. They are a product of insitu weathering of rocks under tropical conditions and are generally gap graded, containing mainly gravel size and clay size particles. The particles greater than 5 mm in size were removed from the original soil considering the smaller size of the model tyres. The fines had a liquid limit of 58.0% and a plastic limit of 42.6%. The specific gravity of the particles was 2.60. The optimum moisture content was found to be 25.0 % under Standard Proctor conditions and the maximum dry density was 1515 kg/m^3 .

The wall was constructed layer by layer and the lateritic fill material placed at its optimum moisture content and compacted with a specially made drop hammer of weight 6.0 kg and fall 0.550 m providing a compaction effort equivalent to that in the standard Proctor compaction test. The fill material is found to have shear strength parameters of $c = 30.4 \text{ kN/m}^2$ and $\phi = 28.1 \text{ deg}$ when tested in the standard direct shear test setup at a strain rate of 0.29 mm/min. The somewhat high cohesion value obtained could be mainly due to the matric suction of the unsaturated compacted fill.

Initial tests were done with a smaller model of height 250 mm (13 layers of tyres), and width 200 mm and the later tests were performed with larger models of height 375 mm (20 layers of tyre) and width 1120 mm.

Results Tests with Loading within the Anchor Zone

Tests Done with a Smaller Model

In the initial series of tests nylon wires of diameter 6 mm were used to connect the anchor tyres to the facing tyres. The vertical load could be increased to an intensity of 660 kN/m^2 without any indication of a catastrophic failure. At this stage the wall facing has experienced an outward movement of around 18 mm. The vertical settlements in the surface were much larger nearer the wall facing. This differential settlement caused difficulties in the vertical loading system and it slipped. The wall deformations observed at the very high loading intensities of 660 kN/m^2 corresponds to strains of around 9.0% which is well above acceptable serviceability limit states of any structure. However within much smaller realistic load levels deformations were well within acceptable serviceability limits.

A second series of tests was done again with the smaller size model with 3mm diameter nylon wires used for the connection of anchor and facing tyres. The model could be loaded to a vertical load intensity of 176 kN/m^2 until maximum outward movements of the facing tyres were 25 mm. The large differential settlements of the surface at this stage caused the loading system to slip and further loading was not possible. However there were no signs of catastrophic failure. Model was excavated carefully layer by layer in order to identify the outward movement of the anchor tyres. Observations made in the top most layer was ignored due to the high level of disturbance caused by surface settlements. The outward movements of the anchor tyres were measured to be 3 mm at level 2, 2 mm at level 3 and around 1 mm at level 4 (Figure 11). No measurable movements were seen in the anchor tyres below this level. Thus the somewhat larger outward movements of the facing can be attributed to the larger extensions in the wires of smaller cross section. The use of wires of larger stiffness will help to minimise the wall deformations.

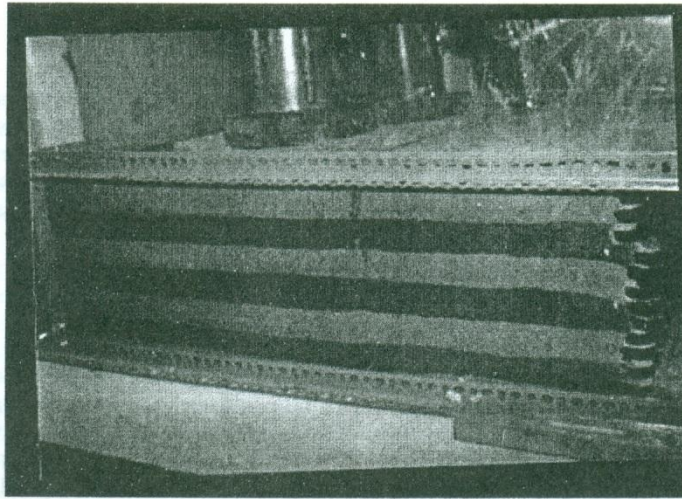


Figure 10 – Separation of the Wall Unit
Loading Behind the Anchor Zone

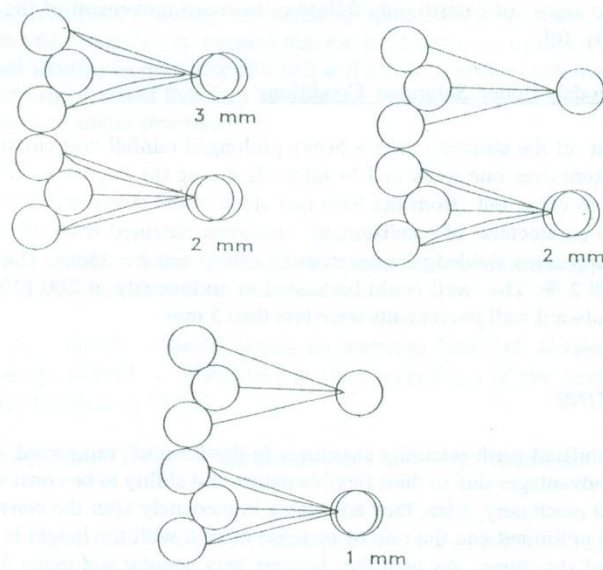


Figure 11 – Outward Movement of Anchor Tyres – Lateritic Fill

The next series of tests were done to simulate the saturation condition that may occur in the field after a heavy prolonged rainfall. The model prepared was kept in a shallow container and was saturated by pouring water frequently on the surface. Subsequently the saturation was found to have reached 100 %. During the application of the vertical load the saturated soggy soil settled by more than 40 mm and outward movements of the order of 40 mm were recorded at a vertical loading intensity of 325 kN/mm^2 .

Results of the Larger Model Tests (Loading within the Anchor Zone)

A larger models of height 375 mm, width 1100 mm and sectional width 400 mm were used in the following tests. The construction was done in a similar manner and the loading was applied within the anchor zone incrementally using two jacks. The anchor and facing tyres were tied with nylon wires of diameter 3 mm. The loading intensity was increased to 300 kN/m^2 incrementally without any indication of a catastrophic failure. The load was not increased beyond 300 kN/m^2 due to excessive bulging of the box.

Results of the Model Tests (Loading Behind the Anchor Zone)

A model constructed in the same manner as above in the large Perspex box was loaded from behind using two jacks. The loading intensity was increased to an intensity of 280 kN/m^2 before the loading system slipped. The observed outward wall movements were less than 3 mm at this stage. There were no signs of catastrophic failure or outward movement of the wall unit as seen in the case with sandy fill.

Testing Of Models Under Saturated Conditions

The condition of the structure after a heavy prolonged rainfall was simulated by sprinkling water over the structure over one week at 1 hr intervals during the day time. By this time the sprinkled water is seen to come out from the base and sides of the structure. Subsequent measurement of shear strength parameters of undisturbed specimen obtained from the model, made using the Direct Shear apparatus yielded parameters $c=15 \text{ kN/m}^2$ and $\phi = 33\text{deg}$. The degree of saturation was found to be 99.2 %. The wall could be loaded to an intensity of 200 kN/m^2 without any signs of failure. The outward wall movements were less than 5 mm.

CONCLUSIONS

Internally stabilised earth retaining structures in the form of reinforced earth on anchored earth posses many advantages due to their flexible nature and ability to be constructed quickly without the use of special machinery. Also, they are usable immediately after the construction. The achievable wall height is unlimited and the rate of increase of cost with the height is much lower than for the gravity form of structures. As such they became very popular and many different innovative forms were developed. Most of the retaining structures constructed today to support highway embankments, bridge abutments etc. are of this form. For a developing country further advantages could be gained by the use of locally available material in these constructions.

Models studies reported in the paper were done to study the performance of anchored earth retaining structures made up of discarded motor vehicle tyres. It was also expected to develop

rational design procedures. The cost of these structures was as low as 30 - 40 % of an alternate gravity form of structure.

The model studies on the anchored tyre earth retaining structures revealed that the anchor tyre has a very high pullout resistance and when loaded within the anchor zone it can support very high loading intensities. The applied surcharge itself will increase the pullout resistance and catastrophic failure can be seen only if the connecting wires fail in tension. If wires of smaller stiffness were used the tensile stresses mobilised in them will cause greater extensions which in turn will lead to larger outward movements of the wall. As such, the use of wires of larger stiffness (larger diameter and elastic modulus) will be effective in minimising the wall deformations.

Model walls constructed with lateritic fill showed lesser deformations compared with the models constructed with sandy soils. Even after the saturation of the model, a catastrophic failure could not be induced in model anchor tyre walls constructed with lateritic fill. When the load is applied behind the reinforced zone, there was more resistance to overturning or sliding than in the case of an equivalent gravity retaining wall of same weight with both types of fill. Motor car tyres and nylon wires have a long life (at least 50 years), and there would not be any problem arising from deteriorating strength.


A design procedure was developed for the anchored tyre earth retaining structures (Kulathilaka 1998) and bamboo reinforced earth retaining structures by application of the findings of the pullout resistances observed in this research. It revealed that the field retaining structure of this form has safety factors on internal stability in the order of 7 to 8 and safety factors on external stability in the order of 3 to 4. Thus it can be stated that they are not only inexpensive but are more stable than alternate gravity type earth retaining structures.

REFERENCES

1. *Bandl and Dalmatiner (1986)* – New Retaining wall system - Federal Ministry of Construction and Engineering Road Research, Vol 280, Vienna 1986
2. *Kulathilaka S A S, (1998)* - Model studies on Anchored Tyre Earth Retaining Systems and Development of a Design Method - Published in the Proceedings of the Seminar on Earth Retaining Structures organised by SLGS
3. *Murray R T and Irwing M J (1981)* - Preliminary study of TRRL Anchored Earth – TRRL Report 674
4. *Sumanarathna I H D, Mallawarchchi D P, Kulathilaka S A S – (1997)* - Stabilisation of Slopes by Anchored Type Retaining Structures. Published in the 14th International Conference in Soil Mechanics and Foundation Engineering held in Germany

Improving the Efficiency of Electro Discharge Machining by Dual Voltage Excitation

Dr. J.A.K.S Jayasinghe, University of Moratuwa



Improving the Efficiency of Electro Discharge Machining by Dual Voltage Excitation

Dr. J.A.K.S. Jayasinghe, University of Moratuwa

Abstract

An Electrical Discharge Machine (EDM) is a vital machine used in manufacture of tools and dies. Its operation is based on discharge of an electrical current across the tool and the work-piece. Due to limitations of the servo control system, the EDM operates with a low efficiency using a high spark voltage. This paper presents a novel technique based on a dual voltage excitation for an EDM. Although this technique was developed primarily to improve the efficiency, it reduces the cost and size of the electronic controller as well.

INTRODUCTION

An Electrical Discharge Machine (EDM) cuts metal by discharging electrical current across a thin gap between the tool electrode and work-piece electrode. Each electrical discharge produces a tiny crater by melting and vaporization, thus eroding the shape of the tool electrode into the work-piece electrode. In EDM, each spark contains a discrete, measured and controllable amount of energy; hence the surface finish of the work can be properly controlled. EDM is widely used in manufacture of tools and dies for casting, forging, stamping, extrusions and molding [2]. The absence of mechanical forces makes it possible to machine fragile parts without distortions.

In EDM, the work-piece and tool are submerged in a dielectric fluid and it flushes out the "chips" generated due to the electrical spark. Figure 1 depicts the schematic diagram of a typical EDM machine. The tool feed mechanism maintains the distance between the tool and the work-piece very accurately. No electrical spark is created when the gap is too large. Usually the spark gap is maintained to its optimum distance by a servo control system. Under the control of the servo control system, the tool is lowered from its rest-position. During this process, tool and work-piece should not touch each other, as it creates a short circuit. Under the short circuit condition, no spark is generated but a heavy current is drawn from the supply. To prevent any short circuit conditions during operation of the servo control system, a sufficient spark gap must be allowed. In practice, a spark voltage (V_{spark}) of approximately 100 V is required for this purpose. The energy delivered in each spark determines the accuracy of the machining process, and hence the spark current and the spark duration determine the accuracy. The spark current is usually maintained to the required strength by using a current limiting resistor (R) as depicted in Figure 2 [1]. During the spark, the voltage between the spark gap (V_{Gap}) drops to a value as low as 20 V while remaining 80 V is dropped across the current limiting resistor. This makes the EDM very inefficient. For a typical operation condition with a 100 V spark voltage and 20 V spark gap drop, the efficiency of the machine is only 20%. This paper

presents a novel technique to improve the efficiency of the EDM using a dual voltage excitation source.

TOOL DYNAMICS

The servo control system that positions the tool is depicted in Figure 3. It consists of a servomotor with a reduction gear or a belt drive, tool holder and tool holder guide. A typical servo control system used in EDM can be modeled as in Figure 3. In this block diagram, the servo controller is represented as a proportional controller with gain K_p . To reduce the effect of friction, a velocity feedback with a gain K_r has been used. The parameter J represents the inertia of the system. The closed loop transfer function of the system is given by

$$\frac{C(s)}{R(s)} = \frac{K_p}{J s^2 + K_r s + K_p}$$

Therefore the system is second order with its characteristics equation

$$s^2 + 2\xi\omega_n s + \omega_n^2 = 0$$

where ξ is the damping coefficient and ω_n is the natural frequency of the system. The maximum system overshoot and the corresponding time at which it occurs are given respectively by [3]

$$ov_{\max} = e^{-\frac{\pi\xi}{\sqrt{1-\xi^2}}}$$

and

$$T_{\max} = \frac{\pi}{\omega_n \sqrt{1-\xi^2}}$$

To obtain a fast response time, the servo control system must operate with small damping coefficient, but it creates large overshoots. In practice, $\xi = 0.7$ is selected as the optimum damping coefficient, as it creates only a 5% overshoot [3].

The spark gap between the tool and the work-piece is directly proportional to the applied voltage between the tool and the work-piece. Usually, the dielectric fluids used in EDM have dielectric strengths in the order of 20 kV/mm and hence the spark gap is approximately given by 0.05 $\mu\text{m}/V$. With a 5% overshoot in the servo control system and initial tool position of 0.1 mm above the work-piece, a 5 μm spark gap is required to prevent any short circuit conditions being developed during the tool movement. In order to maintain a 5 μm spark gap, 100 V spark voltage is required. As the voltage drop across the gap during the spark (i.e. V_{Gap}) is as low as 20 V, and 80 V drop is developed across the current

limiting resistor, the system operates with a low efficiency in the order of 20%. It is now clear that direct system efficiency improvement needs reduction in the spark voltage V_{spark} . Any reduction in spark gap voltage is associated with a reduction in the spark gap and hence reduction in system overshoot is required. For example, a 25 V spark voltage may increase the efficiency of the system to 80%, but it reduces the spark gap to 1 μm . Positioning the tool to maintain a 1 μm spark gap from the original tool position of 0.1 mm above the work-piece allows only a 1% overshoot. When the system damping is increased to reduce the system overshoot to 1%, the system operates slower. Hence any attempt to improve the system efficiency by reducing the spark voltage is not successful as it slows down the tool positioning speed.

DUAL VOLTAGE EXCITAION TECHNIQUE

A careful examination of the spark generation process, tool positioning process and spark maintenance process reveals the following facts:

- a) A high voltage is required to generate the spark with a high tool positioning speed.
- b) A low voltage is sufficient to maintain the spark once the spark is generated without any effect on the tool positioning speed.

These two facts can be easily met with a dual voltage excitation as depicted in Figure 4. It contains a high voltage source (V_h) to generate the spark and a low voltage source (V_l) to maintain the spark. Two resistors in combination with a diode are used to improve the efficiency. The high voltage path resistance (R_h) is very high to prevent excessive power dissipation. The low voltage path resistance (R_l) is selected according to the spark current, and it is fairly low as the low voltage supply is in the order of 25 V. One can now note that with a 20 V spark gap voltage drop, only 5 V is dropped across the current limiting resistor R_l and hence the system efficiency is now as high as 80%.

The dual voltage excitation not only improves the system efficiency, but also reduces the cost of the system as well. The power dissipation on the current limiting resistor for an 80 V drop at 50 A current is 4 kW. Hence the single source excitation requires high wattage resistors and a good cooling system must be employed. Usually an array of 300 W resistors is used in practice and the cost of a single 300 W resistor is approximately Rs. 5000/=. To meet the required 4 kW capacity, the cost of the current limiting resistor array alone is around Rs. 70,000/=.

On the other hand, power dissipation on the current limiting resistor with a 5 V drop at 50 A current is only 250 W. The wattage rating of the current limiting resistors is reduced by a factor of 16. Hence it reduces the cooling requirements as well. This low power dissipation current limiting resistor can be constructed by using a 50 W resistor array. The cost of a 50 W resistor is around Rs. 400/=:, and hence the cost of the current limiting resistor array is now only Rs. 2000/=. The cost of the current limiting resistor is reduced by a factor of 35.

Furthermore, the dual voltage excitation reduces the capacity of the power transformer. In order to draw a 50 A current from a 100 V supply, at least 5000 VA transformer is required. For the dual voltage excitation system supplying 50 A from a 25 V supply, only 1250 VA transformer is required.

The reduction in the power rating of the current limiting resistors, cooling requirements and transformer capacity not only reduces the size of the electronic controller but the cost of the system is also reduced by a significant factor. Figure 5 show a photograph of an EDM system developed by the author using the dual voltage excitation technique described in this paper. This system has been used in the field successfully for more than a year to manufacture moulds for the plastic industry.

CONCLUSION

A dual voltage excitation technique for improving the efficiency of the EDM was presented in this paper. Although the primary aim was to improve the efficiency, the new technique reduces the cost and size of the system due to reduction in the power rating of the current limiting resistors. The new technique has been field tested in manufacture of plastic moulds and shows good performance.

Acknowledgement

The author wishes to acknowledge Mr. G. Dharmaratna of *Tech Masters* at Nugegoda for providing financial support to design an EDM controller for plastic mold manufacturing. The contribution of Mr. H.A.S. Perera and R.S. Thimirachandra in electronic circuit design is acknowledged.

References

- [1] Corisma Corporation, *Operation Manual CM50*.
- [2] E. P. De Gramo et.al., *Materials and Processes in Manufacturing*, Prentice-Hall of India, New Delhi, 1997.
- [3] B.C. Kuo, *Automatic Control Systems*, Prentice-Hall, Englewood cliffs, N.J., 1975.

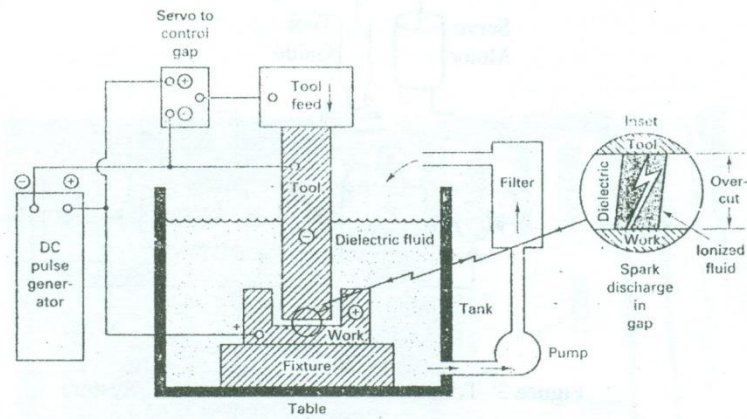


Figure 1: Schematic Diagram of a Typical EDM

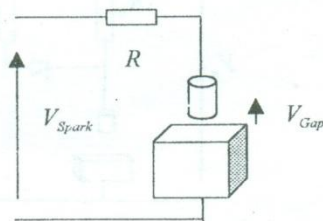


Figure 2: Electrical Circuit of a Typical EDM

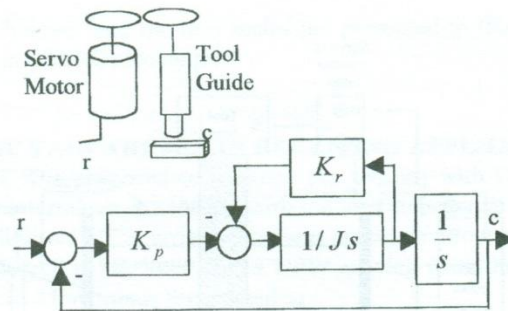


Figure 3: Tool Positioning Servo Control System

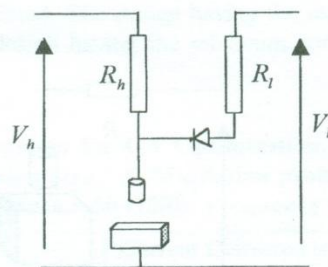


Figure 4: Dual Voltage Excitation Scheme

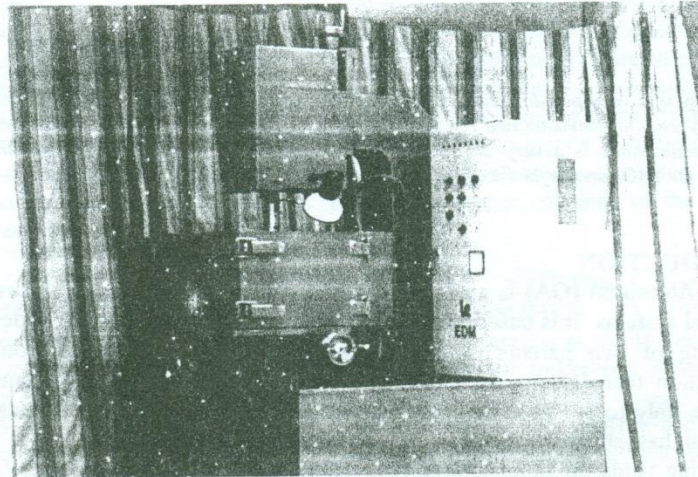


Figure 5: Photograph of the EDM based on Dual Voltage Excitation

Design of YAGI Array Receiving Antennas Using Genetic Optimization

Dr. J.A.K.S. Jayasinghe, University of Moratuwa

Design of YAGI Array Receiving Antennas Using Genetic Optimization

Dr. J.A.K.S. Jayasinghe, University of Moratuwa

Abstract

YAGI array is a very popular antenna for VHF/UHF applications due to its simple construction. It is extensively used in television and FM radio reception. However, design of YAGI arrays to meet a given set of specifications is a very difficult task. This paper presents a genetic algorithm based design technique for YAGI arrays for receiving applications.

INTRODUCTION

Genetic Algorithm (GA) is an optimization technique based on the natural evolution of biological systems. It is based on the structure of a chromosome and its development due to mating of two parents to conduct a global search in the solution space. Many optimization techniques search the solution space around the initial guess, and hence converge only to the best local optimum at the vicinity of the initial guess. The genetic algorithm has shown better results in many applications. It has been used in many engineering fields for optimization. Antenna design, Jet Turbine design, VLSI design are some examples [6]. In antenna design, GA has been used in the design of YAGI Array Antennas [3], Loaded Monopole Antenna [1] and Broad Band Microwave Absorbers [4].

The YAGI array has been used extensively since its introduction in 1928 [5] by H. Yagi due to its simple construction. However, the design of a YAGI array to meet a given set of specification is a complicated task. Cheng et.al. [2] have developed a gradient search technique to design YAGI arrays by optimizing its gain. In many applications, one may have to meet specifications other than the gain. Input impedance, side lobe levels, front-to-back ratio are some other important specifications. Optimization of YAGI arrays with these parameters using the gradient search technique is extremely difficult.

As an alternative, Jones et.al. [3] developed a YAGI array optimization technique based on the genetic algorithm. In this technique, the antenna dimensions are coded into a chromosome and its performance is evaluated when the antenna is in the transmitting mode. A new genetic algorithm based optimization technique for design of YAGI arrays for receiving applications is presented in this paper. A comparison of the performance the designs resulting from the Jones' technique and the new technique for receiving applications is also presented.

GENETIC ALGORITHM

The genetic algorithm is based on the development of species characterized by genes in the nucleus of the chromosome. In natural evolution of species, offspring of a sexual reproduction inherit properties from their parents with some mutations. Each individual species possesses unique structure in its chromosome made up of individual genes.

Individuals who are fit to survive in a given environment will get the chance to create the next generation. This natural phenomena is used in the genetic algorithm. In the genetic algorithm, a set of solutions to a given problem is coded into a set of chromosomes. Each optimization parameter for the given problem is taken as a gene in the chromosome. The fitness of each chromosome is then evaluated with a user defined objective function. The unfit individuals are allowed to die while fit individuals are allowed to mate to produce their offspring. The chromosome of the offspring is generated by breaking the chromosomes of the parents at a randomly chosen location and joining them together to form two children. During this process, few bits are allowed to mutate. This process is repeated for several generations and, as only fit individuals are allowed to mate, the fitness of the generation increases with evolution. This creates better solutions to the given problem as it evolves.

REPRESENTATION OF A YAGI ARRAY BY CHROMOSOMES

A YAGI array consists of one driven element with several parasitic elements known as directors and reflectors. Usually the directors are shorter in length and several of them are placed in front of the driven element. The reflectors are placed behind the driven element and longer than the driven element. Figure 1 shows a typical YAGI array and some important parameters. The spacing between the elements, the lengths of the elements and the diameter of the elements are the design parameters that one can vary to meet the given set of specifications.

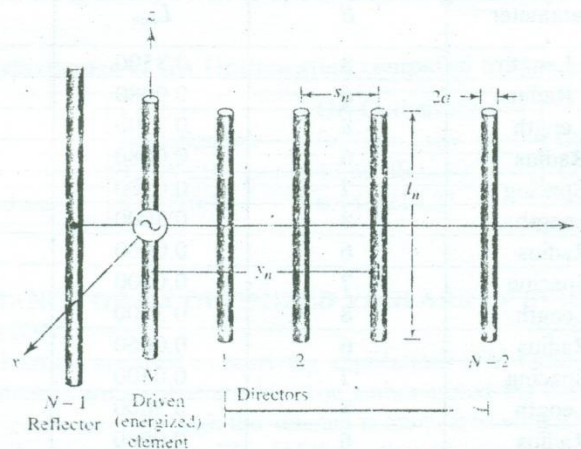


Figure 1: A YAGI Array

In order to exploit the power of the genetic algorithm, the YAGI array must be represented by a chromosome. In [3], Jones *et.al.* proposed a binary string as the chromosome where variable length bit groups are allocated to represent the spacing between the elements, length of the elements and diameters of elements. Each parameter is assigned a maximum and minimum value to limit the search space. Then each parameter is encoded into B bit block where B is determined from the following equation

$$B = \log_2 \left(\frac{L_{\max} - L_{\min}}{L_{\text{res}}} + 1 \right)$$

The parameters L_{\max} and L_{\min} define the range over which the parameter L can vary and L_{res} is the resolution of discretization. When B is not an integer, it is rounded up to the next integer value. The coded binary representation of the parameter L is given by

$$L = L_{\min} + \sum_{k=1}^B L_{\text{res}} l_k 2^{k-1}$$

Table 1 shows a typical set of maximum and minimum values, number of bits allocated to a four-element YAGI array.

Table 1: Parameters for a Typical Four-Element YAGI Array

Gene Number	Parameter	B	L_{\min}	L_{\max}
1	Refl. Length	8	0.3500	0.6060
2	Refl. Radius	6	0.0080	0.0120
3	DE Length	8	0.3500	0.6000
4	DE Radius	6	0.0080	0.0100
5	DE Spacing	7	0.0500	0.5620
6	D1 Length	8	0.3000	0.5560
7	D1 Radius	6	0.0060	0.0090
8	D1 Spacing	7	0.0500	0.5000
9	D2 Length	8	0.3000	0.5560
10	D2 Radius	6	0.0060	0.0090
11	D2 Spacing	7	0.0500	0.5000
12	D3 Length	8	0.3000	0.5560
13	D3 Radius	6	0.0060	0.0090
14	D3 Spacing	7	0.0500	0.5000

EVOLUTION PROCESS OF THE GENETIC ALGORITHM FOR YAGI ARRAY DESIGN

In order to carry out the evolution process, the genetic algorithm requires a simulator to obtain the performance of each individual represented by a chromosome. In the YAGI array design, the antenna represented by a chromosome is decoded into its geometric structure and simulated to obtain its performance. The well-known Numeric Electromagnetic Coding (NEC) has been used extensively to evaluate the performance of wire antennas. The NEC is capable of simulation of a wire antenna under any given condition. It can provide simulation results on many parameters such as gain in any give direction, received power or current from any direction, driving point impedance etc.

In [3], Jones. et.al. proposed the following objective function for the evolution process of the YAGI array design problem for an antenna with a 50Ω input impedance.

$$O(x) = aG(x) - b|50 - \text{Re}(Z(x))| - c|\text{Im}(Z(x))| - d\text{MaxSLL}(x)$$

Here $G(x)$ represents the gain, $Z(x)$ represents the driving point impedance and $\text{MaxSLL}(x)$ represents the maximum side lobe level of the antenna. The constants were set to $a=40, b=c=1$ and $d=2$. The parameters $G(x)$, $Z(x)$ and $\text{MaxSLL}(x)$ in the above equation are extracted from the NEC simulation runs. In order to extract above parameters the antenna is simulated when it is in the transmitting mode. The results reported in [3] for a six-element YAGI array are tabulated in Table 2. These results indicate that the genetic algorithm based YAGI array designs provide a better gain and impedance matching than a YAGI array based on the gradient optimization method.

Table 2: Performance of GA Optimization compared to Gradient Optimization

	Gradient Optimization	GA Optimization for Gain Only	GA Optimization for Gain and Impedance
Gain	12.98 dB	13.60 dB	12.58 dB
Input Impedance	$8.4+j20.1$	$6.14+j216.21$	$49.64-j5.08$

PERFORMANCE OF GA OPTIMIZED YAGI ARRAY IN RECEIVING APPLICATIONS

Many YAGI arrays are used in receiving applications. FM radio receiving antennas, TV receiving antennas are some examples. The author tested the design reported in [3] as a TV receiving antenna. Although the antenna is associated with a very high gain, the tests failed to produce good results. This led the author to investigate the performance of the antenna in receiving mode. The antenna was simulated in receiving mode by NEC with a uniform plane wave (UPW), and simulation results indicated a gain lower than 13 dB which is in agreement with the field tests. This led to the investigation of alternative GA optimization techniques for design of YAGI array antennas for receiving applications. Hence, we refer to the technique presented by Jones et.al. as "GA based Transmit

Optimization (GATO) technique” and the new technique presented in this paper as “GA based Receive Optimization (GARO) technique”.

GA OPTIMIZATION OF YAGI ARRAYS IN RECEIVING APPLICATIONS

For receiving applications, it is proposed to evaluate the antenna with UPW excitation. For evaluation, the antenna terminals are loaded with the load impedance and the current delivered to the load for different UPW arrival directions are taken into consideration. Let us assume the current delivered to the load from a UPW arriving from the direction θ_j is given by I_j . Now the objective function is formulated as

$$O = \sum_{j=1}^N a_j I_j$$

where a_j is a weighting factor. Assigning high values to the weighting factor gives preference to selected wave arrival directions. With this objective function, the GA optimization was carried out for different sizes of the YAGI array. First 2-element YAGI array was designed using GARO technique with a population size of 10 members evolved over 5 generations with $a_1=1$ and $a_2=a_3=..a_N=0$. The current delivered to the load by the best individual is given in Table 3 for ten different design sessions. In order to compare the performance of the new technique, currents delivered to the load by designs created by GATO technique are also tabulated. The design having the maximum current is depicted with bold characters and the design having the minimum current is depicted with italic characters for easy comparison.

Table 3: Performance Comparison for GA Optimization, 2-Element YAGI Array, Population size = 10, Generation Size = 5, Mutation probability = 0.02, Cross over probability = 0.8, Input impedance = 50 Ohms, Frequency = 299.8 MHz.

	Current Delivered to a 50 Ohm load by a UPW arriving from the front of the antenna (A/V)	
	GARO Technique	GATO Technique
Design Session 1	0.004432	0.004267
Design Session 2	0.004397	0.004436
Design Session 3	0.004386	0.004047
Design Session 4	0.004337	0.003158
Design Session 5	0.004123	0.003554
Design Session 6	0.004450	<i>0.002956</i>
Design Session 7	0.004364	0.003352
Design Session 8	0.004316	0.003948
Design Session 9	0.004210	0.003760
Design Session 10	<i>0.004124</i>	0.003742
Mean	0.004314	0.003722
Standard Deviation	0.0001206	0.0004755

The results tabulated in Table 3 indicate that the designs resulting from GARO technique have delivered the highest load current while a significant variation in load current is observed for the designs resulting from GATO technique.

In order to compare the performance of large YAGI arrays, a 9-element YAGI array was then designed with a population size of 10 members evolved over 5 generations. The current delivered to the load by the best individual is given in Table 4 for ten different design sessions.

Table 4: Performance Comparison for GA Optimization, 9-Element YAGI Array, Population size = 10, Generation Size = 5, Mutation probability = 0.02, Cross over probability = 0.8, Input impedance = 50 Ohms, Frequency = 299.8 MHz.

	Current Delivered to a 50 Ohm load by a UPW arriving from the front of the antenna (A/V)	
	GARO Technique	GATO Technique
Design Session 1	0.006471	0.003032
Design Session 2	0.005561	0.004006
Design Session 3	0.005261	0.004085
Design Session 4	0.004750	0.005381
Design Session 5	<i>0.004713</i>	0.004102
Design Session 6	0.005002	<i>0.002934</i>
Design Session 7	0.006287	0.003544
Design Session 8	0.005603	0.003368
Design Session 9	0.005356	0.003968
Design Session 10	0.005101	0.006349
Mean	0.005411	0.004076
Standard Deviation	0.0005928	0.001057

The results tabulated in Table 4 indicate that the designs resulting from GARO technique have delivered the highest load current while a significant variation in load current is observed for the designs resulting from GATO technique. The variation in load current for designs resulting from GATO technique has increased as the dimension of the array increases.

In order to compare the performance with increased population size and generation size, a 9-element YAGI array was then designed with a population size of 20 members evolved over 10 generations. The current delivered to the load by the best individual is given in Table 5 for ten different design sessions.

Table 5: Performance Comparison for GA Optimization, 9-Element YAGI Array, Population size = 20, Generation Size = 10, Mutation probability = 0.02, Cross over probability = 0.8, Input impedance = 50 Ohms, Frequency = 299.8 MHz.

	Current Delivered to a 50 Ohm load by a UPW arriving from the front of the antenna (A/V)	
	GARO Technique	GATO Technique
Design Session 1	0.007036	0.004057
Design Session 2	0.006799	0.004221
Design Session 3	0.006225	0.004095
Design Session 4	0.005937	0.004627
Design Session 5	0.005197	0.005630
Design Session 6	0.006708	0.003761
Design Session 7	0.005821	<i>0.003518</i>
Design Session 8	0.005396	0.003715
Design Session 9	0.005235	0.005088
Design Session 10	<i>0.005151</i>	0.005608
Mean	0.005950	0.004432
Standard Deviation	0.0007142	0.0007735

The results tabulated in Table 5 indicate that the designs resulting from GARO technique have delivered the highest load current while a significant variation in load current is observed for the designs resulted from GATO technique. The variation in load current for designs resulting from GATO technique has decreased as the population size and number of generations are increased. However, this reduction is achieved with a significant increase in computer simulation time.

The best 9-element YAGI array design generated by the GARO techniques delivers a load current of 0.007036 A/V. A half-wave dipole operating under same conditions delivers a load current of 0.002536 A/V, hence the gain of this antenna is approximately 11dB. Field tests carried out with this antenna verify its superior performance.

CONCLUSION

The GARO technique presented in this paper generates YAGI arrays with better receiving capabilities compared to the GATO technique reported in literature. The YAGI antennas used for Television reception and FM radio reception are always used in receiving mode. Hence design of such antennas using GARO technique guarantees better performance.

Acknowledgement

The author wishes to acknowledge Mr. Chandana Perera for his contributions in writing software for implementation of the GARO technique.

References

- [1] E. E. Altshuler and D. S. Linden, *Design of a Loaded Monopole Having Hemispherical Coverage Using a Genetic Algorithm*, IEEE Transactions on Antennas and Propagation, Vol. 45, No. 1, p. 1, January 1997.
- [2] D.K. Chen and C.A Cheng, *Optimum element Spacings for Yagi-Uda Arrays*, IEEE Transactions on Antennas and Propagation, Vol. AP-21, p. 615, September 1973.
- [3] E. A. Jones and William T. Joines, *Design of Yagi-Uda Antennas Using Genetic Algorithms*, IEEE Transactions on Antennas and Propagation, Vol. 45, No. 9, p. 1386, September 1997.
- [4] D.S. Weile and E. Michielssen, *Genetic Algorithm Optimization Applied to Electromagnetics*, IEEE Transactions on Antennas and Propagation, Vol. 45, No. 3, p. 343, March 1997.
- [5] H. Yagi, *Beam transmission of Ultra-Short Waves*, Proceedings of IRE, Vol. 26 p. 715, June 1928.
- [6] A.M.S. Zalzal and P.L. Fleming, *Genetic Algorithms in Engineering*, First Edition, The Institution of Electrical Engineers, 1997.

OPTICAL CHARACTERISTICS OF CARBON BASED SEMICONDUCTORS

D A I Munindradasa and G A J Amaratunga *

Department of Electronics and Telecom. Eng.
University of Moratuwa,
Moratuwa,
Sri Lanka.

*Electronics Division,
Department of Engineering,
University of Cambridge,
Trumpington Street,
Cambridge CB2 1PZ,
United Kingdom.

OPTICAL CHARACTERISTICS OF CARBON BASED SEMICONDUCTORS

D A I Munindradasa and G A J Amaratunga*

Department of Electronics and Telecom. Eng.
University of Moratuwa,
Moratuwa,
Sri Lanka.

*Electronics Division,
Department of Engineering,
University of Cambridge,
Trumpington Street,
Cambridge CB2 1PZ,
United Kingdom.

Abstract

The photoluminescence (PL) in a-C:H:N was measured using a 2.41eV Ar ion laser line for varying N content. The PL results show a lowering of the PL peak energy and a spectral line width broadening as the N content in the film increases. Decomposition of the PL spectra into a series of Gaussian sub-peak levels shows two distinct peaks at 2.2 and 2.1eV and a broad peak at 1.7eV. It is found that the apparent lowering in the PL peak energy and the spectral line width broadening with increasing N content can be understood in terms of an increase in intensity of the sub-peak at 2.1eV with respect to that at the higher energy (2.2eV). The 1.7eV, 2.1eV and 2.2eV sub-peaks are also found in a-C:H without N.

Introduction

Hydrogenated amorphous carbon (a-C:H) films can be deposited using a plasma enhanced chemical vapour deposition (PECVD) process with a hydrocarbon gas as the source[1]. The ability of carbon to bond in a variety of configurations - sp^3 (diamond-like), sp^2 (graphite-like), and sp , in amorphous carbon leads to a material which can have a wide range of mechanical, electrical and optical properties depending on the relative fraction of the different bond types[2-6]. Kruangam et. al. [7] and Hamakawa et. al. [8] have reported the use of a-C:H as the active layer in electroluminescent devices. A new alloy, nitrogenated and hydrogenated amorphous carbon (a-C:H:N) obtained when nitrogen is incorporated into the gas mixture, has

drawn the interest due to its superior mechanical and optical properties [9] and also as a cold cathode which emits at low electric fields [10]. Materials containing (C-H) bonds show strong room temperature photoluminescence [11-14]. It is thought that this behaviour is due to photo excitation resulting in generation of confined electron hole pairs in π and π^* states. Since the π - π^* states associated with sp^2 sites are surrounded by wider gap sp^3 sites, it creates sharp band edge fluctuations leading to localised band edge states[15]. In this report we present the influence of nitrogen on the room temperature photoluminescence (PL) of amorphous carbon.

Experimental Work

The a-C:H:N films in this work were deposited by decomposition of methane (CH_4) and nitrogen (N_2) at 900mTorr, in an inductively coupled PECVD system operated at 27MHz, with variable RF power (600W - 1050W). In inductively coupled PECVD the ionised plasma oscillations are parallel to the substrate, minimising induced self bias voltage with respect to the substrate and secondary back sputtering, which is not the case in conventional capacitively coupled PECVD. Films were deposited on Si {100} substrates for PL studies and on fused quartz substrates for optical measurements. All substrates were chemically cleaned using a standard process prior to deposition [**The cleaning procedure** : boiled in deionized water, heated in trichloro ethylene, rinsed in 2-propanol, washed in deionized water, heated in hydrogen peroxide and ammonium hydroxide, washed in deionized water, heated in a hydrogen peroxide and hydrochloric acid mixture washed in deionized water and spin-dried]. In addition all substrates were given an in situ He plasma clean for 30 seconds in order to sputter clean any remaining impurities.

Optical measurements were carried out on 100nm - 300nm thick films deposited on quartz substrates. Absorption data were collected both in transmission and reflection with near normal incidence in a Philips UV-VIS spectrophotometer (188nm - 900nm). Optical parameters (refractive index - n and absorption constant - k) were computed, by considering reflection and transmission in a multilayer system comprising the film and substrate.

For the PL spectra measurement the 514nm line of an Ar ion laser operated at 600mW was used as the excitation source. The sample was excited at a glancing angle by a modulated laser beam, the PL emission was dispersed by a monochromator and detected by a photomultiplier placed normal to the sample. The amplifier was locked-in with the modulating frequency in order to remove any dc bias induced on the detector by the scattered ambient, and an optical filter in front of the detector is used to exclude the exciting laser line. All PL spectra were corrected for the system response.

Results and Discussion

The PL spectra measured from films with varying N content from no detectable N to 30 at% N [The N content was determined using scanning neutral mass spectroscopy (SNMS) with a structure factor adjusted for the density of a-C:H:N] are shown in Fig. 1. The PL peak energy position moves from 2.23eV for the film with no N to 2.12eV for the film with the highest nitrogen content. The Tauc optical band gap of the nitrogenated films remains constant at around 2.7eV for all nitrogen ratios while that of a-C:H without nitrogen is 3.0eV. With nitrogen incorporation into the film, the refractive index of the material n , does not shift from its behaviour without nitrogen in the film, as shown in Fig. 2a. The behaviour of the absorption constant k also remains the same with varying nitrogen contents [Fig. 2b]. However it shifts from its position at 0 at% N with the presence of nitrogen in the film. The deconvolution of the composite PL envelope for all the a-C:H:N and a-C:H films reveals two prominent Gaussian sub-peaks around 2.1eV and 2.2eV, and another relatively broad minor peak around 1.7-1.8eV. The apparent shift in peak position of the composite PL envelope with increasing N content is due to the change in the relative intensities of the two prominent sub-peaks with variation in nitrogen content, see Fig. 3a-Fig. 3d. As nitrogen content increases, the intensity of the sub-peak at 2.1eV increases with respect to that at 2.2eV, this effect is manifested as an apparent shift in PL peak position of the composite envelope towards lower energies. The relationship between the relative intensity of the sub-peaks and the measured PL peak is clearly seen in Fig.

4. In Fig. 4 the N ratios of 0.4, 1 and 3 correspond to N contents of 3.6 at%, 9 at% and 27 at%. The highest ratio of N is expected to be at the saturation level of N in a-C:H:N, 30 at%, as also measured previously [15]. When the ratio of $P_{S1(2.1\text{eV})} / P_{S2(2.2\text{eV})}$ and the composite PL peak is plotted against N content, the change in peak position with N content closely corresponds to the inverse change of the major sub-peak ratio. This is a strong evidence for the apparent shift in peak position of the composite envelope being due to intensity competition between these two sub-peaks. It is not due to any movement of the recombination centre within the band-gap as the N content increases.

As N content in the film increases the density of states related to N-centre, which on the basis of the PL results we propose to be $\sim 2.1\text{eV}$ above the π edge, increases making the intensity of PL associated with that centre higher. As shown in Fig. 5, the spectral width of the composite spectra gets broader with N content in the film. The spectral widths are comparable with those reported previously for similar materials [16]. The spectral broadening seen can be understood within the same context of there being two dominant recombination centres. The width of the two sub-peaks remains unchanged with changing N content, with a width of 0.18eV for the sub-peak at 2.2eV and 0.31eV for the sub-peak at 2.1eV . This shows that inclusion of nitrogen does not influence the line shape. Rather, nitrogenation leads to a higher intensity of the PL sub-peak at 2.1eV . Although the width of the sub-peaks remains unchanged, as relative N content, intensity increases, the intensity level at which half maximum occurs goes up. This is reflected as a broadening in the composite PL profile.

Conclusions

In this work we have studied the effect of nitrogen on photoluminescence in a-C:H:N, and we suggest that the apparent shift in PL peak and line with broadening of the PL spectra with nitrogen content is in fact due to increased intensity of a nitrogen associated recombination centre at 2.1eV from the π edge, within the bandgap electronic density of states (DOS). The fact that the spectral width of the PL sub-peak associated with N does not change as the N content is increased up to the saturation

value, also points to the N states associated with this centre being very strongly localised. We conclude that the PL is a very sensitive measurement of relative variation in such DOS in a-C:H due to inclusion of N compared to conventional optical absorption.

References

- [1] H. Nakaue, T. Mitani, H. Kurakawa and T. Yonezawa; Thin Solid Films, **212**, 240-244 (1992).
- [2] B. Dischler, A. Bubenzer and P. Koidl; Appl. Phys. Lett., **42**, 636 (1983).
- [3] J. Robertson; Adv. Phys., **35**, 317 (1986).
- [4] S. R. P. Silva, G.A.J. Amaratunga and C.P. Constantinu; J. Appl. Phys., **72**, 1149 (1992).
- [5] B. Meyerson and F W Smith ; Solid State Commun.; **41**, 68 (1982).
- [6] K K Chan, G A J Amaratunga, S P Wong and V S Veerasamy ; Solid State Electron., **36**, 3 (1993).
- [7] D Kruangam, T Endo, M Deguchi, W Guang-Pu, H Okamoto and Y Hamakawa ; Optoelectronics **1**, 67 (1986).
- [8] Y. Hamakawa, T. Toyama and H. Okamoto; J. Non-Cryst. Solids, **115**, 180 (1989).
- [9] J.H. Kim, D.H. Ahn, Y.H. Kim and H.K. Baik; J. Appl. Phys., **82** (2), 658 (1997).
- [10] G.A.J. Amaratunga and S.R.P. Silva ; App. Phys. Letts., **68** (18), 2529 (1996).
- [11] Z. Vardeny, E. Ehrenfreund, J. Shinar and F. Wudl; Phys. Rev. B, **32** (2), 2498 (1987).
- [12] J. Wanger and Lautenschlager; J. Appl. Phys., **59**, 2044 (1986).
- [13] S. Schuhnte, S. Will, H. Mell and W. Fuhs; Diamond Relat. Mater., **2**, 1360 (1993).
- [14] Rusli, G. A. J. Amaratunga and J. Robertson ; Phys. Rev. B **53** (24), 16306 (1996).
- [15] S. R. P. Silva, J. Robertson, Rusli and G. A. J. Amaratunga; Phil. Mag. B, **74** (4), 369 (1996).
- [16] S. Liu, S. Gangopadhyay, G. Sreenivas, S.S. Ang and H.A. Naseem; J. Appl. Phys. **82** (9), (1997).

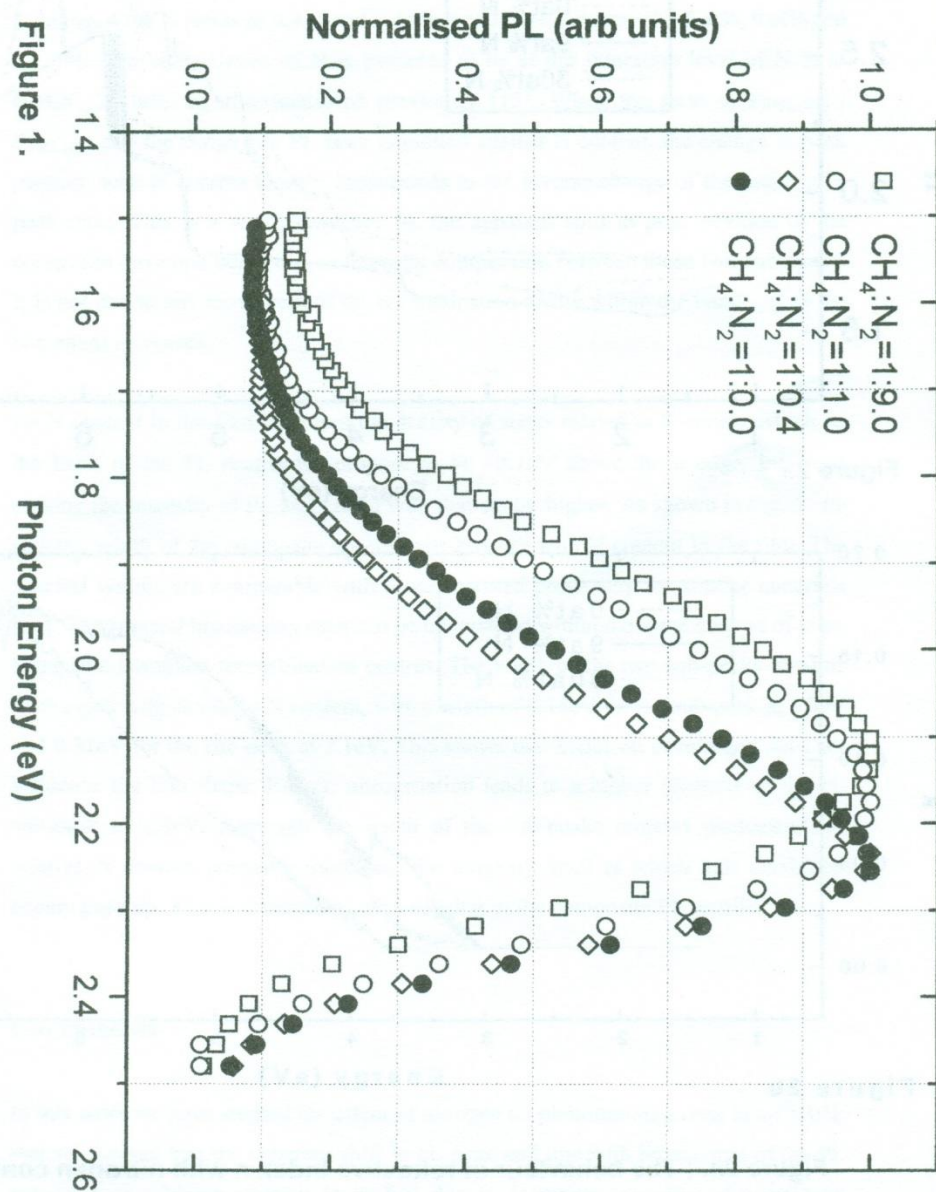


Figure 1.

PL spectra of a-C:H:N with varying N contents from no detectable N to ~30% N. Excitation energy used was the 2.41 eV Ar ion laser line. As N content in the film increases, PL peak position shifts from higher photon energy of 2.23 eV to 2.12 eV. The spectral width of the spectra also broadens with N content in the film.

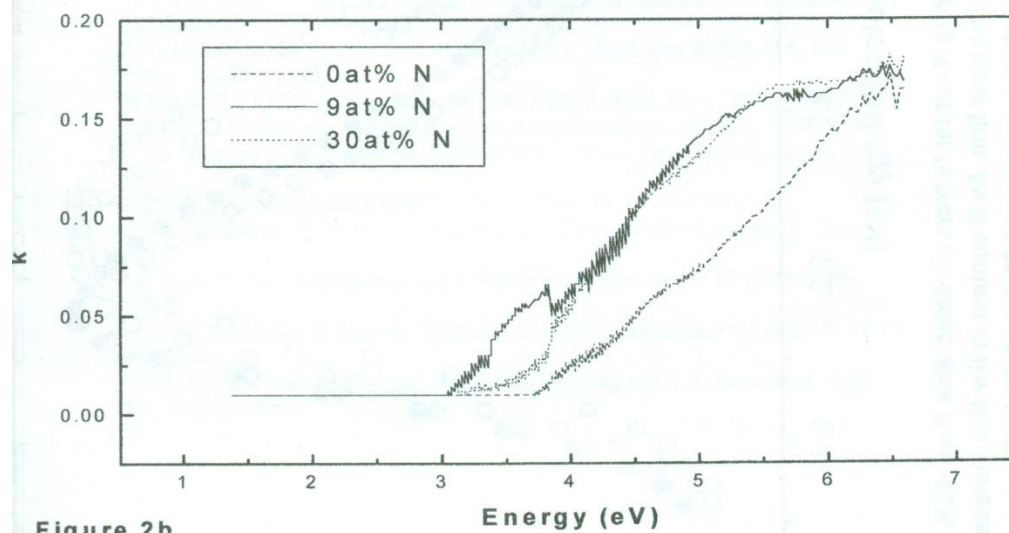
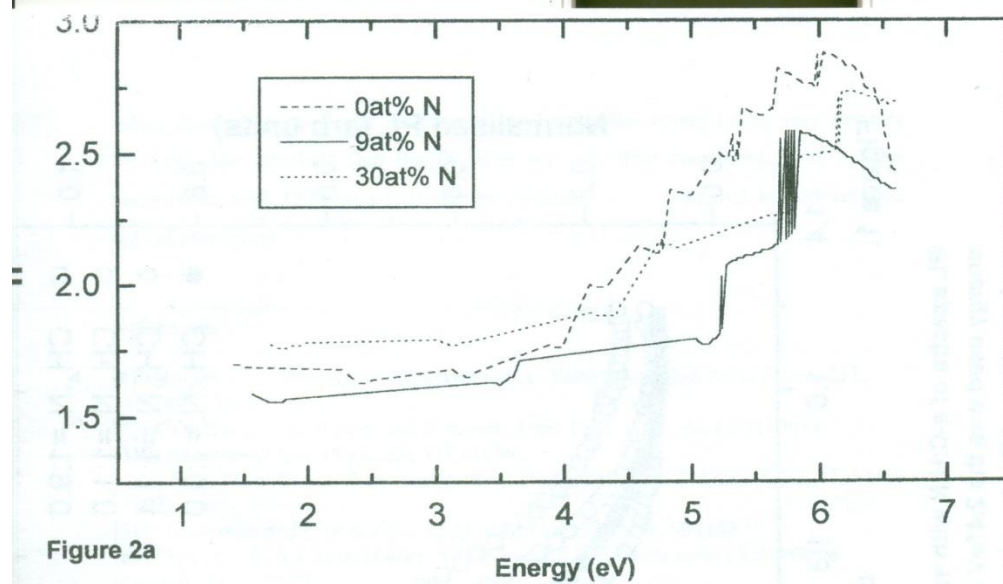


Figure 2a. : The behaviour of refractive index n with nitrogen content for three different N levels in the film. Incorporation of N does not affect the behaviour of n with photon energy.

Figure 2b. : The absorption constant k , shifts from nitrogen free position indicating the presence of N in the film. However it does not change further with varying N content.

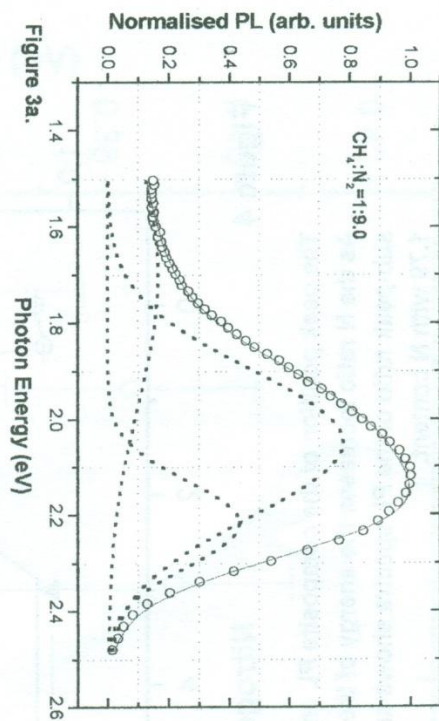


Figure 3a.

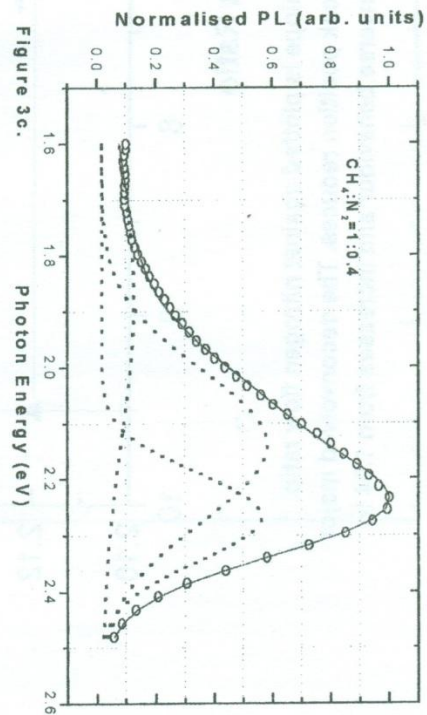


Figure 3c.

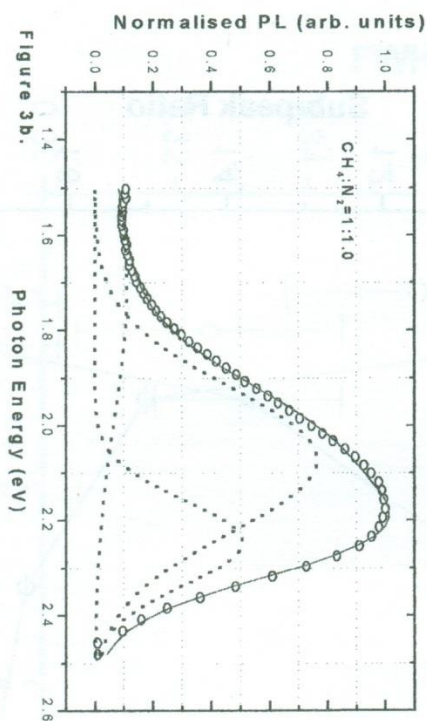


Figure 3b.

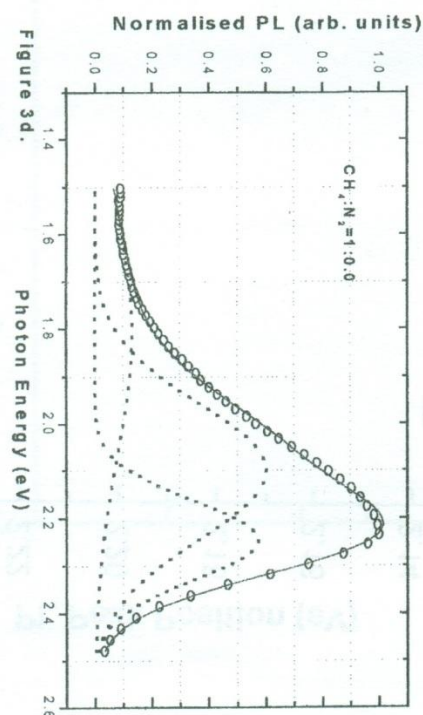


Figure 3d.

Figure 3 : The PL spectrum at the highest N content is in 3a. Deconvolution yields three Gaussian sub-peaks. The intensity ratio of two major sub-peaks, ~2.1eV to ~2.2eV is 1.79. In 3b the deconvolution shows similar sub-peaks as in 3a. But as N content goes down, major sub-peak ratio also goes down to 1.5. Further reduction in N content brings the deconvolved major sub-peak ratio down to 1.03. Deconvolved spectrum of the film containing no detectable N has a major sub-peak ratio of 1.04.

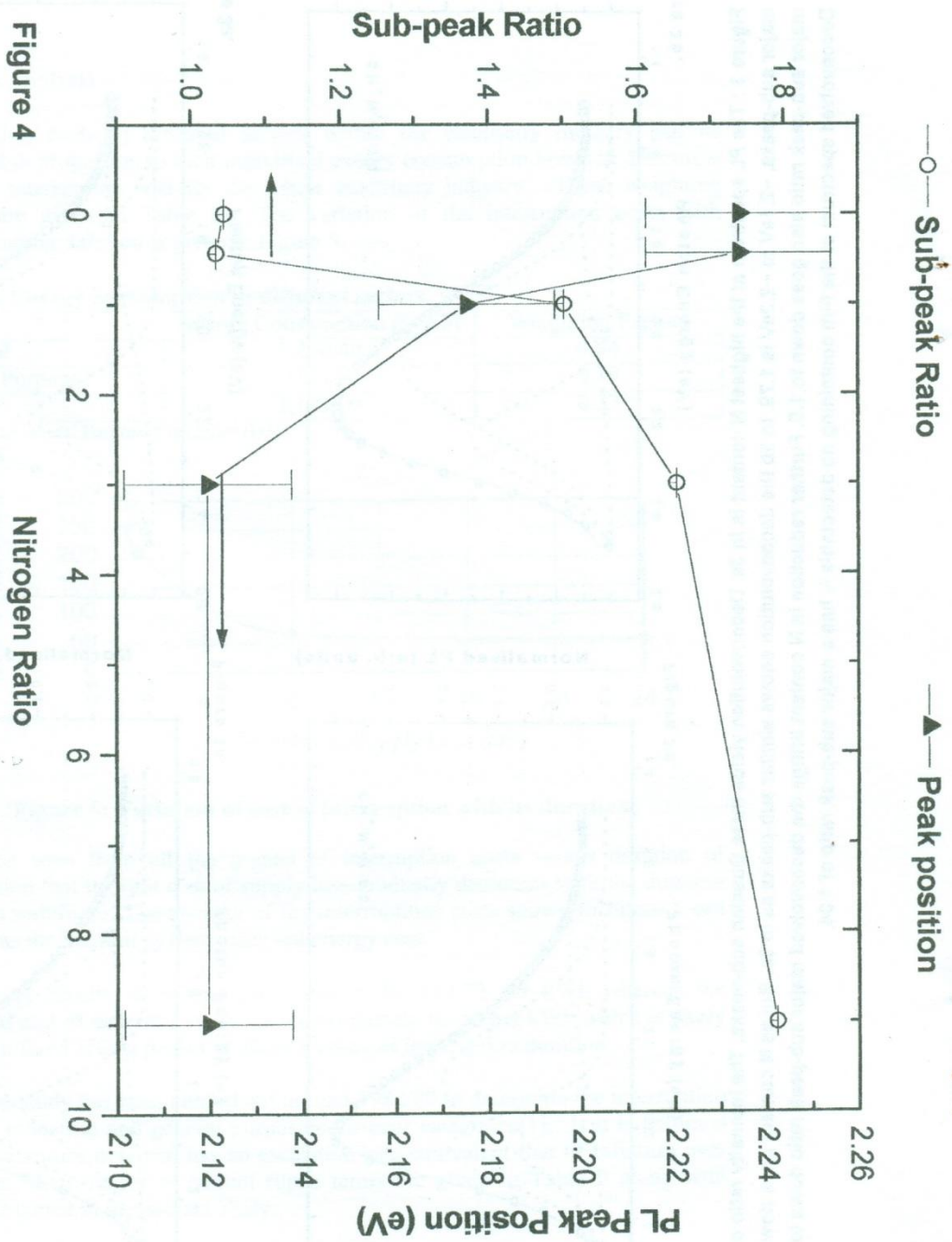


Figure 4

The peak position of the composite PL envelope is plotted against nitrogen flow ratio. As the N ratio increases the energy of the peak position reduces. The deconvolved major sub-peak ratio of the PL spectra shows an inverse behaviour and increases from 1.04 to 1.79 with N content.

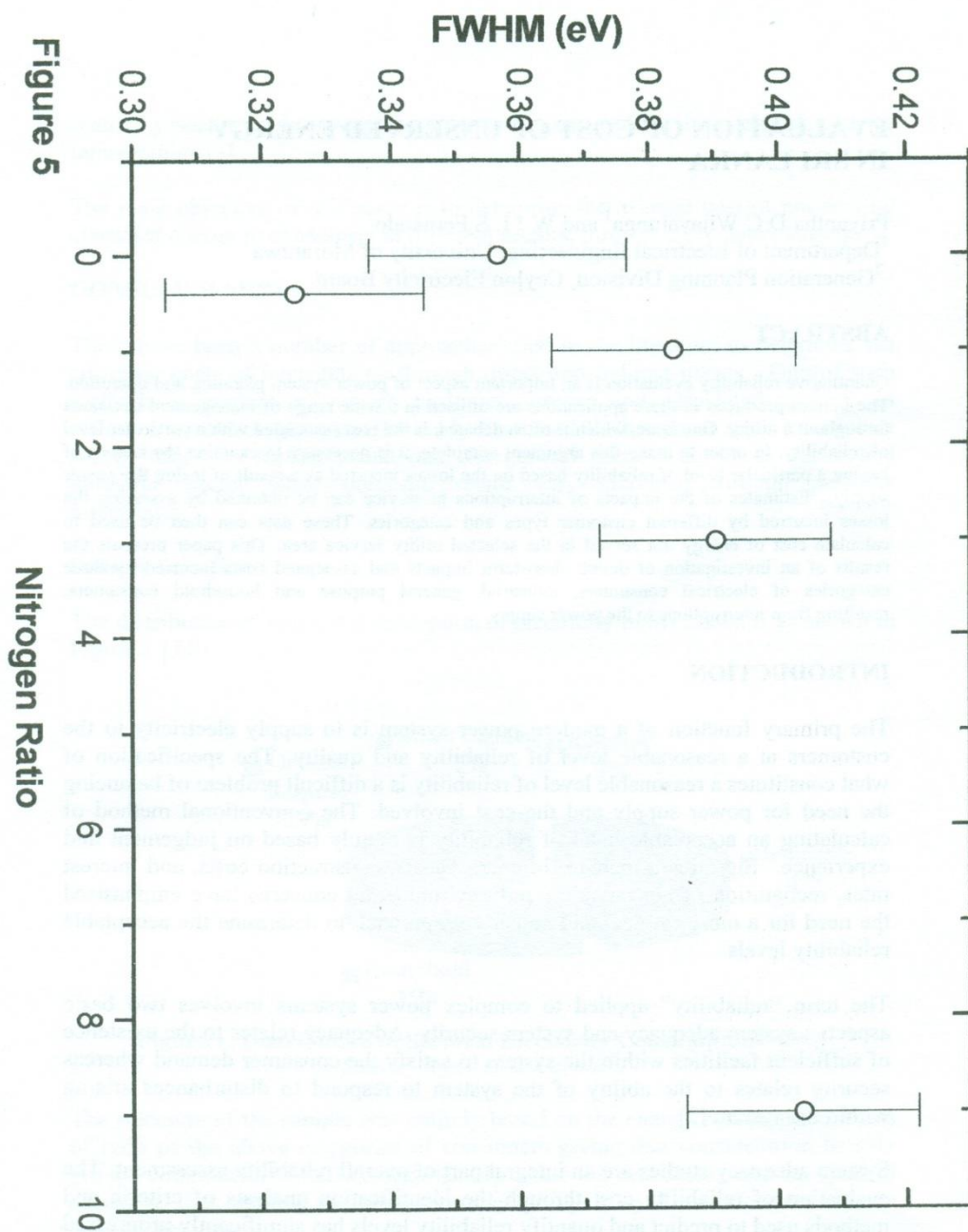


Figure 5

Nitrogen Ratio

The spectral width of the composite PL envelope as N content increases

EVALUATION OF COST OF UNSERVED ENERGY IN SRI LANKA

Priyantha D C Wijayatunga ⁽¹⁾ and W J L S Fernando ⁽²⁾

1. Department of Electrical Engineering, University of Moratuwa
2. Generation Planning Division, Ceylon Electricity Board

EVALUATION OF COST OF UNSERVED ENERGY IN SRI LANKA

Priyantha D C Wijayatunga¹ and W J L S Fernando²

¹Department of Electrical Engineering, University of Moratuwa

²Generation Planning Division, Ceylon Electricity Board

ABSTRACT

Quantitative reliability evaluation is an important aspect of power system planning and operation. The indices produced in these applications are utilised in a wide range of management decisions throughout a utility. One issue, which is often debated, is the cost associated with a particular level of reliability. In order to make this argument complete, it is necessary to examine the benefit of having a particular level of reliability based on the losses incurred as a result of losing the power supply. Estimates of the impacts of interruptions in service can be obtained by assessing the losses incurred by different customer types and categories. These data can then be used to calculate cost of energy not served in the selected utility service area. This paper presents the results of an investigation of direct, short-term impacts and associated costs incurred by three categories of electrical consumers, industrial, general purpose and household consumers, resulting from interruptions to the power supply.

INTRODUCTION

The primary function of a modern power system is to supply electricity to the customers at a reasonable level of reliability and quality. The specification of what constitutes a reasonable level of reliability is a difficult problem of balancing the need for power supply and the cost involved. The conventional method of calculating an acceptable level of reliability is mainly based on judgement and experience. Significant increase in energy costs, construction costs, and interest rates, recognition of conservation and environmental concerns have emphasised the need for a more rational and consistent approach to determine the acceptable reliability levels.

The term "reliability" applied to complex power systems involves two basic aspects : system adequacy and system security. Adequacy relates to the existence of sufficient facilities within the system to satisfy the consumer demand whereas security relates to the ability of the system to respond to disturbances arising within the system [2]

System adequacy studies are an integral part of overall reliability assessment. The evaluation of reliability cost through the identification analysis of criteria and methods used to predict and quantify reliability levels has significantly progressed during the past decade. By comparison, the assessment of reliability worth is in its infancy with most approaches used providing only an indirect or a boundary evaluation. This is because the assessment of societal worth of electric service reliability is a very complex task. One method, which has been used to successfully establish reliability worth estimates is to survey electrical consumers,

sector by sector to determine the costs or losses resulting from electric service interruptions [3].

The main objective of this study is to determine the average cost of not serving electrical energy to consumers in different sectors, through a consumer survey.

CONSUMER SURVEY

There have been a number of approaches used in the literature to determine the customer costs of interruptions through direct and indirect means. One of such methods is evaluation through customer surveys and associated analysis of different consumer groups. The study discussed in this paper used a customer survey based on regular postal mail for general purpose consumer sector and industrial sector while domestic sector was addressed through personal interviews.

Sample Selection

The distribution of sectoral consumption of electricity in Sri Lanka is as shown in Figure 1 [5,8].

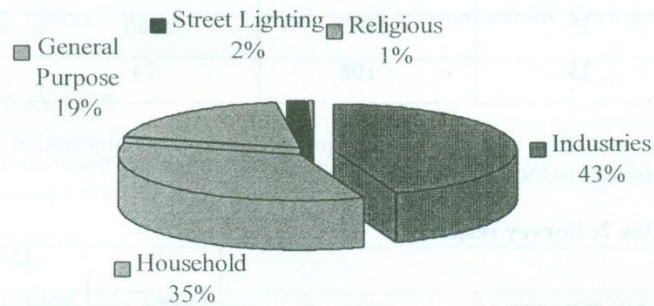


Figure 1: Distribution of Sectoral Electricity Consumption –1997

Source: Ceylon Electricity Board

The selection of the sample was entirely based on the energy consumption levels of each of the above categories of consumers giving due consideration to sub-groups within each of these categories [4]. Also the availability and the level of access to data relating to these consumer groups played an important role in sample selection.

Three categories of industrial consumers and three categories of General-Purpose consumers were separately addressed in the study along with one household consumer category. They are,

- I1, G1- Industrial 1/ General Purpose 1 Contract Demand <42kVA supplied at 400/230V
 I2, G2- Industrial 2/ General Purpose 2 Contract Demand >42kVA supplied at 400/230V
 I3, G3- Industrial 3/ General Purpose 3 supplied at 11/33/132kV

The sample was selected based on the availability of information in the consumer database as given in Table 1[7].

Table 1: Number of consumers and sample sizes

Category	No of Accounts 1997	No of consumers in the computer database	Selected sample size
General Purpose			
G1	202509	101	86
G2	1346	1283	641
G3	26	24	23
Industrial			
I1	19889	423	423
I2	3013	2366	1253
I3	108	74	74

The statistics related to the requests for supply interruption information and responses to them are shown in Table 2.

Table 2: Survey responses

	I1	I2	I3
No of consumers	19889	3013	108
No of questionnaires Mailed	423	1253	74
No of completed questionnaires Received	10	67	13
	G1	G2	G3
No of consumers	202509	1346	26
No of questionnaires Mailed	86	641	23
No of completed questionnaires Received	8	58	-

Questionnaire

Three separate questionnaires giving due consideration to specific details of each category, were prepared for industrial, general purpose and domestic consumers to obtain the cost of electricity interruption information.

The information requested from the consumers included estimates of the costs per kW for different supply interruption periods such as momentary, 1 minute, 30minutes, 1hour, 4hours, 12hours and 24hours.

CALCULATION METHODOLOGY

The values obtained for each type of industrial consumers were weighted based on their relative contribution towards value addition in the national economy, to determine the average cost of electricity supply losses within each industry group. Then these values for each group were further weighted based on their relative energy consumption patterns to obtain the final average value for the industrial sector.

The same approach was employed to determine the average value of cost of electricity supply losses in the general-purpose consumer sector with weighting factors based on relative energy consumption patterns. In the domestic sector equal weighting factors were used for all types of households during the calculations.

RESULTS & ANALYSIS

Data acquired for different categories of consumers were processed to fit into the above calculation requirements.

Industrial Sector

The cost data related to nine sub groups of the industrial sector directly obtained from the survey have been weighted in proportion to the value addition of each of these sub groups in the national economy. Table 3 shows these weighted averages of losses in each industrial sector tariff category (I1, I2 & I3).

Table 3: Interruption costs in the Industrial Sector

Duration	Loss Incurred (Rs/kW)					
	Momentary	30mins	1hour	4hour	8hour	24hour
Industrial 1	4.35	56.75	109.15	431.65	882.99	1790.24
Industrial 2	37.67	57.75	78.69	180.3	332.12	621.75
Industrial3	115.9	127.15	138.41	205.94	295.98	656.15

Later the average value corresponding to I1, I2 and I3 values was calculated by weighting each of them in proportion to the energy consumption within each of

these categories since the final impact of supply loss to the national economy will be in those proportions. Table 4 provides these weighting factors based on 1997 electricity consumption data.

Table 4: Energy consumption in different sub groups in Industrial Sector

	Energy Consumption (GWh)	Weighting Factors
Industrial 1	101.40	0.07
Industrial 2	805.00	0.56
Industrial3	524.00	0.37

The variation of cost of interruptions with duration of the interruption is shown in figure 2.

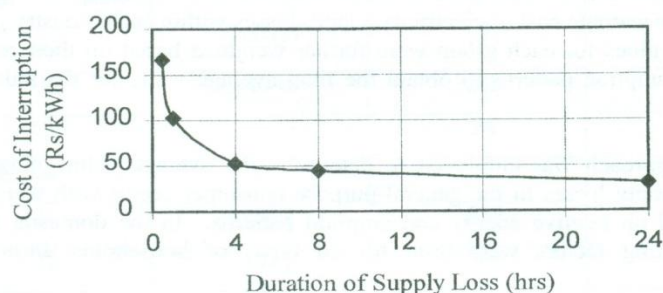


Figure 2: Variation of cost of interruption with its duration - Industrial Sector

General Purpose

The monetary values of losses obtained from the general purpose consumer sector through the survey were averaged giving equal weightage to all forms of General Purpose institutions due to unavailability of data on contributions to the national economy by individual subsectors. These weighted averages are given in Table 5.

Table 5: Interruption costs in the General Purpose Consumer Sector

Duration	Loss Incurred (Rs/kW)						
	momentary	10mins	30mins	1hour	4hour	12hour	24hour
General Purpose 1	8.07	246.85	511.67	1004	2278.8	4835.7	6430.2
General Purpose 2	302.03	310.14	333.91	370.2	569.74	1010.5	1331.1

Similar to the approach used in the industrial sector calculation of the average monetary values related to energy losses was based on weighting factors derived using 1997 consumption pattern. These weighting factors are given in Table 6.

Table 6: Energy consumption in different sub groups in General Purpose consumer Sector

	Energy Consumption (GWh)	Weighting Factors
General Purpose 1	389	0.65
General Purpose 2	214	0.35

The variation of cost of energy losses with duration of interruption is shown in Figure 3 for the General-Purpose category.

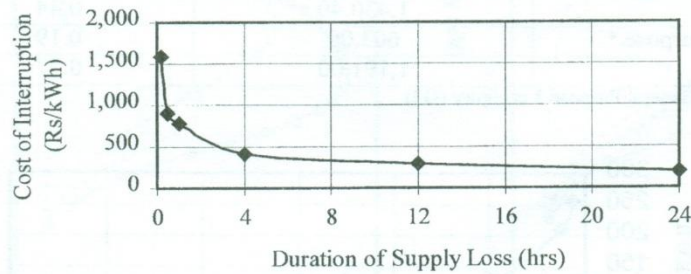


Figure 3: Variation of cost of interruption with its duration - General Purpose Consumer Sector

Domestic Sector

Data obtained for the domestic sector were averaged with all types of households given equal weightage. These final values are shown in Table 7 with the variation presented in Figure 4.

Table 7: Interruption costs in the Domestic Sector

Duration	30mins	1hour	4hour	8hour	24hour
Loss Incurred (Rs/kW)	16.26	50.16	196.23	226.31	341.27

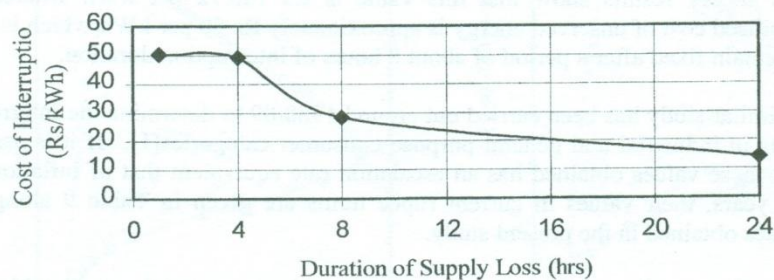


Figure 4: Variation of cost of interruption with its duration - Domestic Sector

General Analysis

Interruption costs in different sectors within the electricity industry can be weighted in proportion to their individual energy consumption levels to determine a single interruption cost for the whole electricity industry. These weighting factors are given in Table 8. The variation of the interruption costs with corresponding duration is given in Figure 5.

Table 8: Energy consumption in different sectors

	Energy Consumption (GWh)	Weighting Factors
Industrial	1,430.40	0.44
General Purpose *	603.00	0.19
Domestic	1,191.00	0.37

* Excludes General Purpose 3 category (G3)

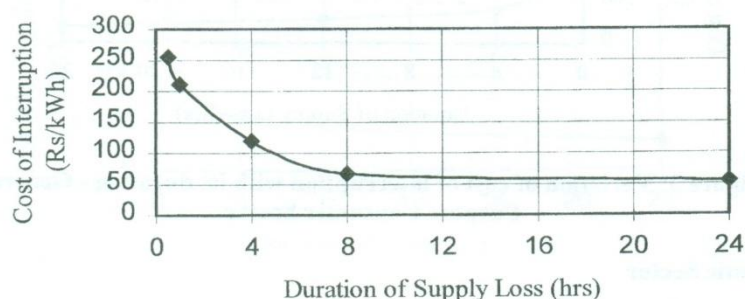


Figure 5: Variation of cost of interruption with its duration

It can be seen from all the graphs of interruption costs versus duration of interruption that the unit cost of supply loss gradually decreases with the duration and then stabilises. The average of the interruptions costs shown in figure 5 can be used as the per unit system unserved energy cost.

The survey results show that this value is Rs 140.72 per kWh whereas the stabilised cost of unserved energy is approximately Rs 50 per kWh which is likely to remain fixed after a period of about 8 hours of interruption duration.

A similar study has been carried out around 1988/89 to determine the interruption costs in industrial and general purpose consumer categories[1]. If it is assumed that these values obtained has an escalation rate equivalent that of inflation over the years, their values in current rupee terms are given in Table 9 along with values obtained in the present study.

It can be seen that while the industrial sector values agree to a considerable level, general-purpose consumer related values are approximately 10 to 25 times higher in the present study than those in the previous study.

Table 9: Comparison of results from previous and present studies

Industrial Sector					
<i>Duration</i>	<i>30 minutes</i>	<i>1 hour</i>	<i>4 hours</i>	<i>8 hours</i>	<i>24 hours</i>
Previous Study (Rs/kWh)	119.68	104.13	70.20	60.60	41.58
Present Study (Rs/kWh)	166.20	102.73	51.88	44.74	29.88
General Purpose					
Previous Study (Rs/kWh)		29.00	26.23	26.26	17.07
Present Study (Rs/kWh)	897.17	779.06	418.07	(12hr) 289.85	192.52

This clearly shows that the general-purpose consumers consisting of large commercial institutions now experience major losses due to power supply interruptions and it has escalated at a faster rate than the general rate of inflation. This may be largely due to rapid expansion of the commercial sector and higher energy intensity of activities carried out within these institutions in comparison to those around 10 years ago.

LIMITATIONS

The major limitation of the survey and the analysis is the absence of a large response to the set questionnaires in different sectors. This was particularly apparent in General Purpose Consumer Sector G3 category where the response was nil. Even in other sub sectors response rate was less than 10% of the total number of questionnaires mailed.

The cost of interruptions is entirely dependent on the estimates given by the individual respondents in the survey. The accuracy of these estimates is likely to vary from one respondent to another, which will have an impact on the final results.

CONCLUSIONS

The interruption cost estimates evaluated from this research project may be used in electrical system planning purposes in Sri Lanka bearing in mind the limitations of the consumer survey carried out. These values can be used as a good guideline for generation planning or any related analysis in the absence of a recently carried out study addressing the cost of supply interruptions. The dynamic nature of the unserved energy cost obtained in this can be effectively utilised in the calculations rather than using a single value across all interruption periods. Where necessary sectoral studies can be carried out using the unserved energy cost for the sector instead of using the average value for the whole electricity industry.

ACKNOWLEDGMENT

The authors are grateful to Mr H P I P Nandasena, Mr J C Nananyakkara, Mr P S Liyanaarachchi and Mr N T G Punchihewa, University of Moratuwa for their contribution in data collection and analysis and the Ceylon Electricity Board for providing data.

Financial Assistance extended by the University of Moratuwa and Sri Lanka Energy Managers Association is also gratefully acknowledged.

REFERENCES:

- [1] WA Methsiri, Evaluation of National costs of electricity interruptions in Sri Lanka, MSc Research Report, University of Moratuwa, 1990.
- [2] Roy Billinton, Ronald N Allan, Luigi Salvaderi, Applied reliability assessment in electric power systems, IEEE power power engineering society
- [3] G Wacker, E wojeznski, R Billnton, Customer damage resulting from electric service interruptions, Power system research group, University of Saskatchewan, Saskatoon, Saskatchewan
- [4] Annual Report 1997, Central Bank of Sri Lanka, 1998
- [5] Long Term Generation Expansion Plan 1997, Ceylon Electricity Board, 1997
- [6] KKYW Perera, Energy status of Sri Lanka; Issues-Policy-Suggestions, Institute of Policy Studies, 1992
- [7] Statistical digest, Ceylon Electricity Board, 1997
- [8] Sri Lanka Energy Balance-1996, Energy Conservation Fund, Sri Lanka, 1997
- [10] V.H. Wickramaratne et al, Distribution System Reliability, Final year project report, Department of Electrical Engineering, University of Moratuwa 1996

ENERGY CONSERVATION IN INDUSTRY: MOTOR DRIVES

Priyantha D C Wijayatunga¹ and D A U Daranagama²

1.Department of Electrical Engineering, University of Moratuwa

2.Energy Conservation Fund

ENERGY CONSERVATION IN INDUSTRY: MOTOR DRIVES

Priyantha D C Wijayatunga¹ and D A U Daranagama²

¹Department of Electrical Engineering, University of Moratuwa

²Energy Conservation Fund

ABSTRACT

A significant proportion of electrical energy generated is utilised in industrial motor drives in addition to it being used for electric lighting and heating. Also, oversized and under-utilised motors in the industrial sector are a common occurrence in Sri Lanka as a result of poor design and inappropriate replacement of equipment. These provide great opportunities for energy savings in motor drives particularly due to the fact that modern designs offer improved energy efficiencies in motor drive systems. This paper examines the present electricity consumption levels in motor drives used in the industrial sector and explores the opportunities for improvement by analysing data obtained through an industrial consumer survey carried out by personal visits to different industrial installations. The paper concludes with estimates of energy savings in the industrial sector as a result of possible energy efficiency improvements in industrial motor drives.

INTRODUCTION

Electrical energy is mainly used for lighting, heating and to drive motors particularly in the industrial sector. A significant proportion of electrical energy generated is consumed by electrical motor drive systems. This provides an opportunity to save a considerable amount of energy by proper selection of motors. The electric motor being a device converting electrical energy to rotating mechanical energy, the only form of power consumed is electricity while the output is the useful mechanical energy and mechanical energy losses within the motor. The losses within the motor can vary between 5% and 25% of the input power.

Modern motors are designed and manufactured using high quality materials and improved technology. For many years, the trend in motor manufacture has been to produce smaller and lighter motors in order to bring down the unit costs and no significant attention was given to efficiency and the power factor improvement beyond the levels required to achieve allowable temperatures. One of the major reasons for this trend is the higher priority given by the users for price, reliability, availability and quick delivery of motors as against operating costs. Thus energy efficiency did not rank at the top of purchaser concerns.

With the increasing cost of electric power and more emphasis on energy conservation, motor manufacturers have been addressing the area of energy efficiency improvement in electric motors to the levels that would lead to significant savings in energy.

Energy efficient motors are designed to generate a given mechanical power output with minimum mechanical and electrical losses within the motor. These energy efficient machines contain more copper and iron and have low frictional

and wind losses in comparison to their counterparts with standard designs. Although, Energy efficient motors typically cost more than standard motors, the benefit of lower operating cost can often offset the price premium [6,7,8].

ELECTRICITY CONSUMPTION TRENDS

Energy is a vital input to the national economic activity. Electricity is a major component within the energy sector. The electricity sector consists of three main consumer groups and few others having relatively low consumption levels. The main groups are the industrial consumers, households and the commercial sector. Electrical energy consumption has been increasing over the years with the total electricity sales in 1985 standing at 2060 GWh while it has increased to 3865 GWh in 1995 recording an increase of 1.9 times within a period of 10 years. The annual average growth rate of total electricity demand has been around 6.6 % during this period. The share of the electricity consumption in the industrial sector during the same period increased from 872 GWh to 1689 GWh at an average annual rate of 7.03 % [1,2,4].

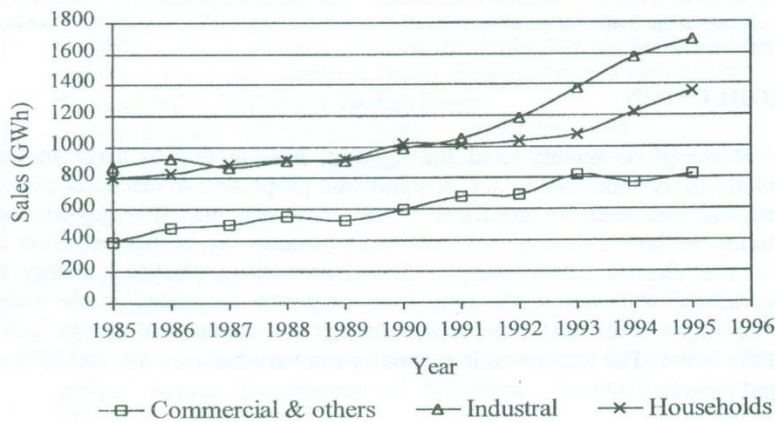


Figure 1: Sectoral electricity consumption growth over the years

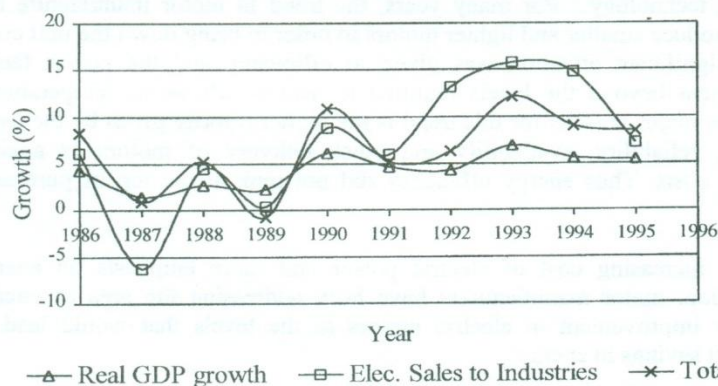


Figure 2: Variation of growth rate in the economy and electricity sector

As can be seen from figure 2 the economic growth in country is strongly correlated to the electricity consumption. In 1985 it required 18.807 MWh to produce one million rupees worth of national output while it has increased to 23.012 MWh in 1995 in current rupee terms. The electricity intensity of the industrial consumers grew from 7.95 MWh per rupees million to 10.05 MWh per rupees million in 1995 [3].

These changes in the electricity intensity can be due to two reasons

- a) Changes in the structure of the economy and of electricity use, possibly with more energy consuming industries being established resulting in reduction in the overall economic efficiency of electricity use.
- b) Decline in technical efficiency of electricity use.

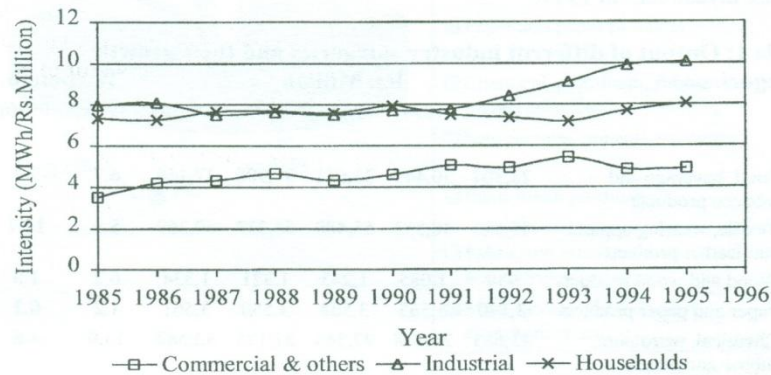


Figure 3: Electricity intensity in different sectors

These factors indicate that a strong emphasis on energy conservation and a move towards less energy intensive industries is necessary to bring down the electricity intensity in industry.

SRI LANKA INDUSTRIAL SECTOR

The industrial sector in Sri Lanka can be classified into nine categories. They are

1. Food, Beverages and Tobacco
2. Textile, Wearing Apparel & Leather
3. Wood, Wood production & Furniture
4. Paper, Paper Production, Printing, Publishing
5. Chemical, Petroleum, Rubber & Plastics
6. Non-metallic mineral
7. Basic Metal
8. Fabricated Metal Production Machinery & Equipment
9. Other Manufacturing Industries

Overall Trends

The industrial sectors grew by 10.3% in 1997, reflecting a significant expansion of both export oriented and domestic market oriented industries. Textiles and garment, the largest sub-sector in manufacturing, grew by 19%. Its share in GDP rose from 4.5% in 1996 to 5.1% in 1997. Its share in value addition in the industrial sector, which had remained around 38% during the last four years, increased to 41%. Many other industrial sector activities also reflected higher output levels. Among others, plastic, paints, milk products, tea processing, beverages, confectionery products, meat products, electrical items, batteries and rubber products, showed significantly high growth rate during the year. The manufacturing sector contributed 29% to the overall economic growth in 1997. Private sector industrial output grew by 12% compared to 7% in 1996. The Central Bank's Annual Survey of Industrial Production of 470 firms revealed an expansion in industrial sector capacity by 5%, in line with the growth of overall private investment in 1997.

Table 1: Output of different industry categories and their growth

Categories	Rs. Million					% change	
	1993	1994	1995	1996	1997(a)	1996	1997(a)
1. Food, beverage and tobacco products	28,304	30,445	33,641	35,908	37,146	6.7	3.4
2. Textile, wearing apparel and leather products	45,540	48,333	55,480	58,332	69,269	5.1	18.7
3. Wood and wood products	939	1,085	1,243	1,321	1,334	6.2	1.0
4. Paper and paper products	3,140	3,565	3,508	3,550	3,561	1.2	0.3
5. Chemical, petroleum, rubber and plastic products	23,683	25,838	27,543	31,135	32,582	13.0	4.6
6. Non-metallic mineral products	10,349	11,643	12,516	13,360	13,914	6.7	4.1
7. Basic metal products	1,178	1,568	1,377	1,636	1,671	18.8	2.1
8. Fabricated metal products, machinery and transport equipment	5,203	5,931	6,139	6,252	7,437	1.8	18.9
9. Manufacture products not elsewhere specified	2,366	2,617	3,005	3,443	3,904	14.5	13.4
Total	120,702	131,025	144,452	154,937	170,818	7.3	10.3

SAMPLE SURVEY AND ANALYSIS

A survey was carried out to identify the different kinds of motors used in industrial sector of Sri Lanka in order to collect their nameplate data and electricity consumption details of different companies. A sample of twenty-seven companies was selected to visit, on the basis of electricity intensity. Each of the nine industrial categories was divided into three electricity intensity levels. The intensity levels are

1. Electricity intensity less than 5%
2. Electricity intensity more than 5% and less than 15%
3. Electricity intensity more than 15%

One company from each of these intensity levels in each industrial category constitutes a sample of twenty-seven companies. Of the selected sample of twenty seven, only ten institutions responded positively to personal visits by the researchers which resulted in group 7, basic metal products, being completely left out.

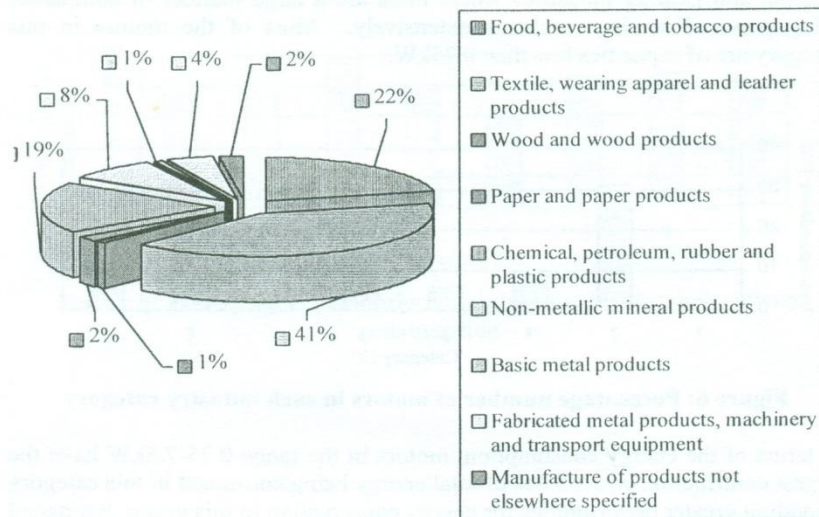


Figure 4: Composition of Industrial Production

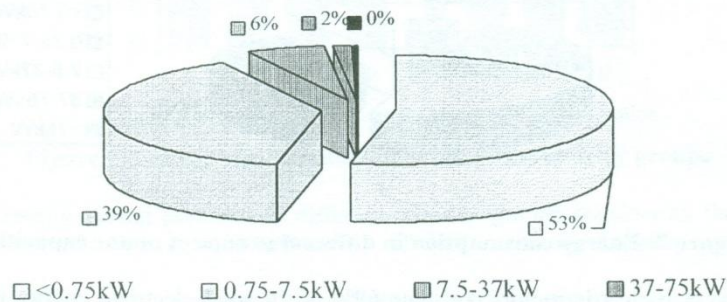


Figure 5: Distribution of different capacities of motors within the sample

Survey Results

Identification of motor population of different power rating ranges and their energy consumption is important in determining the saving potentials of different motor categories. Estimates of motor population of different power rating ranges within the sample are shown in figure 5.

It can be seen that most of the motors in the industry are of small capacities and those exceeding 75kW represents only around 0.3% of the total number of motors in the sample. The highest number of motors are used in the Textile, Apparel and Leather industries where there are a large number of companies using powered sewing machines extensively. Most of the motors in this category are of capacities less than 0.75kW.

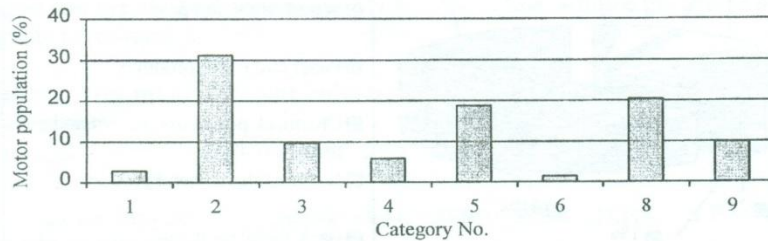


Figure 6: Percentage number of motors in each industry category

In terms of the energy consumption, motors in the range 0.75-7.5kW have the largest contribution with 35.6% of total energy being consumed in this category providing greater opportunities for energy conservation in this group. Estimated motor energy consumptions are shown in the figure 7.

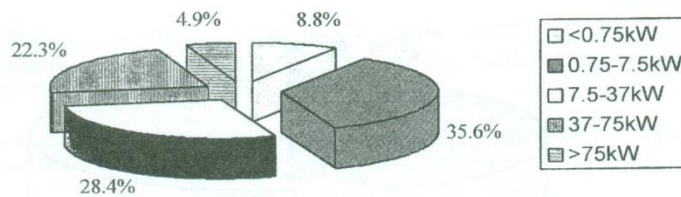


Figure 7: Energy consumption in different groups of motor capacities

On average electric motors consume 69% of the total electrical energy in the industrial sector. The contribution of motors to overall electricity consumption in each industrial category is shown in figure 8.

Although the category of wood, wood products and furniture has the highest motor energy consumption, its saving potential is relatively low because of the low motor population within that category.

Energy saving potential

The calculation of conservation potential of motors in the industry is done on the basis of National Electric Manufacturers Association (NEMA) standards. The existing standard motors in the industry are assumed to be at the average efficiency of the NEMA standard motors. Corresponding improvement in the existing standard motors are assumed to be the nominal efficiency values given for the energy efficient motors on NEMA standard MG1- 12.55A.

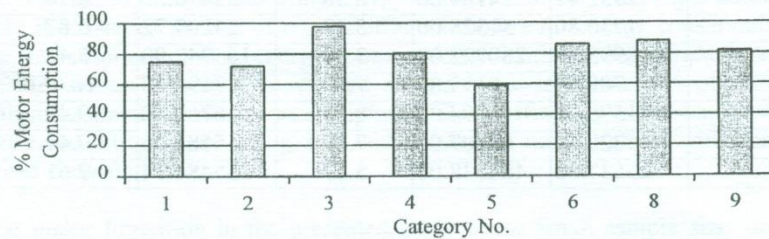


Figure 8: Electricity consumption in motors against total electricity consumption

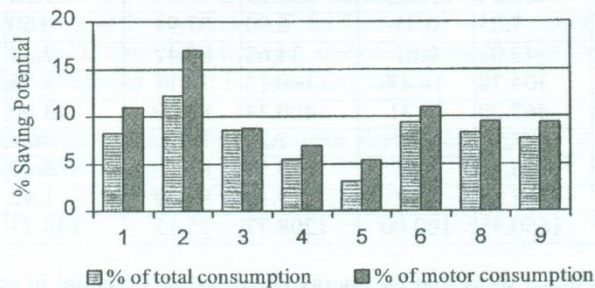


Figure 9: Energy saving potential in different industry groups

The energy saving potential in different industry groups considering that the existing motors are replaced with energy efficient motors are shown in figure 9.

Total energy saving potential in motors is 5.3% of total electrical energy consumption in the industry. It is also 7.6% of the total motor energy consumption in the industry. The highest motor energy saving potential is in the Textile, apparel and leather category. This category has a large number of small power motors where the possibility of efficiency improvement is high compared to large motors.

These results can be extended to the national situation and the corresponding figures are given in table 3.

Table 2: Energy saving potential in motors in different industry groups in the sample

Category No.	Energy Saving potential	Total Energy Consumption		Motor Energy Consumption	
	KWh	kWh	%	kWh	%
1	1915.44	23340.00	8.21	17451.12	10.98
2	2356.67	19270.00	12.23	13863.56	17.00
3	2932.41	34184.00	8.58	33478.20	8.76
4	1730.80	31328.00	5.52	25209.72	6.87
5	8993.59	280722.00	3.20	165942.90	5.42
6	788.64	8393.00	9.40	7192.38	10.96
8	1590.70	19094.00	8.33	16760.80	9.49
9	5229.59	68207.00	7.67	55581.46	9.41
Total	25537.85	484538.00	5.27	335480.14	7.61

Table 3: Projected national energy saving potential in motors within different industry groups

Category No.	Total Energy Consumption		Motor Energy Consumption		Conservation Potential	
	GWh	%	GWh	%	GWh	%
1	196.24	11.89	146.73	74.77	16.10	8.21
2	485.54	29.42	349.29	71.94	59.38	12.23
3	7.05	0.43	6.90	97.94	0.60	8.56
4	43.03	2.61	34.63	80.47	2.38	5.52
5	304.78	18.47	180.15	59.11	9.76	3.20
6	467.20	28.31	400.34	85.69	43.90	9.40
7	41.95	2.54	N/A	N/A	N/A	N/A
8	86.11	5.22	75.59	87.78	7.17	8.33
9	18.57	1.12	15.13	81.49	1.42	7.67
Total	1650.45	100.00	1208.77	75.15	140.73	8.75

These calculations show that the energy conservation potential in motors in the Sri Lanka industrial sector is around 141 GWh, which amounts to approximately 9% of the total electrical energy consumption in the industry. These values are likely to be higher if the industrial category of Basic Metals is also considered in the calculations.

Cost of Efficiency Improvement

The energy efficient motors are around 20-30% higher in cost compared to standard motor [7] whereas the efficiency gain is in the range of 2-8% [9]. For instance a 10hp (7.46kW) standard motor costs US\$ 614 and a same capacity efficient motor costs US\$ 795. The corresponding efficiency values are 86.5% and 91.6% [9]. If it is assumed that the average daily loading of the motor is 75% with 8hours of daily operation and 300 days annually, the additional

investment will be paid back within less than 5 years at an average electricity cost of Rs 4.75 per kWh. It is considered that an import tax of 50% is imposed on motors. The pay back period will be halved if one considers a two-shift operation in the industry leading to 16hrs of daily operation.

CONCLUSIONS

It can be seen from this study that industrial motor drives consists of a significant a component of industrial electrical energy consumption providing a vast opportunity for energy efficiency improvement in the sector. These efficiency gains can be achieved through proper sizing of motors, having variable speed controls and using energy efficient motors. This paper addressed only the issue of the use of energy efficient motors for energy conservation in the industrial sector. The energy conservation potential through replacement of existing motor drives with efficient motors alone is around 9% of the total industrial electrical energy consumption. These efficiency gains can be vastly improved with proper sizing and replacement of motors along with variable speed controls.

The major limitation in the presented study is the small sample size and the absence of relevant data from one of the industry categories. Further, the estimation of proportion of electricity consumption in motors is based on walk-through audits conducted in the selected sample.

ACKNOWLEDGEMENT

The authors are grateful to Mr H D Chaminda, Mr P S D Dabare, Mr G J Susantha and Mr U N Dahanayake of the University of Moratuwa for their assistance extended in data collection and analysis and the Energy Conservation Fund & Ceylon Electricity Board for providing data.

Financial Assistance extended by Sri Lanka Energy Managers Association is also gratefully acknowledged.

REFERENCES

1. Sri Lanka Energy Balance-1996, Energy Conservation Fund, Sri Lanka, 1997
2. Statistical digest, Ceylon Electricity Board, 1997
3. Annual Report 1997, Central Bank of Sri Lanka, 1998
4. Long Term Generation Expansion Plan 1997, Ceylon Electricity Board, 1997
5. KKYW Perera, Energy status of Sri Lanka; Issues-Policy-Suggestions, , Institute of Policy Studies, 1992
6. John C Andreas, "Energy Efficient Electric Motors", Second Edition, Marcel Dekker Inc, New York, USA, 1996
7. David Walters, "Energy Efficient Motors-Part 1", IEE Power Engineering Journal, London, Volume 13, Number 1, February 1999
8. David Walters, "Energy Efficient Motors-Part 2", IEE Power Engineering Journal, London, Volume 13, Number 3, April 1999
9. <http://www.energy.ca.gov/water/motors.html>, Energy-Water Connection California Energy Commission, Sacramento, USA

Annex A

Industries in different sub-groups within the industrial sector

- | | |
|---------------------------------------|-------------------------------------|
| 1. Food, Beverages and Tobacco | 5.5 Drugs & Medicines |
| 1.1 Meat Products | 5.6 Soap, Cosmetics |
| 1.2 Dairy Products | 5.7 Chemical Products N.E.C. |
| 1.3 Vegetable Products | 5.8 Petroleum |
| 1.4 Fish Products | 5.9 Miscellaneous Prod. |
| 1.5 Oil and Fat Products | of Petroleum |
| 1.6 Grain mill products | 5.10 Rubber Prod |
| 1.7 Bakery products | 5.11 Plastic Prod. |
| 1.8 Sugar refined | 6 Non-metallic Mineral |
| 1.9 Cocoa, chocolate, | 6.1 Pottery & Earthenware |
| sugar confectionery | 6.2 Glassware |
| 1.10 Food prod. N.E.C. | 6.3 Structural Clay Prod. |
| 1.11 Distilled Bottled Spirits | 6.4 Cement, Lime & Plaster |
| 1.12 Wine industry | 6.5 Non-metallic Mineral Prod. |
| 1.13 Malt industry | 7 Basic Metal |
| 1.14 Soft drinks | 7.1 Iron/ Steel Base Industries |
| 1.15 Tobacco | 7.2 Non-ferrous Metal Industries. |
| 2 Textile, Wearing Apparels & Leather | 8 Fabricated Metal Prod. |
| 2.1 Spinning & Weaving Textile | Machinery & Equipment |
| 2.2 Made-up Textile Goods | 8.1 Hand Tool & General Hardware |
| 2.3 Knitting Mills | 8.2 Furniture & Fixtures (Metal) |
| 2.4 Carpets & Rugs | 8.3 Structural Metal Prod. |
| 2.5 Cordage, Rope & Twine | 8.4 Fabricated Metal Prod. |
| 2.6 Textile N.E.C. | 8.5 Engines & Turbines |
| 2.7 Wearing Apparels | 8.6 Agriculture Machinery |
| 2.8 Tanneries & Leather Finishing | 8.7 Metal & Wood Work Machinery |
| 2.9 Prod. Of Leather | 8.8 Special Industrial Machinery |
| 2.10 Footwear | 8.9 Office Machinery |
| 3 Wood, Wood production. & Furniture | 8.10 Machinery & Equipment |
| 3.1 Saw Mills & Articles | 8.11 Elect. Industrial. Machinery |
| 3.2 Wood/Cane Containers/Boxes | 8.12 Radio, TV, Communication Eqpt. |
| 3.3 Wood/Cork Prod. N.E.C. | 8.13 Machinery & Eqpt. (Households) |
| 3.4 Furniture | 8.14 Electrical Apparatus |
| 4 Paper, Paper Prod., | 8.15 Ship Building |
| Printing, Publishing | 8.16 Railways |
| 4.1 Pulp, Paper, Paper Board | 8.17 Motor Vehicles |
| 4.2 Paper Containers & Boxes | 8.18 Motorcycles & Bicycles |
| 4.3 Paper & Paper Board Articles | 8.19 Transport Eqpt. |
| 4.4 Printing & Publishing | 8.20 Professional Scie. Eqpt. |
| 5 Chemical, Petroleum, | 8.21 Photographic & Optical Eqpt. |
| Rubber & Plastics | 8.22 Watches & Clocks |
| 5.1 Basic Inds. Chemicals | 9 Other Manufacturing Industries |
| 5.2 Fertiliser & Pesticide | 9.1 Gem & Jewellery |
| 5.3 Synthetic, Plastic Materials | 9.2 Musical Eqpt. |
| 5.4 Paint & Varnish | 9.3 Sport Eqpt. |

DESIGNING FUZZY LOGIC DAMPING CONTROLLERS FOR LARGE PRACTICAL POWER SYSTEMS

HJC Peiris

Department of Electrical Engineering, University of Moratuwa

DESIGNING FUZZY LOGIC DAMPING CONTROLLERS FOR LARGE PRACTICAL POWER SYSTEMS

HJC Peiris

Department of Electrical Engineering, University of Moratuwa

ABSTRACT

A methodology for designing fuzzy logic damping controllers for large practical power systems is presented in this paper. The proposed approach uses (i) the Prony Signal & Transfer Function Identification Technique to identify (a) the critical oscillation modes in the system (b) suitable damping control options and feedback signals to improve the damping of critical modes without significantly affecting the other modes; (ii) Pulse Test Response Technique to identify the rule base of fuzzy logic damping controllers. The advantage is that, the proposed approach can be utilized with the practical system or a simulated model of the system. In this paper, this approach is utilized to design fuzzy logic damping controllers for an ac-dc multi-area interconnected system. The system and controllers used in this study are simulated using EMTDC/PSCAD Transient Simulation Software. The simulation results observed reveal that, the proposed approach can be successfully utilized to design fuzzy logic damping controllers for large power systems.

INTRODUCTION

Electric power systems worldwide have continued to expand over the years owing to the growth in interconnections among neighbouring utilities. This is mainly because, the interconnections among utilities lead to improved security from mutual emergency assistance and economic system operation through the reduction of reserve capacity needed on each system and sharing of the most economical sources of power. These interconnections have resulted in very large systems of immense complexity and their secure operation has become very challenging. A major issue for consideration due to the increased interconnections is the formation of groups of closely coupled machines connected by weak lines that results in poorly damped oscillations in the system under different power transfer conditions. In addition, the increased use of continuously acting faster responding excitation systems for improving the transient stability and steady state power transfer levels have prompted decreased damping of power swings associated with generating plants. Moreover, the increased use of power electronic devices has contributed to significant changes in system dynamic characteristics. Primarily due to these reasons, the maintenance of small-signal stability has become an important aspect during design and operation of modern day power systems.

In general, the small-signal instability occurs due to the lack of sufficient synchronizing torque or damping torque on rotors of the synchronous machines in the power system. Insufficient synchronizing torque causes a steady increase in

the rotor angle and insufficient damping torque causes rotor oscillations of increasing amplitude. In the present day practical interconnected power systems, the small-signal instability is primarily a problem due to insufficient damping of the oscillations [1].

The most popular approach to improve the damping of system oscillations is the use of Power System Stabilizers to modulate the generator excitation control. Modulation control of power electronic devices such as High Voltage Direct Current Converters (HVDC), Static Var Compensators (SVC), Thyristor Controlled Series Compensators (TCSC) and Superconducting Magnetic Energy Storage units (SMES) have also been used in number of situations for enhancing damping of power system oscillations [1-6].

Choosing control algorithms for deriving these modulation signals to realize the desired stabilization objectives in a robust manner with minimal risk of adverse side effects is an important issue in power system controller design. In recent years, a considerable enthusiasm has been shown in the development and application of artificial intelligence techniques to design damping modulation controllers [7,8]. Fuzzy Logic Control is one such technique. Fuzzy logic controllers can handle imprecise, vague or "fuzzy" information to a significant extent and capable of producing good results under changing operating conditions and uncertainties in system parameters or observed variables. Hence, fuzzy logic control techniques are suitable for large, interconnected power systems, which usually possess a significant amount of uncertainties and experience frequent changes in operating conditions.

However, the difficulties in identifying a suitable rule base (relationships between input and control variables that are usually represented as a set of if ... then ... statements) have hindered the application of fuzzy logic control for large systems. Further, since a linearized model of the system is usually not obtained in designing fuzzy logic controllers and also, since the derivation of such a model is extremely difficult with large/complex interconnected systems, the identification of critical oscillation modes, suitable control options and feedback signals for improving damping of the critical modes without adversely affecting the other modes have become major issues.

A methodology, which uses the response of system variables to pulse test signals applied at chosen instants, is utilized in this paper to identify the suitable relationships that are needed to develop the rule base of fuzzy logic damping controllers. Further, the use of the Prony signal and transfer function identification techniques are proposed in this paper to identify the critical oscillation modes, the suitable damping control options and feedback signals. These approaches along with sequential de-centralized controller design are proposed and utilized to develop fuzzy logic damping controllers for large interconnected power systems in this paper. Sequential de-centralized controller design means development of each controller one after the other, so that dynamics of the previously designed controllers are taken into account in designing the next

controller [9]. Use of this approach enables us to enhance power system damping with simple fuzzy logic controllers.

TEST SYSTEM

Figure 1 shows the schematic diagram of the multi-area ac-dc interconnected system considered in this study.

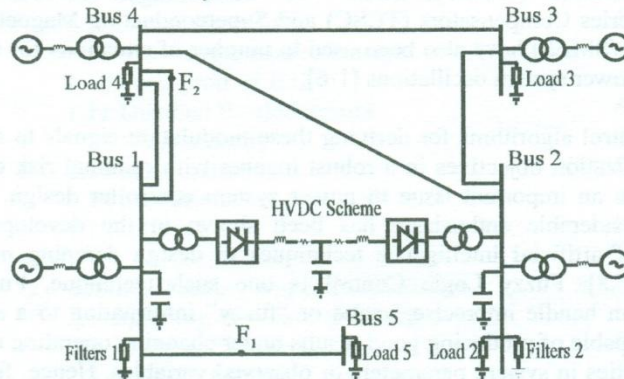


Figure 1: AC-DC power system

In this model, the ac systems are represented by synchronous generators equipped with excitation systems and governor-turbines. The converters of the dc scheme consist of two series connected six-pulse bridges. Harmonic Filters and capacitor banks are connected to the converter ac buses. Data for the synchronous generators, associated excitation systems and governor-turbines, transmission lines and ac loads are obtained from [10]. Data for the hvdc scheme, associated firing angle controllers, harmonic filters and capacitor banks are obtained from the CIGRE Benchmark Model [11]. In normal operation of the dc scheme, the rectifier firing angle controller is in constant current mode and the inverter firing angle controller is in constant extinction angle mode.

IDENTIFICATION OF CRITICAL OSCILLATION MODES

In this study, a number of simulations was performed with different disturbances to excite all the significant modes in the system. The variables such as the power output of the generators and the power flow in the lines (the lines between the buses 4 & 1, 4 & 3, 4 & 2, and 3 & 2) were observed and subjected to Prony Signal Analysis in order to identify the frequency and damping information of oscillation modes in the system.

In Prony Analysis, the time-domain signals are decomposed into a collection of damped sinusoids with four parameters per mode: frequency, damping, amplitude and phase. That is, the Prony Analysis gives an optimal fit (in a least square-error sense) to a signal $y(t)$ in the form:

$$\begin{aligned}\hat{y}(t) &= \sum_{i=1}^n A_i \exp(\sigma_i t) \cos(2\pi f_i t + \phi_i) \\ &= \sum_{i=1}^n B_i \exp(\lambda_i t)\end{aligned}\quad (1)$$

where, $\hat{y}(t)$ = estimated value for $y(t)$ from Prony Analysis Solution, f_i = frequency of the i^{th} mode, σ_i = damping of the i^{th} mode, A_i = amplitude (strength) of the i^{th} mode, ϕ_i = phase of the i^{th} mode, B_i = signal residues corresponding to i^{th} mode, λ_i = i^{th} eigen value (mode), n = number of modes in the system. A detailed derivation of the Prony Algorithm can be found in [12].

For example, the variation of the power output of the four generators (Pg1, Pg2, Pg3 and Pg4) and the power flow in the transmission lines between the areas 4 & 1, 4 & 3, 4 & 2 and 3 & 2 (P41, P43, P42 and P32) when the current order of the dc link is increased by 10% for a duration of 0.1s, is given in Figure 2. The information obtained by analysing these responses using the Prony Algorithm are given in Table 1.

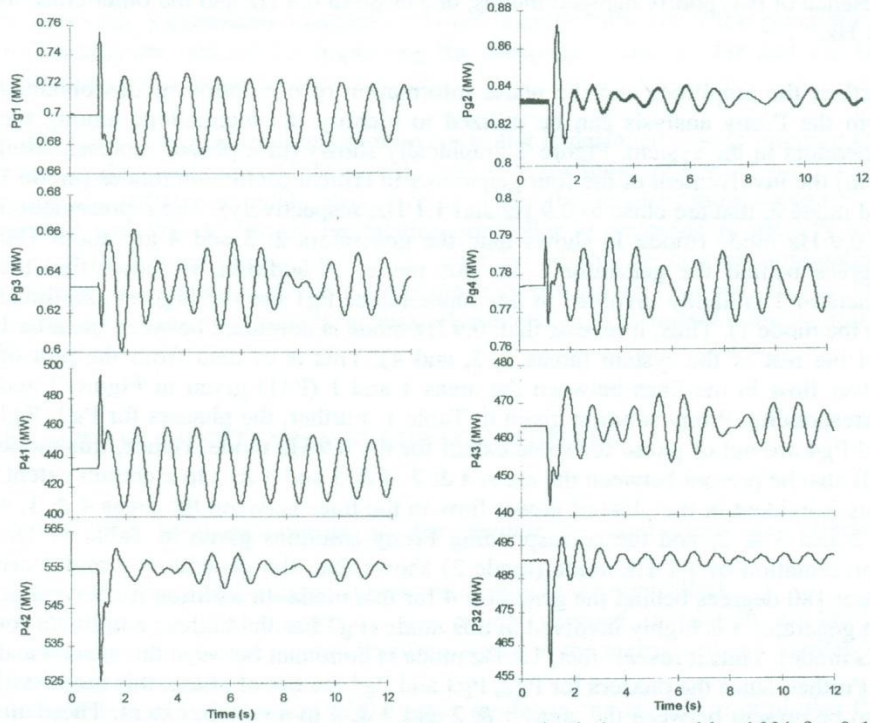


Figure 2: System response when the dc current order is increased by 10% for 0.1s

Table 1: Prony Analysis Solutions

signal	frequency (Hz)	damping	amplitude	relative strength	phase (deg)
Pg1	0.93	0.003	0.013	1.000	114.9
Pg2	0.94	0.003	0.003	0.60	-74.9
	1.07	0.034	0.005	1.00	-0.58
Pg3	0.91	0.003	0.006	0.75	-32.61
	1.10	0.033	0.008	1.00	-8.41
Pg4	0.89	0.003	0.005	1.00	-24.83
	1.09	0.030	0.004	0.80	154.35
P41	0.92	0.004	16.62	1.00	-66.0
P43	0.91	0.003	2.45	0.57	121.4
	1.12	0.025	4.31	1.00	132.2
P42	0.89	0.003	0.957	1.00	143.3
	1.12	0.029	0.937	0.98	114.9
P32	0.89	0.004	0.71	0.81	51.3
	1.11	0.022	0.88	1.00	-9.3

According to the Prony Analysis Solutions given in the Table 1, the dominant mode in the signal Pg1 is the oscillation mode with a frequency of around 0.9 Hz. Damping of this mode is slightly positive (0.003). The Prony solution for the signal Pg2 shows the presence of two poorly damped oscillation modes, one close to 0.9 Hz and the other close to 1.1 Hz. Participation of 1.1 Hz mode is slightly higher than the 0.9 Hz mode. Solutions for the signals Pg3 and Pg4 show the presence of two poorly damped modes, one close to 0.9 Hz and the other close to 1.1 Hz.

Further, the amplitude and the phase information of oscillation modes obtained from the Prony analysis can be utilized to identify the interactions among the generators in the system. Figure 3 graphically shows (in a phasor representation form) the involvement of the four generators in critical oscillation modes (mode 1 and mode 2, that are close to 0.9 Hz and 1.1 Hz, respectively). The representation of 0.9 Hz mode (mode 1) shows that, the generators 2, 3 and 4 are about 180 degrees behind the generator 1 for this mode. In addition, it shows that the generator 1 is highly involved in this mode (since Pg1 has the highest amplitude for the mode 1). Thus, it reveals that, 0.9 Hz mode is dominant between the area 1 and the rest of the system (areas 2, 3, and 4). This is evident from the plot of power flow in the lines between the areas 4 and 1 (P41) given in Figure 2 and corresponding Prony solution given in Table 1. Further, the phasors for Pg2, Pg3 and Pg4 are out of phase for some extent for the 0.9 Hz mode. Hence, this mode will also be present between the areas 4 & 2, 4 & 3 and 3 & 2 to a certain extent. This is evident in the plots of power flow in the lines between the areas 4 & 3, 4 & 2 and 3 & 2, and the corresponding Prony solutions given in Table 1. The representation of 1.1 Hz mode (mode 2) shows that, the generators 2 and 3 are about 180 degrees behind the generator 4 for this mode. In addition it shows that, the generator 3 is highly involved in this mode (Pg3 has the highest amplitude for this mode). Thus it reveals that, 1.1 Hz mode is dominant between the areas 4 and 3. Further, since the phasors for Pg2, Pg3 and Pg4 are out of phase, this mode will also be present between the areas 4 & 2 and 3 & 2 to a certain extent. These are

evident in the plots of power flow in the lines between the areas 4 & 3, 4 & 2 and 3 & 2 given in Figure 2 and corresponding Prony solutions given in Table 1.

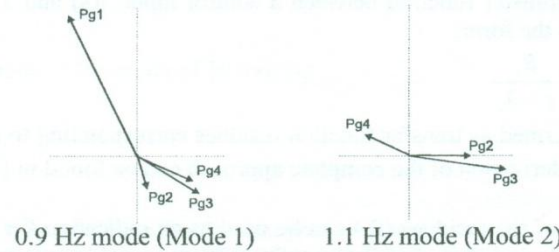


Figure 3: Involvement of generators in oscillation modes

DAMPING IMPROVEMENT OF THE CRITICAL MODES

In the test system considered, the modulation control of the dc current and the excitation of the four generators (generators 1 to 4) are possible options for improving the damping of poorly damped oscillation modes. Since generators 1 and 3 are mainly involved with critical oscillation modes 1 and 2 respectively, the dc current modulation (which significantly affect the generator 1 oscillations) and the generator 3 excitation modulation (which significantly affect the generator 3 oscillations) are utilized for improving the damping of the 0.9 Hz and 1.1 Hz oscillation modes, respectively.

In this study, the dc current modulation controller is designed first to improve the damping of more critical 0.9 Hz oscillation mode (damping of 0.9 Hz and 1.1 Hz modes are 0.003 and 0.03, respectively). Then the identification approach is repeated with the dc current modulation controller in operation to identify any changes in system modes due to the addition of the dc current modulation controller. It is found that, the 1.1 Hz mode is still poorly damped. Hence, the generator 3 excitation modulation controller is designed to improve the damping of this mode.

SELECTION OF SUITABLE FEEDBACK SIGNALS

The suitable feedback signals to the modulation controllers are selected considering,

- (a) the availability of the signal at close proximity to the controllers,
- (b) the extent of participation of the poorly damped oscillation modes in consideration (i.e. the sensitivity of the signal to the poorly damped oscillation modes), and
- (c) the extent of participation of the other modes in the signal (to minimize the effects of respective modulation control on those modes).

An extension of Prony Algorithm (Prony Transfer Function Identification Technique) is utilized to facilitate the feedback signal selection process by identifying the transfer function between a control input, $I(s)$ and a system state variable, $Y(s)$ in the form:

$$G(s) = \sum_{i=1}^n \frac{R_i}{s - \lambda_i} \quad (2)$$

where, R_i are termed as transfer function residues corresponding to system eigen values λ_i . The derivation of the complete approach can be found in [13].

The amplitudes of the residues (R_i) can be used as an indication for the extent to which each mode is affected if the respective state variable $y(t)$ is used as the feedback signal to the corresponding controller [13]. Hence, the amplitudes of these transfer function residues can be utilized to facilitate the feedback signal selection process.

In this study, local signals such as current (I), real power (P) and reactive power (Q) in the lines between the areas are subjected to the above analysis in order to identify suitable feedback signals to respective modulation control schemes. Accordingly, in the case of dc current modulation, current (I41), real power (P41) and reactive power (Q41) in the lines between the areas 4 & 1 are observed when a pulse signal is applied at dc current controller input. In the case of generator 3 excitation modulation, current (I43), real power (P43) and reactive power (Q43) in the line between the areas 4 & 3 are observed when a pulse signal is applied at the generator 3 excitation controller input. A summary of the corresponding transfer function solutions is given in Table 3.

Table 3: Transfer function residues
(a) dc current modulation controller.

Signal	Mode 1 (0.9 Hz)	Mode 2 (1.1 Hz)
I41	2.33	0.28
P41	1690.50	18.42
Q41	276.03	55.04

(b) generator 3 excitation modulation controller

Signal	Mode 1 (0.9 Hz)	Mode 2 (1.1 Hz)
I43	0.10	1.17
P43	38.25	767.53
Q43	41.82	83.47

The feedback signals selected for the dc current and the generator 3 excitation modulation controllers according to the above information are power flows in the lines between the buses 4 & 1 and 4 & 3, respectively (which have highest residues). Further, these feedback signals are passed through washout filters to eliminate the effects of offsets in steady state values due to change in steady state operating conditions. The time constants of these washout filters are chosen to allow oscillations of interest to pass through unchanged [1].

FUZZY LOGIC MODULATION CONTROLLERS

Fuzzy Logic (Fuzzy Sets)

Fuzzy logic can be viewed as a superset of conventional (boolean) logic that has been extended to handle the concept of partial truth values between “completely true” and “completely false” [14].

Thus, a fuzzy set \tilde{A} in the universe of discourse U is defined as a set of ordered pairs $\tilde{A} = \{(x, \mu_{\tilde{A}}(x)) | x \in U\}$ where $\mu_{\tilde{A}}(x)$ is called the membership function (or characteristic function) of \tilde{A} . Actually, $\mu_{\tilde{A}}(x)$ is the grade (degree) of membership of x in \tilde{A} , which indicates the degree that x belongs to \tilde{A} .

For example, let \tilde{A} represent the test scores achieving an excellent grade. Then, there is,

$$\tilde{A} = \{(x, \mu_{\tilde{A}}(x)) | x \in U\}$$

where the membership function $\mu_{\tilde{A}}(x)$ can be expressed as,

$$\mu_{\tilde{A}}(x) = \frac{1}{1 + [e^{(x-75)}]^{-p}}$$

which is shown in Figure 4. Here increasing p changes the definition of the term to become less fuzzy, or sharper.

According to this definition, a test score of 85 will belong to the fuzzy set “excellent grade” with a membership of 0.73 (when $p = 0.1$).

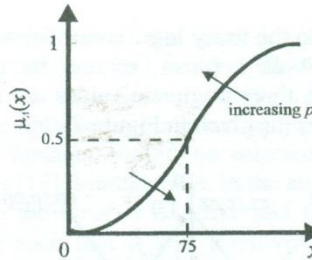


Figure 4: Characteristic (membership) function of a fuzzy set

Fuzzy Logic Controller

A fuzzy logic controller consists of three main processors; fuzzification, rule base & inference and de-fuzzification [15] as given in Figure 5. Fuzzification is the process of transforming crisp variables to respective fuzzy variables according to the chosen membership functions. The Rule Base of a fuzzy logic controller consists of all the necessary relationships among the input and output (control) variables. These relationships are expressed in the form **if ... then ...** statements. These are usually derived based on analytical, heuristical or expert knowledge

about the system behavior. In the inference stage, the rules are evaluated to determine the values of fuzzy output variables. De-fuzzification is the process of combining the results of inference process to find crisp outputs.

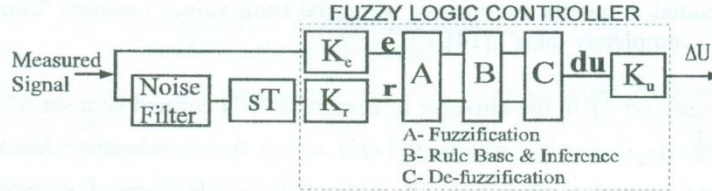


Figure 5: Fuzzy logic controller

Modulation Controllers

DC current modulation to improve the damping is done by adding a signal (derived in response to power flow oscillations in the lines between the buses 4 & 1) to the current reference of the rectifier firing angle controller (Figure 6).

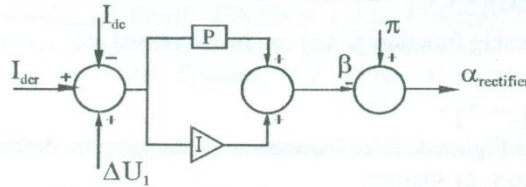


Figure 6: Rectifier firing angle controller

The derivation of the dc current modulation signal (ΔU_1) using fuzzy logic control techniques consists of the processes mentioned in Figure 5.

In this case, chosen inputs to the fuzzy logic controller are, the deviation of power flow between the buses 4 & 1 (error, e) and its rate of change (rate, r). Membership functions with three linguistic values are chosen for the input (e, r) and the output (du) variables (as given in Figure 7).

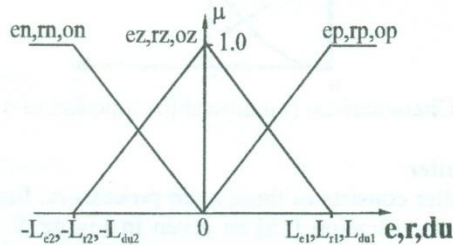


Figure 7: Membership functions of input and output variables

The derivation of the rule base needs the knowledge about suitable control actions for all combinations of the input variables; that is, suitable control actions to the rectifier firing angle controller for all combinations of the deviation of power flow

in the lines between the buses 4 & 1 (e) and its rate of change (r). The response of power system variables to pulse test signals applied at chosen instants (the Pulse Test Response Technique) is utilized in this paper to identify the suitable relationships that are needed to develop the rule base of fuzzy logic controllers. This technique has two main steps [10]:

- (a) apply test signals to the actual system or to the simulated model and observe the response,
- (b) derive the suitable fuzzy rules by comparing the responses with and without the test signals.

For example, assume that, the variation of the error and rate (after a disturbance) is as given in Figure 8.

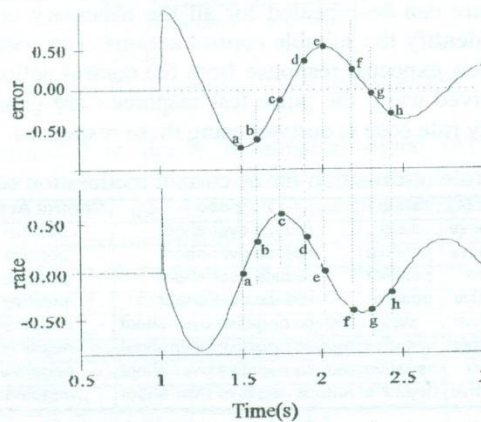


Figure 8: Input variables to the fuzzy logic controller

In order to develop the rule base of the fuzzy logic controller to improve the system response, the suitable control actions should be known for different combinations of the error and rate. Some instants on the system trajectory where such combinations can be obtained are marked in Figure 8 (instants a, b, ... , h). Control actions at such instants should be selected according to the system performance requirements [16]. For example, in the above case: close to point 'a', where the error is negative and the rate is almost zero, the control action should be such that it will improve the rise time (to speed up system response).

To find the suitable control action close to point 'a', where the error is negative and the rate is almost zero, a positive (P) pulse signal is applied at that instant. After the response is observed, the test is repeated with a negative (N) pulse signal of the same magnitude and duration. The variation of the error observed for these cases is compared with the original error signal (Figure 9). It can be seen from the responses that the negative pulse signal improves the system rise time. Therefore, when the error is negative and the rate is zero, the control action is selected as negative in order to improve the rise time. However, this has a

negative effect on the over-shoot (Figure 9). Therefore, if the over-shoot reduction is more important, then the corresponding control action is set either to zero to have no effect on the over-shoot or to positive to reduce the over-shoot.

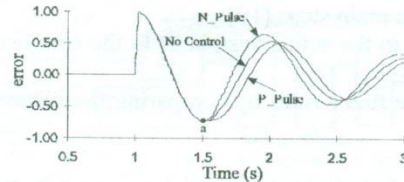


Figure 9: Pulse test response comparison at point 'a'

The above procedure can be repeated for all the necessary combinations of the input variables to identify the suitable control actions. The possible combinations of the input variables, expected response from the control actions and the suitable control actions derived using the pulse test responses are given in Table 4. The corresponding fuzzy rule base is derived using these responses.

Table 4: Fuzzy rule information for dc current modulation controller design

error (e)	rate (r)	Purpose	Control Action
negative	zero	reduce over-shoot	positive
negative	positive	reduce over-shoot	positive
zero	positive	reduce over-shoot	positive
positive	positive	reduce over-shoot	positive
positive	zero	reduce negative over-shoot	negative
positive	negative	reduce negative over-shoot	negative
zero	negative	reduce negative over-shoot	negative
negative	negative	reduce negative over-shoot	negative

The intersection operator, "product" is used to evaluate the fuzzy rules. Then the union operator, "maximum" is used to assess the results of the intersection operations that give the same output linguistic value. The Center of Gravity defuzzification technique is used to combine the inference outputs. The values that define the membership functions of the input and the output variables are set to have normalized domains (that is, $L_{e1} = L_{e2} = L_{r1} = L_{r2} = L_{u1} = L_{u2} = 1$). The input scaling gains, K_e and K_r , are chosen considering the probable maximum range of the input variables, error and rate (that is, so that $K_e \cdot \text{error}_{\max} \approx K_r \cdot \text{rate}_{\max} \approx 1$). The output scaling gain K_u is chosen to transform the control signal to a suitable range considering the probable limits of the modulation signal (that is, if the probable safe limit of the modulation signal is ± 0.1 , then K_u is selected as 0.1). Then, the chosen scaling gains K_e , K_r and K_u are adjusted until the controller performance is satisfactory.

Once the dc current modulation controller is designed, the system response is observed under different disturbances in order to identify the significant oscillation modes present in the current system. As expected, it was found that, still there is the other oscillation mode (close to 1.1 Hz) that has not been properly damped out. The frequency and the damping information at this stage are given in Table 5.

Table 5: Significant modes with the dc current modulation controller

Oscillation Mode	Eigen values (λ)	Frequency = $\text{imag}(\lambda)/2\pi$	Damping = $-\text{real}(\lambda)/2\pi$
1	$-1.26 + j 5.65$	0.9	0.2
2	$-0.19 + j 6.91$	1.1	0.03

A modulation control signal (which is derived in response to power flow oscillations in the line between the buses 4 & 3) is added to the excitation system of the generator in the area 3 (Figure 10) to improve the damping of this oscillation mode (close to 1.1 Hz).

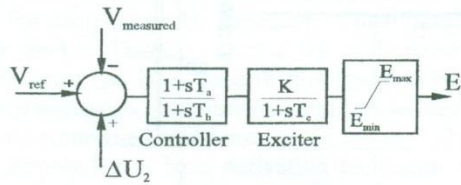


Figure 10: Generator 3 excitation system

A fuzzy logic controller to derive modulation signal (ΔU_2) is designed by following a similar procedure to that of the dc current fuzzy logic modulation controller. Information about the damping of oscillation modes after the addition of the generator 3 excitation modulation controller are given in Table 6. It can be observed that, the addition of the generator 3 excitation modulation controller has increased the damping of 1.1 Hz oscillation mode.

Table 6: Significant modes with both modulation controllers

Oscillation Mode	Eigen values (λ)	Frequency = $\text{imag}(\lambda)/2\pi$	Damping = $-\text{real}(\lambda)/2\pi$
1	$-1.26 + j 5.65$	0.9	0.2
2	$-0.63 + j 6.91$	1.1	0.1

SIMULATION RESULTS

To evaluate the performance of the designed controllers of which the parameters are given in the Appendix, the system response without modulation control (NC), with dc current modulation control (CC) and with both dc current and generator 3 excitation modulation control (CEC) under different disturbances, is observed.

The results given in Figure 11 show the response when one of the transmission lines between the buses 4 & 1 is tripped 5 cycles after a 3 phase line to ground fault occurred in that line at a point close to bus 4 (F_2 in Figure 1). This disturbance excites both poorly damped oscillation modes in the system (curves NC). It can be observed from these results that, with the addition of the dc current modulation controller (curves CC), the power flow oscillations in the remaining line between the buses 4 & 1 (P41) are significantly damped out, but there exists poorly damped oscillations between the areas 4 & 3 (P43), 4 & 2 (P42) and 3 & 2 (P32); specially between the areas 4 & 3 (in P43). After the addition of the excitation modulation controller (curves CEC) these oscillations are also

significantly damped out. The current in the dc link, the excitation of the generator 3, and the voltages at the buses 1 & 3, are also given in order to show that, there are no significant deviations in these signals due to modulation.

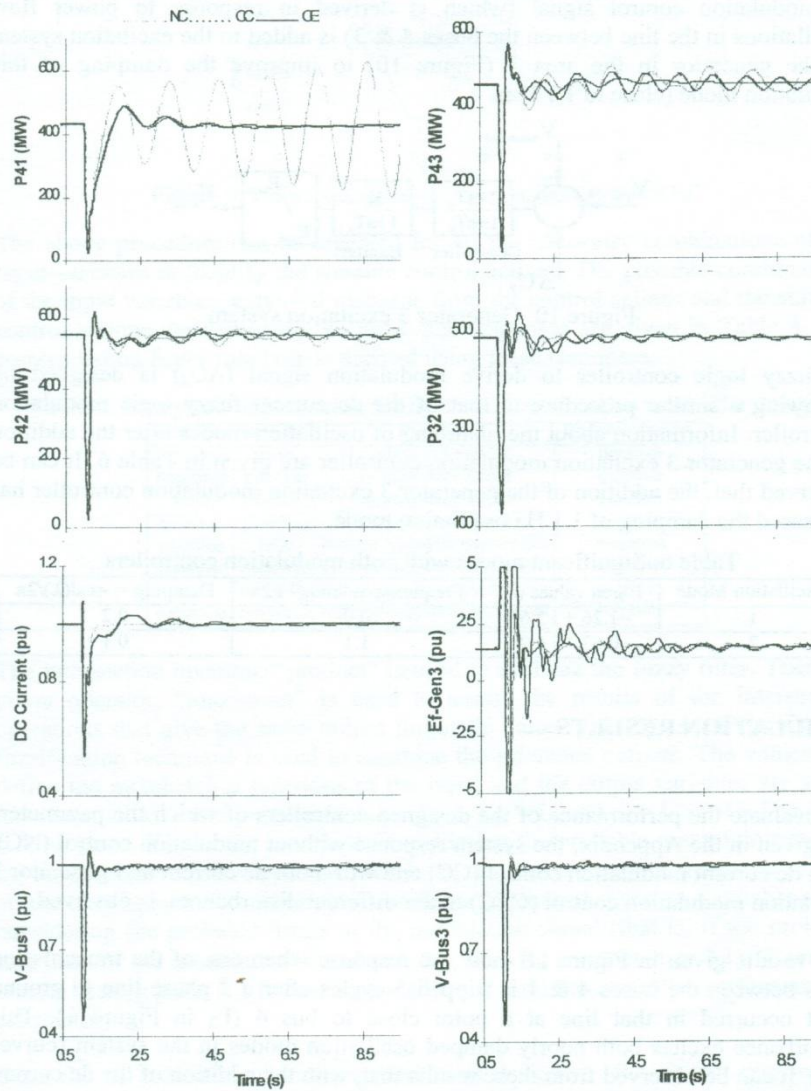


Figure 11: Response when one of the lines between the buses 4 & 1 is tripped after a three phase line to ground fault

CONCLUSIONS

A methodology to apply fuzzy logic control techniques to enhance damping of oscillations in large, interconnected power systems has been presented in this paper. The proposed method combines the Pulse Test Response Technique for rule base development and Prony Analysis for identifying (i) the critical oscillation modes in the system, and (ii) the suitable control options and feedback signals to improve the damping of the respective critical modes without adversely affecting the other modes. This approach along with sequential de-centralized control design techniques has been used in this study to design fuzzy logic dc current and generator excitation modulation controllers to improve the damping of oscillations in an interconnected multi-area ac-dc system. The simulation results revealed that the proposed rule base derivation technique can be successfully applied to design simple fuzzy logic controllers for improving damping of oscillations in large/complex power systems. It can be also stated that, since the designed controllers are very simple and contain only few rules, they are suitable for on-line implementation in practical power systems.

REFERENCES

- [1] P Kundur, *Power System Stability and Control*, McGraw-Hill, Inc., 1993.
- [2] P Kundur, M Klein, G J Rogers and M S Zywno, "Application of Power System Stabilisers for Enhancement of Overall System Stability," *IEEE Transactions on Power Systems*, Vol. 4, No. 2, pp. 614-626, May 1989.
- [3] R L Cresap and W A Mittelstadt, "Small-Signal Modulation of the Pacific HVDC Intertie," *IEEE Transactions on Power Apparatus and Systems*, Vol. 95, No. 2, pp. 536-541, March/April 1976.
- [4] S E M de Oliveira, "Synchronising and Damping Torque Coefficients and Power System Steady-State Stability as Affected by Static Var Compensators," *IEEE Transactions on Power Systems*, Vol. 9, No. 1, pp. 109-119, February 1994.
- [5] E W Kimbark, "Improvement of System Stability by Switched Series Capacitors," *IEEE Transactions on Power Apparatus and Systems*, Vol. 85, No. 2, pp. 180-190, February 1966.
- [6] H J Boenig and J F Hauer, 'Commissioning test of the Bonneville Power Administration 30 MJ Superconducting Magnetic Storage Unit,' *IEEE Transactions on Power Apparatus and Systems*, Vol. 104, No. 2, pp. 302-312, February 1985.
- [7] P J M Van Son, "Practical Aspects of Intelligent Machines in the Control Room," *Electra*, No. 159, pp. 103-115, April 1995.

- [8] Y H Song and A T Johns, "Applications of Fuzzy Logic in Power Systems," *Power Engineering Journal*, Part 1: pp. 219-222, October 1997; Part 2: pp. 185-190, August 1998; Part 3: pp. 97-103, April 1999.
- [9] E J Davison and U Ozguner, "Decentralised Control Using Local Models for Large-Scale Systems," *Control and Dynamic Systems*, Vol. 22, Part 1, pp. 195-231, Academic Press, Inc., 1985
- [10] H J C Peiris, U D Annakkage and N C Pahalawaththa, "Generation of fuzzy rules to develop fuzzy logic modulation controllers for damping of power system oscillations", *IEEE Transactions on Power Systems*, Vol. 14, No. 4, pp. 1440-1445, November 1999.
- [11] EMTDC/PSCAD User's Manual, Manitoba HVDC Research Centre, Canada, 1994.
- [12] J F Hauer, C J Demeure and L L Scharf, "Initial Results in Prony Analysis of Power System Response Signals," *IEEE Transactions on Power Systems*, Vol. 5, No.1, pp. 80-89, February 1990.
- [13] D J Trudnowski, J R Smith, T A Short and D A Pierre, "An Application of Prony Methods in PSS Design for Multimachine Systems," *IEEE Transactions on Power Systems*, Vol. 6, No. 1, pp. 118-126, February 1991.
- [14] L A Zadeh, "Fuzzy Sets," *Information and Control*, Vol. 8, pp. 338-353, 1965.
- [15] Lee, C.C., "Fuzzy Logic in Control Systems: Fuzzy Logic Controller-Part I and Part II", *IEEE Transactions on Systems, Man, and Cybernetics*, Vol. 20, No. 2, pp. 404-435, March/April 1990.
- [16] H X Li and H B Gatland, "Conventional Fuzzy Control and its Enhancement," *IEEE Transactions on Systems, Man and Cybernetics-Part B: Cybernetics*, Vol. 26, No. 5, pp. 791-797, October 1996.

APPENDIX

Noise Filter parameters:

Transfer function = $G/(1+sT)$

$G = 1.0$, $T = 0.05s$

Washout Filter parameters:

Transfer function = $G.sT/(1+sT)$

$G = 0.01$, $T = 1.0s$

Parameters of fuzzy logic controllers:

(a) DC current modulation controller

$K_e = 0.5$, $K_r = 0.04$, $K_u = 0.4$

(b) Generator 3 excitation modulation controller

$K_e = 0.35$, $K_r = 0.02$, $K_u = 0.5$

AN OVER-CURRENT INDICATOR

A. Ranaweera, D. Chandanandana, M. T. K. de Silva,
H. Y. A. Hewawasam, K. Indika
Department of Electrical Engineering, University of Moratuwa
M. Kalyanapala, Electroteks (Pte) Ltd.

AN OVER-CURRENT INDICATOR

A. Ranaweera, D. Chandanandana, M. T. K. de Silva,
H. Y. A. Hewawasam, K. Indika
Department of Electrical Engineering, University of Moratuwa
M. Kalyanapala, Electroteks (Pte) Ltd.

ABSTRACT

The over-current indicator indicates to the user that the current in a circuit is exceeding its rated value as soon as it occurs. The current is sensed by a current transformer (CT) and the rectified and regulated output of the CT is fed to a comparator for detecting over-current. The output of the comparator triggers the indicator circuit that lights up a light emitting diode (LED) when the over-current is detected. The device is designed for operation in 5 A or 10 A rated current circuits, as selected by a toggle switch. The paper describes the device, its principle of operation and the design procedure.

INTRODUCTION

The purpose of the over-current indicator is to immediately indicate to the user that the current flowing in a circuit is exceeding its rated value. The user can then take remedial action before the current increases further and circuit breakers operate due to the over-current to switch off the power supply to the circuit. Most widely used over-current protective device in both industrial and domestic sectors is the miniature circuit breaker (MCB). The tripping factors of MCBs vary from 1.5 to 2.0, which means that they allow a current of 1.5 to 2.0 times the rated value before operating to disconnect the circuit. In contrast, the over-current indicator acts as soon as the current exceeds the rated value and indicates to the user that the rated value has been exceeded. The user can take remedial actions such as not increasing the loads beyond that point or switching off of less important sub-circuits, in order to prevent sudden tripping-off of the entire circuit due to the over-current.

It is very important especially in industrial environments to maintain the processes uninterrupted to ensure the quality of products. Sudden shut-off of processes can also seriously affect the productivity of factories. Moreover, certain sensitive components of equipment may be damaged due to a slight over-current that is not sufficient to activate the MCBs. Thus, the use of the over-current indicator along with MCBs can further improve the reliability and protection of a distribution system.

This paper describes the over-current indicator, its principle of operation and the steps in the design procedure.

DESCRIPTION OF THE DEVICE

Figure 1 shows photographs of the exterior and interior of the constructed over-current indicator with the current transformer. The actual dimensions of the unit are 4 cm x 4 cm x 1 cm. The unit can be connected in series with the MCBs in a suitable location.

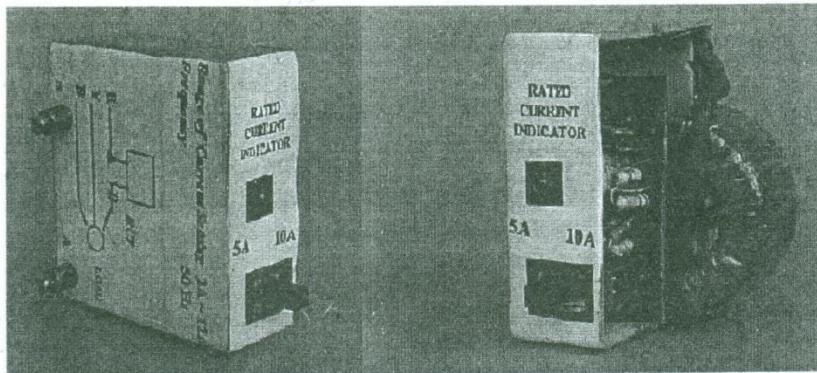


Figure 1. Exterior and interior views of the over-current indicator

PRINCIPLE OF OPERATION

Basic components of the over-current indicator are shown schematically in Figure 2. The current of the circuit is sensed by the use of a current transformer (CT). The output of the CT is rectified and regulated before being fed to the comparator for deciding whether the limit has been reached. When the current exceeds the rated value, the output of the comparator triggers the LED or the alarm to warn the user.

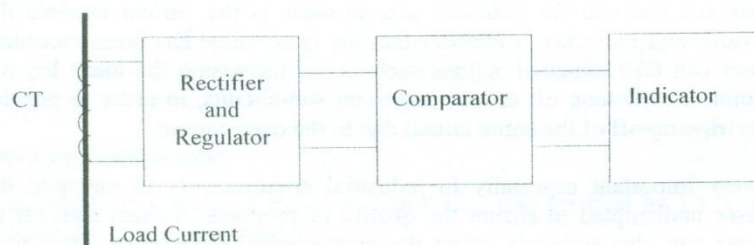


Figure 2. Basic components of the over-current indicator

The complete circuit diagram of the over-current indicator is shown in Figure 3. The rectified output voltage of the CT is smoothed by the capacitor C and regulated by the zener diode D . The reference voltage to the op-amp comparator V_{ref} is derived from this regulated voltage V_R . The other input to the comparator is a voltage proportional to the output voltage of the CT, which is proportional to the current in the CT primary. The device is designed to be used for two current ratings 5 A and 10 A, which can be manually selected using an on-off switch. As shown in the figure, when the switch is in the off position the lower arm resistance is only R_{41} . But when the switch is in the on position, the lower arm resistance is the parallel combination of the R_{41} and R_{42} . Thus the switch operation provides two resistor values for the lower arm

of the potential divider, thereby providing the necessary voltage to the comparator for the selected rated current.

The output of the op-amp is connected to the base of the pnp transistor. When the opamp output voltage V_o is high, the transistor is in the off state. Therefore, there is no current through the LED and there is no indication. When V_o is low, the transistor and in turn the LED are turned on.

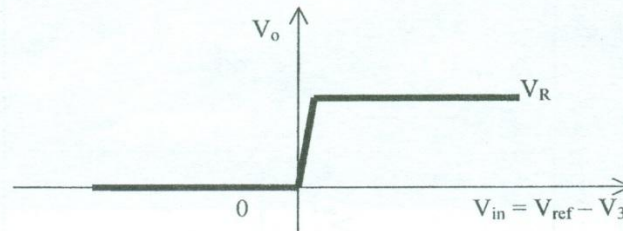


Figure 4. Variation of the comparator output V_o against the input V_{in}

The output of the op-amp comparator varies between its minimum and maximum voltage levels, zero and V_R depending on the voltage difference between its inputs, as shown in Figure 4. When V_3 is less than the reference voltage to the comparator V_{ref} , the comparator output remains at the regulator output voltage V_R . Hence the transistor remains switched off. When V_3 exceeds V_{ref} , the comparator output changes from V_R to zero, the minimum output voltage of the comparator. This turns the transistor on, allowing a current through the resistor R_c and the LED, to light up the LED and warn the user. An audible alarm used in place of the LED can further ensure the attention of the user on the detected over-current in the circuit.

DESIGN PROCEDURE

The V_Z of the zener diode D and hence the regulated voltage V_R is selected as 3 V.

The reference voltage of the comparator V_{ref} is selected as 1.5 V and therefore, we select

$$R_1 = R_2 = 4.7 \text{ k}\Omega \quad \text{for} \quad V_R = 3 \text{ V} \quad (1)$$

Transistor Inverter

The transistor selected is a low cost general purpose 2SC828. The transistor works as an inverter in its switching operation. When the transistor is switched on, it is in the saturation region and the voltage V_{CE} is nearly zero [1].

The rated I_C of the 2SC828 is 30 mA. But the rated current of the LED is 20 mA and a current of 10 mA is enough to light up the LED. In order to ensure transistor saturation, select the minimum β for the transistor which is 50.

Therefore,

$$I_{b,s} = \frac{I_{c(sat)}}{\beta} = \frac{10 \text{ mA}}{50} = 0.2 \text{ mA} \quad (2)$$

The opamp draws this current from the power supply to switch the transistor on when V_o is high.

The value of R_c can be calculated using the equation

$$V_s = R_c I_c + V_{LED} + V_{CE} \quad (3)$$

$$R_c = \frac{V_s - V_{LED} - V_{CE}}{I_c} = \frac{3.0 - 2.0 - 0.2}{10} = 80 \Omega$$

R_c can be 82 Ω or 100 Ω in order to provide an I_c of just below 10 mA.

Voltage Regulator

The ratings of the 3 V zener diode are 500 mW and minimum current of 5 mA. Therefore, the maximum and minimum values of the zener current are, $I_{Z,max} = 500/3 = 166.67 \text{ mA}$, and $I_{Z,min} = 5 \text{ mA}$.

The load current I_L of the zener voltage regulator is the sum of the currents in the transistor base and the collector, and the current taken by the potential divider R_1 and R_2 as shown in Figure 3. Thus

$$I_L = I_1 + I_b + I_c \quad (4)$$

Values of I_b and I_c vary depending on whether the transistor is switched on or off. If the transistor is in the off state, both I_b and I_c are equal to zero. Otherwise, $I_b = 0.2 \text{ mA}$ and $I_c = 10 \text{ mA}$. The constant value of $I_1 = V_R/(R_1 + R_2) = 3/(2 \times 4.7) = 0.3 \text{ mA}$. Therefore, the maximum and minimum values of I_L are

$$I_{L,max} = 10.5 \text{ mA} \quad (\text{Transistor ON}), \quad I_{L,min} = 0.3 \text{ mA} \quad (\text{Transistor OFF})$$

The input current to the regulator $I_R = I_Z + I_L$. The following inequalities must hold for the proper operation of the zener regulator:

$$I_{R,max} - I_{L,min} \leq I_{Z,max} \quad \text{and} \quad I_{R,min} - I_{L,max} \geq I_{Z,min} \quad (5)$$

Therefore, $I_{R,max} \leq 166.67 + 0.3 = 167 \text{ mA}$ and $I_{R,min} \geq 5 + 10.5 = 15.5 \text{ mA}$. Select $I_{R,max} = 100 \text{ mA}$ and $I_{R,min} = 20 \text{ mA}$.

Current Transformer

The maximum and minimum values of the average dc output voltage needed across the capacitor can be calculated as

$$V_{dc,max} = V_R + I_{R,max} R_S \text{ and } V_{dc,min} = V_R + I_{R,min} R_S \quad (6)$$

The resistance R_s is selected as 68Ω . Thus, $V_{dc,max} = 3.0 + 0.1 \times 68 = 9.8 \text{ V}$ and $V_{dc,min} = 3.0 + .02 \times 68 = 4.36 \text{ V}$.

Figure 5 shows the voltage across the smoothing capacitor connected across the full-wave diode bridge, which rectifies the output voltage of the current transformer. V_{2p} is the peak value of the CT secondary voltage. The frequency of the waveform is 100 Hz, twice the supply frequency. For the purpose of design calculations this waveform can be approximated to a saw-tooth waveform with zero charging time and constant discharging current indicated by a constant slope as shown in Figure 6 [2].

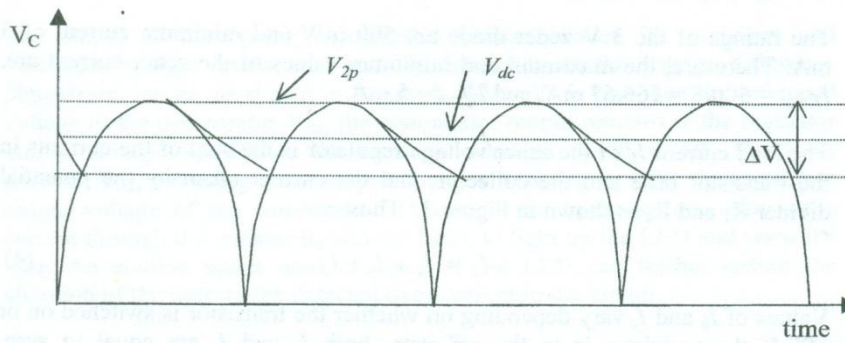


Figure 5. Voltage across the smoothing capacitor

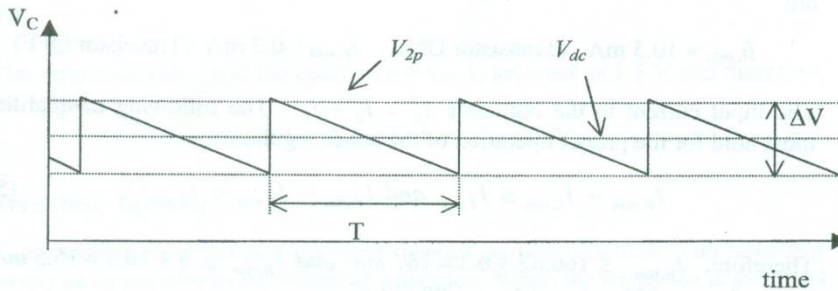


Figure 6. Approximated voltage waveform across the capacitor

It can be seen from Figure 6 that the average dc output voltage of the capacitor $V_{dc} = V_{2p} - \frac{\Delta V}{2}$ and the voltage variation $\Delta V = \frac{\Delta Q}{C} = \frac{I_R T}{C}$ that can be combined to obtain

$$V_{dc} = V_{2p} - \frac{I_R T}{2C} \quad (7)$$

where $T = 1/100 = 10$ ms and the capacitance C is selected as $470 \mu\text{F}$.

V_{2p} is determined by the primary current in the CT and is independent of I_R . Therefore, the maximum value of V_{dc} occurs when V_{2p} is maximum and I_R is minimum.

Thus,

$$V_{2p,\max} = V_{dc,\max} + \frac{I_{R,\min} T}{2C} = 9.8 + \frac{20 \times 10}{2 \times 470} = 10.0 \text{ V}$$

Similarly, minimum value of V_{dc} occur when V_{2p} is minimum and I_R is maximum and therefore,

$$V_{2p,\min} = V_{dc,\min} + \frac{I_{R,\max} T}{2C} = 4.36 + \frac{100 \times 10}{2 \times 470} = 5.42 \text{ V}$$

The core of the CT is made of Silicon Steel, which has the following maximum values of the flux density B and field strength H :

$$B_{\max} = 1.7 \text{ T}, \quad H_{\max} = 200 \text{ A/m}$$

Current flows in the secondary of the CT only during the charging of the capacitor, when the diodes in the CT secondary are forward biased. During other times, the secondary current is zero, and therefore, there is no secondary mmf to balance the primary mmf. Thus the entire primary mmf is used for the magnetization of the CT core. The maximum magnetic field strength occurs during this period when the maximum current flows in the primary [3]. Thus,

$$N_1 I_{1p,\max} = H_{\max} l \quad (8)$$

where, $I_{1p,\max}$ is the peak value of the maximum primary current and l is the mean length of the toroidal core of the CT as shown in Figure 7. N_1 is the number of primary turns of the CT which is 1.

The over-current indicator is to be designed for the rated currents of 5 A and 10 A. A maximum current of 12 A is assumed in the 10 A rated current circuit. Thus, the minimum mean length of the toroidal core can be calculated from equation (8) as

$$l = \frac{N_1 I_{1p,\max}}{H_{\max}} = \frac{1 \times 12 \sqrt{2}}{200} = 8.48 \text{ cm}$$

A toroidal core of mean length 9.5 cm was selected for the CT in order to ensure a magnetic field strength of less than H_{max} . The cross sectional area of the core is 1.68 cm^2 .

The peak induced voltage of the CT secondary can be expressed as [3]

$$V_{2p,max} = B_{max} N_2 A \omega \quad (9)$$

where A is the cross sectional area of the toroidal core of the CT as shown in Figure 7, N_2 is the number of secondary turns of the CT and $\omega = 2\pi f$ where f is the frequency of the supply voltage.

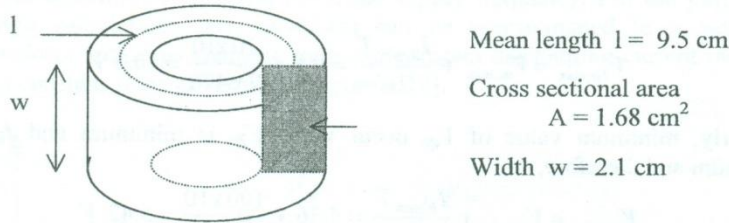


Figure 7. Dimensions of the toroidal core

The maximum number of turns of the CT secondary can now be calculated using equation (9) as

$$N_2 = \frac{V_{2p,max}}{B_{max} A \omega} = \frac{10.0}{1.7 \times 1.68 \times 10^{-4} \times 100\pi} = 112$$

Op-amp Comparator

The reference voltage of the comparator V_{ref} was selected as 1.5 V at the beginning of the design procedure.

The output of the comparator remains at V_R when V_3 is less than V_{ref} , but becomes zero when V_3 exceeds V_{ref} as shown in Figure 4. The LED lights up to indicate over-current when the comparator output is zero. Therefore, V_3 has to exceed V_{ref} when the current in the CT primary exceeds the rated current 5 A or 10 A. Let this value of V_3 be 1.6 V.

The lower arm resistance is R_{41} for rated current of 5 A, and is the parallel combination of R_{41} and R_{42} for 10 A. Therefore,

$$V_3 = \frac{R_{41}}{R_3 + R_{41}} V_{dc@5A} \quad \text{and} \quad V_3 = \frac{R_p}{R_3 + R_p} V_{dc@10A} \quad (10)$$

where R_p is the parallel combination of R_{41} and R_{42} .

The actual variation of V_{dc} with the primary load current of the CT is given in Figure 8.

It can be seen from Figure 8 that,

$$V_{dc @ 5A} = 4.8 \text{ V} \quad \text{and} \quad V_{dc @ 10A} = 10 \text{ V}$$

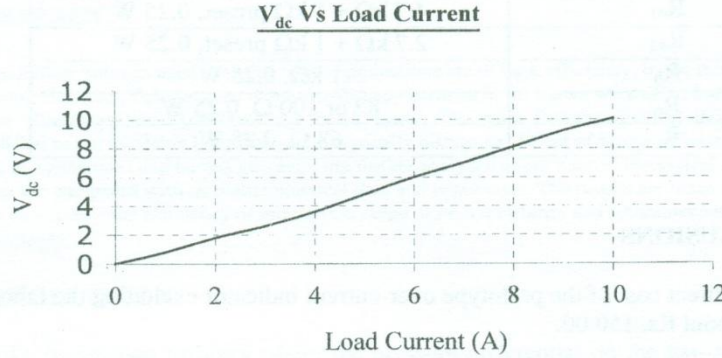


Figure 8. Variation of the Capacitor voltage V_{dc} with load current I_1

Select $R_3 = 10 \text{ k}\Omega$ and the above values can be used in equation (10) to calculate

$$R_{41} = \frac{V_3}{V_{dc \text{ at } 5A} - V_3} R_3 = \frac{1.6}{4.8 - 1.6} 10 = 5 \text{ k}\Omega$$

$$R_p = \frac{V_3}{V_{dc \text{ at } 10A} - V_3} R_3 = \frac{1.6}{10 - 1.6} 10 = 1.9 \text{ k}\Omega$$

where, R_p is the parallel combination of R_{41} and R_{42} .

Therefore $R_{42} = 5 \times 1.9 / (5 - 1.9) = 3 \text{ k}\Omega$. A $4.7 \text{ k}\Omega$ resistor with a $1 \text{ k}\Omega$ preset for fine tuning can be used for R_{41} whereas, a $2.7 \text{ k}\Omega$ resistor with a $1 \text{ k}\Omega$ preset can be used for R_{42} .

Short Circuit Protection

In the case of a direct short circuit of the primary load side of the current transformer, a large current may flow in the CT primary until the circuit breakers operate and disconnect the power supply. Assuming a current of 40 A under short circuit conditions for the 10 A rated circuit, the maximum CT secondary current would be $40/112 = 357 \text{ mA}$. The voltage that may build on the CT secondary could be between 30 to 40 V . A capacitor of rated voltage

Component Ratings

Component	Rating
Zener diode	3 V, 1.3 W
Capacitor C	470 μ F, 63 V
R ₁ , R ₂	4.7 k Ω , 0.25 W
R ₃	10 k Ω , 0.25 W
R ₄₁	4.7 k Ω + 1 k Ω preset, 0.25 W
R ₄₂	2.7 k Ω + 1 k Ω preset, 0.25 W
R _b	1 k Ω , 0.25 W
R _c	82 or 100 Ω , 0.25 W
R _s	68 Ω , 0.25 W

CONCLUSIONS

The net direct cost of the prototype over-current indicator excluding the labour cost is about Rs. 150.00.

The prototype was designed for rated currents of 5 A and 10 A. However, with the use of a variable resistor in place of the fixed value resistors in the potential divider, the selector switch can be eliminated and the device can be made to respond to any rated current within the designed range.

The device does not require any external power supplies and the dc power supply needed for the op-amp is obtained from the same CT output voltage which indicates the current level.

The over-current indicator would be very useful in various industrial and commercial applications where maintaining uninterrupted operation is important. Various other alarms can be incorporated instead of the LED with additional circuits for their operation as necessary.

REFERENCES

1. *Electronic Devices and Circuits*, Bogart T. F, Universal Book Stall, 1986.
2. *Power Electronics: Converters, Applications and Design*, Mohan N, Undeland T. M., Robbins W. P., John Wiley and Sons, 1989.
3. *Electromagnetic and Electromechanical Machines*, Matsch L. W., Morgan J. D., 3rd Edition, Harper & Row Publishers, 1986.
4. *IC Op-Amp Cookbook*, W. G. Jung, 3rd Edition, BPB Publishers, 1997.

AN ANALYSIS OF PELTON TURBINES AS RELATED TO MINI-MICRO HYDRO APPLICATIONS

Eng (Dr) M.A.R.V.Fernando, B.Sc, Ph.D., C.Eng., F.I.E.(SL)
Department of Mechanical Engineering, University of Moratuwa

AN ANALYSIS OF PELTON TURBINES AS RELATED TO MINI-MICRO HYDRO APPLICATIONS

Eng (Dr) M.A.R.V.Fernando, B.Sc., Ph.D., C.Eng., F.I.E.(SL)
Department of Mechanical Engineering, University of Moratuwa

ABSTRACT:

Large Pelton turbines used in major hydro applications are of high efficiency, in the range of 92% or more. However, Peltons used in mini-hydro applications in Sri Lanka were often found to be of lower efficiency, and of micro range much lower. The main factors affecting efficiency are identified as per available literature and analytically discussed. Effect of nozzle efficiency, bucket friction, speed ratio and bucket geometry are further analyzed as per a novel theoretical derivation. These are compared with available practical data and experience. The results are discussed with a view to improve the efficiency of mini/micro range of Pelton turbines and recommendations made accordingly.

INTRODUCTION:

Unlike in reaction turbines where the pressure differential on the two sides of a vane provides the driving force, the energy transfer in impulse turbines is by the impingement of a jet of water on a set of buckets or vanes in the turbine runner. Thus it is essential to convert the potential energy in a source to kinetic energy by passing it through a nozzle to form a jet. Peltons and Turgos are pure impulse turbines. The degree of "impulse" and "reaction" in a Banki (or cross flow) turbine is questionable though it is often categorized as impulse.

Large Pelton turbines used in major hydro applications are of very high efficiency in the range of 92% or more. However Peltons used in mini and micro applications are usually found to be of much lower efficiency with minis in the range of 80% and micros below 70%, with some (village levels) even less than 65%. Turgo wheels, which perhaps is a development of "GHATTA", the village water wheel with a long history and widely used in Nepal [1], seldom achieve efficiencies of more than 75%.

Peltons are widely used in mini and micro hydro applications owing to their ease of construction. Even with dimensionally similar bucket shapes, it was observed that the efficiency of smaller units was much less than that of their larger counterparts. When a jet is made to impinge even on a set of flat plates mounted on a rim an efficiency of 50% could be obtained. It may be interesting to note that even the crude device shown in figure 1, made at village level by mounting aluminium bowls on a rim has achieved an efficiency of 62%. Thus it is necessary to investigate the reasons for the observed low efficiencies of mini and micro Peltons. Accordingly, an analysis of the energy transfer in a Pelton bucket was carried out and compared with practical data available. Results analyzed and recommendations made for improvement of Mini and Micro Peltons.

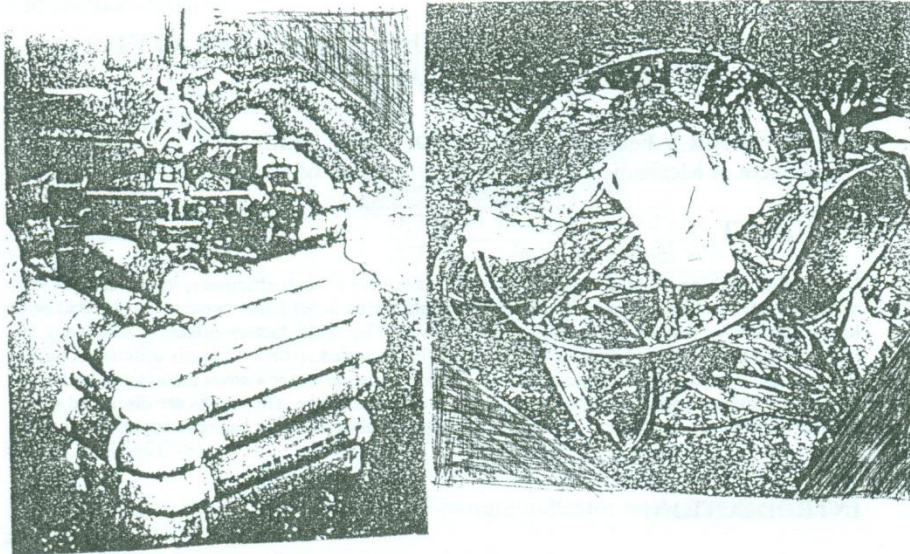


Fig 1: A CRUDE PELTON TURBINE SET UP

Analysis of impulse turbines are often over simplified and only a two dimensional flow is considered. Effect of friction in buckets is also often disregarded. Of the two pure impulse turbines, the efficiency of Turgo is less as the water jet entry is at an angle (inlet angle), while it is (supposed to be) tangential in Peltons. However the Turgo has the advantage of incorporating a larger jet as the jet is simultaneously impinging on several buckets. Attempts have been made to increase the discharge of Peltons by using multiple jets, which may be acceptable up to about 3 jets, provided other conditions are satisfactory. Beyond this the interference of exiting jets with other buckets may drastically reduce the efficiency. On the other hand Turgos can also be provided with multiple jets without such adverse effects.

Efficiency of a turbine unit is usually defined from the point of entry to the unit (standard method used by most of the manufacturers). That is the nozzle is included in the unit and the head condition based on the net head available after Penstock.

FACTORS AFFECTING TURBINE EFFICIENCY:

Factors affecting turbine efficiency can be broadly divided in to three categories, viz:

- 1 Pre runner i.e: nozzle efficiency.
- 2 Mechanical and windage losses
- 3 Energy absorbed by runner from jet.

Nozzle Efficiency:

There are varying claims about the efficiency of well-designed nozzles with spear (needle) valves. While Addison [2] gives it in the range of 98% to 99%, Nechleba [3] specifies it over a range of 95% to 98% with an average of around 97%. Addison seems to have specified data obtained from certain large hydro turbine manufacturers, while Nechleba, (an accepted authority on this subject) specifies a more realistic figure as per practical experience. Thus it can be considered that a well-designed and properly manufactured Nozzle can have an efficiency of more than 95% and usually around 97%. However in certain mini, and many micro hydro applications, (particularly as advocated for intermediate technology manufacture [4]), simple nozzle shapes are being used. Kishioka [5] says that the nozzle efficiency is not appreciably affected by the shape as long as the straight portion after the usual bend, to accommodate valve spindle, is sufficiently long. Contrary to this claim investigations carried out by Fernando [6] indicates a considerable variation of nozzle efficiency depending on its shape and also fabrication and surface conditions. Nozzle shapes often advocated in [4] were found to be of rather low efficiency and seldom achieve 92%. However, as shown by Fernando [6], these can be much improved by proper manufacture with improved surface conditions. Further there is no appreciable difference in efficiency with the shape of the nozzle for elliptical or extended elliptical sections. (see fig 2).

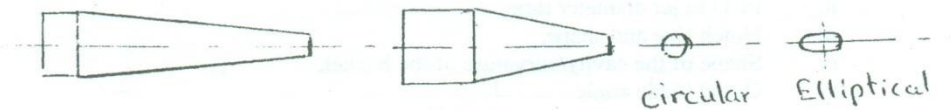


Fig 2: NOZZLE SHAPES

Mechanical and Windage Losses:

Mechanical losses are mainly in bearings and drives. In this regard direct coupling has a definite advantage over speed variators, often belt drives, provided the other parameters are the same. Runners mounted on generator shaft, often found in micro applications are the best to reduce mechanical losses, but the compromise thus carried out with optimum speed may some times be disadvantageous.

Windage losses depend mainly on the clearance between the casing and the runner, and surface conditions of the back of the buckets. Sierro [7] specifies a minimum gap, from casing to bucket, of 15 times the bucket width. Other literature [5] too agrees with this.

Another factor affecting efficiency is the interference of exiting water with other buckets some times acting even as reverse jets in extreme cases. Outlet angle of the bucket, number of jets, jet diameter to bucket width ratio, pitch circle diameter to jet diameter ratio are some other factors affecting this.

Energy Absorbed by Runner from Jet:

This is the most important part in turbine design. The ideal is to absorb 100% of the energy available in the jet by runner. However in practice only a part is absorbed by the runner, with a part lost as kinetic energy of the exiting water, and another part lost due to friction in the bucket. Some times interference of exiting jets, particularly with multi jet machines, and when exit angle is very small, may lead to further drop of power at turbine shaft [8].

Many a literature (eg:[2], [7]), repeat what Nechleba [3] has said regarding bucket geometry and construction. In analysis of Pelton buckets it is normally considered as a simple 2-D case, and that the inlet blade angle is zero with the jet entering the bucket tangentially. How accurate these assumptions are, is questionable. Kishioke [5] and Bachman [8] has analyzed these effects.

In a Pelton turbine the main factors within the control of a designer / manufacturer are;

- a). Blade geometry. This includes;
 - i. bucket width to jet diameter ratio,
 - ii. PCD to jet diameter ratio,
 - iii. Notch size and shape,
 - iv. Shape of the cavity/curvature of the bucket,
 - v. Outlet blade angle.
- b). Friction condition of the bucket surface,
- c). Ratio of jet velocity to peripheral speed (at PCD) of runner.

Factors "a. i to iv" above, had been analyzed in great detail by Nechleba [3] and thus is not intended to repeat here. However, the available literature (to the authors knowledge) does not properly explain the abnormally low efficiency often observed in mini/micro Peltons. {Certain manufacturers of mini range Peltons, eg [9], claim relatively higher efficiencies compared to what is often observed. However, how they achieved such, if their claims are true, is not very clear}.

Accordingly,

1. the friction conditions of bucket, 2. speed ratio, and 3. outlet blade angle, are investigated here in detail with a view to find the reasons for the said drop of efficiency in mini/micro Peltons.

FLOW ANALYSIS:

Let the:

Velocity of JET of water relative to EARTH be V_i (at inlet), V_o (at outlet)
 Velocity of JET of water relative to BUCKET W_i (at inlet), W_o (at outlet)
 Velocity of BUCKET, relative to EARTH U_i (at inlet), U_o (at outlet)
 α_i and α_o are the inlet and outlet Jet angles with the tangent at point of entry
 β_i and β_o are the inlet and blade angles respectively.

Energy of the incoming jet of water $= M.V_i^2/2$, and
 Energy of the exiting jet of water $= M.V_o^2/2$,

Let W_i at entry to blade (bucket) is reduced to W_o due to friction between Bucket and Water jet, and is given by $W_o = f.W_i$, where " f " (<1) is the "Friction factor".

In the case of Pelton turbines it is assumed that the water enters and leaves at the same PCD (this is not strictly correct) and therefore $U_i = U_o =$ (say) $c.V_i$, where " c " is the Speed ratio, ie. Bucket speed / Jet speed.

Consider the most general case of above system with Inlet and Outlet Velocity Triangles combined (as shown in fig: 3).

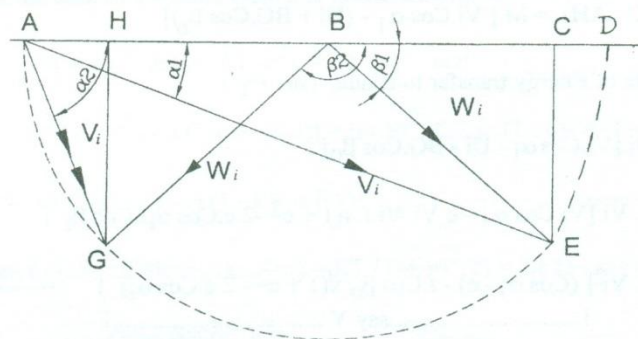


Fig. 3 - VELOCITY TRIANGLES (Inlet & Outlet)

Now, $AE = AD = V_i$, $AB = U_i = U_o = c.V_i = c.AE = c.AD$, $BE = W_i = BF$,
 $BG = W_o = f.W_i = f.BF$

At inlet, $AC = V_i \cos \alpha_i$, $CE = V_i \sin \alpha_i$,
 $BC = AC - AB = V_i \cos \alpha_i - U_i = V_i \cos \alpha_i - c \cdot V_i = V_i (\cos \alpha_i - c)$,

$$\begin{aligned} W_i = BE &= \sqrt{BC^2 + CE^2} = \sqrt{V_i^2 \cos^2 \alpha_i - 2V_i^2 \cos \alpha_i \cdot c + V_i^2 c^2 + V_i^2 \sin^2 \alpha_i} \\ &= V_i \sqrt{1 + c^2 - 2c \cos \alpha_i} = V_i \cdot S = BF \quad \text{-----} \quad \text{-----} \quad (1) \\ &\quad \text{!.....S.....!} \end{aligned}$$

$$W_o = BG = BF \cdot f = V_i \cdot f \cdot \sqrt{1 + c^2 - 2c \cos \alpha_i} = f \cdot V_i \cdot S \quad \text{-----} \quad (2)$$

$$HG = BG \sin (180 - \beta_o) = BG \sin \beta_o$$

$$HB = BG \cos (180 - \beta_o) = -BG \cos \beta_o$$

$$V_o \cos \alpha_o = AH = U_i - HB = U_i + BG \cos \beta_o$$

$$\begin{aligned} V_o &= AG = \sqrt{AH^2 + HG^2} = \sqrt{BG^2 \sin^2 \beta_o + BG^2 \cos^2 \beta_o + 2U_i \cdot BG \cos \beta_o + U_i^2} \\ &= \sqrt{BG^2 + 2U_i \cdot BG \cos \beta_o + U_i^2} \end{aligned}$$

Change of Momentum in direction of U is: (where M is the mass flow rate),

$$= M \cdot (AC - AH) = M \cdot [V_i \cos \alpha_i - (U_i + BG \cos \beta_o)]$$

Therefore, rate of Energy transfer to Blade, (say E_T)

$$\begin{aligned} E_T &= M \cdot U_i \cdot [V_i \cos \alpha_i - U_i - BG \cos \beta_o] \\ &= M \cdot c \cdot V_i \cdot [V_i \cos \alpha_i - c \cdot V_i - V_i \cdot f \cdot \sqrt{1 + c^2 - 2c \cos \alpha_i} \cdot \cos \beta_i] \\ &= M \cdot c \cdot V_i^2 [(\cos \alpha_i - c) - f \cos \beta_o \cdot \sqrt{1 + c^2 - 2c \cos \alpha_i}] \quad \text{-----} \quad (3) \\ &\quad \text{!..... say Y!} \end{aligned}$$

As the energy of the initial jet is $(M \cdot V_i^2)/2$, the efficiency is given by;

$$\eta = (M \cdot c \cdot V_i^2 \cdot Y) / (M \cdot V_i^2 / 2) = 2 \cdot c \cdot Y \quad \text{-----} \quad \text{-----} \quad (4)$$

Energy lost with "out let water" (exiting jet), say E_L

$$\begin{aligned}
EL &= (M.V_o^2)/2 = (M/2).AG^2 = (M/2).[BG^2 + 2.U_i.BG.\cos \beta_o + U_i^2] \\
&= (M/2) [V_i^2.f^2.(1 + c^2 - 2c.\cos \alpha_i) + c^2.V_i^2 + 2.V_i.c.\cos \beta_o.V_i.f.S] \\
&= (M.V_i^2/2).[f^2.S^2 + c^2 + 2.c.f.S.\cos \beta_o] \quad \text{-----} \quad \text{-----} (5)
\end{aligned}$$

Energy Lost due to Bucket Friction (say EF)

$$\begin{aligned}
EF &= (M/2).[W_i^2 - W_o^2] = (M/2).[W_i^2.(1 - f^2)], \\
&= (M/2).[V_i^2.S^2.(1 - f^2)] = (M.V_i^2/2).S^2.(1 - f^2) \quad \text{-----} \quad \text{-----} (6)
\end{aligned}$$

Now, ET + EL + EF =

$$\begin{aligned}
&= (M.V_i^2/2).2.(c.\cos \alpha_i - c^2 - c.f.S.\cos \beta_o) + (M.V_i^2/2).(f^2.S^2 + c^2 \\
&+ 2.c.f.S.\cos \beta_o) + (M.V_i^2/2).S^2.(1 - f^2) \\
&= (M.V_i^2/2).[2.c.\cos \alpha_i - c^2 + S^2] = (M.V_i^2/2).1 = \text{Input Energy}
\end{aligned}$$

Therefore Energy equation balances

Factors that can be varied (at the discretion of designer) are α_i , β_i , β_o , c , & f

Consider the case of a Pelton. Here it is presumed that $\alpha_i = 0 = \beta_i$

Then, $S = \sqrt{1 + c^2 - 2c} = \sqrt{1 - c^2} = (1 - c)$ and

$$\begin{aligned}
ET &= M.V_i^2.[c - c^2 - c.f.\cos \beta_o (1 - c)] = (m.V_i^2/2).2.[c.(1 - c) - c.(1 - c).f.\cos \beta_o] \\
&= (M.V_i^2/2).2.c.(1 - c).(1 - f.\cos \beta_o) \quad \text{-----} \quad \text{-----} (7)
\end{aligned}$$

Therefore turbine efficiency (say η_T) = $ET / (M.V_i^2/2) = 2.c.(1 - c).(1 - f.\cos \beta_o)$

$$\eta_T = 2.(1 - f.\cos \beta_o).(c - c^2) \quad \text{-----} \quad \text{-----} (8)$$

$d\eta_T / dc = 2.(1 - f.\cos \beta_o).(1 - 2c)$, Thus η_T is maximum when $c = 1/2$, or $\cos \beta_o = 1/f$, but as $f < 1$, $\cos \beta_o \neq 1/f$

Therefore Turbine efficiency is maximum when $c = 1/2$, (for what ever the friction condition or the out let blade angle)

VARIATION OF TURBINE EFFICIENCY WITH SPEED RATIO

Now $V_i = k \cdot \sqrt{2gH}$, where k is the Nozzle coefficient.
For large turbines " k " usually lies between 0.95 to 0.99 [3]

Therefore, $U_i = U_o = V_i/2 = 0.5 \times 0.95 \sqrt{2gH}$ to $0.5 \times 0.99 \sqrt{2gH}$
 $= (0.475 \text{ to } 0.499) \sqrt{2gH}$,

In mini hydros U_i is often set to about $0.45 \sqrt{2gH}$ (which condition is suitable only when " k " = 0.9, ie; nozzles of very low efficiency).

Consider equation 8, when " c " = $1/2$,

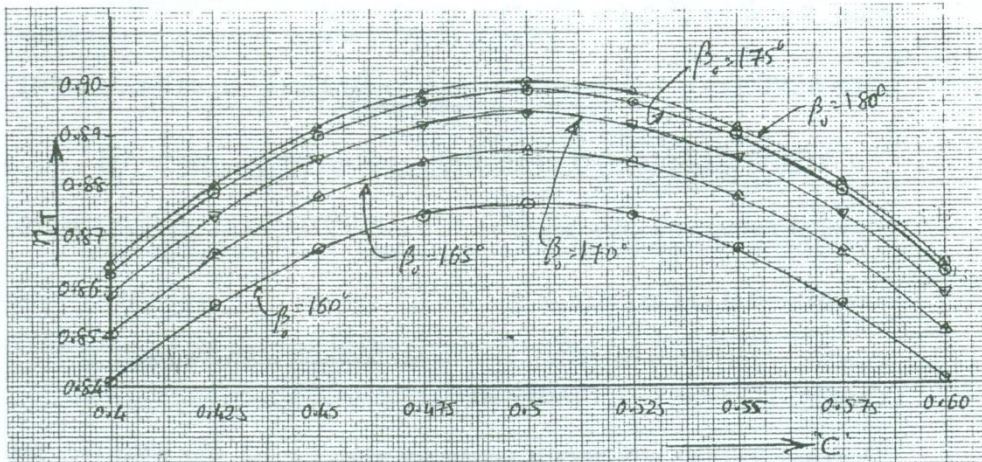
$$\eta_T = 2 \cdot (1 - f \cdot \cos \beta_o) \cdot (1/2 - 1/4) = 2 \cdot (1/4) \cdot (1 - f \cdot \cos \beta_o) = 0.5 \cdot (1 - f \cdot \cos \beta_o)$$

This is maximum when " f " = 1, and " β_o " = 180° , which is the ideal condition and the Turbine efficiency η_T will be then be $= 0.5 \times (1 + 1) = 1$

In practice β_o is often kept around 170° to 160° to prevent out let water splashing and interfering with the subsequent buckets. For mini peltons " f " is in the range of 0.8

VARIATION OF TURBINE EFFICIENCY WITH NOZZLE FACTOR

The variation of " η_T " with " c ", for $\beta_o = 160^\circ, 165^\circ, 170^\circ, 175^\circ$ & 180° , and " f " = 0.8 is shown in the graph 1

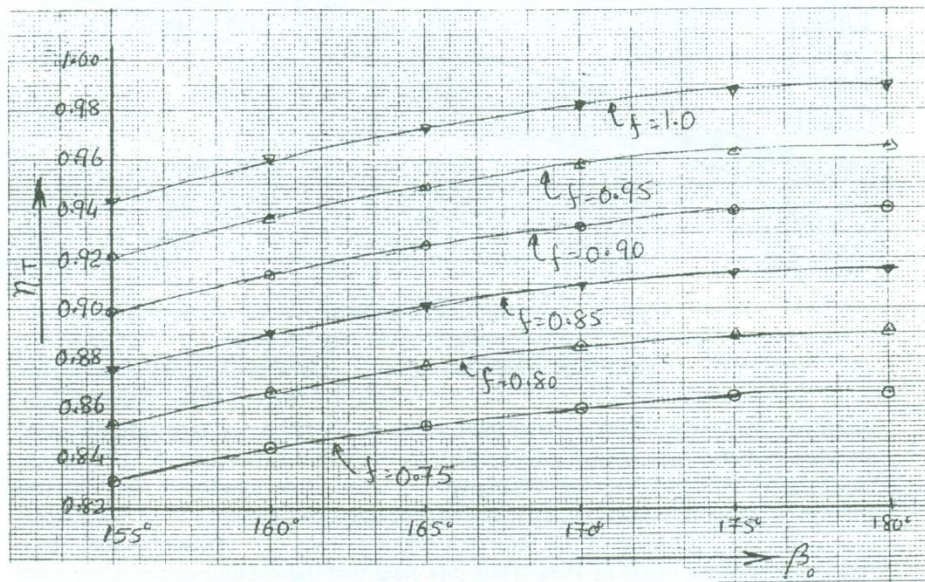


GRAPH 1: " η_T " Vs " C "

From the above it is clear that " c " = 0.5 is the best condition for what ever the friction or outlet angle conditions. However, loss of efficiency for " c " up to 0.475 (or 0.525) is not very significant (only a loss of 0.2%). Speed ratios " c " up to 0.45 (or 0.55) may be tolerated (with a drop of efficiency of 0.8%), but beyond these are not recommended unless due to very special reasons.

VARIATION OF TURBINE EFFICIENCY WITH BLADE OUT LET ANGLE

Variation of " η_T " with " β_0 ", for " f " = 0.75, 0.8, 0.85, 0.9, 0.95 and 1, with " c " = 0.45 is given in the graph 2

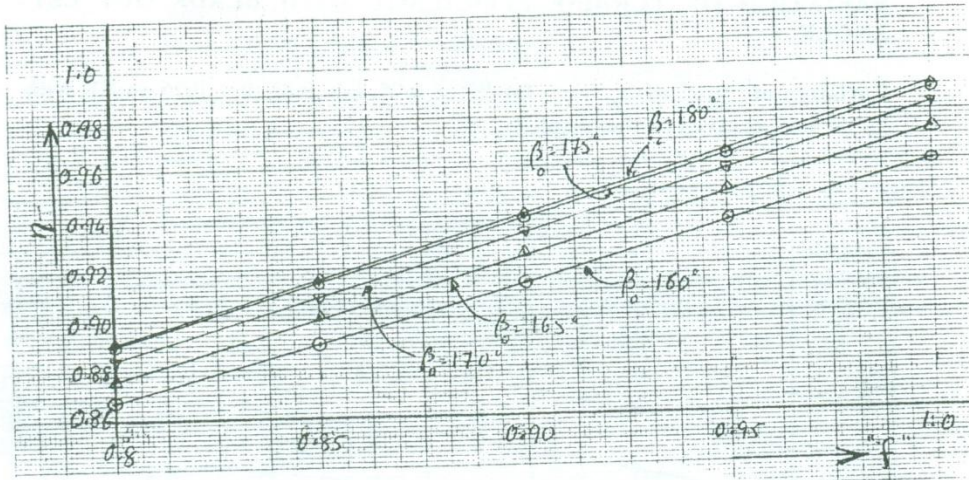


GRAPH 2: " η_T " Vs " $\cos \beta_0$ "

Though $\beta_0 = 180^\circ$ (the ideal) is the best, it cannot be practically achieved. From the graph it is clear that the drop of efficiency for variation of β_0 up to about 175° is not significant (only about 0.2%), but at 170° efficiency drops by about 0.6% to 0.7%. At $\beta_0 = 165^\circ$ drop in efficiency is considerable, 1.3% to 1.6%, and at $\beta_0 = 155^\circ$ rather high (2.3% to 3.0%). It must be remembered that this is the actual exit angle which may be lower than the geometric outlet angle of the blade due to spreading and 3-D effect of the flow.

VARIATION OF TURBINE EFFICIENCY WITH FRICTION FACTOR

Variation of " η_T " with " β_0 " for " c " = 0.45, and " β_0 " = 160° , 165° , 170° , 175° & 180° is given in graph 3



GRAPH 3: " η_T " Vs " f "

From the graph it can be seen that the friction factor " f " is the most important of all above. Efficiency drops almost linearly with reduction of " f ", practically independent of other factors. Changing " f " from ideal condition of "1" (no friction) to about 0.9 drops the efficiency by about 05%, and at " f " = 0.8, which is very common with most of the mini and micro peltons, the efficiency drop from this alone is in the range of 10%. Thus it is clear that the friction factor is the most significant, and accordingly every endeavour must be made to improve this. This can easily be practically achieved, by being aware of this and accordingly taking necessary precautions during selection of materials and manufacture.

MAJOR HYDRO PELTONS

Practical case for **major hydro** as given by Nechleba [3],
 $k = 0.97$ (average), $f = 0.88$ (safely attainable), $\beta_0 = 170^\circ$

for $U_i = 0.5\sqrt{2g.H}$ and $k = 0.97$, " c " = 0.464,

$$\begin{aligned}\text{Then } \eta_T &= 2 \cdot (1 - f \cdot \cos B_o) \cdot (c - c_2) = 2 \times (1 + 0.88 \times .9848) \times (0.464 - 0.215296) \\ &= 0.92846\end{aligned}$$

Thus an efficiency of 92% to 93 % can be expected with major Peltons, and agrees with practice.

CASE OF MINI HYDRO

Now let us consider a typical mini hydro pelton [10].

$$k < \text{or} = 0.92, \quad f < \text{or} = 0.8, \quad c = 0.45, \quad B_o = 160^\circ \text{ (effective)}$$

$$\text{Then Turbine Efficiency } \eta_T = 2 \times (1 + 0.8 \times 0.937) (0.45 - 0.2025) \times 0.92 = 0.7968$$

This shows that the efficiency that can be expected from a typical mini hydro is in the range of 80% only. This agrees well with practically observed values [10]

This analysis can shed some light on the reasons for the often observed low efficiency of Mini - Micro Peltons, and the factors that should be given due attention to improve the efficiency. Now let us consider some of the most important factors in more detail.

NOZZLE EFFICIENCY;

The nozzle converts the potential energy of the water source to kinetic energy as a jet of water. **Any loss at this stage cannot be recovered** and therefore every effort must be made to achieve maximum efficiency of nozzle. Experience show that turbines with properly designed nozzles with spear (needle) valves are of much higher efficiency than those which incorporate simple taper shaped nozzles. In addition to shape, the smoothness of the inner surface of the nozzle (and the surface of spear valve) is also very important. Fernando describes [6] experimental investigations carried out with;

- a). a well designed Nozzle and Spear valve of a unit in actual operation for more than six years,
- b) Tapered Nozzles made of
 - i, Fibre Glass and Resin with and without a coat of Liquid Ceramic (Devcon),
 - ii. Mild Steel with surface a). "as machined", b). manually ground and cleaned, and
 - c). "Nickel Plated",
 - iii With a Stainless Steel inner surface.

It is stated that the Nozzle with a spear valve as it is after six years of service was still giving an efficiency ("k" value) of 92%, and once the inner surface of the nozzle and the spear valve surface were cleaned, the efficiency improved to about

95%. If properly rehabilitated it could have been possible to achieve better efficiency. Claims of **efficiencies in the range of 98% to 99%** with stainless steel nozzle with spear valve properly ground and polished, as made by certain manufacturers [9] may accordingly be correct. Further, "k" value does not vary appreciably with jet diameter (needle opening),

Simple **tapered nozzles are of much lower efficiency** than would have been anticipated and often claimed .

Fibre Glass / Resin units which have a reasonably good surface finish are said to be marginally better than Mild Steel nozzle manually ground and cleaned. This may be representing the condition of most of the units of this type in use.

Efficiency of the Mild Steel nozzle with "as machined" surface has been observed to be really poor. **This may be depicting the condition of many Micro hydro installations made according intermediate technology and /or for village level applications.**

Nickel plating has drastically improved the efficiency (93%) bringing it close to properly designed nozzles. **Application of a Ceramic Coat too has increased the efficiency to high levels (92%),** just slightly below that of Nickel plated unit.

These confirm the importance of properly designed contour as well as the smoothness of the wetted surface of the nozzle. This further shows the importance of regular and proper maintenance to keep the wetted surface of the nozzle in best possible condition.

BUCKET FRICTION

This is perhaps one of the most neglected, or rather un-investigated aspects in Mini-Micro hydro applications. Large Peltons, used in major hydros are invariably model tested after the design. Strictly speaking the surface roughness too must be dimensionally proportioned in a model testing. In specific speed considerations and model analysis it is assumed that the hydraulic losses are in exact proportion to the square of velocity when the same Reynolds number of flow is encountered [3]. Thus roughness of the blade too must be increased or decreased according to the same proportions as the diameters for model testing. Pelton units made for major hydro applications are invariably hand buffed to ensure the best possible smoothness in the wetted surface of the buckets. During model testing this cannot be dimensionally ratioed, for a finer surface, but has to be satisfied with the same surface finish as the proto type at best. Thus the actual friction loss in the proto-type will be less than that derived from the model test. It is the reverse in cases of mini and micro peltons when the designs are based on dimensional ratios as per tested models or larger machines.

Nechleba [3] says that the actual force on bucket by jet reduces when the jet is turned more than 90° relative to the bucket. This seems to have been deduced by the fact that the loss of momentum, and thus the resulting force is with a positive component in the direction of bucket movement till the jet is turned by 90° , and only after it has turned more than 90° that the component of force becomes negative. However Nechleba's statement is a little mis-leading as the energy loss due to bucket friction is lost energy, whatever the angle of turn, and cannot be recovered.

Experimental investigations carried out by Fernando [6] has shown that the friction factor "f" of buckets, of pelton turbine of mini hydro range, cast out of Brass and hand finished by "pin mounted grinding balls" are less than 0.8, and can be as low as 0.75 if surface finishing is not very good. Fibre Glass / Resin buckets are also of the same range, but was improved to about 0.85 to 0.88 with application of a liquid ceramic coating.

From graph 3 it can be seen that the friction condition of the wetted surface of a bucket is a very important factor affecting the over all efficiency. **Dropping the friction factor "k" to 0.9 will reduce the efficiency by almost 05%, while 10% of efficiency will be sacrificed by allowing it to be dropped to 0.8 range**, which is not uncommon in so called low cost designs.

Finely finished and nickel plated Brass buckets of proper geometry has yielded friction factors "k" as high as 0.94. These show that proper and very smooth finish of the wetted surface of bucket is of paramount importance to achieve high efficiencies.

GEOMETRY OF THE BUCKET

Outlet Angle of Bucket:

The lower the out let angle better the efficiency of a pelton bucket. But this will lead to interference of the exiting jet with other buckets. So a compromise has to be achieved. From the graph of Efficiency Vs outlet angle it is clear that the decrease in efficiency is not very appreciable for an outlet angle of about 175° , and can be tolerated even up to about 170° (with a loss of efficiency of about 0.6% to 0.7% only). In practice it has been observed that the jet does not follow the exact contour (angle) of the bucket due to reduction of thickness of jet, due to spread, close to out let and also due to the 3-D nature of outlet. That is the actual outlet angle of the jet is less than the geometrical out let of the bucket. Thus it is important to keep a proper allowance for this in the bucket geometry when the bucket is designed and constructed. An extended portion, or a lip, of a few mm in the bucket outlet to act as a calibration zone to guide outlet water along bucket contour may thus be advantageous. In certain major hydro peltons the outlet angle is said to be as low as 4° .

3-D Flow in Bucket

Another important factor to be considered is the "Pebbling" effect or spread of fine water bubbles interfering with the buckets that follow. This was well analyzed by Bachman [8]. Though 2-D flow is usually assumed for ease of analysis in pelton buckets it really is a 3-D process. Further at the point of first contact of the water jet with bucket, only a part is entering the bucket tangentially and the others at a reasonable angle. Further leading angle of about 18 to 20 degrees of the bucket at commencement of entry, and lagging at exit too causes rather complicated flow patterns. Bachman [8], Nechleba [3] and Kishioka [5] have made reasonable analyses of these aspects. However these need further experimental investigations.

SPEED RATIO

From the above analysis it is clear that the best efficiency is when the speed ratio "c" is 0.5. ie; $U = 0.5 V_i$. However the known data for a hydraulic site usually is the net head. In major Peltons the Nozzle factor "k" is evaluated exactly and the exact "c" could then be arrived at. But in Mini hydro, and particularly in Micro hydro pelton designs, "k" is not known, or calculated, precisely. Vague values obtained from unreliable data books and normograms are often used by unskilled designers and $U_i = 0.45\sqrt{(2gH)}$, which is not correct, is often used as a standard value irrespective of nozzle conditions.

From graph 1 it can be seen that the **best speed ratio is 0.5**. However speed ratios up to about 0.475 (or 0.525) do not cause a significant loss in efficiency (only about 0.2%), and up to about **"c" = 0.45 (or 0.55) may be tolerated** with a loss efficiency of only about 0.8%. In certain instances in order to direct couple to the generator, thereby avoiding the loss in transmission (speed variation), may be possible with further deviation for "c" value. In such cases, it must be individually and properly analyzed and efficiency loss Vs gain be compared before taking a decision. Thus it can be seen that **speed factor is one of the factors contributing to the often observed low efficiency of Mini and Micro Peltons particularly with the so called peltric types.**

PCD TO JET DIAMETER RATIO

Nechleba [3] Strongly recommends a PCD to Jet diameter ratio of 11 or above, and in any case not less than 9. Addison [2] recommends it to be 11 to 15. However, certain micro peltons, particularly the so called "Peltric" sets are designed for very low ratios in the range of 7 and even up to 6 in extreme cases. This is often done to achieve the required speed of runner to connect it direct to the generator, or sometimes to mount the runner directly on the generator shaft, when the head is limited. This arrangement, though it has the advantage of avoiding losses at a drive, seems to lead to a higher loss due to interference of the exiting jets and splashing with the subsequent buckets and also often to restricted

and thus poor bucket geometry (shape). Attempting multi jets with such low ratios may lead to serious loss in efficiency.

Thus it is recommended to retain a PCD to Jet diameter of 11 or more, where ever possible.

CONCLUSIONS

From the above analysis it is clear that several very important factors are often disregarded in Mini/micro Pelton Design and Construction. **With correction of these factors it should be possible to improve the efficiency of such turbines appreciably**, at least close to those values observed with major peltons. Some of the main factors that should be given due consideration are given below.

1. Nozzle

- a. Use properly designed nozzles and a spear valves,
- b. Ensure the wetted surfaces of nozzles and valves are given the best possible surface finish,
- c. If possible use Stainless steel for the nozzles and spear valves. Grind and Polish the wetted surfaces,
- d. For non-stainless steel materials, Chrome or Nickel plating can be recommended,
- e. A Ceramic Coat on wetted surface is also advantageous
- f. Make sure the nozzle and spear valves are maintained well by cleaning and polishing regularly.
- g. Simple tapered nozzles are not recommended

2. Buckets

- a. Ensure the wetted surfaces of the Buckets are given the best possible surface finish,
- b. If possible use stainless steel. Grind and Polish the wetted surfaces
- c. For non-stainless steel materials, Chrome or Nickel plating can be recommended,
- d. For relatively low cost applications a Ceramic Coating on the wetted surface is recommended,

Further investigations are necessary to arrive at best bucket geometry. However, an equalizing lip at the edge of the bucket can be considered as a good practice.

3. Speed Ratio

- a. Peripheral bucket speed (at the PCD) of half the jet speed is the best

- b. When ever possible try to adhere to this condition. However if a speed variator could be avoided by slight deviation from above, such may be permissible after complete evaluation of loss of efficiency due to this compared with the gain by avoiding a drive.

4. PCD to Jet Diameter Ratio

- a. It is strongly recommended to retain a PCD to Jet Diameter ratio of 11 or more. A lower ratio may be used in extreme circumstances, but with proper investigation of its effects.

REFERENCES:

- [1] Kathmandu Metal Industries - 1995, SIBAIT -Phillipines
- [2] ADDISON.H, - "A Treatise on Applied Hydraulics", Chapman & Hall Ltd.,
- [3] NECHLEBA. Miroslav, - "HYDRAULIC TURBINES - Their Design & Equipment", - 1957, ARTIA, PRAHA
- [4] HARVEY. A, et al. "Micro Hydro Design Manual", - 1993, ITP
- [5] KISHIOKA.E, & OSAWA.K, - "Investigation in to the problem of losses of the Pelton Wheels", The 2nd International J S M E Symposium, Fluidmachinery and Fluidics - Tokya, 1972
- [6] FERNANDO.M.A.R.V, -"Experimental Investigations of Effect of Geometry and Friction Conditions of Nozzles and Buckets on Pelton Turbine Efficiency" - Yet Unpublished,
- [7] de SIERVO.F, and LUGARESINT, - "Modern Trends in Selecting and Designing Pelton Turbines", Water Power & Dam Construction, December 1978,
- [8] BACHMAN.P, et al. - "Experimental Flow Studies on a 1 jet Model Pelton Turbine", 1991, Symposium in Belgrade,
- [9] DAN, N, - Trade Literature of Canyon Industries Inc, Deming , USA
- [10] FERNANDO.M.A.R.V, - " Rehabilitation of Small Hydro Plants in Sri Lanka" Small Hydro Power & Fluid Machinery in 1982, American Society of Mechanical Engineers.

Recommended General References;

- ROGER.E.A.Arndt, - "Fundamentals of Hydraulic Turbine Design", Small Hydro Ppower for Asian Rural development, 1981, AIT, Bangkok,
- "Micro Pelton Turbines", - MHPG Series Vol 9, 1993, SKAT

KNOWLEDGE BASED SOFTWARE FOR LOADING AND STABILITY OF SHIPS

W.K. Wimal Siri

Department of Mechanical Engineering, University of Moratuwa.

KNOWLEDGE BASED SOFTWARE FOR LOADING AND STABILITY OF SHIPS

W.K. Wimalasiri

Department of Mechanical Engineering, University of Moratuwa.

ABSTRACT

Loading and Stability calculations of ships became a more and more complicated and time consuming process as the ship sizes and design complexity increased. Accurate and efficient methods of evaluating and analysing stability of ships for a given loading condition became very important as the safety become equally comparable with efficiency of operation. These requirements lead to introduction of dedicated computer systems onboard ships for loading and stability monitoring in the past. At present Ports-State Control requires details of loading and stability of the ship as it arrives to a particular port. With the development of the personal computer and windows environment, it is now possible to demonstrate actual loading and stability not only on onboard computer, but also at the shore based offices of the shipping agencies that do cargo planning. Any loading condition can be studied together with required stability prior to actual loading taking place. Alterations of loading can be suggested to optimize any loading condition. Although there are specialized producers of such software to the global shipping industries, this paper presents development of such software for a local ship owner.

INTRODUCTION

Complexity of "Loading and Stability" software depends upon the ship size and configuration, specially when the ship has more tanks and compartments with integrated cargo loading. Loading sequence should satisfy the strength requirements (limits of shear forces and bending moments) and stability of the ship at harbour condition and sea-going condition. Manual calculation and assessing of strength and stability becomes a cumbersome process if the ship is to be loaded with hundreds of containers. It is impossible to perform same calculation manually for alternative loading arrangements. In practice, experiences of a few loading conditions and stability calculations and their results are used to make judgement on any other situation with a level of uncertainty. The risk involved with such approximation and judgement may depend upon the type of ship and the loaded draft. However, when an onboard computer is available to study all possible and practical options of loading, cargo spaces can be utilized to an optimum level without risk and uncertainty. This paper presents development of such software on windows environment using Visual Basic as the programming language.

DATABASE NEEDED FOR THE DEVELOPMENT

General Arrangement of the Ship

The General Arrangement and subdivisions of the vessel into different tanks and cargo holds are required. This information is used to obtain tank and cargo hold locations, capacities, their vertical and longitudinal centers of gravity and free surfaces as the capacity varies from zero to maximum. Container profile plan (elevation of tiers) and bay plans (cross sections of bays) are required if the ship is a container ship. Container planning would be based on the profile plan and bay plans.

Hydrostatics Particulars and Cross Curves of Stability.

The following particulars of the underwater hullform are used to calculate the trim and stability of the vessel. These data are stored against set of draft or displacement and interpolated where necessary.

- i. Volume of displacement
- ii. Waterplane area and their location of centre of gravity (LCF – Longitudinal Centre of Floatation)
- iii. Longitudinal Centre of Buoyancy of the underwater volume (LCB)
- iv. Vertical Center of Buoyancy of the underwater volume (VCB)
- v. Height to Metacentre from the keel (KM)
- vi. Moment to Change Trim by a Centimetre (MCTC)
- vii. Stability lever (KN) for different displacements as the ship heel increases (Cross-curves of stability).

The above data are used to determine trim, drafts and centre of buoyancy and stability of the ship for a given loading condition. Instantaneous values of all the particulars are calculated to check the stability of the vessel as the ship displacement is changed even by a very small value.

Types of Load and Loading Data.

In the case of tank loading, the type of liquid in each tank is needed to estimate the weight of the liquid when volumetric capacity is given as the loading data. Stowage factor and weight of cargo are required in case of Bale or Grain cargo loading. If Grain cargo is carried, heeling moment due to grain shifting should be taken into consideration when estimating the stability of the vessel. Container cargo loading should include weight, size, type of cargo and port of discharge. Sequence of container loading depends on the weight and port of discharge in order to facilitate quick discharging.

Distribution of Structural Weight of the Lightship.

The distribution of the lightweight of the ship should be added to the distribution of other loads (tank load, cargo loads) to calculate total weight distribution along the ship length. Shear Force and Bending Moment estimation involve the determination of resultant force distribution as the difference between the weight and buoyancy. This is further discussed in the section on shear force and bending moment.

Loadline and Stability Criteria

There are statutory criteria to be satisfied by the ship for each loading condition. The loaded draft should not exceed the maximum draft specified by the Loadline Rules and stability criteria applicable to all weather conditions should be satisfied. In addition, maximum values of shear force and bending moment should not exceed the allowable values for harbour condition and sea-going condition.

BACKGROUND OF THE DEVELOPMENT

Particulars of the lightship and all hydrostatics particulars are stored in the program and user is not allowed to change these data. Displacement, center of gravity and all hydrostatics particulars relevant to the displacement are calculated when there is an addition or subtraction of any item. Trim and stability criteria are assessed and a warning displayed if any criterion fails. The load, shear force and bending moment variation along the length of the ship are assessed and displayed graphically against frames of the ship structure.

For each type of tank loading, a window is displayed. This window provides the information on default data and data to be input for each tank. Any item can be loaded as its volume or weight, and the specific gravity value is set default. Fig.1 shows an algorithm of tank loading. A similar algorithm is used for cargo loading as well.

Stability Criteria

In general, all ships should satisfy certain stability criteria. These criteria are imposed to ensure stability of the ship, or in other words, resistance to capsize under any weather condition. These criteria are specified with respect to the righting lever and area under the righting lever that represent the potential energy of the ship at any angle of inclination (Fig 2).

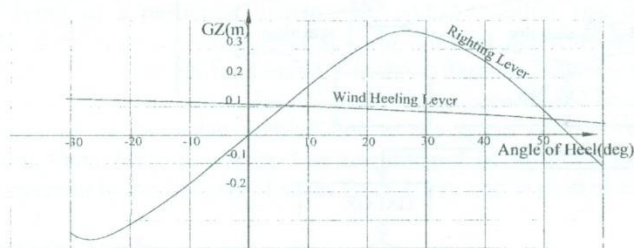


Fig.2:- Righting Lever of a Ship

The following intact stability criteria are recommended by IMO (International Maritime Organization):

1. Initial metacentric height GM should be not less than 0.15 m.
2. Righting lever should be at least 0.2 m at an angle of heel equal to 30 deg.
3. Area under the righting lever curve should be not less than 0.055 m.rad upto an angle of heel of 30 deg.
4. Area under the righting lever curve should be not less than 0.09 m.rad. upto an angle of heel of 40 deg. or upto an angle where the non-weathertight openings come under water (whichever is less)
5. Area under the righting lever curve should be not less than 0.03 m.rad. between the angles of heel of 30 to 40 deg. or such lesser angle mentioned under criterion 4.
6. Maximum righting lever should occur at an angle of heel exceeding 30 deg.
7. Angle of heel due to turning of the vessel should be less than 10.
8. Wind heeling moment criterion should be satisfied.

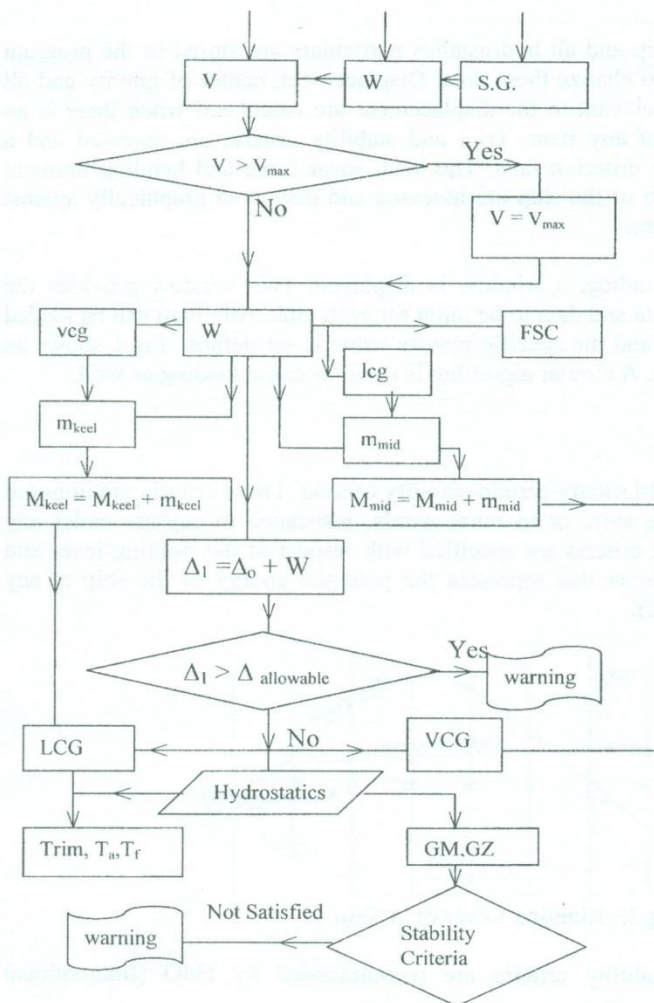


Fig. 1:- Algorithm for Tank Loading

V-Volume of liquid loaded

W- Weight of liquid loaded

Δ_0 = Original displacement

Δ_1 = New displacement

$\Delta_{allowable}$ = Allowable displacement for the specified loadline

FSC = Free surface correction of liquid

M_{keel} = moment of the ship about keel

M_{mid} = moment of the ship about midship

VCG = vcg of the ship

LCG = lcg of the ship

S.G.= Specific Gravity of liquid loaded

V_{max} = Maximum volume of the tank

lcg = longitudinal centre of gravity of liquid loaded

vcg = vertical centre of gravity of liquid loaded

m_{keel} = moment of weight of liquid about keel

m_{mid} = moment of weight of liquid about midship

Trim = trim of the ship

T_a and T_f = Draft aft and forward

GM = Metacentric height of the ship

GZ= Righting lever of the ship

Shear Force and Bending Moment.

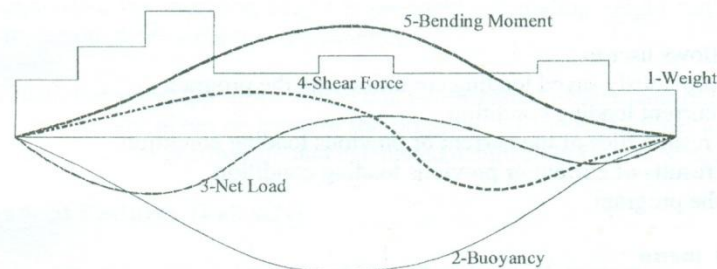


Fig. 3- Shear Force and Bending Moment Distribution

Figure 3 illustrates typical longitudinal distributions of weight and buoyancy for a ship afloat in calm water. Curve 2 represents buoyancy force variation in still water condition. Curve 1 is the distribution of the weight. Areas under these two curves should be equal, as the weight is equal to the buoyancy force.

In this procedure, the length of the ship is divided into a number of equal frame spaces corresponding to frame sections. All of the weights of hull, equipment and contents lying in a particular spacing are added together and treated as a single uniformly distributed load over this spacing. Having determined the buoyancy and weight distribution, the net load curve 3 is the difference between the two. Under the condition of static equilibrium, the net area of this curve should be zero and the center of buoyancy be on the same vertical line as the center of gravity. As in any beam calculation, shear force is obtained as the integral of resultant load (Curve-4). The bending moment is the integral of shear force curve and is plotted as Curve 5.

Wave Induced Loads

The calculation of the bending moment, shear force and torsional loading on a ship hull in waves require a knowledge of the time-varying distribution of fluid forces over the wetted surface of the hull together with the distribution of inertial reaction loads. The fluid load corresponds to the wave induced motion of the water and the corresponding motion of the ship. The inertial forces equal to the product of the local mass of the ship and absolute acceleration. The shear force and bending moments are obtained based on these combined forces and then become time-varying force and moment.

However, experiments have shown that worst case for an average sea going condition can be assumed to be when either the crest or trough of a wave whose length is equal to ship length L , and height is $L/20$ is at the midship. This approach is used here in calculating shear force and bending moment at sea-going condition.

PROGRAM STRUCTURE & FEATURES

The program is structured into the following main menus (see Annexes)

1. File menu

This menu allows user to :

- i. load previously saved loading condition into the program
- ii. save current loading condition
- iii. open results files of the current or previous loading condition
- iv. print results of current or previous loading condition
- v. quit the program

2. Deadweight menu

This menu allows user to load

(a) Consumables as follows (Annex-A)

- i. load or unload Fresh Water tanks either by volume or weight. (Specific gravity is a default value. However user can alter this value if he wishes)
- ii. load or unload Heavy Fuel tanks with the facilities given in i
- iii. load or unload Diesel Oil tanks with the facilities given in i.
- iv. load or unload Ballast Water tanks with the facilities given in i.
- v. load or unload Miscellaneous tanks with the facilities given in i.
- vi. load or unload Lubrication oil tanks with the facilities given in i.
- vii. 10%, 98% or 100% of the capacity as stated in the ship stability booklet can be loaded with single mouse click.

(b) Cargo as follows (Annex-B)

- i. load or unload Cargo Holds with either Bale cargo or Grain cargo. Cargo can be loaded either by volume and stowage factor or weight.
- ii. to load or unload containers.
Profile plan of the container stowage is displayed when containers are to be loaded. Each slot in Bay of containers can be selected for loading. Container information can be loaded either as (Annex-C)
 - 1) weight of the container only
 - or 2) weight and discharge port of the container
 - or 3) weight, discharge port and container numberContainers can be unloaded by a double clicking of the mouse.

3. Crane Loading menu

This menu provides the facility of using onboard Cranes for loading and unloading of cargo. Options are provided to understand the effect of loading or discharging either by a single crane or both cranes simultaneously from both port side and starboard side of the ship. Any adverse heeling or stability of the ship while using these cranes is warned. Program provides the information on Ballast to be loaded or unloaded to correct the adverse heel while using these cranes. Officer in-charge of loading the ship is made knowledgeable on any dangerous situation and precautions can be taken before actual loading or unloading commences.

4. Sounding and Draft Survey menu (Annex-D)

This menu provides information on existing volume or weight of liquid in each tank when the sounding height is the input. Sounding height can be obtained as the results if the weight is fed as input.

Existing deadweight of the vessel can be estimated when measured draft values of the vessel are given as input to the program. At the same time, any discrepancy between actual deadweight and calculated deadweight is warned against.

Advanced Features (Fail safe)

1. The program calculates the centers of gravity of respective volume of liquid loaded and hence user does not need to input these values.
2. Specific gravity of different liquids (Diesel, Heavy Fuel, Lubrication oil) can be altered by the user, however warning is displayed in message box, if these values are out of range.
3. Stowage factor of cargo is checked against recommended values.
4. Empty upper slot of a container-bay is inactive until the slot just below is loaded.
5. Loaded slot of a container-bay is inactive until the slot just above is unloaded.
6. The port of discharge of containers can be selected with a color. This color appears in all loaded slots with containers belonging to the same port of discharge.
7. If loading of the ship continues without selecting an operating draft (loadline), program warns to select an operating draft when the loaded draft reaches the minimum recommended loadline.
8. Program does not permit to load any item if the vessel's draft exceed operating draft.

CONCLUSION

This is the first attempt to develop window-based ships loading software by the author and it is fully successful to the owner's requirements. The results of the software have been validated and in agreement with the calculation given in the stability booklet of the ship. The software could be further improved by adding animated graphical display of the ship and its position with respect to waterplane as loading or unloading take place. Also tank loading and unloading can be integrated with feed pumps parameters to estimate the time of loading or unloading tanks.

Further, this software is already used in the Division of Maritime Studies for teaching purposes and to demonstrate variation trim and stability of a ship during loading and unloading.

REFERENCES

1. General Arrangement Plan of the Ship
2. Capacity Plan of the Ship
3. Stability Booklet of the Ship
4. Principles of Naval Architecture, Volume I, 1988, Published by The Society of Naval Architects and Marine Engineers.

Annex -A :- Description of the labels in the form for loading of Tanks

Load-Expert

Ruhunupura - Loading Heavy Fuel and Diesel

Items	Location	Weight(t)	Vol.(m3)	Sp.Gravity	Vcg(m)	Lcg(m)	Tcg(m)	FSM(t.m)	%Full
Tank 8 DB-SB	Fr 82 1/2 - 13	126.44	131.71	0.960	0.74	80.70	1.26	49.90	98.00
Tank 8 DB-PS	Fr 82 1/2 -	126.44	131.71	0.960	0.74	80.70	1.26	49.90	98.00
Tank 9 Overfl	Fr 81 - 86	16.28	16.95	0.960	0.74	61.81	0.03	12.30	98.00
Tank 10 DB-SB	Fr 31 - 83	143.00	148.96	0.960	0.74	40.73	1.32	56.80	98.00
Tank 10 DB-PS	Fr 31 - 83	143.00	148.96	0.960	0.74	40.73	1.32	56.80	98.00
Tank 31 Sett-PS	Fr 26 -32	23.61	24.60	0.960	6.93	19.30	-4.01	12.00	98.00
Tank 32 day-PS	Fr 26 -323	21.54	22.44	0.960	6.95	19.38	-7.16	11.30	98.00
Total		600.32	625.34	0.959999	1.20	56.53	-0.41	249.00	98.00

HEAVY FUEL

☐ All Empty ☐ 10% ☒ 98% ☐ 100%

Finish

Items	Location	Weight(t)	Vol.(m3)	Sp.Gravity	Vcg(m)	Lcg(m)	Tcg(m)	FSM(t.m)	%Full
Tank 11 Overfl-PS	Fr 30 - 32	5.06	5.88	0.860	0.88	20.69	-4.16	6.00	98.00
Tank 12 Storage-SB	Fr 20 - 32	27.98	32.54	0.860	0.98	17.78	3.17	27.40	98.00
Tank 13 Storage-PS	Fr 20 - 31	25.37	29.50	0.860	1.00	17.39	3.08	26.50	98.00
Tank 33 Day-PS	Fr 18 - 22	8.85	10.29	0.860	7.57	13.00	6.42	2.10	98.00
Tank 34 Sille-PS	Fr 18 - 22	10.54	12.25	0.860	7.45	13.05	8.11	1.90	98.00
Total		77.79	90.45	0.86	2.61	16.66	-1.96	63.90	98.00

DIESEL

☐ All Empty ☐ 10% ☒ 98% ☐ 100%

Stability - During Loading

Displ	DWT	KG	LCG	TCG	FSC	LCG/LCB/LCF are from	GZ at degrees of heel
3888	1	0748.1	06.94	49.26	0.531	0.00	0 10 20 30 40 50 60
LCB	LCF	MCTC	TPC	KMT	GM	Select an Operating Draft	-0.53 0.43 1.24 1.56 1.63 1.34 0.87 0
56.17	57.23	93.24	16.75	12.42	5.41		GM_o = 5.41 (m) > 0.400 Satis
Trim	Ta_mk	Tm_mk	Tf_mk	Tmean	Enter Water Density		GZ at 30 deg = 1.56 (m) > 0.200 Satis
2.883	4.053	2.631	1.178	2.648	1.025		Area GZ_30 = 0.394 (rad/s) > 0.055 Satis
							Area GZ_40 = 0.670 (rad/s) > 0.090 Satis

Start | Project1 - Microsoft Visual ... | Load-Expert | 9:15 AM

Label	Description
Item	Name of each tank (ex: Tank 8DB-SB – Tank no 8 double bottom starboard)
Location	Location of the tank in the ship with respect to the frames
Weight	Weight of liquid
Vol	Volume of liquid in the tank
Sp.Gravity	Specific gravity of the liquid
VCG	Vertical Centre of gravity of the liquid in the tank
LCG	Longitudinal centre of gravity of the liquid in the tank
TCG	Transverse centre of gravity of the liquid in the tank
FSM	Free surface moment of the liquid
%Full	% of the filled volume of the tanks

Annex -B :- Description of the labels in the form for Loading of Cargo Stability details of the ship

Load-Expert

Ruhunupura- Cargo Loading

Items	Location	Weight(t)	Volume(m3)	Stow.Fac.	Vcg(m)	Lcg(m)	Tcg(m)	%Full
Hold 1	Fr 83 - 134	2300.00	3450.00	1.500	5.86	80.42	0.00	70.19
Hold 2	Fr 33 - 83	3430.00	5145.00	1.500	5.72	41.65	0.00	100.00
Total		5730.00	8595.00	0.67	5.78	57.21	0.00	0.0

Grain Cargo

Stowage Factor

☐ m3/Tonne ☐ ft3/Tonne

Bale Cargo

Stability - During Loading

Displ.	DWT	KG_f	LCG	TCG	FSC	LCG/LCB/LCF	are from	GZ at degrees of heel
9618.1	6478.1	06.25	54.00	-0.215	0.03		<input checked="" type="radio"/> AP <input type="radio"/> Midship	0 10 20 30 40 50 60
LCB	LCF	MCTC	TPC	KMT	GM_f	Select an Operating Draft		-0.21 0.24 0.78 1.17 1.40 1.29 0.97 0
57.13	56.72	134.86	19.60	8.78	2.50			GM_o = 2.50 (m) > 0.400 Satisf
Trim	Ta_mk	Tm_mk	Tf_mk	Tmean	Enter Water Density			GZ at 30 deg = 1.17 (m) > 0.200 Satisf
2.233	6.895	5.793	4.668	5.816	1.025			Area GZ_30 = 0.263 (rad/s) > 0.055 Satisf
								Area GZ_40 = 0.488 (rad/s) > 0.090 Satisf
								A40 - A30 = 0.263 (rad/s) > 0.030 Satisf
								GZ_max = 1.4 (m) > 0.200 Satisf
								Occut at = 40 (deg) > 30 Satisf

DISTRIBUTION OF SF [- - - -] and BM [———]

F0 F16 F32 F48 F64 F80 F96 F112 F128 F144 F160

Start **Project1 - Microsoft Visual** **Load-Expert** 9:16 AM

Label	Description
Displ	Displacement of the loaded ship
DWT	Deadweight of the loaded ship
KG_f	Vertical Centre of gravity (fluid) of the loaded ship
LCG	Longitudinal centre of gravity of the loaded ship
TCG	Transverse centre of gravity of the loaded ship
FSC	Free surface correction of the ship
LCB	Longitudinal centre of buoyancy of the ship
LCF	Longitudinal centre of floatation of the loaded ship
TPC	Tonnes per centimeter immersion of the ship
KMT	Height to the transverse metacentre from the keel
GM_f	Metacentric height (fluid)
Trim	Trim of the ship
Ta_mk	Draft aft marks
Tm_mk	Draft midship mark
Tf_mk	Draft forward mark
Tmean	Draft mean draft
GZ	Righting lever
AreaGZ_30	Area of GZ curve up to 30deg of heel
A40-A30	Area of GZ between 30 and 40 degrees
GZ_max	Maximum value of GZ

Annex -C :- Description of the labels in the form for Loading of Containers

BAY05

	08	06	04	02	01	03	05	07	
	0.0	0.0	0.0	0.0	0.0	0.0	0.0	0.0	86
	0.0	0.0	0.0	0.0	0.0	0.0	0.0	0.0	84
	0.0	0.0	0.0	0.0	0.0	0.0	0.0	0.0	82
06	2.74 (cmb)	2.73 (cmb)	2.72 (cmb)	2.71 (cmb)	2.7 (cmb)	2.69 (cmb)			Finish
04		6 (JPN)	5.9 (JPN)	5.8 (JPN)	5.7 (JPN)				
02			13.7 (JPN)	11.5 (JPN)					Weight Mom. C/L 64.89 -4.47

Weight Kg Lcg Tcg

Enter Discharge

cmb

JPN

188

186

184

182

180

178

176

174

172

170

168

166

164

162

160

158

156

154

152

150

148

146

144

142

140

138

136

134

132

130

128

126

124

122

120

118

116

114

112

110

108

106

104

102

100

98

96

94

92

90

88

86

84

82

80

78

76

74

72

70

68

66

64

62

60

58

56

54

52

50

48

46

44

42

40

38

36

34

32

30

28

26

24

22

20

18

16

14

12

10

8

6

4

2

0

16.29 8.24 91.85 -0.03

23.40 5.59 91.85 -0.05

25.20 2.82 91.85 -0.11

Dis.Port

Finish

B09 B07 B05 B03 B01

Stability - During Loading

Displ.	DWT	KG	LCG	TCG	FSC	LCG/LCB/LCF are from	GZ at degrees of heel
6459.1	5319.1	06.62	51.61	0.163	0.00	AP Midship	0 10 20 30 40 50 60
LCB	LCF	MCTC	TPC	KMT	GM_I	Select an Operating Draft	-0.16 0.26 0.78 1.14 1.38 1.22 0.84 0
57.12	57.64	121.19	18.83	8.91	2.28		GM_o = 2.28 (m) > 0.400 Sati
Trim	Ta_mk	Tm_mk	Tf_mk	Tmean	Enter Water Density		GZ at 30 deg = 1.19 (m) > 0.200 Sati
3.844	7.101	5.204	3.266	5.213	1.025		Area GZ_30 = 0.272 (rad/s) > 0.055 Sati
							Area GZ_40 = 0.500 (rad/s) > 0.090 Sati

Start Project1 - Micros... Load-Expert BAY07 BAY05 8:56 AM

Label	Description
B01 – B27	Container Bay number
Form B05	Cross section of the bay 5
T2- T86	Tier numbers
No	Number of containers in each tier
Weight	Weight of containers in each tier
Kg	Equivalent vertical centre of gravity of containers in each tier
Lcg	Equivalent longitudinal centre of gravity of containers in each tier
Tcg	Equivalent transverse centre of gravity of containers in each tier

Annex -D :- Description of the labels in the form for Sounding and Draft Survey

Load-Expert
File Deadweight Crane Operation Sounding and Draft Survey

Soundings **Draft Survey**

Enter TRIM in metres (+ By Stern) 0

BALLAST TANKS **LUB OIL TANKS** **DIESEL OIL TANKS**

TANK3-DB-PS
HEAVY FUEL TANKS
MISCELLANEOUS TANKS

Enter Either Soundings(m) or Weight(t)
1 8.61

Specific Gravity 1.025

Enter Drafts (m)
3.131 3.131 Fore
5.17 5.17 Mid
7.168 7.168 Aft
Port Starbd

Mean draft with Hog-Sag Correction = 5.179m
Estimated Displacement = 8393.89t
Descrepancy of Displacement = 0.29t

Exit

SUMMARY OF LOADING

Items	Weight(t)
Lightship	3140.00
Crew Stores	70.00
Heavy Fuel Oil	0.00
Diesel Oil	0.00
Lub Oil	47.97
Fresh Water	142.88
Ballast Water	0.00
Miscellaneous	0.00
Grain/Bale	4993.33
Containers	0.00
Displacement	8394.18

Stability - During Loading

Displ	DWT	KG_f	LCG	TCG	FSC	LCG/LCB/LCF are from	GZ at degrees of heel
8394.2	5254.2	06.63	51.30	0.164	0.00	AP Midship	0 10 20 30 40 50 60
LCB	LCF	MCTC	TPC	KMI	GM_f	Select an Operating Draft	0.16 0.26 0.70 1.20 1.38 1.22 0.84 0
57.12	57.67	120.67	10.80	8.92	2.28	6.85 m - Tropic FW	GM_o = 2.28 (m) > 0.400 Satis
Trim	Ta_mk	Tm_mk	Tf_mk	Tmean	Enter Water Density	1.025	GZ at 30 deg = 1.20 (m) > 0.200 Satis
4.045	7.166	5.170	3.131	5.179			Area GZ_30 = 0.272 (rad/s) > 0.055 Satis
							Area GZ_40 = 0.501 (rad/s) > 0.090 Satis
							A40 - A30 = 0.272 (rad/s) > 0.030 Satis
							GZ_max = 1.38 (m) > 0.200 Satis
							Occut at = 40 (deg) > 30 Satisfie

DISTRIBUTION OF SF [- - - -] and BM [- - - -]

F0 F16 F32 F48 F64 F80 F96 F112 F128 F144 F160

Start Project1 - Microsoft Visual ... Load-Expert 8:52 AM

1. This frame can be used to find the amount of fluid (Fuel oil, Freshwater, Lubrication oil and Ballast water in each tank when the sounding value of the tank is input.
 2. When the actual draft values of the ship are input the displacement of the ship displayed.
- Drop down menu show the different tank carrying different type of fluids.

Label	Description
Sounding	Reading of the sounding of a particular tank
Weight	Weight of liquid
Sp.Gravity	Specific gravity of the liquid
Fore	Forward of the ship
Mid	Midship of the ship
Aft	Aft of the ship

